DEPARTMENT OF BIOCHEMICAL ENGINEERING

Scale Down Mimics for Viral Vaccine Harvest and Early Purification

EngD Submission

Beatrice Melinek

I, Beatrice Judith Melinek confirm that the work presented in this thesis is my own. Where information has been derived from other sources, I confirm that this has been indicated in the thesis.

Signed……..

Acknowledgments

I would like to thank my supervisor, Tarit Mukhopadhyay, and secondary supervisor, Dan Bracewell, for all their invaluable advice and guidance.

My thanks to GSK and my industrial supervisor Sandrine Dessoy for their support.

I would also like to thank (in no particular order) (i) the many fellow students who have taken the time to show me how to use the various pieces of laboratory equipment and offer their advice; (ii) Bernice Wright for her suggestion of looking at gels and western blots and training to do so and various other pieces of guidance over the last year; (iii) Jelena Ruscic and Bernice Wright for using their expertise to optimise the BFU assay; (iv) the team at GSK, who as well as welcoming me at the Rixensart site and enabling my work there also helped by performing $TCID_{50}$ assays and worked with me on the PKII nanobead runs and offered various pieces of guidance; (v) Mark Turmaine for his guidance and training on the use of TEM; (vi) Gareth Mannell for training on and help running, taking apart and putting back together the CSA-1, CARR and PSC-1 centrifuges, and many helpful suggestions for conducting the cell mimic work on these industrial centrifuges.

Abstract

The project focused on the Ultra Scale-Down (USD) modelling of harvest and early purification for viral vaccine and vector production processes. USD models seek to mimic the commercial scale process environment using only millilitres of material. Many commercial processes include a disc-stack centrifuge, micro-filtration, tangential flow ultrafiltration and density gradient ultracentrifugation steps, which are investigated in this work.

A key parameter of USD, in particular for centrifugation, has been shown to be shear, which may cause significant damage to biological products and increase the difficulty of subsequent processing steps. To quantify shear rate therefore the PSC-5 disk-stack centrifuge and PKII density gradient ultra-centrifuge have been modelled using Comsol Multiphysics®.

This EngD project extended existing Computational Fluid Dynamic (CFD) analysis by treating the centrifuge as a 3 dimensional system, drawing comparison to the rotating disc shear device based on a simple population balance analysis (accounting for different shear rate levels and time of exposure), and identifying the nature of the shear (simple versus extensional). This modified approach produced a good prediction of shear rate as validated against experimental results, as well as intuitively representing a closer match to the physically important points of comparison between the two systems.

In order to overcoming the challenge of experimentally validating CFD predictions in downstream process units a novel approach was adopted: use of synthetic particles that mimic mammalian cells. Adju-Phos was applied successfully for the prediction of shear rate in a number of pilot scale centrifuges of both tubular bowl and disk-stack design, by correlating changes in the particle size distribution against that seen in the USD shear device. The significant advantages of using Adju-Phos include reduced cost, pre-work and time.

For the PKII density gradient ultracentrifuge, a smaller virus shear mimic, consisting of an off-the-shelf polystyrene nanobead coated with streptavidin, was used for experimental validation of CFD. This work also represents the first steps in developing an USD model for the continuous feed industrial ultracentrifuge, consisting of the rotating disc shear device and laboratory ultracentrifuge matched to the large scale on the basis or $\omega^2 t$ and head at the product layer. The fact that these nanobeads showed an impact from hydrodynamic forces despite their small size, raised the possibility that viruses, which had been thought to be too small for damage by hydrodynamic or other forms of shear, might also be susceptible.

There is limited if any literature on the impact of shear rate on cells used to produce viral products, or on the viral products themselves. The existing USD tool was used to provide some insight into the performance of the harvest step for influenza and adenovirus production processes in continuous cell-lines.

The results indicated that virus infected cells do not actually show any increase in sensitivity to shear forces, and may indeed become less shear sensitive, in a similar manner to that previously observed in old or dead cell cultures. Clarification may be most significantly dependent on the virus release mechanism, with the budding influenza virus producing a much greater decrease in clarification than the lytic, non-enveloped adenovirus. A good match was also demonstrated to the industrial scale performance in terms of clarification, protein release and impurity profile.

The impact on the influenza and adenoviruses themselves was measured using infectivity assays, TEM and particle size distribution and protein contents of post shear purified viral particles. Whilst no impact was recorded based on the infectivity assays or TEM, a small but significant change in particle size distribution was shown for adenovirus, and is indicated for influenza. The influenza virus also showed a possible change in protein make-up of purified viral particles, indicating possibly a loss of those proteins from the virus structure. The significance of these morphological changes, if any, remains to be confirmed.

Key words: Scale-down, centrifugation, viral vaccine, shear, gene-therapy

Impact Statement

Traditional regulatory approaches involve testing representative batches to confirm that a range of quality and safety criteria are met. This approach is changing, with the emphasis, for new processes, shifting to understanding the impact of varying process conditions on the quality of the final product. This new approach is known as Quality by Design (QbD). The aim is to use QbD approaches to improve the robustness and reduce the risks associated with pharmaceutical processes. This has the potential to improve the success rate of production processes and allow pharmaceutical producers greater flexibility, both reducing the final product cost.

The use of qualified scale-down models is an essential component of the QbD process; allowing characterisation of the design space for a new product/process economically and rapidly, producing sufficiently comprehensive quantities of data for confidence and to generate knowledge of the product-process interactions and to test design space boundaries in a manner which is not feasible at large/pilot scale (Garcia et al., 2012, McCreath and Shivhare, 2011, Chhatre et al., 2011). This is of particular use for low-volume, high-cost products (Garcia et al., 2012), which describes viral vaccines, particularly during early stage process development. The shift from animal/tissue based (e.g. ova) production to cell based manufacturing in the vaccines industry (Whitford and Fairbank, 2011) also implies that Ultra-Scale Down (USD) models for vaccine purification steps may have considerable utility going forwards. In this work an existing USD methodology for the centrifugal harvest step is used to characterise, for the first time, a viral vaccine production process.

To address cost and safety concerns, the first stage of the project was to develop and characterise synthetic shear tracer particles which can be used as a mimic for various biological products (cells and viruses). The focus on shear is based on previous work (Maybury et al., 2000, Boychyn et al., 2004) in scaling down continuous centrifugation which showed shear rate to be the key scaling parameter. The shear mimics may also be useful tools in characterising shear rate in large-scale equipment and reducing the cost of USD development.

Contents

List of Appendices

Table of Figures

Nomenclature

Symbol	Description	Page #	Eqn #
Q_1, Q_2	the flow rate through centrifuge 1 and 2		
Σ_1, Σ_2	the settling area or sigma for centrifuge 1 and 2	46	1
Z_0	the number of revolutions per second following acceleration to full speed		
x	the fraction of run time spent accelerating		
y	the fraction of run time spent decelerating		
V	the volume of material being centrifuged		
R_2	the radius to the base of the centrifuge tube		
R_1	the radius to the surface of the liquid in the centrifuge tube	46	2
N	the number of active discs		
Z	the number of revolutions per second		
R_0	the outer disc radius		
R_i	the inner disc radius		
θ	the half disc cone angle		
f_l	a correction factor accounting for the flow area occupied by the strips which hold the discs apart	46	3
ρ	the solution density		
ΔP	the pressure drop along the pipe		
D	the pipe diameter		
L	the pipe length		
μ	the solution viscosity	48	4
λ	the Kolmogorov scale		
ν	the kinematic viscosity		
EDR	the local energy dissipation rate	55	5
μ	the dynamic viscosity		
U	the velocity vector		
∇U	the velocity gradient vector	55	6
A	a constant, typically 1		
V'	the fluctuating velocity, typically using root mean square fluctuating velocity		
L	a characteristic length, typically larger than turbulent eddies	55	7
u, v and w	the fluid velocities in the x, y and z directions respectively		
subscript of x, y or z	denotes differentiation in the indicated direction	74	8

Symbol	Description	Page #	Eqn #
Q	the volumetric pumping rate		
v_r	the velocity at a given distance (r) from the disc		
A	the flow area		
N	the number of passes over the time (t) (typically 20seconds)		
V	the volume of liquid in the chamber of the rotating disc device (typically 15ml)	74	9 / 10
b	breakage kernel / rate		
C_4, β, α and γ	constant parameters		
EDR	the energy dissipation rate		
k_{vis}	the kinematic viscosity (assumed to be that of water)		
D_P	the particle diameter	78	11

1. Introduction

1.1. Thesis overview

The project aim is to produce laboratory scale mimics for the purification steps in a vaccine manufacturing process. A number of technologies can be used in the downstream purification processes, however, in this project the focus was on disk-stack centrifugation, ultrafiltration clarification and density gradient ultracentrifugation, of which the first and last were successfully explored in some detail. Within industrial centrifugation shear and related phenomena have previously been identified as a key scaling parameter. This remained to be confirmed for viral vaccine production processes. It was envisioned that this work be made as generic as possible, first involving the identification and use of a synthetic shear tracer particle.

This review will therefore briefly introduce downstream separation and the above technologies in particular, with reference to trends in vaccines, vaccine types and production technology and the implications of these for downstream separation processes; the role of ultra-scale down in bioprocess development and optimisation; the nature of shear; the impact of hydrodynamic shear forces within bio-processing and particularly its impact on downstream purification and subsequent product efficacy.

1.1.1. Vaccines

Vaccines are a diverse group of biological products, coming in various forms. Traditionally including attenuated viruses, inactivated bacteria and toxoids (Josefsberg and Buckland, 2012), novel product types including molecule subunit antigens, virus-like particles, combination vaccines and gene-therapy therapeutic vaccines have been developed since the 1980s. A broader range of product types and applications have been developed in recent decades thanks to factors such as greater systematisation of product testing, through well plates and automated methods, and unlocking of the human and pathogen genomes, potentially allowing more logical direction of research efforts (Yarmush, 2003).

The earliest products were derived by extraction from infected animals or humans, through to ova based culture and have evolved through greater understanding of how to manipulate existing organisms and cell culture based technologies (Josefsberg and Buckland, 2012). Cell culture in better defined cells, using processes such as recombinant DNA technology or virus infection are the current standard and better understood and controlled. By contrast, the use of human and animal blood serum is less acceptable for the risk of transmission of adventitious agents. Ova based culture techniques are still used for legacy and cost reasons, especially in influenza vaccine manufacture (Yarmush, 2003).

Differences between viruses include size, shape, chemical composition and surface structure, including charge distribution and density, hydrophobicity or hydrophobic components, addition of poly or oligosaccharides to surface proteins (Wolff and Reichl, 2011). Protein size ranges from 0.005×10^6Da to 0.08×10^6Da. Viruses are much larger, generally larger than 5×10^6 Da with virus particles as big as 100s of nm.

During this EngD project two separate virus production processes have been explored, which represent enveloped virus (influenza) and non-enveloped virus (adenovirus) processing. The work aims to draw lessons from work done at UCL and apply this to work done in collaboration with GSK. This has the added advantage potentially of broadening the processes examined, and by comparing and contrasting, drawing some indication of how general the results obtained might be. Adenovirus was grown at UCL in an adherent culture of the continuous HEK 293 cell-line, in stationary T-flasks. The latter is not expected to be representative of a

large scale culture. The influenza viral vaccine was produced, using a continuous EB66 cell-line, in a stirred tank reactor at a scale of 50Litres. The section below details some of the existing literature on these two viral products and their production processes. Section 1.1.2.4 discusses the impact of shear forces on viruses in more detail.

1.1.1.1. Influenza

Historic flu pandemics have had a devastating toll, with tens of millions of deaths around the world, and concerns for the possibility of another such pandemic remain high (Kamps et al. (2006),Osterhaus et al. (2011)). Seasonal flu alone causes millions of cases of severe illness and hundreds of thousands of deaths annually (WHO, 2014). Prevention by vaccination has been the most widely used and successful strategy for combating influenza (Hedlund et al. (2010), Salomon and Webster (2009), Muennig and Khan (2001)).

Historically influenza vaccine production has used a live egg-based system. This traditional production process has numerous limitations including the imperfect and fragile supply of appropriately sourced eggs, the risk of contamination, cost and allergenic nature of some egg constituents (Feng et al., 2011). There is a need for more efficient and cost-effective processes to meet the demand for a rapid response capacity, and billions of doses of stock piles, which are required to deal with emergent pandemic strains, alongside the ongoing annual seasonal flu vaccine production (Chua and Chen (2010), Osterhaus et al. (2011)). The degree of investment and support from public and commercial projects, and the number of continuous cell-line based candidates and processes in development, are witness to the importance placed on improving production (Genzel and Reichl, 2009). For example the continuous cell lines currently under investigation for production of influenza vaccine include Vero, MDCK, CEFs, PER.C6, AGE1.CR, EB66, PBS-1, QOR/2E11, SogE and MFF-8C1 (Genzel, 2015). For development and a smooth transition to production these new processes must be well characterised.

The seasonal nature of influenza, and the evolution of different strains, means that each year process development, troubleshooting and clinical safety trial must be complete all within very tight timeframes. This is also likely to limit the amount of material, expert personnel and resources available for any new or alternative

process developments which may be occurring in parallel with annual production (Proctor, 2012). Moving on from legacy processes also requires meeting modern regulatory expectations, including QbD, and a full understanding of process-product interaction (Rathore and Winkle, 2009). The complex nature of the product, virus-cell and immune-virus interactions in the context of products mechanisms of action, and of the virus-cell interaction, in the context of production, make viral vaccine production a particularly difficult process to characterise.

Influenza virus is a member of the orthomyxoviridae family. It is enveloped, pleomorphic and varies in size between 80 and 120nm. In its core are segmented negative-sense, single RNA strands. It has 9 viral proteins forming a capsid layer, composed largely of a single matrix (M1) protein, and embedded in the viral envelope, of which haemagglutinin (HA) and neuraminidase (NA) are identified as of chief importance in the viral vaccine for their role in stimulating the immune response (Dimitrov (2004), Chang et al. (2015), Shaw et al. (2008), Osterhaus et al. (2011)).

Figure 1.1-1 and Table 1.1-1 gives a summary of the proteins in influenza virus for later reference.

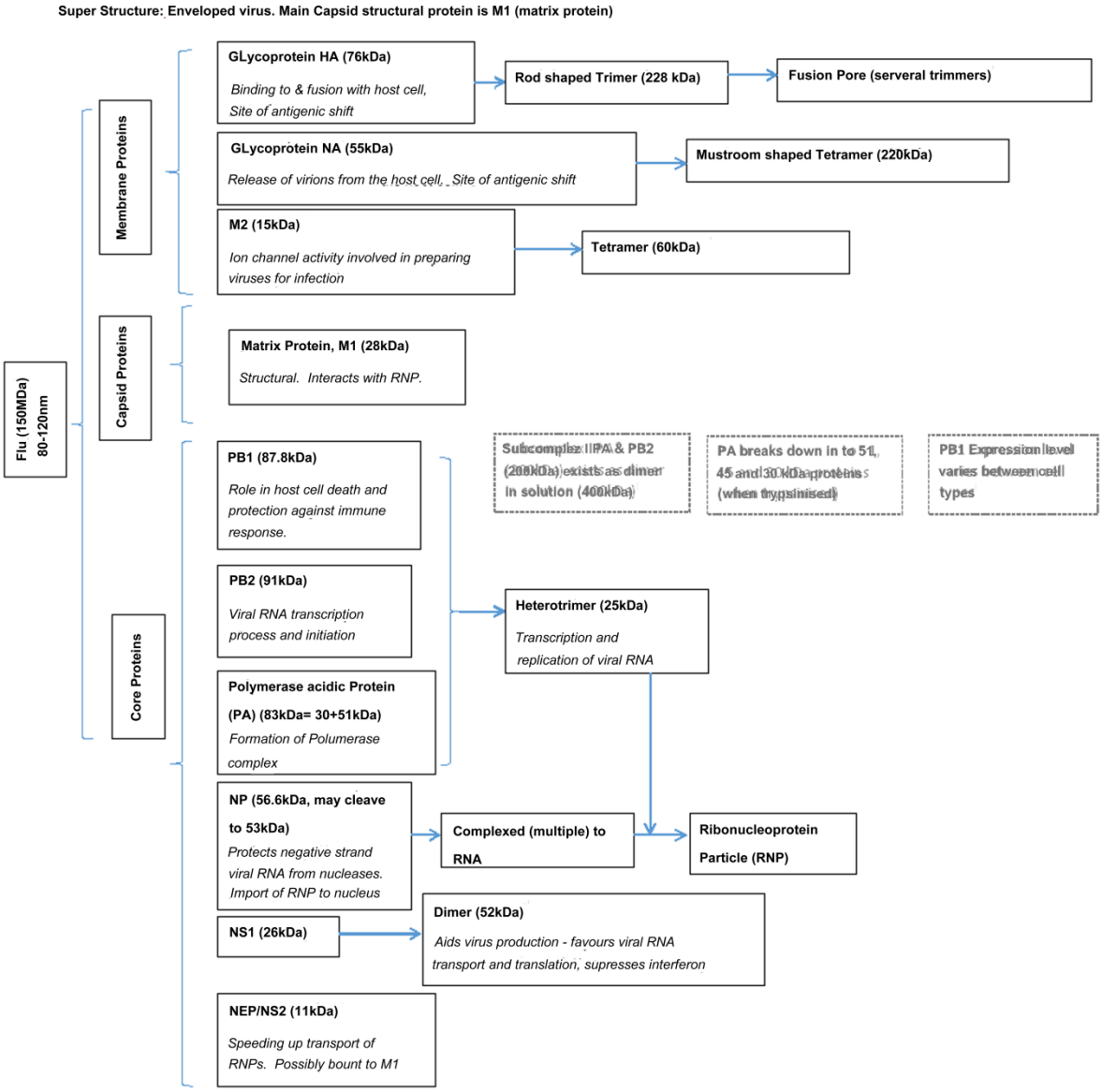

Figure 1.1-1. Schematic summary of influenza virus proteins and structure (The Rapid Reference to Influenza Resource Center Team. Adapted from Wilschut (2006), (Gürtler, 2006), (Lamb et al., 1994), (UniProt, 2016a), (Guu et al., 2008), (SinoBiologicalInc), (Pflug et al., 2014), Chang et al. (2015)).

Protein ID		MW (kDa)	Prevalence/Copy Number per virion
	Dimer of PA, P2 subcomplex I	400	
	PA, PB1 & PB2 heterotrimer	250	
	HA trimer	228	167*
	NA tetramer	220	25*
	PA, P2 subcomplex I	200	
PB2	Polymerase basic protein 2	91	30-60
PB1	Polymerase basic protein 1	87.8	30-60
PA	Polymerase acidic Protein	83	30-60
HA0	Haemagglutinin	76	500
	M2 tetramer	60	5-15*
NP	Nucleoprotein	56.6	1000
HA1	Haemogglutinin (post cleavage)	55	500
NA	Neuraminidase	55	100
Nucleoprotein post cleavage		53	1000
	Dimer of NS1	52	
	PA trypsinised	51	30-60*
		45	30-60*
		30	30-60*
M1	Matrix protein M1	28	3000
NS1	Non-structural proteins	26	
HA2	Haemogglutinin (post cleavage)	25	500
M2	Matrix protein M2	15	20-60
NS2	Non-structural proteins	11	130-200

Table 1.1-1. Summary of protein molecular weight and prevalence in influenza virus (The Rapid Reference to Influenza Resource Center Team. Adapted from Wilschut, 2006, Guu et al., 2008), (Zhirnov et al., 2002). *Assumed values

It might be speculated that the mechanical properties of the cell and thus its response to process conditions would be most greatly affected by the entry and release stages of the viral life cycle.

The entry route of influenza is by endocytosis, via attachment of the HA to siallic acid receptors on the host cell surface (Dimitrov (2004), Gürtler (2006)). Influenza crosses the cell membrane very rapidly and with high efficacy, i.e. the majority of viruses which attach to a cell go on to enter that cell. Dimitrov (2004) shows the stages of influenza viral entry in to the cell, following attachment, as internalisation in

an endosome, conformational changes in the attachment protein leading to fusion of the viral and endosomal membrane, leading in turn to the release of the viral genome into the cell cytoplasm.

Influenza buds from the cytoplasmic membrane, which is first modified to create lipid rafts, the characteristics of which include concentration of viral membrane proteins, and a different cholesterol/lipid compositions from that of the standard cell membrane. These lipid rafts may be isolated, or may coalesce to form large lipid raft zones from which multiple viruses bud. The capsid and core are assembled at the membrane where it buds, and the receptors for HA are destroyed prior to budding in order to allow the virus to leave the cell unencumbered, and presumably to minimize self-aggregation of virus. The local membrane properties, chemical and physical, are also modified to allow it to bend, forming an envelope around the virus, and eventually separate from the host cell membrane. Virus release from the cell is associated predominantly with the action of NA (Handel et al., 2014).

Enveloped viruses in particular may contain host encoded protein, which it is presumed is due to host cell proteins which are 'caught up' in the viral membrane during budding. In addition, as with therapeutic proteins, processes such as glycosylation may vary from one host cell type to another. The properties of the viruses themselves may therefore vary as a function of the type of cell line used to produce them (Shaw et al. (2008), Schaap et al. (2012), Shigematsu et al. (2014)).

The above gives some sense of the complexity of the virus life cycle and structure for influenza. To some extent its historic usage, under circumstances where full evaluation of that structure was impossible, set a precedent for use of this killed virus product in humans without the same kind of quality assurance / quality control (QA/QC) burden which might apply to future such attenuated or killed viral vaccine. The European Medicines Agency (EMA) Vaccines Working Party (VWP (2013)) provide guidelines for measuring flu vaccine quality, including HA antigen identification against calibration strain by immunodiffusion, HA physicochemical properties, NA antigen identification, ratio of NA to HA, purity, aggregate size etc.

1.1.1.2. Adenovirus

Gene therapy has great potential in healthcare and therapeutics, particularly for unmet medical needs (Carr and Bradshaw, 2016). Adenovirus is one of the leading candidates currently being studied for use as a vector in gene therapy (Silva et al. (2010), Waehler et al. (2007), Zhang and Godbey (2006)), with particular potential in oncology, and immunotherapies / vaccines (Kotterman et al., 2015). 526 reported trials are currently ongoing (Edelstein, 2016) and licenced products include Gendicine in China for head and neck cancer (Kotterman et al. (2015), Kasala et al. (2016)).

As with influenza there is considerable interest in scaling up production as gene therapy treatments move through clinical trial, towards production phases. This scale-up is set to pose a number of challenges, including the shift from existing adherent culture at laboratory scale to large scale bioreactors. This project focuses on shear rate, as a particularly challenging factor, associated with downstream processing, which is likely to be significantly different between laboratory and production scales (Pettitt et al., 2016). One of the many significant differences between influenza and adenovirus for gene therapy is the relative stage of development in view of regulation: gene therapy is at a much earlier stage in terms of its applications as a therapeutic, and therefore likely to be subject to considerably more stringent demands with respect to understanding of its structure, mechanism of action and critical quality attributes (CQA) (Scherman, 2014).

Adenovirus is part of the Adenoviridae family, unenveloped, icosahedral in structure, with a double strand of Deoxyribonucleic acid (DNA) at its core, a diameter of 70-100nm, a large number of serotypes (>=52), with serotype 5 being used for this project, and c. 13 structural proteins (Waehler et al. (2007), Harrison (2010), Russell (2009)). The structural proteins include a trimerised hexon which constitutes the majority of the outer capsid, and which are arranged systematically around a penton base with fibre proteins attached (Lynch et al., 2011). These fibres give adenovirus its distinct pattern of spikes, and are responsible for initial cell attachment (Vellinga et al., 2005).

Figure 1.1-2 and Table 1.1-2 gives a summary of the proteins in adenovirus for later reference.

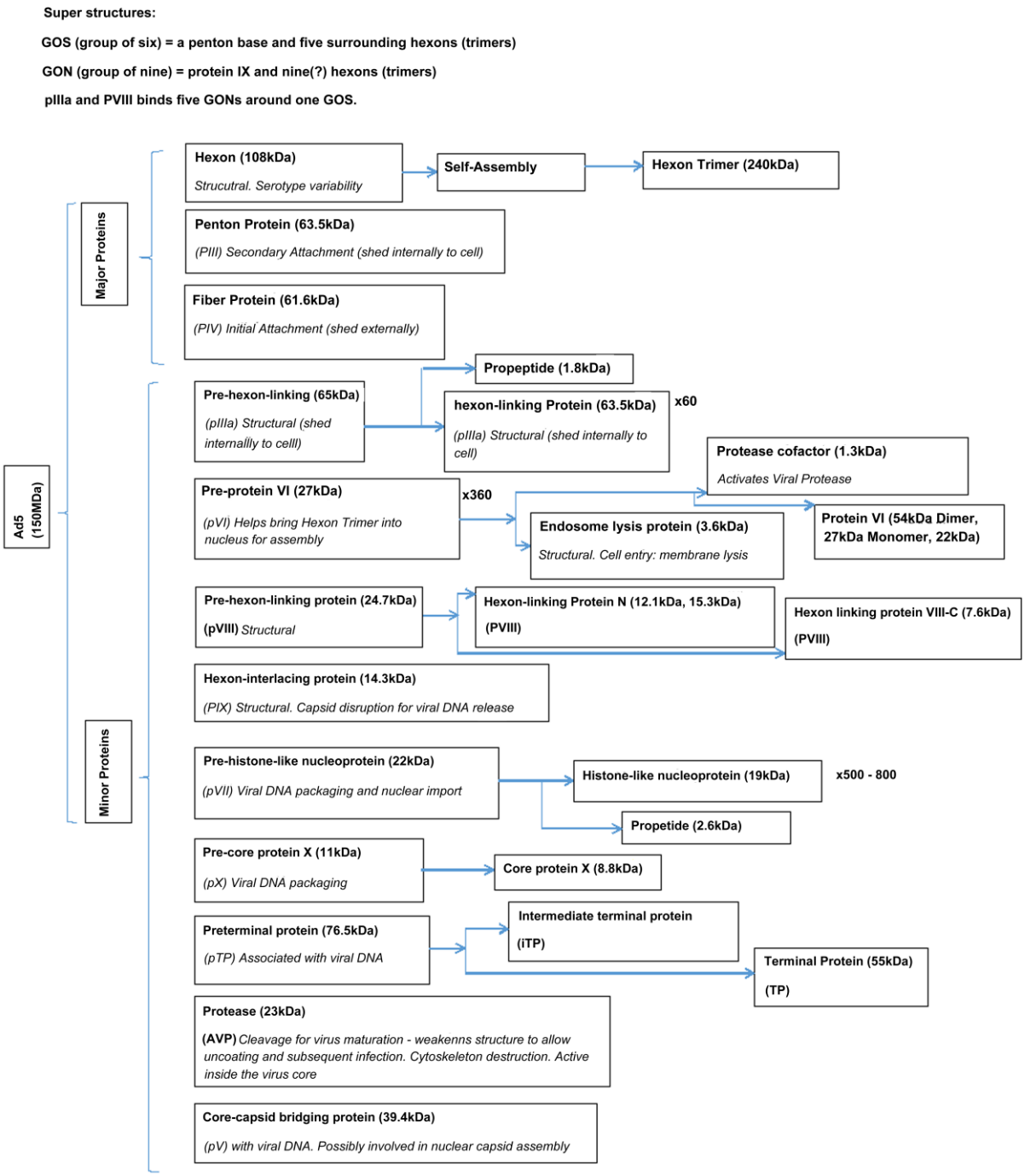

Figure 1.1-2. Schematic summary of Adenovirus proteins and structure ((Liu et al., 2010), (Vellinga et al., 2005), (Perez-Berna et al., 2009), (Moyer and Nemerow, 2012), (Haruki et al., 2003), (UniProt, 2016b), (UniProt, 2015), (MyBioSource.com, 2016))

Protein ID		MW (kDa)	Prevalence/Copy Number per virion	References (Wisniewski et al., 2014)
Hexon Trimer		240	240	(Vellinga et al., 2005)
Hexon		108	720	(Vellinga et al., 2005, Silvestry et al., 2009)
pTP	Preterminal protein	76	2	(Perez-Berna et al., 2009)
pIIIa	Pre-Hexon Linking	65	60	(Perez-Berna et al., 2009)
PIIIa	Hexon Linking	63.5	(60)	
Penton Protein		63.2	60	(Christensen et al., 2008, Silvestry et al., 2009)
Fiber Protein		61.6	12, 36	(Henning et al., 2006) (Campos and Barry, 2006, Silvestry et al., 2009)
TP	Terminal Protein	55	(2)	
Protein VI Dimer		54	(360/2)	
Protein V		39.4	170	(Silvestry et al., 2009)
Pre-protein VI		27	360, 369	(Perez-Berna et al., 2009) (Silvestry et al., 2009)
pVIII	Pre-hexon-linking protein	24.7	120	(Perez-Berna et al., 2009, Silvestry et al., 2009)
AVP	Protease	23	10, 43	(Silvestry et al., 2009)
Protein VI monomer		22	(360?)	
pVII	Pre-histone-like nucleoprotein	22	800, 633	(Perez-Berna et al., 2009) (Silvestry et al., 2009)
PVII	Histone-like nucleoprotein	19	(800)	
PIX	Hexon interlacing protein	14.3	240	(Campos and Barry, 2006, Silvestry et al., 2009)
PVIII	Hexon-linking Protein N	12.1	(120)	
pX	Pre-core protein X	11	126-160	
PVIII	Hexon-linking Protein C	7.6	(120)	
PX	Core Protein X	8.8	125	(Silvestry et al., 2009)

Table 1.1-2. Summary of protein molecular weight and prevalence in adenovirus

Of the structural differences between influenza and adenovirus the critical one is likely to be the unenveloped nature of the latter. In the mechanism by which they penetrate and release from the cell non-enveloped viruses differ considerably from enveloped (Garoff et al. (1998), Wiethoff et al. (2005)).

For adenovirus the entry route is by clathrin-mediated endocytosis, via the coxsackie adenovirus receptor (CAR) (Dimitrov, 2004). Transcription, replication and assembly occur in the cell nucleus and release is by cell lysis (McLean et al., 2008), via viroporins introduced to the cell membrane (Hulo et al., 2011). This release is described as inefficient by Gros and Guedan (2010) as much of the virus remains inside the cells. This may be linked to the similarity in concentration of virus between the cell pellet and liquor, although there appears to be a preponderance of processes which focus on extraction of viral product from the former as oppose to the latter, and some uncertainty about the relative qualities (Altaras et al., 2005).

One additional complexity of particular concern within gene therapy is the presence of empty or partially filled capsids, which may provoke a greater immune response without providing any additional therapeutic benefit, generating vector-immunity by the host. This is one of a long list of product characteristics which is likely to constitute the regulatory requirements for release (Scherman (2014), Altaras et al. (2005), Silva et al. (2010)).

1.1.2. Downstream Processing

Downstream processing covers the stages between the outlet from the bioreactor through to the final purification stages. The stages of downstream processing may include: cell recovery; product inactivation; initial separation and purification steps, which may also provide volume and therefore cost reduction for subsequent process units; ultrafiltration and/or diafiltration, which allow buffer exchange in preparation for subsequent processing steps or for formulation purposes; and final purification, e.g. filtration (Rathore and Sofer, 2005).

Recovery stages separate whole cells from supernatant, where the biological product is likely to reside predominantly in one or the other. This is typically done by centrifugation or filtration, depending on the volume or flow to be processes and the solids quantities to be handles in each batch. If the biological product is contained within the cells there are the additional stages of cell lysis using either high pressure homogenisation, or agitation with beads, heat or chemical lysis or freeze thaw. This is usually followed by another stage of either centrifugation or filtration to remove cell debris (Yarmush, 2003).

Removal of the product from in process impurities (or visa-versa) at later stages relies on smaller differences, e.g. in density, size, hydrophobicity or charge, with or without treatment. Density gradient centrifugation is one such later stage unit, and is commonly used for viruses for both concentration and purification. (Yarmush, 2003)

Optimisation of yields at the upstream stage in cell culture based processes has been the focus of considerable effort. This has resulted in downstream separation in some cases being limiting and representing a higher proportion of costs (Wolff and Reichl, 2011), with values given for the percentage of operating costs incurred at the downstream separation stage as high as 70% (Morenweiser, 2005). In addition safety and reactogenicity concerns continue to drive towards greater purity processes, with potential particularly in filters and highly specific chromatography as material science progresses (Yarmush, 2003).

1.1.2.1. Continuous Centrifugation

The principle of centrifugation is that particles of a different size and density will respond differently under the effects of a centrifugal force, which acts in a manner analogous to gravity (Hsu and Perry, 1981). It is a common unit operation for solid-liquid separation. The force acting on a particle is proportional to its mass, the square of the angular velocity and the distance from the centre of rotation. The movement of the particle is inhibited by the viscosity of the fluid and its own size. Under the effects of gravity alone the back diffusion of solute particles can play a significant role in maintaining small particles with minimal differential density in suspension.

Centrifuges are used to separate cells and particulates from liquids and for fractionation. For cell harvesting the disc-stack configuration is the most commonly used. The feed is continuous as is the liquid extraction at the top. The solid removal may be either continuous or batch. The centrifugal force throws the cells or particles outwards, so that they do not flow with the lighter fluid but hit the discs and run down to the solids settling area (Rathore and Sofer, 2005).

Disk-stack centrifuges offer poor de-watering levels (~50-60% (Salte et al., 2006)) when compared to bowl centrifuges, which can be problematic when it comes to maximising the recovery of an extra-cellular product (Lopes and Keshavarz-Moore, 2012). However, bowl centrifuge operation is constrained by other factors such as the requirement for manual intervention (Salte et al., 2006).

1.1.2.2. Filtration

The principle of filtration is that larger particles will pass with greater difficulty, or not at all, through a membrane whose pores are below a certain size, whilst smaller particles may still pass relatively unhindered; filtration is a particulate separation technique based on the size or molecular weight of a heterogeneous feed stream. Filtration is classified according to the filter pore size into microfiltration or ultrafiltration. Microfiltration can be used instead of centrifugation to remove microcarriers, cells and cell debris (Wolff and Reichl, 2011) and for the concentration of viruses, Whilst ultra-filtration is generally used for purification, exchanging buffer for a formulation or prior to a purification step such as chromatography (diafiltration)

and concentrating the product (Sharma et al., 2011), although depending on product size there can be overlap in the application of filters with different pore sizes.

For large volumes at an industrial scale tangential flow filtration is usually used. This involves flow on the retentate side parallel to the surface of the filter, minimizing the build-up of cake, and thus minimizing the resistance to flow of the permeate (Saxena et al., 2009). A slight modification of this is high performance tangential flow filtration involving co-current feeds of retentate and some of the permeate; maintaining a more stable transmembrane pressure (Wolff and Reichl, 2011) and reportedly allowed a closer approach between the sizes of particles being separated (vanReis et al., 1997). Key parameters which can be controlled during operation are transmembrane pressure (TMP), feed flow rate and flux of permeate (Wolff and Reichl, 2011).

There are many different geometries available for filtration including: spiral wound, tubular, hollow fibre, flat sheet. Each has their pros and cons: for hollow fibres the pros are low shear due to laminar flows and high compaction; for flat sheet the advantages are ease of cleaning and unit replacement. (Wolff and Reichl, 2011, Sharma et al., 2011)

The biggest issues with filtration are fouling and the cost of the units (Sharma et al., 2011). Pore size (cut off molecular weight) and size distribution, membrane material, process stream (e.g. contamination, viscosity etc.), virus/product size, aggregation behaviour, buffer used, flux and pore blockage all effect recovery. Product losses can occur due to mechanical damage, separation efficiency, trapping within pores or by adsorption to the membrane surface. Depth filters with reducing pore size reduces blockage. (Wolff and Reichl, 2011)

Viscosity, which is expected to impact upon filter performance, is a function of the process stream make-up particularly in terms of concentration of proteins, nucleic acids and product and concentration and molecular weight of DNA fragments. These concentrations may depend both upon the culture media, culture conditions and the preceding separation processes, for example the degree of shear experienced at cell recovery. Viscosity may also change as filtration proceeds. (Wolff and Reichl, 2011)

Virus particles tend to be quite different in size from most common soluble biomolecules allowing an efficient and economic separation. The size is also relatively independent of strain where this changes regularly. However, the nominal molecular weight cut-off of a membrane only represents the average that a membrane will allow to pass through. Therefore, in practice, larger particles will pass through than the molecular weight cut-off would suggest. A margin must therefore be allowed below the virus size to prevent product loss. Equally smaller pore size increases resistance and thus decreases flux, and therefore increases processing time, and increases TMP. It also means that more large contaminants are retained. (Wolff and Reichl, 2011)

Potential sources of damage to virus particles during filtration might include shear forces introduced by pumps and turbulent shear forces on the membrane screens exacerbated by longer processing time: Li and Qiu (2013) discuss the relative merits and faults of various pump types, highlighting the high levels of shear in lobe pumps and variability in flow/ discharge pressure in peristaltic pumps, both effecting product stability; whilst Bekard et al. (2011) highlight the importance of the duration of shearing on protein stability.

1.1.2.3. Density Gradient Ultra-centrifugation (DG-UC)

Density gradient centrifugation allows for a more complete separation of particulate types and can be used to separate out particles of a far lower mass than other forms of centrifugation. There are a number of different modes of operation described in more detail below, however the common feature is a density gradient in the solvent initially filling the centrifuge to which the sample is added (Hsu and Perry, 1981). The usual density gradient media are caesium chloride (CsCl), iodixanol or sucrose and the density of the solution increases with increasing distance from the centre of rotation (Wolff and Reichl, 2011). The ideal density gradient media will have a maximum density greater than the particle for retention, be inert and safe, should not disrupt measurement of the target product or impurities, have a density determinable by physiochemical analysis, be separable from the target product, have a low viscosity and be iso-osmotic with the target product (Frei, 2011). The US Pharmacopeia (1043) defines density gradient media as a tier 2 auxiliary media, and recommends using for auxiliary media chemicals which are already licenced in a therapeutic context; so iodixanol for example has already been widely used, and was

developed as a contrast medium and sucrose is widely used as a sweetening agent (British Pharmacopoeia).

Density gradient ultra-centrifugation (DG-UC) may work in a number of different modes: rate zonal, isopycnic and differential centrifugation, and may also be used to fractionate products. (Wolff and Reichl, 2011)

The principle of density gradient centrifugation is to an extent dependent on the mode of operation. Rate zonal centrifugation relies on the particle size and mass, which gives a different rate of travel for each species, resulting in layers of different macromolecules forming over a period of time. Isopycnic centrifugation relies on the buoyant density; the centrifuge is left to run until the particles have migrated to a position in the density gradient where their density is equal to that of the surrounding solution. With rate zonal centrifugation the sample in its solution will be layered at the top of the centrifuge, while with isopycnic centrifugation the sample for separation may either form the initial top layer or be mixed with the density gradient solution and substantial time (36-48 hours) allowed for gradient formation and sedimentation. Differential centrifugation allows the separation of the macromolecules fractionally, by pelleting against a sucrose cushion at different centrifugal speeds through a media which is less dense than the particles themselves, so that their rate of sedimentation is dependent upon the particle size; thus a partially purified product may be obtained by removing and washing (and re-centrifuging) the pellet after a certain length of time. The gradient material introduces a resistance to flow, either through increased viscosity or back diffusion or both, further accentuating the differences, based on the sedimentation coefficient between the species to be separated. An ultracentrifuge typically operates at a much higher rate of revolutions than standard centrifugation and in many cases offers better resolution of lower molecular weight species. (Thermo, 2006, Hsu and Perry, 1981).

Density gradient ultra-centrifugation is currently commonly used as one of the later steps in the purification of viruses (Yarmush, 2003). Morenweiser (2005) suggests that sucrose gradient centrifugation is being used less in favour of “more sophisticated methods”. Whilst Wolff and Reichl (2011) suggests that, like standard size dependent filtration, centrifugation will continued to have relevance in that it can

give consistent results across multiple strains, so is less susceptible to problems with viruses like influenza which change frequently and because it can be used to separate the protein shell of the virus (capsid) from the viral vector.

Morenweiser (2005) identify a number of disadvantages of DG-UC including that it is labour intensive, time consuming, difficult to scale down or up and that it may not separate host cell DNA well from viruses. In addition the author states that if a virus is labile its ability to infect (transduction ability) may be reduced due to shear in the ultra-centrifuge, exacerbated by the long processing times required. It is hypothesised that this shear will be concentrated in the entry and exit zones, as with continuous centrifuges (see section 1.1.3.1), and may also be encountered during gradient re-orientation. Meriño (2013) states that some smaller ultracentrifuges use a single dual-flow port which exacerbates shear problems at the inlet and outlet. Hsu and Perry (1981) identify a number of complexities in using density gradient centrifugation including selection of the appropriate density range and gradient shape, balance between sample loading amount and gradient stability and resolution.

1.1.2.4. Application to vaccine processing

Acceptable purification techniques for a virus will depend upon its surface characteristics (such as charge or hydrophobicity), whether it has an envelope, its equivalent diameter and how easily it can be damaged (lability) (Morenweiser, 2005).

Many of the existing separation techniques do not require a very refined understanding of the vaccines molecular make-up. Methods typically used in virus purification include density gradient ultra-centrifugation, ultrafiltration, precipitation, two-phase extraction and size exclusion chromatography (Morenweiser, 2005), of which chromatography is today the most popular method for vaccine/ viral product purification at a large scale (Wolff and Reichl, 2011). However, there are a number of vaccine types for which chromatography is typically not used, including enveloped viruses (Morenweiser, 2005) and it is, in other cases, used in combination with ultracentrifugation (Rappuoli, 2006).

For viral downstream processing (DSP) overall recoveries of greater than 30% are generally considered acceptable. Residual host DNA levels should be below 10pg per dose (Wolff and Reichl, 2011). There are regulations which govern the purity,

biological activity and separation of infective and non-infective vectors and capsids which are acceptable (Morenweiser, 2005).

There are many legacy processes still in use today for the production of vaccines, the transition from which is hampered by the need for clinical trials following any modification to the process, and thus potentially the efficacy of the product. This difficulty is exacerbated by the fact that these vaccines, developed before many modern analytical techniques became available, have rarely been fully analysed in molecular terms (Yarmush, 2003).

Vaccine process design is becoming more systematic, prompted in part by the changing technological platforms, to more well defined systems, such as cell based production, and regulatory frameworks with the introduction of Quality by Design (QbD). As a result many of the old barriers to entry which once protected exclusivity for older vaccines no longer apply. The company will therefore have a shorter period of exclusivity, and the commercial pressure for a faster rate of process development have therefore increased (Mukhopadhyay, 2012).

1.1.3. Ultra-Scale Down

Ultra-scale down (USD) involves use and creation of laboratory scale devices, procedures and methodologies, which can be conducted on process material to imitate the effects of industrial scale processing. Scale-down is required to:

- Allow initial development of downstream purification steps, including selection, optimisation and identification of key process stream / product properties and potential problems associated with these, and thus reduce the risk of delays and failures at a later stage. This is of particular importance given tightening timeframes as the time of exclusivity of a vaccine product decreases (Wolff and Reichl, 2011, Titchener-Hooker et al., 2008)
- Mitigate the prohibitive costs of pilot scale studies, where large quantities of material are required and equipment is more expensive, takes longer to use and clean, and is in demand (Pampel et al., 2008). Evaluate the performance of the selected process in terms of impurity removal, product damage and robustness, i.e. the range of conditions (including variations in feed properties) over which the performance is acceptable (Rathore and Sofer, 2005);
- Troubleshoot existing processes, including evaluating the impact of a process change or assessing factors effecting process performance (Rathore and Sofer, 2005);
- As more scale-down models become available, and are shown to be accurate and robust, it will be possible to evaluate the degree of interactions between steps. Ideally scale-down models should be linked, providing enough material of sufficient fidelity to the industrial product from each stage to accurately assess the impact of a particular step in the downstream process on the performance of the next and allow optimisation of the whole process (Titchener-Hooker et al., 2008).
- Future, early use of scale down models should allow more fundamental initial development route decisions to be made in the realms of target product, culture platform, formulation etc. For example:

    - Purification process will depend on the upstream processing parameters, such as cell type or growth media, or use of alternative vaccine sources, e.g. serum versus cell culture (Yarmush, 2003);
    - Biologically similar molecules not only increase commercial pressure to begin producing and marketing a product which has been proved effective, it also points to another potential benefit in early process analysis in that the processability can be taken into account in choosing between similar molecules. (Titchener-Hooker et al., 2008)
- Meet biosafety concerns, mitigating the risks of introducing pathogens into process equipment and facilities and reducing the amount of pathogen to which the operators may potentially be exposed (Rathore and Sofer, 2005);

Development in this area is also motivated by the need to meet increasingly stringent regulatory requirements, which push for ever improving product quality and safety and the introduction of Quality by Design (QbD), which increases requirements to understand how process conditions impact upon product qualities (Wolff and Reichl, 2011).

To increase the usefulness of the technique and push for the production of directly useable output data, such as a window of operation and systematisation of the ultra-scale-down development a Design of Experiments (DoE) methodology has been proposed. This can allow for the identification of key process parameters. Scale-down models with high throughputs and automation along with good mathematical models will help to speed up optimisation (Wolff and Reichl, 2011). Thus, scale-down model validation needs to develop to the point where it conforms to current good manufacturing practice (cGMP) covering planning of studies and thorough documentation in the form of experimental protocols and reporting of results (Rathore and Sofer, 2005).

The literature (Titchener-Hooker et al. (2008), Pampel et al. (2008), Rathore and Sofer (2005)) attempts to offer some guidance on systematisation, identifying the following stages in a scale-down analysis:

- Identification of the engineering system variables and biological material properties which will affect the outcome and which will differ between laboratory scale and large scale. Engineering system parameters which vary

with time and space, such as concentration gradients establishing themselves, parameters which vary just with time and interfacial phenomena are highlighted as typically where the small scale and large scale systems differ. This highlights in particular the difference in residence time between small and large scale systems. Identifying the important, desirable, process properties that effect function or are significantly impacted by the engineering variables.

- Locate where these engineering variables will have their impact. Computational Fluid Dynamics (CFD) has played a key role in development of a number of scale-down systems. In particular the work done to date on centrifuge scale-down at UCL has relied on unverified and unverifiable CFD modelling. The rotational shear device used in these studies and in those described in this report has also only been characterised using CFD; this therefore potentially represents an important source of error in the development procedure for the shear mimic system. It may be that the USD system itself is more amenable to verification of flow patterns using Particle Image Velocimetry (see section 1.1.4) than the centrifuge whose shear pattern and level it is designed to mimic.
- Measure the impact of these variables on the biological materials. The process of experimentation can be used not only to assess the likely significance of factors, but also to identify new ones.
- Summarize the results in an accessible manner through choice of the right parameters and presentation.
- Consider interaction with subsequent and previous stages and the impact of ancillary equipment such as valves and pumps.
- Inform the pilot scale studies and consider costs and “process variability”.

Future challenges may also be presented by the switch, highlighted by Wolff and Reichl (2011), to single use systems and to continuous flow systems, potentially requiring development of modified ultra-scale down techniques. In addition a number of developments in the biopharmaceutical industry have increased the pressure on downstream process development including shifts in upstream production process technologies towards the use of mammalian cells, and increasing cell and product concentrations.

Scale down models are identified as having been used in the analysis of expanded bed adsorption, chromatography, homogenisation, membrane separation, extraction, filtration, centrifugation, pumping or a sequence of these (Titchener-Hooker et al., 2008). Sections 1.1.3.1 to 1.1.3.3 review the development of key ultra-scale down approaches used for centrifugation, filtration and ultra-centrifugation to date. Although a number of authors including Wolff and Reichl (2011) claim that both filtration and chromatography are likely to be used more and more broadly as material technologies advance, the separation technologies focused on in this review are those on which this work is intended to focus.

1.1.3.1. USD Continuous Centrifugation

Centrifugation is popular because it is relatively robust, easy to clean, and has a large throughput (Sharma et al., 2011). In addition centrifuges come in a number of designs including bucket, tubular and disc-stack which each have their particular uses (Rathore and Sofer, 2005). However, the centrifuge is challenging to scale down because of the number of different models and modes of operation. Centrifugation can introduce high shear. This depends on its design and type, various points of entry and exit, bowl impact (Pampel et al., 2008).

Rathore and Sofer (2005) suggest scale-down parameters for a centrifuge should include flowrate at inlet, centrifugal force, back pressure, process stream properties and temperature. The measured outputs suggested by these authors include product yield, centrate turbidity, shear damage, clarification and temperature increases. Pampel et al. (2008) further suggest that it may be desirable to consider the solid compaction, product damage, product loss, feed flow rate, solids content, solid extraction interval, and contamination. However, monitoring all these parameters may be limiting and Maybury et al. (2000) measured only the clarification, solid protein concentration and particle size distribution.

A good deal of work has been done on the derivation of an ultra-scale-down mimic of the centrifuge, particularly the disc-stack centrifuge. In summary, this work followed a number of incremental development steps, including:

- closing off a number of discs in the full scale disc stack centrifuge to reduce the process volume by a factor of 10 (Mannweiler and Hoare, 1992);

- Deriving a modified sigma (settling area) to account for the acceleration and deceleration of the laboratory centrifuge and demonstrating the importance of shear to the clarification quality at large scale. Sigma, mentioned above, refers to a parameter used to scale between different centrifuges and scales, and is described in more detail in section 1.1.3.1 below (J. Maybury, 1999);
- CFD analysis was conducted on a multi-chamber bowl centrifuge and a rotating disc used to recreate the energy dissipation rate (EDR) for a smaller volume of material (Boychyn et al., 2001): At a laboratory scale the material was first sheared in the rotating disc, at the appropriate speed, then separated using a laboratory centrifuge. A similar principle was used for a filtering centrifuge (Boulding et al., 2002) and a disc stack (Boychyn et al., 2004). The CFD predictions of EDR for the disk stack and USD device are shown side by side in Figure 1.1-3, below. This combined rotating disc shear device and laboratory centrifuge constituted the scale down mimic and was shown to give clarification comparable to the full scale centrifuges;

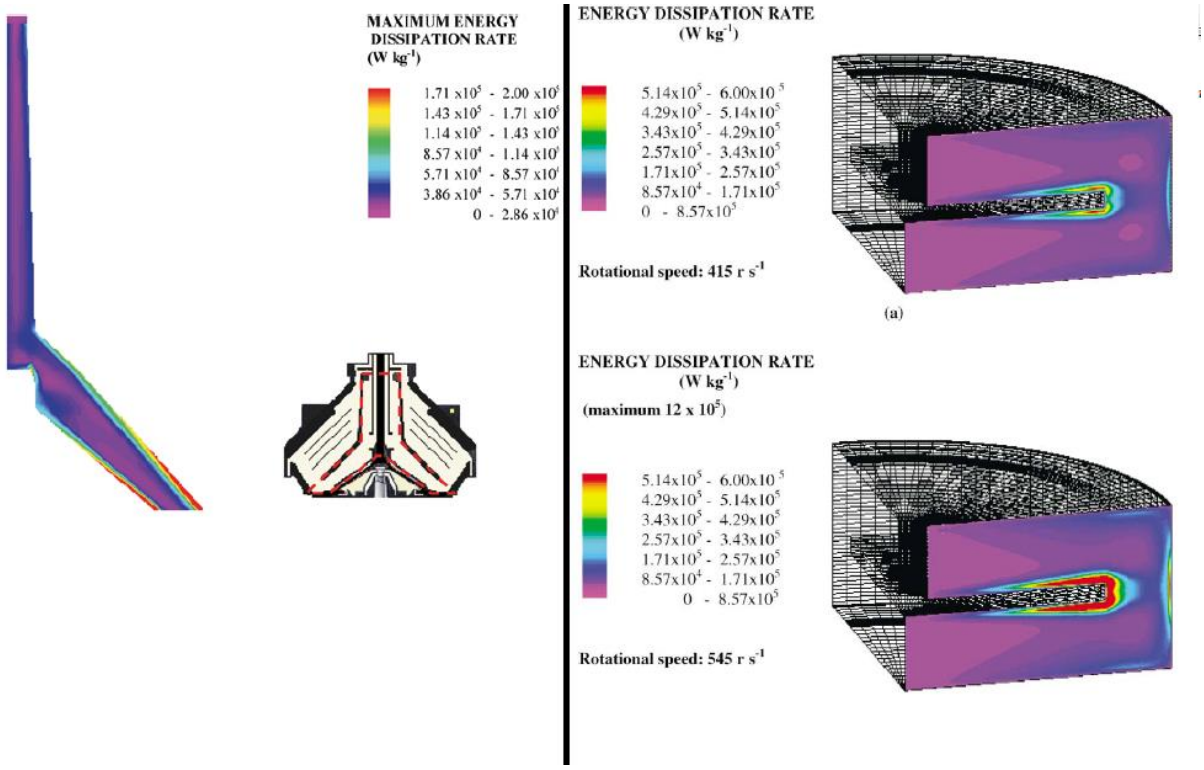

Figure 1.1-3 CFD output for modelling of a disc stack centrifuge and the rotating disk shear device (Boychyn et al., 2004)

- The methodology developed was then used for optimisation of a centrifugation process' rotational speed and centrifugation time for recovery of a virus (Lotfian et al., 2003b) and mammalian cells (Hutchinson et al., 2006);
- A modified version of the rotating shear device was developed to look at the effects of hydrodynamic forces on proteins in the absence of an air-liquid interface and with temperature control (Biddlecombe et al., 2007).
- The methodology was also used in concert with other ultra-scale down devices to demonstrate a procedure for recreating the overall process performance of a large scale process (Pampel et al., 2008).

The starting point of these studies was the poor correlation between industrial scale machines and laboratory centrifuges. This has historically been based on equating the settling time of different centrifuge models, known as sigma theory, which gives the following formula:

$$\frac{Q_1}{\Sigma_1} = \frac{Q_2}{\Sigma_2} \qquad \text{[Eq. 1]}$$

The sigma for any given centrifuge is derived based on the time needed for a particle of a given size to reach the sedimentation surface and the time taken for a package of fluid (containing the settling particles) to pass from the centrifuge inlet to the outlet.

Maybury et al. (2000) describe the derivation of a sigma value for the laboratory scale centrifuge which accounts for acceleration and deceleration periods:

$$\Sigma_{lab} = \frac{(2.\pi.Z_0)^2.(3-2.x-2.y).V}{ln\left(\frac{2.R_2}{R_2+R_1}\right).6.g} \qquad \text{[Eq. 2]}$$

For a disc stack machine the equation for sigma is

$$\Sigma_{ds} = \frac{2.\pi.N.(2.\pi.Z)^2.\left(R_0^3-R_i^3\right)f_l}{3.g.\tan\theta} \qquad \text{[Eq. 3]}$$

However, sigma theory and the equations derived involve a number of assumptions including plug flow through the centrifuge with uniform radial velocity, uniform distribution of particles at point of entry to the clarification sectors, no impedance or interference between particles and no entrainment. It also ignores complexities introduced by feed and discharge zones (Leung, 1998). Rathore and Sofer (2005)

discuss for example initial attempts to scale-down disc-stack centrifuges, which was achieved by decreasing the number of disks between which the fluid could flow and using sigma theory to equate the separation efficiency in laboratory centrifuges. Causes of inconsistencies between the full scale and scale-down suggested by Rathore and Sofer (2005) include disturbance of solids by turbulent flows, solids not being evenly distributed entering the disc-stack channel and between disc-stack channels, acceleration and deceleration times and the disturbance caused by solids discharge with as many as seven to eight bowl volumes needing to pass through the centrifuge before steady state has been restored. Maybury et al. (2000) used polyvinyle acetate particles, which are shear insensitive, to characterise some of these non-ideal factors in the centrifuge in to a single correction factor to multiply the sigma value. For the disc stack centrifuge used in this study the correction factor identified was 0.4.

The study by Maybury et al. (2000) also showed that for shear sensitive material a large inaccuracy was still seen when using a laboratory centrifuge to predict the performance of an industrial scale machine. Shear was identified as the likely cause of this discrepancy. The greatest EDR in the centrifuge is located in the feed distributor at the disc region. It was therefore assumed that accounting only for the shear that occurred in the centrifuge feed zone would be sufficiently representative. A shear device was therefore used to imitate the EDR contours and peak EDR in this region, matching that calculated by CFD. Sigma analysis was then used to predict the residence time (based on full scale flow rate) and centrifugal speed equivalent to the industrial scale machine for a laboratory centrifuge, as in the previous studies. A variety of studies on the impact of centrifuge shear on *E. coli*, mammalian cells and protein precipitates show that significant damage may occur at the impact on the solids collection chamber, in the feed zones or at the discharge depending on the strength of the material concerned, the details of the centrifuge design and the mode of operation (Titchener-Hooker et al., 2008).

In some cases the centrifuge performance prediction quality was shown to be better in ultra-scale down than in pilot because energy dissipation can be adjusted and because in a small pilot scale centrifuge, the control of volume removal is difficult and some sediment may therefore be pulled through in the supernatant effecting measurement of clarity (Pampel et al., 2008).

Hu et al. (2011) question the fact that these experiments were conducted at lower than industrial cell concentration and therefore may have missed some factors such as release of intracellular enzymes. This might for example impact upon the conclusion where this USD mimic showed production of more fine solids, causing problems for subsequent filtration and chromatography steps, but the product structure was not indicated to change.

Westoby et al. (2011) have produced the only other ultra-scale down approach to modelling of centrifuges identified during this literature review. They have done so in response to contended problems which they identify with the UCL shear device; in particular, its specific design and custom manufacture, the only controllable variable is speed, the difficulty of scale-up, and characterisation of the maximum EDR which must be calculated by CFD. They further criticise studies using the shear device citing lack of studies using mammalian cell cultures, and the fact that no correlation between EDR in the scale-down and industrial scale devices has been attempted.

The capillary device described by Westoby et al. (2011) uses a syringe pump and capillaries with reducers and expanders at the inlet and outlet to reduce shear and prevent jetting. As with the UCL shear device, they then used a laboratory centrifuge to separate the solid and liquid phases with the revolution rate and centrifugation time adjusted to make it equivalent to the pilot scale model and flowrate against which they compare.

The maximum EDR in the capillary device is expected to occur in a narrow volume at the pipewall boundary layer and for laminar flow can be calculated from the following equation (Westoby et al., 2011):

$$EDR_{max} = \frac{D^2.\Delta P^2}{16.L^2.\mu.\rho} \quad \text{[Eq. 4]}$$

The main benefit of this approach is clearly the simplicity of the relationship between EDR and pressure drop, a controllable factor. Westoby et al. (2011), however, do not state whether the volume to which this applies has been calculated or give the relationship. It might be expected that this boundary layer volume would also be a function of the flow rate. Boychyn et al. (2001) give an admittedly complicated formula for volume at maximum EDR in the rotatory shear device. It may be

assumed that from a CFD model the EDRs and volumes over which they apply could be derived.

Westoby et al. (2011) identified the appropriate maximum EDR (i.e. system pressure drop) to use in the capillary system by conducting a trial and error comparison of the particle size distribution achieved in the scale down device as compared to the pilot scale it was intended to mimic. The same pressure drop was subsequently applied to different cell stocks from which they showed that the correlation between the pilot and bench scale results remained good.

Westoby et al. (2011) subsequently ran for a range of pressure drops in their capillary device and a range of speeds in their centrifuge, derived a linear relationship between the USD capillary system maximum EDR and turbidity of the supernatant and between the pilot scale angular velocity and supernatant turbidity and equated the two to derive a relationship between the centrifuge angular velocity and the maximum EDR which should be used to mimic it. This study measured turbidity, particle size distribution and the fraction of viable cells. They identified the key size of interest as 3 μm, as it is difficult to remove by centrifugation but large enough to cause blockage in filters.

The key advantages Westoby et al. (2011) identify for their system are that it can be adapted for continuous operation and that calculation of the maximum EDR is simple. However, their comparison was against a pilot scale centrifuge, which Pampel et al. (2008) previously showed can correlate poorly with the industrial scale machine. In addition the maximum EDR values they used were 1.8×10^5 W/kg, where for the industrial scale disc stack 2×10^5 W/kg has previously been identified; they do not state whether their capillary system could function at these higher shear rates or has been tested.

Both Maybury et al. (2000) and Westoby et al. (2011) identified that at lower Q/Σ the error increased and matching clarification became more difficult.

1.1.3.2. Ultra-filtration

The mode of filter operation is a critical parameter identified by Rathore and Sofer (2005), however ultrafiltration is generally run in tangential flow mode. The measures identified for consideration were cross-flow rate for each feed channel, flux across

the membrane, the transmembrane pressure drop, pore size, the number of diafiltration volumes required and set up in terms of parallel or series flows. The values measured to assess the success of the filtration step include the yield of product, the volume concentration factor defined as the ratio of the initial feed volume to the final feed volume, the diafiltration volumes, permeate turbidity, cell lysis / damage, permeate filterability, aggregation generation, contaminant removal and extent of buffer exchange. (Rathore and Sofer, 2005)

If a filter scale-down system is to be re-used a cleaning procedure to return the membrane permeability to the same level consistently must be demonstrated.

Limitations on the scale-down of filtration include: the difference in the nature of the pumps used at the different volume flow rates and pressure generated, which is significant particularly for tangential flow where the fluid is re-circulated a number of times; flux needs to be normalised to transmembrane pressure to account for the different pressure on the feed side; this also gives different process times though larger surface areas can be used to compensate. The internal pressure drops and uniformity of flow distribution may also be different between the scales. (Rathore and Sofer, 2005)

CFD has been used with ultra-filtration to identify and quantify the presence of slug flow (under gas sparged conditions) and wall shear stresses and changing viscosity across the membrane with changing concentrations (Sharma et al., 2011).

1.1.3.3. Density gradient Ultra-Centrifugation

Alfa Wasserman produce a series of density gradient ultra-centrifuges, designed to be run in rate zonal mode. These include a benchtop centrifuge (Promatix 1000^{TM}), a pilot scale centrifuge (PKII) and an industrial scale centrifuge (KII). It is claimed that by scaling for processing time these different scales can be made equivalent to one another.

Although density gradient centrifugation is a standard laboratory technique a number of parameters are likely to vary between the industrial and laboratory scale which prevent linear scaling between the devices, in particular the geometries giving different settling path lengths and local flow effects (Merino et al., 2003). Merino et al. (2003) also highlights residence, rotational speed and gravitational force as

parameters to be maintained constant in scaling. The authors claim that their lower volume device allows linearity in terms of achieving the same gradient and concentration profiles.

Hsu and Perry (1981) indicate that there may be levels of shear rate sufficient to cause damage to biomaterials simply from the passage of the particles through the changing solvent environment. The authors, however, highlight the period of acceleration and deceleration, where gradient re-orientation is taking place, as the key periods of interest with respect to fluid mechanical considerations. Meriño (2013) highlights the dual inflow-outflow design of many density gradient centrifuges as a source of shear.

As described elsewhere it may also be that processing time is a significant factor with respect to the product response, potentially limiting the efficiency of any scale down model trials in terms of time, though set-up at a smaller scale and parallel trials should theoretically be easier and perhaps ideally should be designed into any system developed.

1.1.3.4. Computational Fluid Dynamics (CFD) in bioprocessing

CFD has been used in modelling for fermentation, centrifugation, chromatography, ultrafiltration, microfiltration and freeze drying as part of the parameterisation of the scale-down models. It is also useful to identify key design parameters, quantify power dissipation and shear rates, test design improvements, inform experiments and optimise operating conditions (Sharma et al., 2011).

CFD is based on applying mass, momentum and energy conservation equations, using numerical methods on discretized systems. However, complete resolution of these equations is computationally very difficult and a number of simplifications are therefore routinely made including isotropic turbulence (Doran, 2013). Another limitation of CFD is that the computational time is linked to the shape and size of the mesh, i.e. degree of discretization. It may be expected that the impact of turbulence on biological products may be seen at the scale of the smallest eddies, as Doran (2013) indicates that the volume over which a given amount of energy is dissipated (i.e. the distribution or intensity) has an impact on how damaging it will be, but discretisation to this extent would be unmanageable. This is the basis of interest in the maximum energy dissipation rate and linking this to shear damage . Parameters

to correlate to energy dissipation at the smaller scale and variable mesh sizes are therefore employed.

In building a CFD model one needs to consider system geometry, fluid properties (which may be changeable), meshing (discretization) and boundary conditions. Building of the CFD model is therefore complicated with many possible sources of error. As it stands today validation by experimentation is standard procedure for CFD models (Sharma et al., 2011).

The complexity of CFD modelling software and the computational power of standard computers is continuously evolving however. Comsol Multiphysics for example, the software previously used for a number of CFD simulations, incorporates a number of functionalities which allow different kind of physical phenomena to by modelled in parallel, where at one time iteration between separate models would have been required. Comsol Multiphysics also incorporates a variable parameter, allowing multiple simulations to assess the importance of a given parameter, for example the meshing size (Comsol Workshop).

1.1.4. Shear within the process environment

Hydrodynamic shear is a feature of the process which is frequently identified as requiring special consideration in terms of the difference between the large scale and small scale process, the impact upon the therapeutic efficacy of the biological product and the removal of impurities/ efficiency of product isolation and concentration (Titchener-Hooker et al., 2008). Indeed it has been demonstrated on a number of occasions that incorporating shear into ultra-scale-down mimics renders them more representative of larger scale processes. However, our current understanding of turbulence is incomplete, complicated by the unsteady and unpredictable nature of the phenomena (Doran, 2013). Hu et al. (2011) suggest that this lack of understanding of turbulent flow particularly at the cellular scale has contributed perhaps to the perception of shear as a key detrimental determinant.

In examining the impact of fluid shear on biopharmaceutical processes energy dissipation rate, shear stress and shear strain rate are quoted in the literature. It is therefore important to define explicitly what is meant by these various terms. Shear strain rate or shear rate is the rate at which the local fluid velocity changes with distance and has the units s^{-1}. Shear stress is a force applied to a fluid volume

divided by the area, perpendicular to a given axis, over which that force is applied and has the units $N.m^{-2}$ or $kg.m^{-1}.s^{-2}$. Strictly 'shear stress' refers to the tangential as oppose to normal stress on the fluid, but in this thesis is used to refer to all the various turbulent shear related stresses. In turbulent flow these phenomena are localised within vortices or eddies through which the energy introduced in to the fluid is dissipated and which manifest as spatio-temporal fluctuations. The energy dissipation rate (EDR) is the rate at which the kinetic energy dissipates and is defined mathematically later in this section. (De Nevers, 1991, Morshed et al., 2014)

Figure 1.1-4 illustrates the stages of the viral vaccine production process under investigation. Of these stages the most significant shear rates are expected in the feedzones of the disc stack centrifuge and, as shown in this thesis, the density gradient ultracentrifuge. Cell culture also involves substantial, though lower, shear levels over a substantially longer period of time. Finally the tangential flow ultrafiltration stage may be expected to generate not insignificant levels of shear, particularly in the pumps, as well as concentration of the virus especially in proximity to the membrane, where shearing will also be experienced.

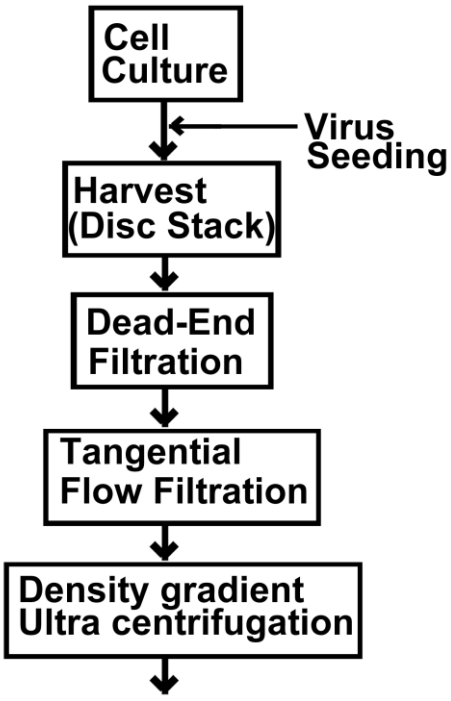

Figure 1.1-4. Schematic of the early steps in the influenza vaccine production process under investigation

Turbulence can only be represented statistically as it is too sensitive to conditions at the start and at the boundary to be 100% reproducible, with the complex spatial and

temporal variations in shear stresses (Hu et al., 2011). Flow on the x, y and z axes are therefore represented by mean and deviation from the mean (root mean square of deviations). In addition the small size of the smallest eddies, being 30 to 100 μm for a low viscosity fluid such as water, means that a very large number of discretization is required to accurately capture turbulent behaviour computationally.

In addition the complexity of the equations describing turbulent behaviour mean that significant simplifications are required for numerical solutions. These simplifications include (Doran, 2013):

- Kolmogorov's theory. This theory states that large eddies lose their energy by passing it to the smaller eddies which they form, and thence on to progressively smaller eddies until dissipation, based on the Richardson energy cascade. At a small enough scale this energy is finally dissipated as heat when the viscosity of the fluid slows its motion; thus increasing Reynolds number (i.e. increasing fluid velocity and decreasing viscosity) decreases the size of the smallest eddies. The size of the largest eddies is typically dictated by the container geometry, but is generally not considered important. The assumptions made within the equations derived by Kolmogorov's theory include high Reynolds number, a wide distribution of eddy sizes, at the smallest scale the only factor which effects the eddy properties are the rate of energy supply (breakdown of larger eddies) and the viscous dissipation.
- Homogeneous turbulence, where the extent of turbulence is independent of the location, both in terms of the average flow and the average turbulent deviations. This simplification can be applied with some accuracy over a small volume, of the order of a small turbulent eddy as described by Kolmogorov's theory.
- Isotropic turbulence is a useful simplification although not seen in many practical scenarios; however at small scales it may be assumed that the directionality imposed by the bulk fluid has been lost by the chaotic nature of progressively smaller eddy formations. Isotropy can also be expected to apply in the regions of highest turbulence.

Hu et al. (2011) suggest that as a rule of thumb if the Kolmogoroff's microscale is of a similar size to the size of the cells in suspension then cell death will occur at a

significant level. The formula for the Kolmogorov scale, which represents the average size of the dissipative eddies, is:

$$\lambda = \left(\frac{\nu^3}{EDR}\right)^{1/4} \quad \text{[Eq. 5]}$$

However, this simple approach relies on the calculation of the local EDR value for which Hu et al. (2011) give the formula:

$$EDR = \mu \sum_i \sum_j [\nabla U + (\nabla U^T)]_{ij} \nabla U_{ji} \quad \text{[Eq. 6]}$$

However, a simplification with the assumption of isotropy gives ((Doran, 2013)):

$$EDR = \frac{AV'^3}{L} \quad \text{[Eq. 7]}$$

In either case the EDR must be either estimated by modelling or measured experimentally. Typically CFD modelling of turbulence will require experimental confirmation given the complexity, number of assumptions, and need to confirm that adequate discretization in terms of both space and time have been applied. Previous studies, (Boychyn et al. (2001), Boychyn et al. (2004)) have to some extent circumvented this by demonstrating comparable impact upon the biological product of interest, the centrifuge being too complicated a system to measure shear rates in directly (Boychyn et al., 2001). To measure turbulence, methods must be quick, to catch an event before direction changes, with good resolution at a small scale, unaffected by a prolonged period of use in order to gain enough measurements over a long enough period to be statistically relevant. The two main methods identified are Laser Doppler Velocimetry (Laser Doppler anemometry) and Particle Image Velocimetry (Doran, 2013).

Laser Doppler Velocimetry relies on the fact that the shift in laser light frequency is proportional to the velocity of particles (constructed of e.g. polystyrene or similar plastic) which are suspended in the fluid. The advantages of the technique include that it requires no calibration and is non-invasive. However the process equipment must be constructed from a material transparent to laser and account taken for the effects of diffraction in the light path. It measures only one small volume (10^{-6} to $10^{-4}m^3$) at a time and only one directional velocity component (Doran, 2013).

Particle Image Velocimetry measures the instantaneous velocity across a large flow area by illuminating and imaging a plane of fluid, again with suspended neutrally buoyant particles, twice in quick succession. The two images are then processed computationally to give velocity vectors. The pros and cons are largely identical to those identified for Laser Doppler Velocimetry above, except that a measurement is taken for a large area in one hit, but less frequent measures are taken so rapid fluctuations may be missed (Doran, 2013).

Much of the research to date on shear has focused on shear rates in impeller driven mixing where turbulence is necessary to good mixing (Doran, 2013). Indeed this interest in shear in bioreactors continues as advances in the fields of cell engineering, culture media formulation and bioprocess engineering allow higher cell densities and larger bioreactors, making mass transfer more problematic and more aggressive mixing / aeration (for oxygen feed and CO_2 removal) is required (Hu et al., 2011).

The changing nature of the feed from upstream and desire to realise the increased product yield, that these advances have produced, through to downstream recovery and purification phases will require a review of hydrodynamic forces in downstream systems. Here hydrodynamic shear has already historically been seen as more of an issue, creating limits for feasible operations and dictating equipment and operational design changes. Further work is needed in downstream systems to quantify hydrodynamic conditions and for design optimisation in terms of minimizing stresses.

The ways of understanding and interpreting shear are also diverse. Shear stress can be divided into normal, perpendicular and elongation stresses with Hu et al. (2011) suggesting that the latter may possibly be the most damaging for cells and Doran (2013) states that cumulative energy dissipation may also be important, with limits of 10^5-$10^9 J/m^3$ for cells. The most significant source of shear stress also appears to be a matter for debate with Biddlecombe et al. (2007) identifying the formation and breakdown of air-liquid interfaces, such as bubbles or a reactor liquid surface, and the velocity gradients caused by non-slip at the interface between a solid surface and the nearby liquid. The centrifuge studies by Boychyn et al. (2001) incorporate the air-liquid and air-solid, liquid-solid interfaces with no slip assumptions

but do not suggest the dominant damage mechanism, calculating instead an energy dissipation rate. Biddlecombe et al. (2007) excluded the air-liquid interface from the system to quantify the impact on protein stability and shows improved stability. Doran (2013) states that the high velocity gradients at small eddies give rise to high shear rates.

The analysis by Hu et al. (2011) does not seem to indicate any correlation between the maximum EDR and average EDR or the fraction of the volume to which the maximum EDR applies. The works referenced use both studies which concentrates exclusively on maximum EDR and studies which use average EDR values. Doran (2013) suggests a link between these: by measuring the dissipation rate in the region of highest turbulence and subtracting this local energy dissipation from the energy input in to the system an average dissipation for the rest might be obtained.

The biological products employed in vaccines are extremely varied, resulting in particles of very different properties, including strength, size and density. Sections 1.1.4.1 to 1.1.4.3 therefore explore in more detail the impact of hydrodynamic forces on two broad categories of product of specific relevance: cells and proteins, viruses and virus-like particles respectively. The degree of variability between these products in terms of their mechanical strength and other factors pertaining to their separation are also quantified briefly. It is worth noting that due to the wide variabilities seen it will always be necessary to conduct tests on the biological material in question, including in most cases mimicking the large scale production techniques, in order to fully parameterize it.

1.1.4.1. Impact of shear rates on cells

Damage to cells in the downstream process can reduce product recovery, damage the product itself and impact negatively on the efficiency of subsequent purification steps (Hu et al., 2011).

It is worth quantifying at the outset the degree of variability within this category. Comparing plant, bacterial and mammalian cells for example, the first has a strong cellulose cell wall, the second a cell wall or secondary membrane and the last a single membrane. Typical diameters might be 1.1μm for *E. Coli*, 5μm for Yeast and 20 μm for a mammalian cell (Milo et al., 2010) whilst aggregates of plant cells may be between 50 and 2000μm (Kolewe et al., 2010). Densities will be approximately

1.095g/ml for a tobacco plant cell (Kumar et al., 2003), 1.1-1.4g/ml for a yeast cell (Bryan et al., 2010), 1.05g/ml for a CHO cell (Anderson et al., 1970), but will vary with the cell age, solution properties, infected status etc. Even the cell shapes are likely to be different.

Yim and Shamlou (2000) compare the size and strength ranges for bacterial, mammalian, yeast and plant cells, amongst others; their diagram is reproduced below in Figure 1.1-5. Their scale shows that plant cells are stronger than the other categories, followed by yeast cells, approximately 4 orders of magnitude weaker and then bacteria, which are a further 5 orders of magnitude weaker. Mammalian cells were the weakest of the species listed, being 2 to 4 orders of magnitude weaker than the bacterial cells. As mammalian cells are of increasing industrial relevance and are likely to be the most susceptible to shear as they are the structurally weakest species and because of their relatively large size, this project will concentrate on development of a mimic for mammalian cells in particular. The following section therefore concentrates on exploring their response to shear forces.

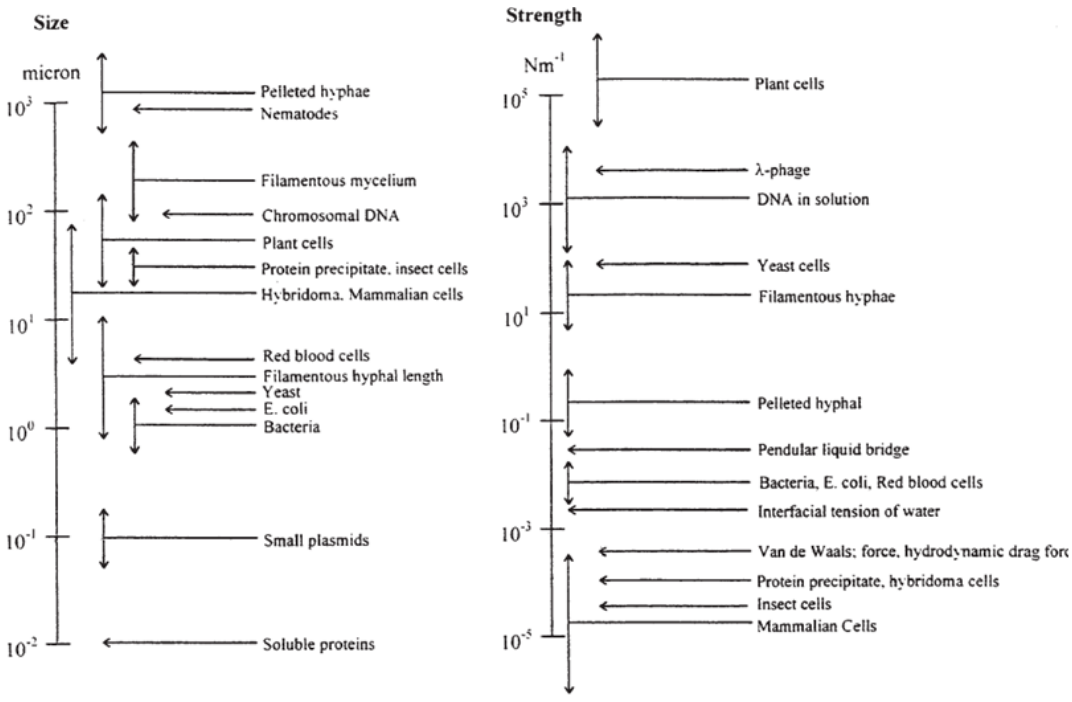

Figure 1.1-5. Diagram giving an indicating the relative size and strength of the different cell classes (Yim and Shamlou, 2000)

The paper by Hu et al. (2011) summarises the results of studies conducted to quantify the impact of hydrodynamic stresses in industrial processes on animal cells. The authors discuss the quantification of hydrodynamic stresses in terms of the EDR

which result in sub-lethal and lethal effects. The paper gives levels of shear rate from bubble rupture, membrane filtration, centrifugation (bowl and disc stack) and capillary scale-down for centrifugation as having similar shear levels (EDR) associated with them. These shear levels were also in the region of shear rates leading to cell death for the majority of studies referenced, where the exceptions used anchored cells. For the sub-lethal effects only a couple of studies are presented, both of which appear to be relevant to culture rather than DSP. As mentioned above Doran (2013) suggests that cumulative energy dissipation may need to be limited for cells to levels of the order 10^5-10^9J/m^3 to avoid damage. It is assumed that the breadth of this range reflects either uncertainties (e.g. different studies using different techniques to measure and quantify significant damage) or the impact on different cell types, although this is not stated in the text.

The impact of turbulent environments on cells is complicated, for example damage to cells may result from the physical stresses such as impact and fluid shear but may also be exacerbated by the release of intracellular enzymes (Mccoy et al., 2009). In addition there are big differences between the shear sensitivity of cells in suspension and cells on microcarriers and additives such as PF-68 can be used to protect cells from damage in bioreactors. The primary mechanism by which PF-68 reduces cell damage is not clear, but two possibilities are integration into cell walls and lowering of interfacial tensions lowering the energy release from bubble rupture or impacting cell to bubble attachment. The latter would be less significant in a centrifuge as oppose to a bioreactor (Hu et al., 2011). The ultra-scale down centrifuge model has shown no time dependence for shearing beyond 5 seconds with respect to solid formation (Hutchinson et al., 2006), although Mccoy et al. (2009) did show time dependence with respect to membrane quality indicators.

The shear sensitivity of the cells have also been shown to be dependent on cell type, cell line, the upstream culture conditions and the culture duration (Lu et al., 1992). A number of human cancer cell lines have been shown to be more sensitive to shear stresses in terms of cell lysis and changes to cell marker receptors. This may have implications for future cell lines entering mass production (Hu et al., 2011).

In order to measure the effects of shear rate, cell viability measurement can be taken, as well as, amount of debris (Hutchinson et al., 2006), amount of released

intracellular protein (Chan et al., 2006), structural changes to released proteins (Hutchinson et al., 2006) and structural changes in cell surface markers (Mccoy et al., 2009).

The impact of shear forces/rate on virus infected cells has not been widely discussed in the literature. Silva et al. (2010) do state that infected cells are more 'fragile'. That virus infected cells would be more easily damaged by stresses such as shear stress seems a logical assumption, and was one of the key hypotheses underlying this thesis work. Due to lack of literature on the topic it is also one of the key novelties / interests of this project.

1.1.4.2. Impact of shear rate on proteins

There are large variations in size, structural and chemical properties of proteins, limited only by their construction from a group of 22 standard amino acid building blocks. Protein density has been shown to be approximately a function of molecular weight with the density of large proteins being approximately 1.4g/ml (Fischer et al., 2004). Susceptibility to shear is a function of protein size and structure, particularly secondary and tertiary although on occasions even very small differences at the primary structure level have been shown to give rise to significant difference in shear response (Bekard et al., 2011). Biddlecombe et al. (2007) singled out monoclonal antibodies as being particularly vulnerable to the effects of shear forces.

They identify a number of possible effects of shear stress on proteins including affects to their secondary, tertiary and/or quaternary structures, altering their activity and causing them to aggregate. Boulding et al. (2002) also identify shear stresses as significant, giving 2×10^4W/kg as the value of the local energy dissipation rate which had been shown to effect antibody activity. Bekard et al. (2011) suggest that extensional forces may lead to aggregation and that the shearing period may in some cases be more important that the shear rate.

A number of authors, by contrast, indicate that the effects of shear stresses on proteins occur in conjunction with other more significant factors and that it is not the shear stress itself that causes damage to the protein structure. Thomas and Geer (2011) state that fluid mechanical shear may not have significant impact; instead it is phenomena linked to "high shear" such as interfacial phenomena, with aggregation linked to collisions or surface phenomena and/or nanoparticles from solid surfaces.

Flickinger and Drew (1999) suggest that shear forces at gas-liquid interfaces causes proteins to unfold, stating that they have demonstrated no aggregation or impact on bioactivity for shear rates greater than 10^5 s^{-1} without gas-liquid interfaces. The authors also link protein damage to adhesion to solid surfaces.

In order to measure the effects of shear Enzyme-Linked Immuno-Assays (ELISA) can be used to assess for conformational changes to significant structural elements using monoclonal antibodies. Many early tests on proteins were conducted on enzymes because their activity could be measured easily as a test for significant degradation or damage. For laxoperoxidase the activity was measured by reacting with a substrate, 2,2'-azino-bis(3-ethylbenzothiazoline-6-sulphonic acid) (ABTS) and measuring the rate of change of absorbance at 405nm (Pampel et al., 2008). Dilute solutions of unbranched homopolymers have been used as a simplified model system for proteins in shearing environments (Bekard et al., 2011).

1.1.4.3. Impact of shear rate on viruses and virus like particles

Like cells, viruses are extremely diverse in nature. They can be constructed of a single or double strands of either Deoxyribonucleic acid (DNA) or Ribonucleic acid (RNA) with a protein coat and with or without a lipid envelop. They range in size from 20-300nm (Lackie and Blackshaw, 2007) and may have a density of the order 1.1 to 1.4 g/ml. They exhibit variations in size, shape, composition, surface chemistry (Wolff and Reichl, 2011), beyond the Baltimore classification (Xu et al., 2011). The presence of the delicate envelope may make enveloped viruses more susceptible to shear stresses (Morenweiser, 2005) and as such the main distinction which will be made in this study, between different virus types, will be between enveloped and non-enveloped viruses. Virus like particles (VLP) are designed to mimic the virus protein capsid by combining many protein particles, typically produced by recombinant technology, into a regular structure, with diameters of between 20 and 120nm (Roldao et al., 2010). The focus of what literature there is on enveloped viruses and VLPs, suggests that these are more sensitive to shear stresses. Although viruses are evolved to maintain integrity, they also need to be capable of releasing the viral genome through disassembly (Castellanos et al., 2012).

The impact of shear stresses on viruses is a possible loss of infectivity (Wolff and Reichl, 2011). This can be measured by plaque assays or detection of early cellular

events associated with viral infection (Pheasey et al., 2006). Pheasey et al. (2006) criticise existing methods for quantifying the amount of infectious virus in a sample as not robust and time consuming. It may be for this reason, or because of the complicated and varied nature of viruses, that the number of articles found dealing with the impact of the shear stresses on viruses was limited.

Andreadis et al. (1999) found a reduced recovery of infective enveloped viruses, which they attribute to shear of the membrane. In non-enveloped viruses such as herpes, shear rates of $14.5 \times 10^{3} s^{-1}$ have been shown to damage Herpes virus in one study by Lotfian et al. (2003a), although the author attributes this to heat damage due to viscous heating. Morenweiser (2005) by contrast, identifies viruses as particularly susceptible to shear stress, citing their non-spherical nature and the fact that they are of such a scale as to be too large to avoid damage by the smallest eddies. Michalsky et al. (2008) found no impact on baculovirus following stirring and pumping experiments.

Sviben et al. (2016) used pipetting and vortexing on measles and mumps, two enveloped viruses, and showed an impact from vortexing, but not from pipetting. Although neither of these methods are well quantified in terms of shear rate, this result probably represents the difference between simple hydrodynamic shear and shear in the presence of an air-liquid interface.

The large size of VLPs is thought to contribute to their immunogenicity, therefore any reduction of stability or change to their complicated structure is likely to be significant (Srivastava, 2012). However, this attitude appears to be partly a result of the lack of fundamental understanding as yet of the interaction of these particles with the immune system.

Given the complexity of VLPs and their interaction with the immune system, and the fact that they are not themselves capable of infecting cells, it is not a trivial problem to measure their response to shear stresses, particularly without the requirement to measure the vaccine's continued efficacy using animal models which is costly and time consuming. Fortunately there are also a wide array of analytical techniques which can be applied, and from which inference can be drawn on the similarity of the vaccine conformation to that of the verified product. A number of these are enumerated here by way of illustration. ELISA may be used to measure potency,

identify components and give conformational information. Size exclusion HPLC will show the proportion of the different constituent proteins. Micro-calorimetry can be used to test the vaccine in terms of number of ‘active sites’ on addition of a given ligand and stability under heating which can show changes in secondary or tertiary structure. Circular dichroism spectroscopy can be used to assess the fraction of alpha helix, beta sheet and random coil structuring there is within the protein, again highlighting any conformational change in the secondary structure (Srivastava, 2012). It is perhaps for this reason that the literature on virus-like particle response to shear also appears to be relatively sparse. (Roldao et al. (2010) and Peixoto et al. (2007))

The complex nature of the viral product, combined with the current sparse nature of the literature, adds motivation and value to the results presented in this report.

1.1.4.4. Shear mimics

For avoidance of confusion:

- Ultra scale-down laboratory mimics refers to a device or collection of devices, and associated protocols, which use millilitre quantities of material and imitate the effect of process scale equipment on the process stream (described in detail in section 1.1.3);
- The cell/virus shear mimic is a novel concept, describing a particulate material, which either by design or as an observed feature can be said to be changed by shear stress in some manner analogous to that seen in (mammalian) cells/ viruses, such as might be used / produced in biopharmaceutical processing.

The aim of employing a non-biological cell/virus shear mimic is to decrease biosafety concerns and validate the comparability of shear rates between the USD and pilot/industrial scale using a more robustly and easily characterised material. The concept is discussed in more detail in sections 4.1, 4.2.1, 5.1 and 5.2.1.

Although artificial materials have been used as cell mimics for the purposes of studying minimum requirements for cellular life (Luisi and Stano, 2011), producing blood cell substitutes (Doshi et al., 2009) and plain liposome products as a mimic for cell membranes (Encapsula) there do not appear to be many instances where microparticles have been used to try to replicate the effects of shear stress on cells.

Lu et al. (1992) used nylon micro-capsules with dextran inside as a mimic system for cells in a bio-reactor in order to analyse where the greatest cell breakage might occur from physical impacts. However, the size range of their mimic system was not in the required size range identified for this project (see section 4.2.1).

It is worth noting, however, that a number of other important properties will differ between the artificial material and the biological, for example the homogeneity of artificial micro-capsules versus biological ones with respect to Young's Modulus was highlighted by Mercade-Prieto and Zhang (2012).

In addition to searching for particle suppliers a limited literature survey was conducted into methods of making micro and nano particles with the aim of identifying any particle materials or categories which may not have been identified

but might still be commercially available and to identify any particle technologies which might be simple and robust enough to use without being too onerous. The outcome of this literature survey indicated that much of the interest in nano/micro-particles to date has been due to their potential use in drug delivery. Factors which research has focused upon tuning therefore have included rate and nature of diffusion from the interior, particles size, solubility (material hydrophobicity), interaction between encapsulated and encapsulating materials, shape, functionalized surfaces (via adsorption, electrostatic interaction, covalent bonding etc.). However, particles in the size range of 10-100nm are likely to have been developed for this application as this is suitable for biological applications in terms of how the body deals with and processes the foreign material (Goldberg et al., 2007). This technology would not therefore be appropriate to the mimicking of all biological products of interest. In addition there was insufficient data to assess whether particulates produced using any of the protocols presented in the literature might be sensitive to shear stresses. For these reasons it was decided not to pursue any attempt to produce micro or nanoparticles in-house for testing as potential shear mimics.

1.1.5. Summary

1.1.5.1. Trends

There are a number of changes on-going in upstream processing which are likely to impact upon future developments in downstream processing. These include:

- Cell engineering, which may for example allow greater control of whether the product is produced in the intra or extra-cellular space (Nesbeth, 2012).
- Higher cell density and titre culture conditions (Wolff and Reichl, 2011).

There are a number of vaccine categories: from classic vaccines such as dead or attenuated bacteria and viruses, developed in the 1700s, to conjugate and recombinant vaccines, developed in earnest in the 1980s (Plotkin and Plotkin, 2011).

Regulatory and market forces are providing impetus for improved quality, systematic development, well characterised products and product process-interactions and reduced time scales respectively. Development of laboratory scale mimics, such as this project intends to explore, will contribute in this respect.

Ultra-scale down models have seen a great deal of interest over the past decade, and the focus appears to be shifting to developing the usability of the output for existing models, linking models to make predictions for overall process performance and process stage interactions and microwell plates to automate testing of a wide range of conditions.

Early production of vaccines was in animal based systems such as embryonic chicken eggs, followed by regulatory permission for use of primary cells, and in the 1960s diploid cells. Continuous cells lines use was only permitted in the 1970s, and in vaccine manufacture in the 1980s, due to fears surrounding the potentially tumorigenic nature of immortalised cell lines. Early cell lines in vaccine manufacture were Vero and MDCK cells. A number of avian cell lines are currently under development, a number of which are at advanced stages, with the Biologics Master File for EB66 being filed with the FDA in 2008. (Reiter et al., 2014)

For influenza vaccine production there is a move towards production in continuous cell lines to replace traditional egg based production. A number of cell line options

are being considered, and new industrial scale processes are being developed to accommodate the different requirements of these production platforms. These processes are required to overcome the limitations of the traditional production process and allow for large scale pandemic vaccine production alongside improving cost of goods for seasonal influenza. Influenza produced in eggs will have already been subject to the stresses and strains of a large scale purification process, although virus quality may vary depending upon the host.

For gene therapy vectors the move is from adherent cell line production at laboratory scale, towards production in bioreactors, and the attendant industrial scale downstream separation train. In contrast to influenza, for adenovirus there is limited experience to date of large scale production processes, though manufacturers such as Crucell (Johnson and Johnson) have heavily invested in adenovirus vector production using their proprietary PER.C6 cell line system.

1.1.5.2. Remaining Questions & Areas of Debate

There appears to be some debate about the future of density gradient centrifugation as an industrial separation method, with some authors (Wolff and Reichl, 2011) implying expanding possible uses (e.g. gene therapy) and others (Morenweiser, 2005) that it will be supplanted by other techniques.

There does not appear to be any literature on the scaling of density gradient ultracentrifugation (DG-UCF), and although there is a laboratory scale DG-UC available the documentation associated with it does not state whether biological function is included in the scaling parameters against which it has been designed. Development of a scale-down device for density gradient will be the focus of this project. The initial approach to this problem was based upon existing centrifuge scale down models, with the focus on quantifying and accounting for non-idealities in settling (likely to be high given the high impedance) and shear effects. There is potential to characterise further the existing Promatix 1000 system in order to take the work in this thesis further.

The impact of solid build up and discharge upon the performance of the centrifuge immediately afterwards and when averaged over the centrifugation cycle cannot currently be accounted for in the scale-down mimic (Pampel et al., 2008). This is not addressed in this project.

Due to its complex nature turbulence cannot be fully modelled nor is its impact upon biological particles understood (Hu et al., 2011). Most studies correlate using energy dissipation rates, either maximum or average, for which there are also a number of calculation approaches. This is further complicated by the degree of variability between biological products, their responsiveness to their environment, identifying and measuring their response(s) to shear stresses and the number of co-variants associated with low or high shear rate conditions. Development of a physical model for shear will require a fairly robust understanding of the factors influencing shear. It is therefore anticipated that this project will contribute towards answering this question by further parameterising the response of a number of sample biological materials (mammalian cell and virus) to shear stresses using a Design of Experiments approach to identify which process parameters show the strongest effect on shear susceptibility. In particular the effect of shear stress on viruses and virus infected cells, for both of which there is highly limited data in the literature, was explored. Further Computational Fluid Dynamics analysis, and application of a simplified population balance analysis method to both the rotating shear device and centrifuges will further add to existing approaches to understanding shear, and the similarities and differences between these two systems.

1.2. Project Introduction

The project was focused on the use and development of ultra scale-down (USD) models for purification steps in a vaccine manufacturing process. The specific vaccine of interest was an inactivated viral (flu) vaccine, but the aim was that the USD models should be as generic as possible. Both with this aim in mind, and to address cost and safety concerns, the first stage of the project was to develop and characterise synthetic shear tracer particles which can be used as a mimic for various biological products (cells and viruses). The focus on shear rates is based on previous work (Maybury et al., 2000, Boychyn et al., 2004) in scaling down continuous centrifugation which showed shear rate to be the key scaling parameter. The methodology already developed for disk stack centrifugation USD was applied to a previously uncharacterised large scale centrifuge model, using the shear mimic tracer particles. The focus then shifted to Density Gradient Ultra-Centrifugation (DG-UCF), which was modelled using Computational Fluid Dynamics to identify shear zones and rates and this information applied to initial work on the creation of a USD for industrial/pilot scale DG-UCF.

The sponsoring company's industrial process included the steps of centrifugal harvest, micro and ultrafiltration, and density gradient ultracentrifugation, at which stage formation of a semi-solid impurity was seen. It is this phenomena which motivated the sponsoring company's interest in the use of scale down as a parameterization and troubleshooting tool.

1.3. Objectives

The completed objectives of the EngD project were to:

- Develop a set of shear mimics, to be used in place of the biological process stream, to measure the equivalence between shear damage inflicted at industrial scale and in the USD rotating shear device. The set of shear mimics comprises a shear mimic for mammalian cells, and another shear mimic for viruses.

- Characterise a previously uncharacterised centrifuge in terms of shear levels and separation efficiency, based on:
    - The methodology previously employed as described in section 1.1.3.1
    - Use of the above mentioned cell shear mimic
    - CFD and population balance modelling over various centrifuge geometries, and operating conditions.
- Investigate the impact of shear stress in virus production processes at the harvest stage, with the aim of answering the hypothesis that virus infected cells will be more shear sensitive, and that consequently minimizing shear in centrifugal harvest is of paramount importance in these industrial units.
- Characterise an industrial density gradient ultra centrifuge (DG-UC) (PKII) in terms of shear levels and separation efficiency, based on:
    - Use of the above mentioned virus shear mimic
    - CFD and population balance modelling
- Investigate the impact of shear stress on viral products, with the aim of answering the hypothesis that viral particles are too small to be impacted by hydrodynamic shear in the absence of an air-liquid interface, and to explore the challenging question of how to measure the impact of shear, if any.
- Begin to explore the question of how the industrial DG-UC may be imitated at laboratory scale in order to provide tools for process development and troubleshooting.

Additional objectives which were not addressed, but which have been explored in the future works section (7) of this thesis included:

- Use of USD tools for predicting the performance of the filtration stages in a virus production process;
- Interaction studies between the centrifugation, filtration and density gradient ultracentrifugation stages.

2. Materials and Methods

2.1. Chapter by Chapter Overview:

This chapter is designed largely as a source of reference for subsequent results chapters. Sections 2.1 provides a high level overview of the sequence of work performed and can be read in isolation, whilst section 2.2 provides a more specific list of materials and individual assays or procedures performed.

2.1.1. Chapter 3: Validated CFD of Process Shear Environments

2.1.1.1. 2D-Axisymettric model

In order to characterise the fluid flow patterns inside the rotational shear device and PSC-5 disc stack centrifuge feed zone Comsol Multiphysics version 4.4 (Comsol Ltd, Cambridge, UK) commercial software was used, with the single phase turbulent flow model, solving RANS k-ε. This was used to derive parameters allowing a broader interpretation of the results presented in this thesis, and to compare shear rates and flow patterns within the rotational shear device and industrial centrifuge.

For the rotating disc shear device the meshing used the standard 'physics-induced sequence', with the following modifications: at the disc tip 'a custom mesh' of minimum size 1μm and maximum size 10μm was employed, along the disc a predefined mesh size of 'extremely fine' (5 to 2500 x10^{-7}m), and at the other walls a predefined mesh size of 'fine' (1.5 to 52.5 x10^{-5}m). A 'normal' mesh (3 to 67.5 x10^{-5}m) was used for the bulk. The rotating shear device was modelled as axisymmetric, using the sliding wall boundary condition for the disc, as illustrated in Figure 2.1-1.

The rotating disc shear device has previously been simulated in relation to a comparison to another model of continuous centrifuge (Boychyn et al., 2001). However, this simulation was repeated in order to validate the comparability of the turbulence modelling in Comsol to those previous Computational Fluid Dynamic (CFD) results.

For the PSC-5 centrifuge, the geometry was based upon manual measurements of the feed-zone. The results of these manual measurements are summarised in Table 2.1-1. Again the standard 'physics-induced sequence' was used for meshing with the following modifications: 'fine' setting for the mesh (6.2 to 218 $x10^{-5}$m), with 'finer' setting at the boundaries (2.5 to 174 $x10^{-5}$m) and 'a custom mesh' at the upper edge of the boundary near the outlet of the feed zone (1 to 20μm). As a first pass the centrifuge was modelled as axisymmetric, using the sliding wall boundary condition to represent the rotation of the equipment, as illustrated in Figure 2.1-2.

It may be noted that Boychyn et al. (2001) also appear to have used an axisymmetric modelling approach for both the centrifuge and rotating shear devices. Physically this is a far closer match to the rotating shear device than to the continuous centrifuge, whose inlet is split into a number of self-contained branches in the feed distributor, with the fluid flowing through, and being moved as a bulk, by forces transmitted by walls moving into the space occupied by the fluid, i.e. normal to the fluid volume, in addition to the movement transmitted through the moving surfaces of the upper and lower walls, i.e. parallel to the fluid volume. For this reason it was considered likely to be a more accurate representation to use the rotating machinery function available in Comsol, as described in section 2.1.1.3.

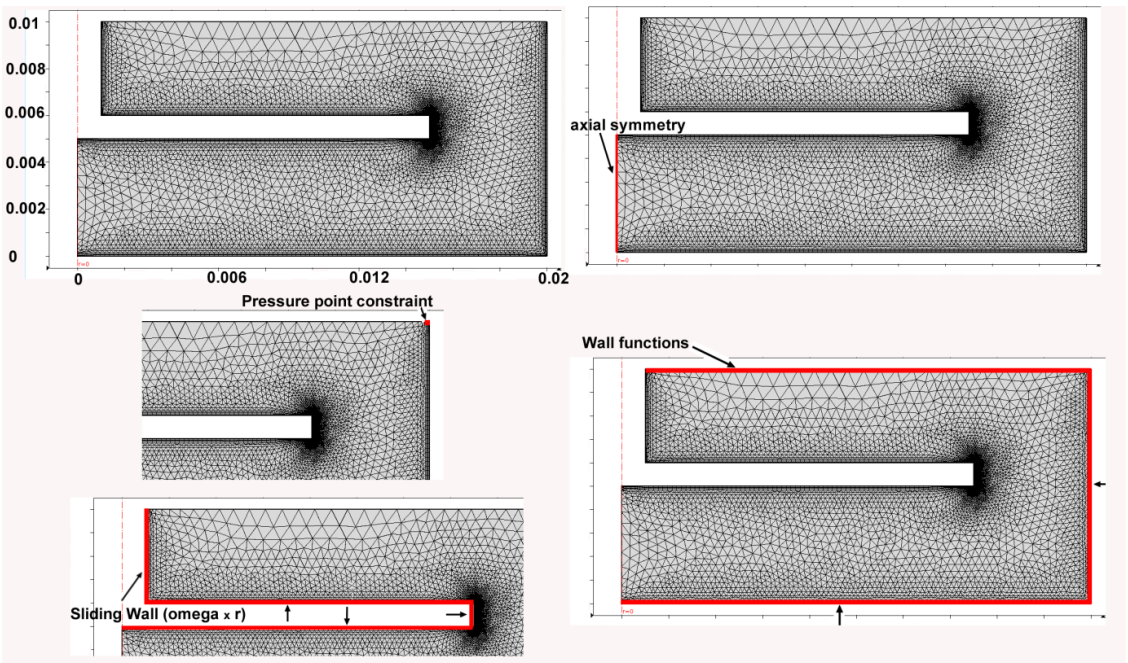

Figure 2.1-1. Schematics of rotating disc shear device 2D axisymmetric CFD model, illustrating the key constraints and boundary conditions imposed (where omega is the angular velocity and r is the radial distance)

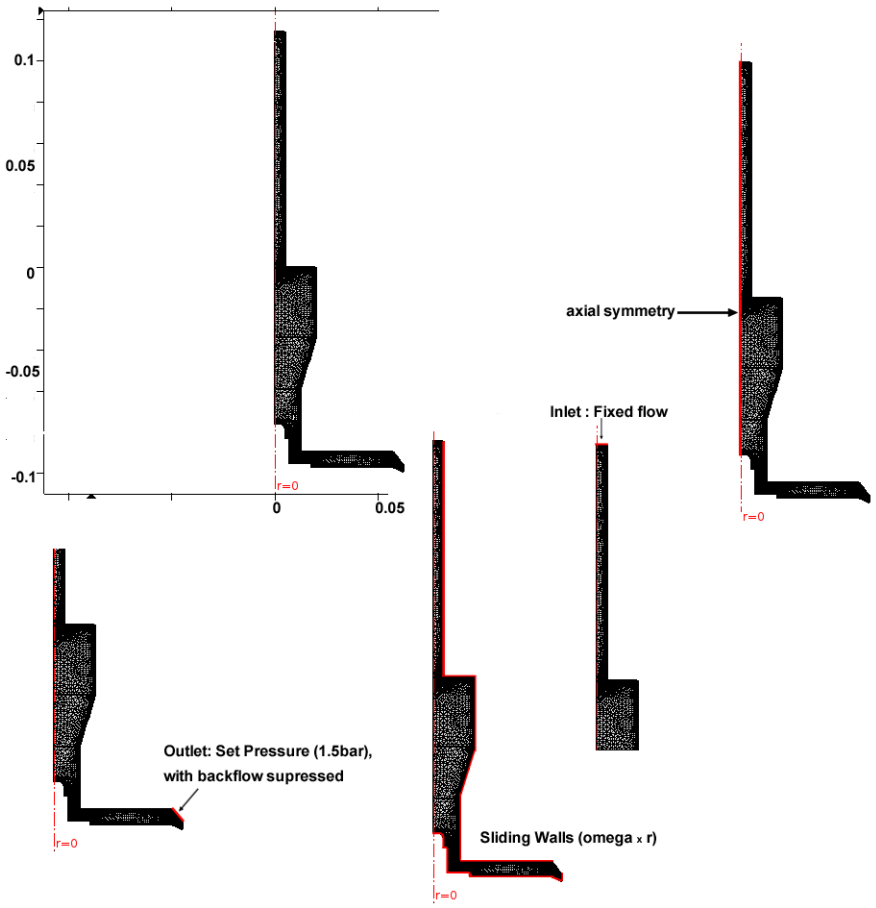

Figure 2.1-2. Schematics of PSC-5 continuous centrifuge feed zone 2-D axisymmetric CFD model, illustrating the key constraints and boundary conditions imposed

2.1.1.2. CFD Analysis 1: Peak shear rate and shear characterisation

In the first pass analysis, as in the previous work by Boychyn et al. (2001), the peak shear rate was used, both for comparison to the aforementioned previous rotating shear device model and between the rotating shear device and centrifuge. It may be noted that peak shear could be expected to be particularly dependent on meshing, and therefore a mesh refinement trial was conducted with the peak shear rate taken as measure of the minimum mesh size required for convergence. How well the peak shear rates in these two very different systems reflects the likely impact on particles processed by those systems is clearly open to question. A further, novel refinement of the modelling approach, which attempts to take account of the broader shear environment is therefore discussed in section 2.1.1.4 below.

In addition calculations of the Eigen values of the stress tensor and the angle between the direction of flow and the maximum shear rates were calculated. These reflect the nature of the shear, i.e. whether it is for example simple or extensional shear. The use of Eigen values and angle to characterise flow has not previously

been applied to this particular problem. The formulae derived from Harshe et al. (2011) were:

$$M = \begin{matrix} e_{11} & e_{12} & e_{13} \\ e_{21} & e_{22} & e_{23} \\ e_{31} & e_{32} & e_{33} \end{matrix} \qquad \text{[Eq. 8]}$$

Where

$e_{11} = u_x,\ e_{22} = v_y,\ e_{33} = w_z,\ e_{12} = e_{21} = 0.5(u_y + v_x), e_{13} = e_{31} = 0.5(u_z + w_x),\ e_{23} = e_{32} = 0.5(v_z + w_y)$

The eigenvalues for this matrix (M) were derived using matlab, where the maximum eigenvalue is denoted as alpha (α), the minimum denoted as gamma (γ) and the remaining eigenvalue denoted as beta (β). The angle between the eigenvector in the direction of the maximum eigenvalue and the vector field for the flow was then calculated. Where an angle of 45° indicates simple shear, and an angle of 0° represents extensional shear.

For the rotating disc the particles were assumed to follow a path which went (i) from the centre, just under the disc, and followed a path parallel to the disc surface until the outer wall was reached, then (ii) returned to the centre along a path midway between the disc and base of the chamber, (iii) returned to the surface of the disc, and (iv) passed along the disc again. The number of passes was derived using the formulae in Zhang et al. (2007) (copied below). It may be noted that a simplified particle tracing model in Comsol showed a movement consistent with the “pumping effect” described in the referenced paper.

$$Q = \int_{-z}^{z} v_r dA \qquad \text{[Eq. 9]}$$

$$N = \frac{tQ}{V} \qquad \text{[Eq. 10]}$$

This analysis was completed in order to better understand the comparability of the shear environment in the two systems, and in recognition of the significance of the nature of the shear as well as its magnitude, which the literature implies.

Data derived from Computational Fluid Dynamics (CFD) output was analysed using a matlab code, where the CFD output for the

- PSC-5 was based on 500 slices in the xy-planes, with a shift of -0.165m to incorporate only the lower sections of the feed zone,
- rotating shear device was based on 5 slices in the y-z planes, and
- PKII ultracentrifuge was based on 1000 slices in the xy-planes, with a shift of 0.12m to incorporate only the upper sections of the model, i.e. feed zone.

2.1.1.3. 3D-Rotating Machinery model

Whilst the axisymmetric model described in section 2.1.1.1 potentially provides an adequate first pass estimate of the shear conditions inside a continuous centrifuge feedzone, and is directly comparable to methods previously used for this purpose, it was considered necessary to assay a model which better represents the continuous centrifuge.

Comsol Multiphysics version 5.2 (Comsol Ltd, Cambridge, UK) commercial software was used, with the rotating machinery, turbulent flow model, solving RANS k-ε. The model set up for the PSC-5 and PKII inlets are illustrated in Figure 2.1-3 and Figure 2.1-4 respectively. The standard 'physics-induced sequence' was used for meshing, with a setting of 'fine' (1.25 to 6.6 $x10^{-3}$m) with the following modifications: custom meshing at the boundary near the outlet of the feed zone (1 to 10 um) and for the boundary walls, with a minimum and maximum element size fixed at 40µm and 4mm respectively, and a parameter sweep used to confirm the impact of meshing tightness on CFD output.

For the PKII only a rotating machinery model was built (i.e. no 2-D axisymmetric model), with the geometry measured manually as for the PSC-5. The results of these manual measurements are summarised in Table 2.1-1. The standard 'physics-induced sequence' was used of meshing with minimum and maximum mesh sizes of 1.7 and 9.1 $x10^{-3}$m respectively; at the boundary walls, excepting in the inlet, a maximum mesh size of $3.9x10^{-3}$m and in the feed $5.2x10^{-3}$m.

		PSC-5	PSC-1	PKII
Inlet angle to horizontal	*Deg*	0	-30	0
Distributor Branch Diameter	*mm*	7.36	7.36	1.5
Number of Branches	-	8	8	6
Radius at distributor branch inlet	*mm*	6.97	6.97	10
Distributor Branch Diameter at outlet	*mm*	11.51	11.51	1.5
Radius at Distributor Branch outlet	*mm*	57.3	57.3	55

Table 2.1-1. Key feed zone geometry parameters for the PSC-5, PSC-1 and PKII centrifuges

Details of the PSC-5 and PKII models have been exported and copied into appendices A and B respectively.

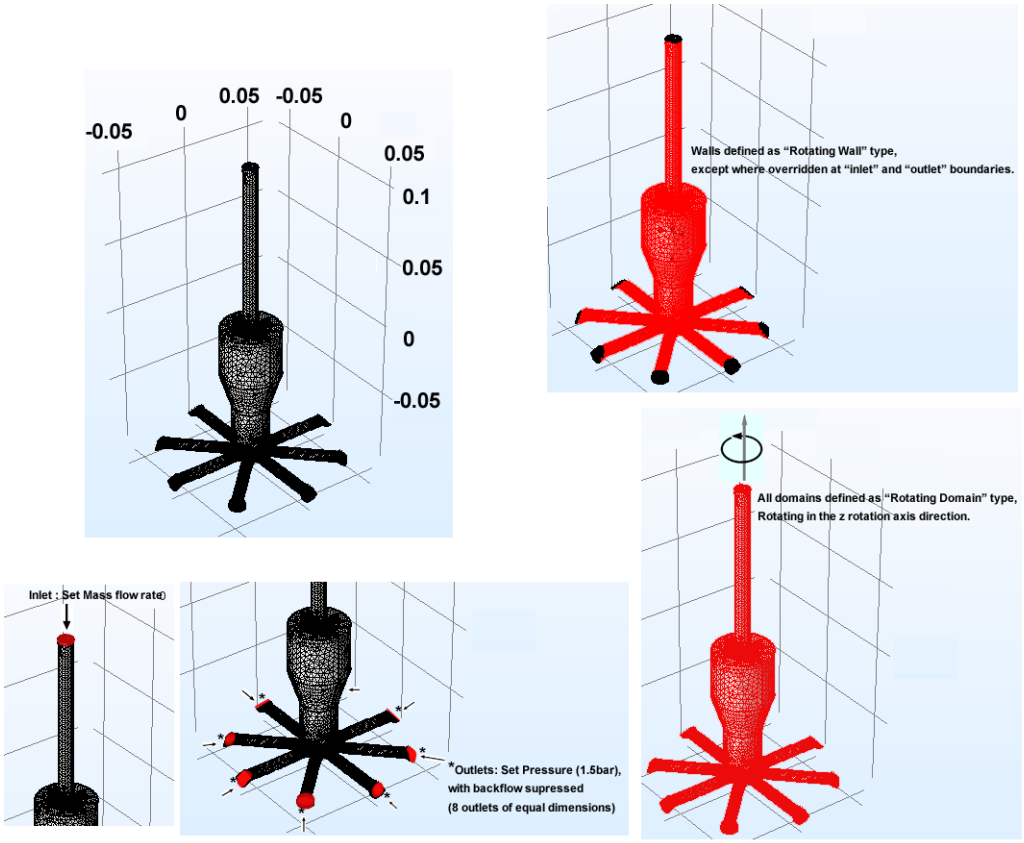

Figure 2.1-3. Schematics of rotating machinery CFD model of the PSC-5 continuous centrifuge feed zone, illustrating the key constraints and boundary conditions imposed

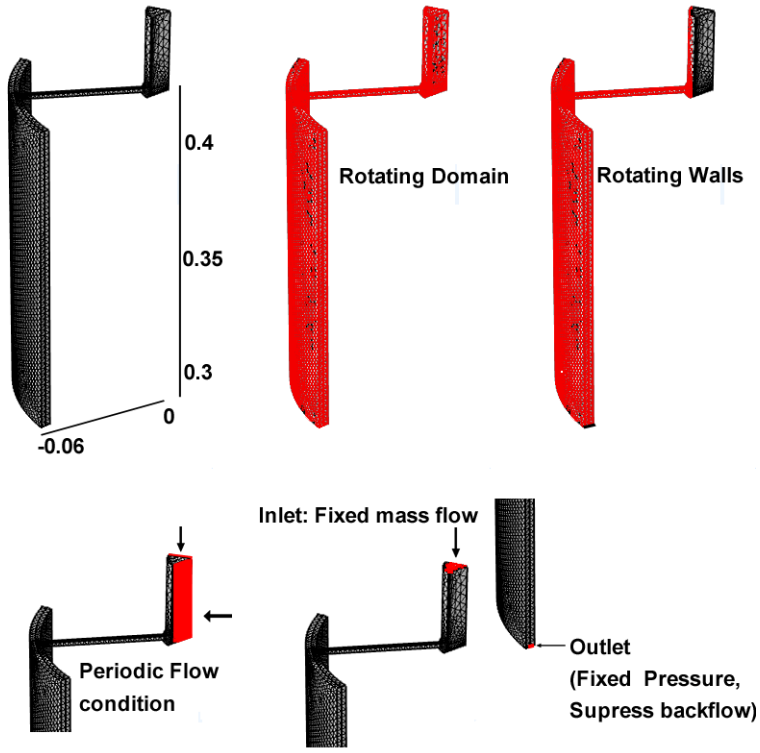

Figure 2.1-4. Schematics of rotating machinery CFD model of the PKII density gradient ultracentrifuge, illustrating the key constraints and boundary conditions imposed

2.1.1.4. CFD Analysis 2: Population Balance Modelling

Population balance modelling is a method used to track the number of discrete elements (gas bubbles, liquid drops or solid particles) in each size bracket within a continuous liquid or gas fluid. It usually incorporates *birth* and *death* processes within each size bracket range. In a continuous liquid- discrete solid particle system new particles, within a given size range, may be formed (*birth*) by aggregation due to interparticle collision through various mechanisms, and through breakage of larger particles through various mechanisms including hydrodynamic stresses and interparticle collision. Both of these phenomena result in the loss (*death*) of particles within a different size range. A wide range of functions exist to model each mechanism of *birth* and *death* which represent different sets of assumptions. In this work, however, a simplified 'population balance model' has been adopted, which incorporates only the breakage phenomena due to hydrodynamic shear, and focuses only on tracking the number of particles in a single size bracket, close to the size range of interest. (Yeoh et al., 2014)

Previous work has been based on the reasonable assumption that two systems, in which the maximum shear rates are comparable, are systems which exert similar

shear damage on particles within them. This assumption ignores, however, certain complications, such as the proportion of the volume for which the shear rate is high, whether the flow or forces are such that particles will be directed into these areas of high shear, and the length of time for which the particles will be exposed to different shear levels. In other words the physical realities of the environment are not fully accounted for simply in comparing maximum shear rates or energy dissipation rates.

Comsol offers an ideal solution to this problem: particle tracing, in to which a stochastic breakage model could be incorporated which responds to environmental factors such as local shear rate and characteristic, and wall/ interparticle collision forces. However, the computational cost and time required for such a model made it infeasible within the time frame of this EngD project.

A compromise solution was therefore devised using a simplified breakage model, as described above, and assumed particle flow paths, and applied to the Computation Fluid Dynamics (CFD) output data using a mixture of matlab, vba macros and excel calculations. With interpolating between the nearest data points available from the CFD output. The formula applied for the breakage kernel / rate, representing the frequency with which the particles are disrupted, (Yeoh et al., 2014) was:

$$b = C_4 \cdot EDR^{\beta} \cdot {k_{vis}}^{-\alpha} \cdot {D_P}^{\gamma} \qquad \text{[Eq. 11]}$$

Where C_4, β, α and γ are constant parameters for which the values in the range 10^{-4} to10^{-3}, 0.25 to 0.9, 0.5 to 2 and 0.25 to 3 respectively are suggested in the literature. Sensitivities were conducted on the effect of the constants, within the suggested ranges, and the particle size. In addition the effect of extensional flow was incorporated by increasing the Energy Dissipation Rate (EDR) linearly, up to 10 fold, for angles less than 10 degrees (see section 2.1.1.2).

In the inlet zone of the PSC-5 and PKII centrifuges the assumed flow path was an even distribution across the cross section of the inlet arms of the centrifuge, with the time to pass from the centre of the centrifuge to the outlet of the arms based on the volumetric flowrate. No account was taken of wall effects (slowing flow in proximity to the walls) or acceleration due to centrifugal forces. Equally no attempt was made to model the particle-particle interactions. Finally the particle size is treated as largely homogeneous, and it is implicitly assumed that the particles are completely or

largely destroyed by shear, therefore only the number of particles in the original size bracket need to be tracked.

For the rotating disc the particle path was based on use of the particle tracing physics option, using 1000 particles. This effectively ignores the effect of particle interaction on the flow path.

In all cases no attempt was made to incorporate particle breakage due to interparticle collision or wall collisions. Rough calculations based on estimated speed and mass of mammalian cells indicate that the forces involved in such collisions would be considerably smaller than those produced by fluid shears in these environments.

2.1.1.5. Validation of disc stack model

As discussed in section 1.1.3.4, for a number of reasons it is standard procedure to validate Computational Fluid Dynamics (CFD) models experimentally where-ever possible. The main reasons include the inaccuracies in geometries, which were measured manually in the absence of any detailed data being provided by the manufacturer, the uncertainties inherent in the turbulent models themselves, which are known to be inaccurate to the order of 50%, and the impact which meshing can have on the modelling output.

Whilst particle image velocimetry is the ideal methodology for validation of velocity field predictions for fluid systems this is impractical in the case of the centrifuge. Two separate approaches were therefore adopted as described below.

On the PSC-5 the clarification of two mammalian cell stocks were measured at a set speed and flowrate, matching the operating conditions used in the flu process. The measured clarification was compared to that produced by the Ultra Scale-Down (USD) mimic as described in section 1.1.3.1, for a range of rotating disc shear device speeds.

On the PSC-1 the particle breakage for a ‘cell shear mimic’ was measured and compared to that produced by the rotating disc shear device. The development of the shear mimic was proposed by GSK biologicals, the industrial sponsor on this project, on the basis of potentially safer, easier and cheaper CFD validation. The process of development is described in section 2.1.2. The use of the shear mimic

provides a somewhat orthogonal method of validation to that described above, in the sense that the shear mimic is a substantially different material from mammalian or bacterial cells which have previously been used in this application, particularly with respect to the apparent mode of breakage. Results which agree with the CFD and mammalian clarification outputs therefore add to the body of evidence that the shear in the rotating shear device and that in the centrifuge feed zone are comparable in scale and character. It will be noted that the model of centrifuge used for the shear mimic work and that used for the CFD and mammalian clarification runs was not identical. This is because the former were carried out at GSK and the latter at UCL. However, the PSC-5 and PSC-1 are understood to be designed to be produce scalable separation within the same product range. This is discussed further in section 2.1.1.7.

2.1.1.6. Validation of PKII model

As for the PSC-5 (section 2.1.1.5) experimental validation of the CFD model predictions for the PKII was necessary. For this purpose the particle breakage/damage for a 'virus shear mimic' was measured and compared to that produced by the rotating shear device. The development of the shear mimic was proposed by GSK biologicals, the industrial sponsor on this project, on the basis of potentially safer, easier and cheaper CFD validation. The process of development is described in section 2.1.3.

2.1.1.7. Geometry Sensitivities

Only rough rules of thumb exist for the expected level of shear in a previously uncharacterised centrifuge. From discussion which Professor M Hoare (UCL) the shear level is anticipated to depend on the outer radius of the feed zone distributor, the speed of rotation and above all the nature of the centrifuge, in terms of hermetically sealed versus not. However, it was noted during the development of the CFD model, and in preparing to use the USD model for continuous centrifugal harvest, that no quantitative answer could be given on the likely impact of specific geometric features. In addition it was noted in dismantling the PSC-5 and PSC-1 centrifuges, that their geometries showed a number of differences, the significance of which needed to be confirmed. Figure 2.1-5 illustrates the key difference between the distributor in the PSC-1 and PSC-5 centrifuges, namely that the inlet branches of the PSC-1 slope, whilst the inlet branches for the PSC-5 are horizontal. As a result

the inlet branch length for the PSC-1 is longer, and the acceleration of the wall in proximity to the fluid is lower. In addition the recommended flow rate range is substantially lower for the PSC-1 (15-30l/hr) than for the PSC-5 (100-200l/hr).

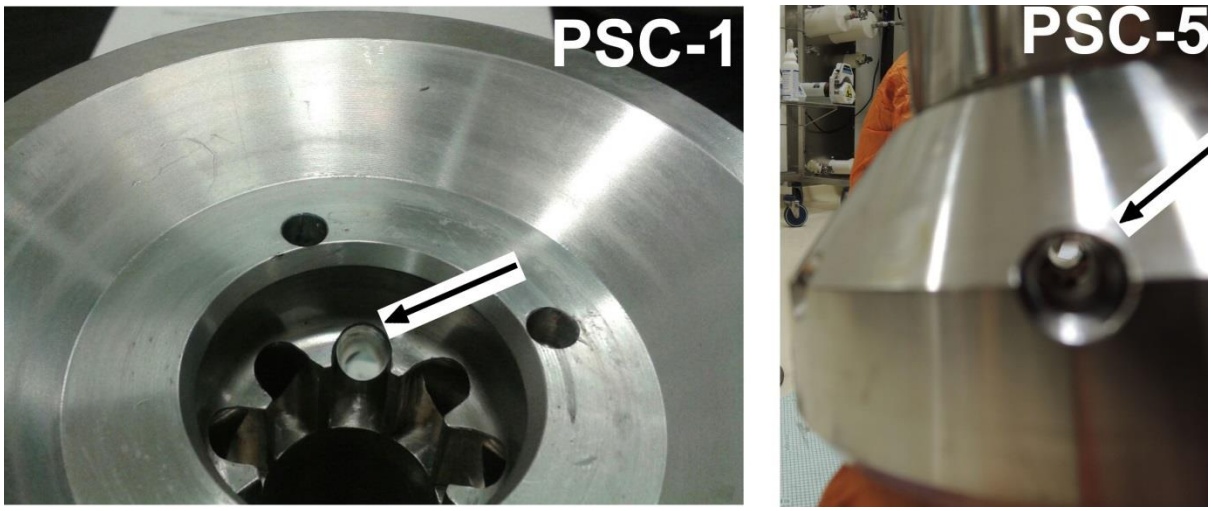

Figure 2.1-5. Photograph demonstrating a key difference between the PSC-5 and PSC-1 inlets, as indicated by the arrow. The PSC-1 inlet branches are pointed upwards at an angle from the base of the centrifuge, in order to exit in to the separation area at the base of the discs, which start higher up in the lower capacity PSC-1 centrifuge. The PSC-5 by contrast has horizontal inlet branches, such that the inlet on one side is in a direct line of sight with the opposite inlet.

The other key geometric features (Figure 2.1-6), including the number and diameter of the branches in the feed distributor, the diameter of the inlet areas which proceed the division of flow into branches, the outer radius of the centrifuge as it feeds in to the separation zone (tip of the distributor) and the operating speed range are identical in both the PSC-1 and PSC-5.

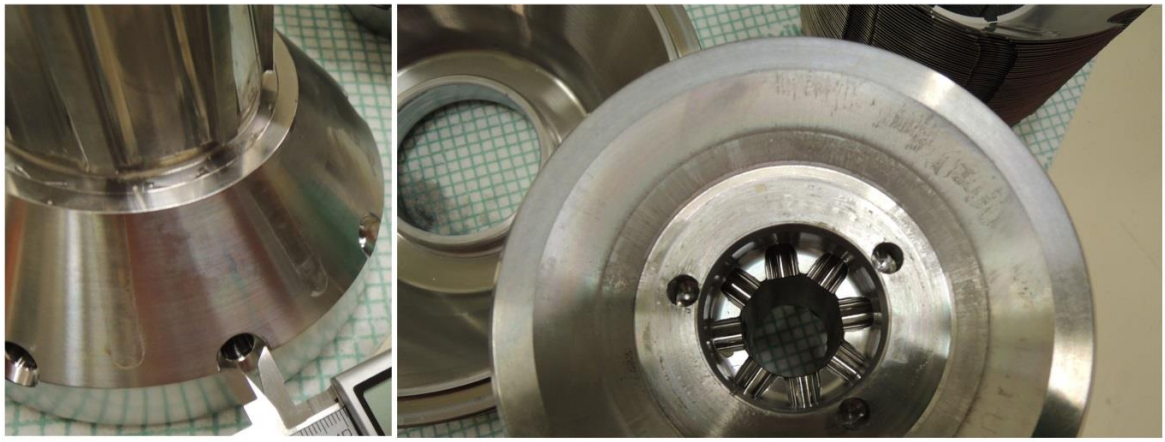

Figure 2.1-6. Photograph of the PSC-5 central section as seen from the side / slightly above (left) and from below (right).

In order to understand the significance of these differences, as well as the impact of any inaccuracies in the geometry measurements and provide an indication for future

similar work, some sensitivities were conducted around the PSC-5 geometry. The scope of this sensitivity analysis was limited due to time constraints, and was entirely simulation based, using the breakage function derived population balance (section 2.1.1.4) as the parameter of comparison between different geometric arrangements. The range of geometries used in this sensitivity analysis are illustrated in Figure 2.1-7, and the geometry parameters are listed in Table 2.1-2. The run parameters used are based on a factorial analysis based around the centre point of the PSC-5 geometry, and derived using Design-Expert® (Stat-Ease).

	Inner radius	Outer radius	Distributor Branch	angle
	mm			*Deg*
Run 1 wide	14.35	67.7	8.36	30
Run 1 narrow	14.35	67.7	6.36	30
Run 2 wide	14.35	67.7	8.36	-30
Run 2 narrow	14.35	67.7	6.36	-30
Run 3 wide	10.35	67.2	8.36	30
Run 3 narrow	10.35	67.2	6.36	30
Run 4 wide	10.35	67.2	8.36	-30
Run 4 narrow	10.35	67.2	6.36	-30
Run 5 wide	14.35	57.7	8.36	30
Run 5 narrow	14.35	57.7	6.36	30
Run 6 wide	14.35	57.7	8.36	-30
Run 6 narrow	14.35	57.7	6.36	-30
Run 7 wide	10.35	57.2	8.36	30
Run 7 narrow	10.35	57.2	6.36	30
Run 8 wide	10.35	57.2	8.36	-30
Run 8 narrow	10.35	57.2	6.36	-30

Table 2.1-2. Geometry parameters for the sensitivity analysis runs

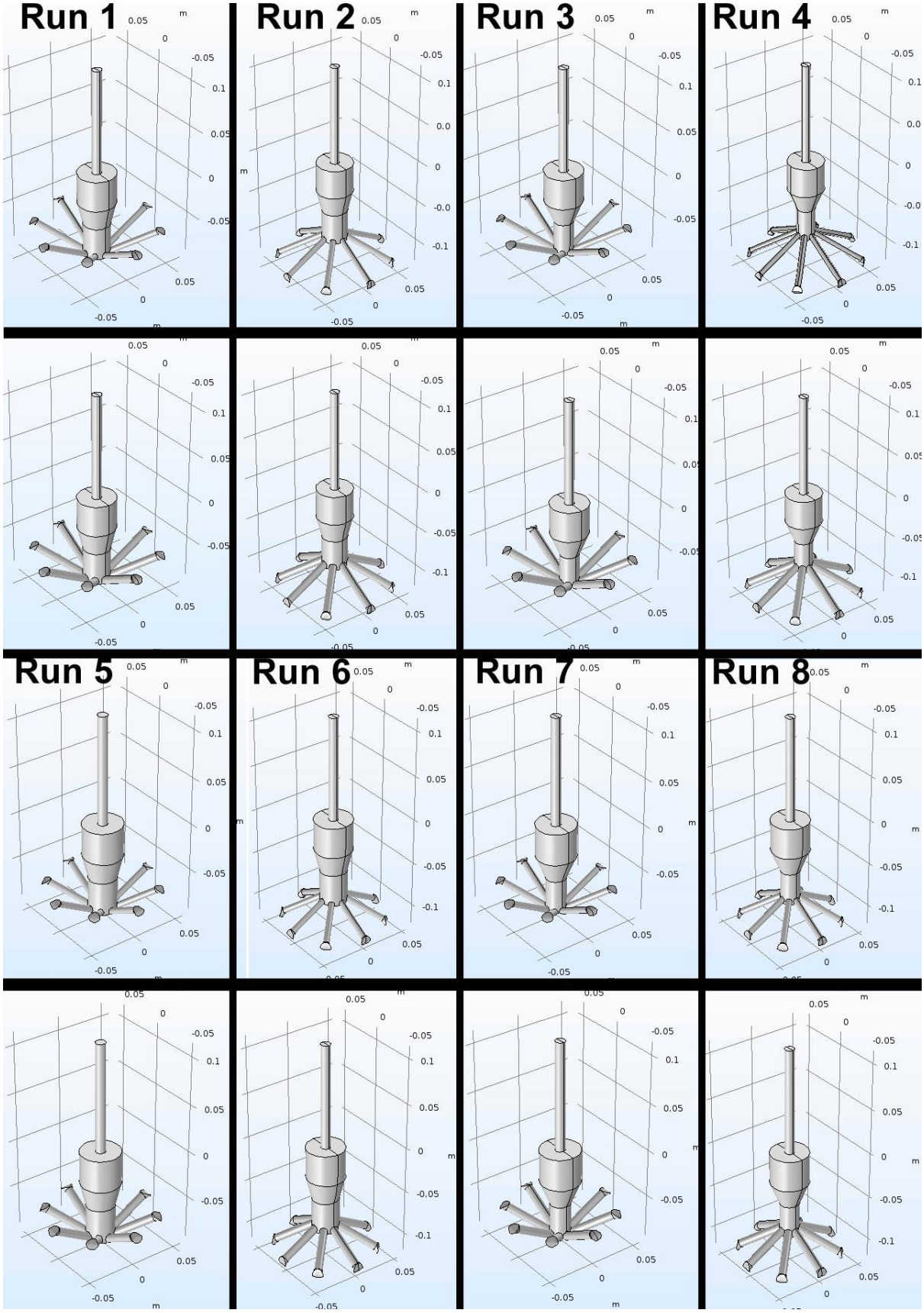

Figure 2.1-7. Schematics of centrifuge geometries for sensitivity analysis runs, where each run had a version with a narrower (upper) and wider (lower) diameter on the inlet branches

2.1.2. Chapter 4: Cell Shear Mimic Development

2.1.2.1. Stress testing Chromatography beads

The first class of particles identified as a potential cell shear mimic, on the basis that these materials are already routinely used in bioprocessing, were chromatographic beads. Initial tests showed agarose was unresponsive to shear forces in the rotating shear device (section 2.2.1.1).

Homogenisation was therefore used, as described in section 2.2.1.3, on 1 ml of Sepharose fast flow in 99ml phosphate buffer saline (PBS) and 100μl of 10μm highly cross-linked agarose beads suspended in 100ml PBS. In both cases the aim was to confirm that at a substantially higher level of shear the material could be broken, and would formed debris on breakage which the selected particle sizing methods could measure.

These homogenisation assays did show damage. Therefore a number of acid treatment methods were assayed for the various agarose species, including:

- 10ml of Sepharose fast flow was added to 40ml of PBS, and 20ml of 1 Molar H_2SO_4 subsequently added (final pH 0.7). This mixture was left for 30 minutes before being neutralised with 1 Molar $NaHCO_3$ (final pH 6.3).
- 10ml of Sepharose fast flow was added to 40ml of PBS, and 20ml of 1 Molar H_2SO_4 subsequently added (final pH 0.7). This mixture was left (not agitated) overnight before being neutralised with 1 Molar $NaHCO_3$ (final pH 6.46).
- 10ml of sepharose CL-4B was added to 40ml of PBS, and 16.7ml of 1 Molar HCl subsequently added (final pH 0.69). This mixture was left (not agitated) over the weekend before being neutralised with 1 Molar $NaHCO_3$ (final pH 6.46).
- For all agarose types except the 10μm superfine highly-crosslinked agarose (ABT) 5 millilitres of agarose was added to 20 ml of PBS, and 8 ml of 1 Molar HCl was subsequently added (final pH 0.73). These mixtures were left (not agitated) overnight before being neutralised with 1 Molar $NaHCO_3$ (final pH ~6.57).
- For sepharose fast flow two sets of 5 ml was measured, and added to 0ml and 12ml PBS respectively and ~3 ml of concentrated H_2SO_4 subsequently

added to each. These mixtures were left (not agitated) for 30 minutes before being neutralised with 1 Molar $NaHCO_3$ (final pH ~6.4).

- For sepharose fast flow, Iberagar, CL-4B, P6-XL agarose types 5 ml of agarose was measured, and ~5 ml of concentrated H_2SO_4 subsequently added. These mixtures were left (not agitated) overnight before being neutralised with 1 Molar $NaHCO_3$ (final pH 6.55-7.45).
- For CL-6B and 10μm highly cross-linked agarose types 10 ml and 10μl was measured respectively, and ~3 ml of concentrated H_2SO_4 subsequently added. These mixtures were left (not agitated) overnight before being neutralised with 1 Molar $NaHCO_3$ (final pH 7.3).
- For CL-6B and 10μm highly cross-linked agarose types 10 ml and 10μl was measured respectively, and ~4.5 and 2.5 ml respectively of concentrated HCl subsequently added. These mixtures were left (not agitated) overnight before being neutralised with 1 Molar $NaHCO_3$ (final pH 7.4/3).
- As concentrated H_2SO_4 was shown to reduce all agarose types to fine debris following overnight treatment the acid concentration was optimised to find a concentration which would not destroy the particles. For CL4B 10ml agarose was added to 1, 2.5 and 3 ml of PBS, then 3, 2.5 and 1 ml respectively of concentrated H_2SO_4 was added. These mixtures were left (not agitated) overnight before being neutralised with 1 Molar $NaHCO_3$ (final pH 6.32, 6.4 and 6.15 respectively). In the second iteration for CL4B 10ml agarose was added to 1.7 and 1.3 ml of PBS, then 2.3 and 2.7 ml respectively of concentrated H_2SO_4 was added. These mixtures were left (not agitated) overnight before being neutralised with 1 Molar $NaHCO_3$ (final pH 7.31and 7.26 respectively).

Both acid and base addition was done at an uncontrolled rate and the shear device used subsequently, as described in section 2.2.1.1, to assess whether the agarose particles susceptibility to shear stresses had been impacted. In all cases no shear sensitivity within the range of interest was identified and experimentation with chromatographic beads was discontinued. Details of acid and base preparations and material vendors can be found in Appendix G.

2.1.2.2. Adju-Phos validation and use as shear mimic

Subsequently similar experiments were conducted with adjuvants, and a promising candidate quickly identified in Adju-Phos.

Figure 2.1-8 summarises the experiments conducted using Adju-Phos as a cell shear mimic to validate the Computational Fluid Dynamics (CFD) results. In summary, both the cell shear mimic and a sample set of mammalian cells were subjected to shear using a rotating shear device (section 2.2.1.1) and the response to shear measured through the change in particle size distribution (section 2.2.7.6). Having demonstrated that the Adju-Phos responded to shear rates in the appropriate range and in a comparable manner to mammalian cells the shear mimic was run through the CSA-1, CARR and PSC-1 centrifuges (section 2.2.1.2). The CSA-1 and CARR centrifuges both being well parameterised were used to validate the use of the cell shear mimic for prediction of shear rate at large scale, and confirm what particle size distribution parameter should be used, as discussed further in section 4.2.4.

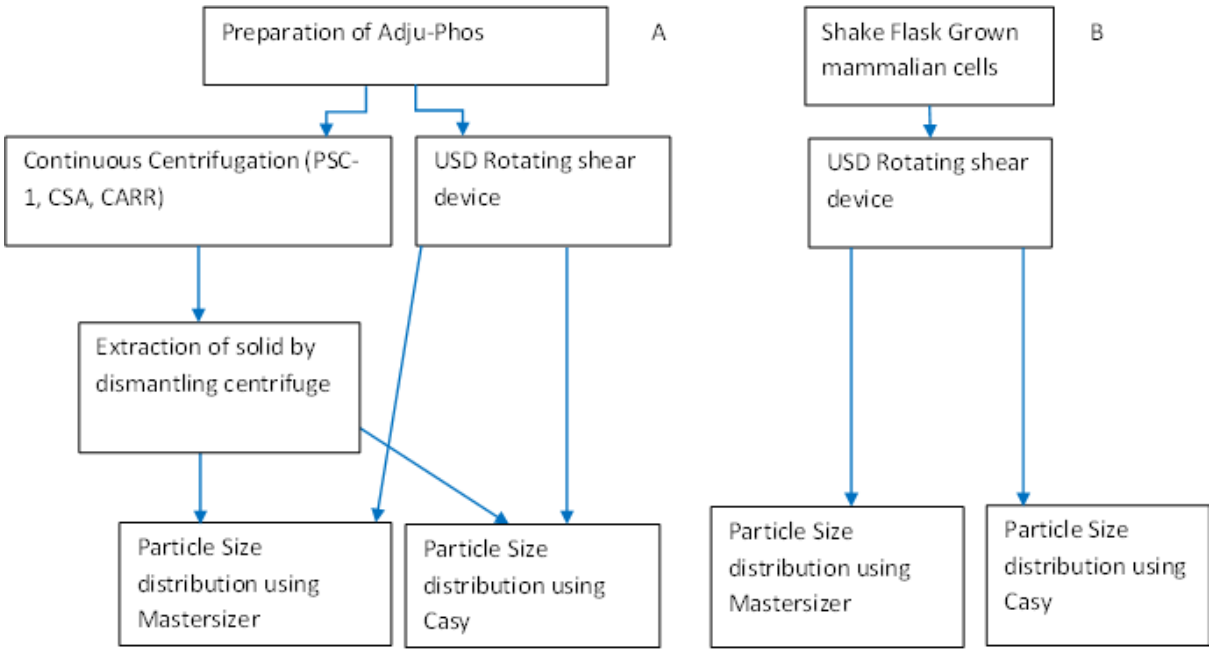

Figure 2.1-8. A. Schematic of parallel runs shearing Adju-Phos at laboratory scale and subjecting it to shear in the industrial scale centrifuge. B. The same laboratory scale procedure was also used with mammalian cells to demonstrate comparability of the response to shear

The CFD prediction of shear in the PSC-5 centrifuge was also validated using mammalian cells as illustrated in Figure 2.1-9. The cells were harvested as per the standard operating conditions in the PSC-5 centrifuge (section 2.2.1.2). The same cell culture material was subjected to shear in a rotating shear device (section

2.2.1.1), and subsequently clarified using a laboratory scale centrifuge (section 2.2.1.3) at a range of conditions covering conditions comparable to those at industrial scale (section 1.1.3.1).

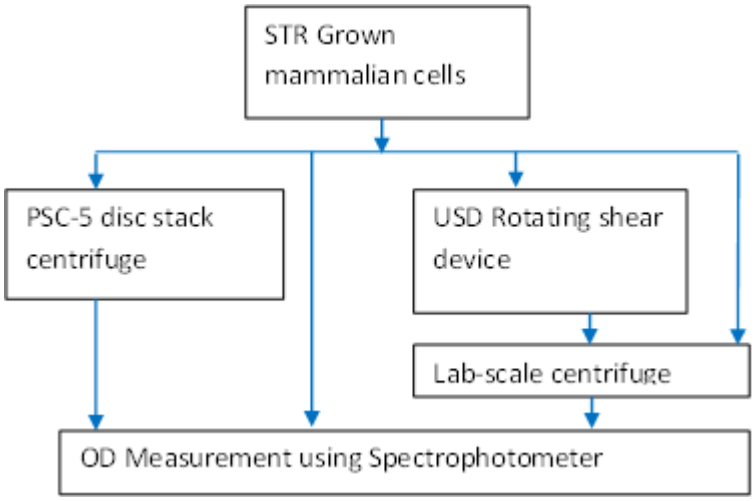

Figure 2.1-9. Schematic of parallel runs, shearing and clarifying mammalian cells at laboratory scale and harvesting using the PSC-5 centrifuge

2.1.3. Chapter 5: Virus Shear Mimic Development

2.1.3.1. Stress testing nanobeads & assay optimisation

Of the potential virus shear mimics only one was examined in detail. The virus shear mimic was a streptavidin coated nanobead (section 2.2.3.1), with the assays identified which might allow measurement of shear rate being particle size distribution and assaying for the streptavidin layer using a biotinylated fluorescein which quenches on binding to streptavidin.

The choice of streptavidin coated nanobeads was prompted by the potential parallel which might be drawn between the outer coating of streptavidin and the viral protein coat. Damage to proteins in the outer coating of a virus would be expected to seriously compromise the virus' ability to interact with cells during the various stages of the virus life cycle / infection processes: sections 1.1.1.1 and 1.1.1.2 list, for example, a number of identified viral proteins in influenza and adenovirus and their roles. Although this approach does rely on the assumption of streptavidin being equally sensitive to the effects of hydrodynamic forces as a viral protein, it was felt none-the-less to be an interesting potential parallel to explore.

For the fluorescence based assay the checkboard method was used in an attempt to optimise the concentration of both fluorescein and nanobead. The methodology

adopted was to compare the fluorescence of unsheared beads to that of beads damaged in one of three ways: by the shear device at speeds up to 12krpm, by acid treatment and by homogenisation. A z-factor (Kada et al., 1999) was used to asses for significance of difference between damaged and undamaged beads. This was based on the original hypothesis that damage to the streptavidin layer might impact upon its ability to quench the fluorescein-biotin when bound.

Acid (Appendix G) was also used to try to create a negative control for the streptavidin coated nanobeads (for the optimisation of the fluorescence assay, section 2.2.7.8):

- 12.5 ml of PBS with nanobeads, to which 5ml of 1 Molar H_2SO_4 was added (final pH 0.66). This mixture was left (not agitated) for 1 hour before being neutralised with 1 Molar $NaHCO_3$ (final pH 6.1). As fluorescence measures may have been effected by pH these results were discarded.
- 50μl of nanobeads was washed and added to 12.5ml of PBS, and 5ml of 1 Molar H_2SO_4 subsequently added (final pH 0.66). This mixture was left (not agitated) overnight before being neutralised with 1 Molar $NaHCO_3$ (final pH 6.35). As fluorescence measures may have been effected by pH these results were discarded.
- 50μl of nanobeads was washed and added to 12.5ml of PBS, and 5ml of 1 Molar HCl subsequently added (final pH 0.63). This mixture was left (not agitated) over weekend before being neutralised with 1 Molar $NaHCO_3$ (final pH 6.35). The acid treated nanobeads were then washed 3 times and concentrated x2 using the vivaspin centrifugal filters.

Both acid and base addition was done at an uncontrolled rate.

100μl of streptavidin nanobeads, were first washed using vivaspins and added to 100ml PBS, then subjected to homogenisation as described in section 2.2.1.3.

These initial assays did not show any significant difference between damaged and undamaged nanobeads, which agrees well with later work implying that there is no significant difference in terms of maximum fluorescence quenching by streptavidin on damaged versus undamaged beads. However, the checkboard titration was used to set an order of magnitude value for the fluorescein and nanobead concentration,

i.e. which gave a clear fluorescence quenching in the presence of beads, and strong fluorescence signal in their absence.

A titration of a fixed quantity of nanobeads against diluted fluorescein showed a difference between undamaged and damaged nanobeads, without being able to distinguish between different levels of shear rate (Melinek, 2013). A method deemed likely to be more accurate, modelled on 96 well plate based immunoassays, was therefore adopted: generating a 4 parameter logistic fit curve of apparent streptavidin concentration with constant fluorescein concentration. This latter is described in more detail in section 2.2.7.8.

2.1.3.2. Finalised methodology

Figure 2.1-10 illustrates the use of the virus shear mimic to validate predicted shear rate in the PKII centrifuge. In summary, the nanobeads appear to form aggregates which when sheared in the rotating shear device (section 2.2.1.1) break down to form a different particle size distribution (section 2.2.7.6), for which there is a relationship to shear rate. The additional step of fractionating the nanobead sample in a density gradient centrifuge (section 2.2.1.4) was completed for direct comparability to the PKII centrifuge (section 2.2.1.2). As the particle size distribution was not maintained, or not easily measured, when suspended in the sucrose gradient / after fractionation, the Nanosight was used to count particles and a fluorescence assay (section 2.2.7.8) used to normalise this count for the quantity of streptavidin attached to the beads.

It may be that this combination of shear device and laboratory scale density gradient ultracentrifugation may have potential as a scale down model for the PKII centrifuge. However, due to lack of time its application to the viral vaccine process stream remains to be assayed.

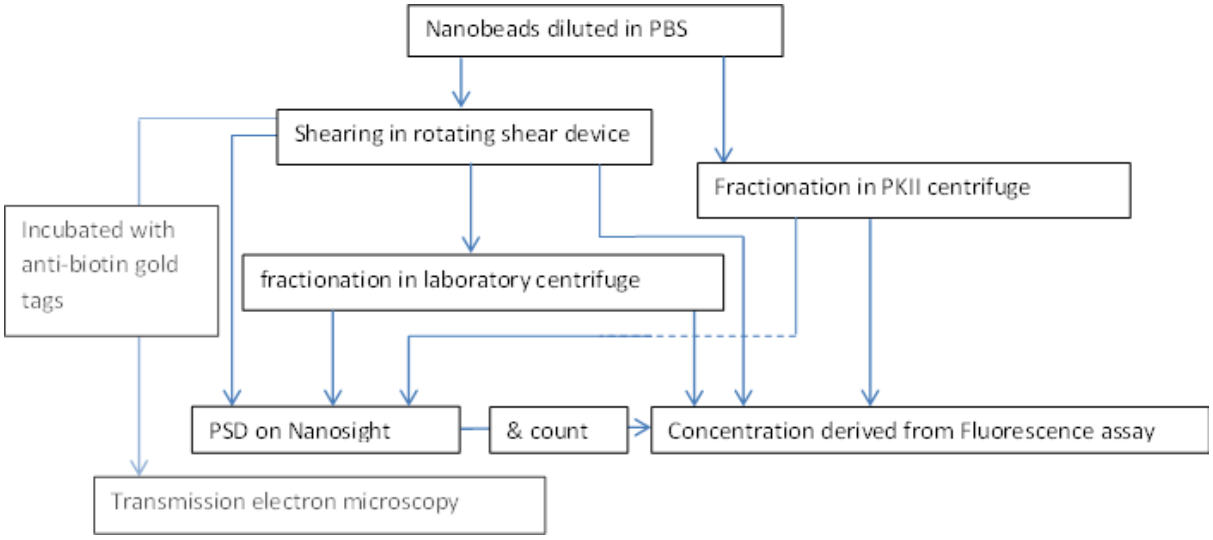

Figure 2.1-10. Schematic showing use of nanobeads as a virus shear mimic for fractionation in the PKII density gradient ultracentrifuge

2.1.3.3. Assays for impact of shear on virus particles

The harvest scale down experiments (section 2.1.4) on the virus infected material were also used to provide sheared viruses, which were assayed for the impact of that shear on the viruses. Figure 2.1-11 illustrates the sequence of assays applied, including infectivity assays (sections 2.2.7.3 and 2.2.7.4), and particle size distribution (section 2.2.7.6) and SDS-PAGE (sections 2.2.7.14 and 2.2.7.18) / western blots (sections 2.2.7.13 and 2.2.7.17) for fractionated viruses (section 2.2.1.4).

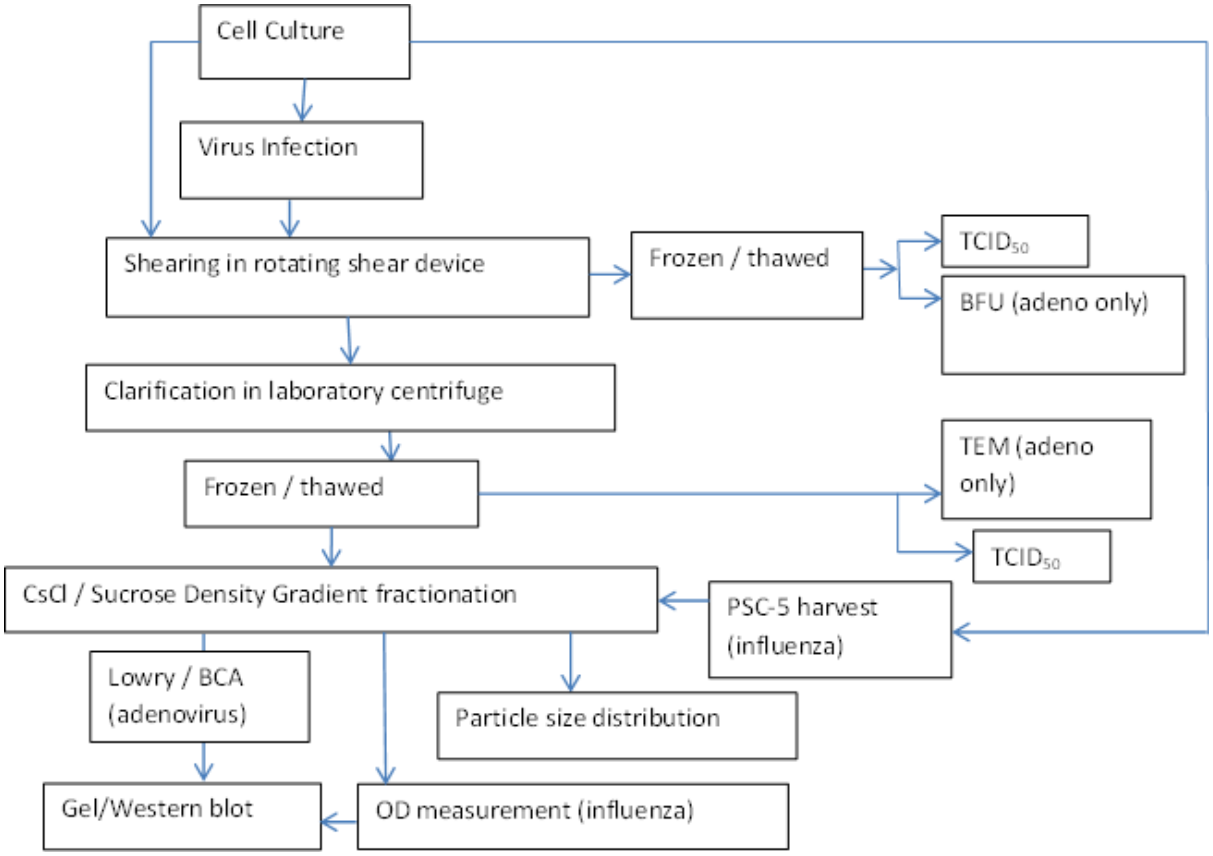

Figure 2.1-11. Schematic showing assays used to assess the impact of shear on adenovirus and influenza virus. Note the viruses was not purified before being subjected to shear, and are thus exposed to all the elements present at cell harvest in the whole cell lysate

2.1.4. Chapter 6: Ultra-Scale Down (USD) for Virus Harvest

Figure 2.1-12 illustrates the procedure used to validate the USD tools for continuous centrifugation, as developed previously be UCL and described in section 1.1.3.1, for the harvest of influenza viral vaccine culture. No literature has previously been published on the use of the USD tool for centrifugal harvest of any viral vaccine. The cells were harvested as per the standard operating conditions in the PSC-5 centrifuge (section 2.2.1.2). The same cell culture material was subjected to shear in a rotating shear device (section 2.2.1.1), and subsequently clarified using a laboratory scale centrifuge (section 2.2.1.3) at a range of conditions covering conditions comparable to those at industrial scale (section 1.1.3.1). The same ultra-scale down procedure was also followed for adenovirus infected HEK cells, to investigate the effect of time of infection on both influenza and adenovirus harvest, and for uninfected HEK and EB66 cells to investigate the effect of the infection process itself (sections 2.2.5 and 2.2.6).

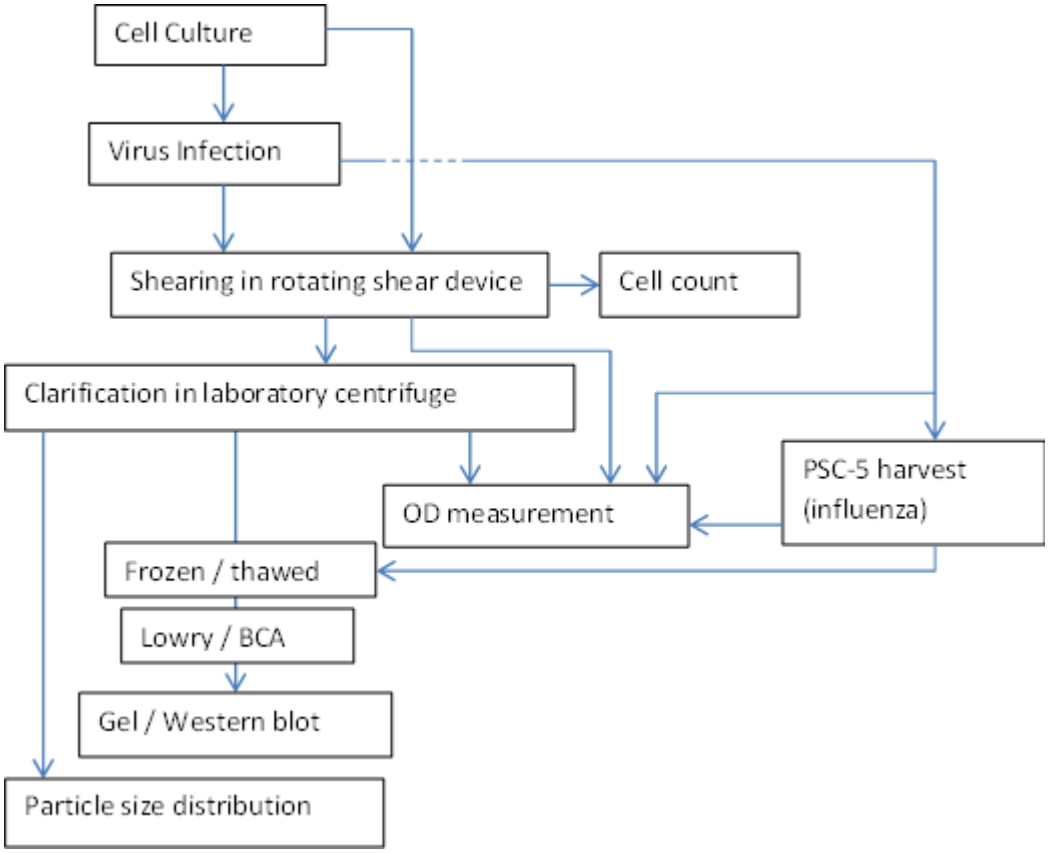

Figure 2.1-12. Schematic of parallel runs, shearing and clarifying influenza infected EB66 cells at laboratory scale and harvesting using the PSC-5 centrifuge, and runs shearing and clarifying adenovirus infected HEK293 cells (laboratory scale only)

2.2. Protocols & Materials

2.2.1. Process Equipment

2.2.1.1. Rotating Shear Device & Ultra Scale-Down (USD)

A rotating disk shear device, constructed at UCL, consisting of an aluminium alloy disk of 4cm diameter and 0.1cm thickness within a chamber of 5cm diameter and 1cm height was used to apply shear to the samples. The model of shear device used for all the results presented in detail in this thesis is shown in Figure 2.2-1 and the motor model was USD SD001 (asset ID 1236). Some initial screening work was completed with earlier versions of the shear device, although the only changes were in external design factors, such as the motor and power pack, which should not have had a substantial impact on the results. The rotating disk is described in detail elsewhere (Boychyn et al., 2001, Boychyn et al., 2004, Hutchinson et al., 2006, Levy et al., 1999, Zaman et al., 2009, Boychyn et al., 2000).

The disk was rotated via a shaft and motor at a number of fixed speeds for a number of fixed time periods. The shear device has a volume of 20ml. The procedure was repeated a minimum of twice for each shear rate to give 40ml of sample for analysis, and as a 'repeat'.

Figure 2.2-1. Equipment: Shear device and power pack

For uninfected CHO, HEK and EB66 cells and infected EB66 cells at GSK, and for uninfected CHO and HEK cells and infected HEK cells at UCL, and Adju-Phos, the rotating shear device was used to shear the material for a period of 20 seconds at fixed speeds of 0, 6, 8, 10 and 12krpm. These speeds are equivalent to a maximum energy dissipation rate of 0, 27, 90, 210 and 420kW/kg respectively. For both infected cell samples an additional shear condition was included, running the shear device at a speed of 18krpm for 1 minute. For experiments focused on clarification the samples were also spun down in a laboratory centrifuge (see section 2.2.1.3) after all samples had been sheared.

Further sensitivities were conducted at 0 and 12krpm for 5 seconds and 30 seconds with Adju-Phos at the same concentration and at lower and higher concentrations (see section 2.2.2.3). The shear rate selected for cells and cell mimics are those which have been shown elsewhere to have a measurable impact on mammalian cells (Hutchinson et al., 2006).

The rotating shear device was used to apply shear to the diluted nanobead samples, by running the motor at a rate of 0, 6, 12 and 18 krpm for 1 minute. Further a sensitivity analysis was conducted running the motor at a rate of 9 and 15 krpm for 0.5 minutes and for 1.5 minutes. Initial work used similar time frames and speeds as

for Adju-Phos, but it was deemed unlikely that such low shear rates, for such a short period would show any impact on nano-scale particles.

Water was used to measure the change in temperature after shearing, with 20 seconds at 12krpm giving an increase of less than 2°C, and shearing at the same speed for a minute gaving a temperature increase of 3.4°C. The ramping rate of the disc is extremely quick, combined with the fact that both cells and Adju-Phos reach an unchanged condition after only 5 seconds; the ramp rate of the disc is therefore not recorded here.

2.2.1.2. Pilot & Industrial Centrifuges

Centrifugation of Adju-Phos was carried out using the CSA-1 disc stack centrifuge (Westphalia Separator, AG, Oelde, Germany) and the CARRPowerfugeTM P6 bowl centrifuge (Carr Centritech Separation Systems, Clearwater, FL), representing characterised, low and high shear centrifuges respectively. The CSA-1 operating conditions were a speed of 9810rpm and a feed flow rate of 100L/hr. The CARRPowerfuge running conditions were a speed of 15000rpm and a feed flow rate of 60L/hr.

Operating conditions in the CSA-1 and CARRPowerfuge are selected according to conditions at which these centrifuges have previously been characterised (Lau et al. (2013) and Lopes and Keshavarz-Moore (2012)). The CSA-1 is an hermetically sealed disc stack centrifuge which has been shown to operate at low shear conditions. The CARRPowerfuge by contrast is a high shear tubular bowl centrifuge. Thus these two centrifuges represent the extremes of possible process conditions in terms of shear rate.

The PSC-5 disc stack centrifuge (Westphalia Separators, AG, Oelde, Germany) was used by GSK for the centrifugal clarification of uninfected HEK cells, uninfected CHO cells (Section 2.2.5.2) and infected EB66 cells (Section 2.2.6.2). The operating conditions were a speed of 8500rpm and a feed flow rate of 200L/hr.

Samples of the supernatant were taken at 30 second intervals and the Optical Density (OD) at 650nm was measured (as per section 2.2.7.7). Steady state was taken as 3 similar consecutive OD measures, with this steady state value being used to calculate the clarification. This steady state was reached within the first 1 minute

30 seconds. For infected EB66 cells, however, this was not possible for biosafety reasons; so a sample of the final well mixed supernatant harvest was taken and measured instead. The feed and well spun OD were based on those measured for the laboratory scale clarification experiments (section 2.2.1.3).

Centrifugation of Adju-Phos was carried out using the PSC-1 disc stack centrifuge (Westphalia Separator, AG, Oelde, Germany) as a substitute for the PSC-5 centrifuge, in the absence of the expertise at GSK to disassemble and reassemble the centrifuge for sample extraction and the equipment to measure particle size distribution. The operating conditions used were a speed of 13500rpm with a feed flow rate of 40L/hr, and a speed of 8000rpm with a feed flow rate of 81L/hr.

The Q/Σ (m/s) for the PSC-5 disc stack centrifuge was calculated as follows (see section 1.1.3.1):

$$\Sigma_{ds} = \frac{2\pi n\omega^2(r_2^3 - r_1^3)}{3g\tan\theta}F_L = \frac{2^{\pi} \times 60 \times 890^2(0.0635^3 - 0.034^3)}{3 \times 9.81\tan(\frac{40}{360} \times 2 \times \pi)}F_L \cong 2622m^2$$

$$F_L = 1 - \left(\frac{3Z_L B_L}{4\pi r_2}\right)\left(\frac{1 - \left(\frac{r_1}{r_2}\right)^2}{1 - \left(\frac{r_1}{r_2}\right)^3}\right) = 1 - \left(\frac{3 \times 8 \times 0.006}{4\pi \times 0.0635}\right)\left(\frac{1 - \left(\frac{0.034}{0.0635}\right)^2}{1 - \left(\frac{0.034}{0.0635}\right)^3}\right) \cong 0.85$$

With addition of a geometric correction factor for the non-idealities in a disc stack environment of 0.4, this gives

$$\frac{Q}{\Sigma} = \frac{200(\frac{l}{hr}) \times 0.001(\frac{m3}{l})}{2622(m^2) \times 0.85 \times 0.4 \times 60(\frac{min}{hr}) \times 60(\frac{s}{min})} \cong 6.25 \times 10^{-8} m/s$$

bowl speed		*min-1*	8500
angular velocity	ω	*rad/s*	890
Flow		*l/hr*	200

Table 2.2-1. PSC-5 run specific parameters

number of discs	*n*	-	60
half disc angle	θ	*Deg*	40
inner radius	*r1*	*M*	0.034
outer radius	*r2*	*M*	0.0635
number of caulks	Z_L	-	8
caulk width	B_L	*M*	0.006

Table 2.2-2. PSC-5 physical parameters

The parameter in Table 2.2-2 were confirmed by taking the centrifuge apart and physically measuring components. These measurements were completed by the author, at GSK, whilst the centrifuge was being serviced.

Centrifugation of nanobeads at pilot scale was conducted using a PKII centrifuge (Alfa Wasserman, Germany). The PKII was loaded with 200ml 55% sucrose and 200ml PBS (pH 7.4) and bought up to speed, with an hour allowed for the gradient to form. The PKII centrifuge, with a K3 rotor was run at a speed of 35000rpm and 100ml of suspended nanobead fed at a flow rate of 20ml/min. Banding was then performed over 1 hour, using PBS (pH 7.4) at a flow of 20ml/min. Offloading was performed automatically in ~12ml fractions.

2.2.1.3. Laboratory Centrifuges & Clarification

Cell samples were first sheared, as described in section 2.2.1.1, then clarified using a laboratory scale centrifuge. As described in section 1.1.3.1 the Q/Σ for the PSC-5 centrifuge (calculated in section 2.2.1.2) was matched by the volume, speed and time of centrifugation at laboratory scale.

For uninfected and adenovirus infected HEK cells (at UCL) the sheared cells were clarified using an Eppendorf 5430 centrifuge with an FA-45-30-11 rotor (Eppendorf, UK). The conditions used were 1ml, 1.5ml and 2ml, spun down for 5 minutes at 3000rpm, and the same volumes spun down for 5 minutes at 6000rpm. Well spun samples were generated by centrifuging 2ml for 30 minutes at 6000rpm. These are the standard conditions used at UCL in the centrifuge USD practicals.

For uninfected and influenza virus infected EB66 cells (at GSK) the sheared cells were clarified using an Eppendorf 5427R centrifuge with an FA-45-48-11 rotor (Eppendorf, UK), and using a larger laboratory scale centrifuge, Allegra X-15R with an SX4750A rotor (Beckmann). In the Eppendorf centrifuge the conditions were identical to those used at UCL. It was observed that the clarification as predicted by

the Eppendorf centrifuge did not match the industrial scale or the larger Beckmann centrifuge used to give a sterile supernatant sample for infectivity assays. Subsequent runs therefore included clarification over a full range of V/Σt for both the larger and smaller laboratory centrifuges. In the Beckmann centrifuge 15ml falcon tubes were used to spin down 7ml and 14ml for 7 minutes at 3000rpm, and the same volumes for 10 minutes at 4000rpm, in addition to 13, 10, 7, 5 and 2ml centrifuged for 5 minutes at 4000rpm. The same well spun samples were used as for the smaller Eppendorf centrifuge.

The conditions listed above for the larger laboratory scale centrifuge are equivalent to a V/tΣ of 6.7, 1.5, 2.8, 5.7, 10.5, 7.8, 5.3, 3.7 and 1.4 $x10^{-8}$ m/s respectively. The first condition was designed to match the Q/Σ conditions in the PSC-5 centrifuge ($6.3x10^{-8}$ m/s). In the Eppendorf 5430 centrifuge the centrifuge conditions listed are equivalent to a V/tΣ of 9.0, 13.2, 17.1, 2.2, 3.3 and 4.3 $x10^{-8}$ m/s respectively, and in the 5427R Eppendorf centrifuge to 5.3, 7.7, 9.8, 1.3, 1.9 and 2.45 $x10^{-8}$m/s respectively. However, it should be noted that the g-forces will also differ between this centrifuge, the smaller laboratory centrifuge and the PSC-5. It has been shown elsewhere that for certain cell types, specifically algal, the g-forces may also be of interest with respect to the clarification and settling (Xu et al., 2015b). The g-forces for the various centrifuges are therefore summarised as follows: the small Eppendorf centrifuge has a g-force ranging from 1,600 to 14,000xg, the larger laboratory centrifuge has a g-force ranging from 5,900 to 41,000xg and the PSC-5 has a g-force ranging from 7,000 to 20,000xg, over the operating ranges used.

For biosafety reasons influenza infected samples were pipetted into the cuvettes under a (micro) biosafety cabinet II and stoppered with a cap. The samples were then agitated just before measurement, by inverting several times, to ensure that particle settling did not affect the accuracy of measurements.

For earlier work at GSK on uninfected CHO and HEK cells the sheared cells were clarified using another large laboratory centrifuge, a 5810 eppendorf centrifuge (VWR, Belgium). A standard 50ml falcon tube with a starting volume of 20ml of process material was spun-down at speeds of 1000 and 2000rpm and 1ml samples of the supernatant taken at intervals of between 5 and 10 minutes. In calculating V/Σt the acceleration and deceleration times were discounted and the removed

sample volume accounted for by assuming uninterrupted centrifugation at the time averaged volume. Well spun samples were generated by centrifugation of 25ml of unsheared material at 4000rpm for 30 minutes.

		Eppendorf 5430 (UCL)	Eppendorf 5427R (GSK)	Allegra X-15R (GSK)	Eppendorf 5810 (GSK)
Outer Radius (m)	R_2	0.095	0.101	0.208	0.075
Angle from vertical (degrees)	θ	45	60	90	90
Tube type		2ml Eppendorf		15ml falcon	50ml falcon
Minimum Volume (ml)	V	1		14	20
Maximum Volume (ml)		2		2	30

Table 2.2-3. Physical parameters of laboratory centrifuges

Sample Calculation of V/Σt for Eppendorf 5427 centrifuge:

R_2 (m)	θ (degree)	Volume	Speed (krpm)	Time (mins)
0.101	60	2ml	3	5

Height of Eppendorf centrifuge tube to 2ml is ~4cm.

$$R_1 \cong R_2 - h \times \cos\theta = 0.101 - \frac{4cm}{100\left(\frac{cm}{m}\right)} \times \cos\left(\frac{60}{360} \times 2 \times \pi\right) = 0.081$$

$$\Sigma_{lab} = \frac{(2.\pi.Z_0)^2.(3-2.x-2.y).V}{ln\left(\frac{2.R_2}{R_2+R_1}\right).6.g}$$

$$= \frac{\left(2.\pi \times 3000rpm \times \frac{1}{60\left(\frac{s}{\min}\right)}\right)^2 \times 3 \times 2(ml) \times \frac{1}{1000(\frac{ml}{l})} \frac{1}{1000(\frac{l}{m^3})}}{ln\left(\frac{2 \times 0.101}{0.101+0.081}\right) \times 6 \times 9.81}$$

$$= 0.096m^2$$

$$\frac{V}{t.\Sigma_{lab}} = \frac{2(ml) \times \frac{1}{1000(\frac{ml}{l})} \frac{1}{1000(\frac{l}{m^3})}}{5(\text{mins}) \times 60(\frac{s}{\min}) \times 0.096(m^2)} = 6.9 \times 10^{-8} m/s$$

The absorbance of the samples were measured as per section 2.2.7.7. By comparing the absorbance of the supernatant to that seen in the feed stock, and in the supernatant of a well spun sample, the clarification was derived (Maybury et al. (2000)):

$$Clarification\ (\%) = \frac{OD_{Feed} - OD_{sample\_supernatant}}{OD_{Feed} - OD_{Well\ Centrifuged\_supernatant}} \times 100 \quad \text{[Eq. 12]}$$

For EB66 (influenza infected, and uninfected) the supernatant samples used for western blots and protein assays were produced by spinning down 7ml of the sheared sample at 3000rpm for 7minutes, conditions which should roughly match the Q/Σ of the PSC-5 centrifuge at the run conditions used in this process.

2.2.1.4. Laboratory-scale batch density gradient ultracentrifugation

In order to look for impact on the adenovirus and influenza virus these needed to be separated from the whole cell lysate, removing the background from measurement of the particle size distribution (section 2.2.7.6), and average protein composition of the virus particles (sections 2.2.7.13, 2.2.7.14, 2.2.7.17 and 2.2.7.18). The protein composition assays were also used in this case to confirm the presence, and attempt to confirm the relative purity of, the viruses in the fractions for which the particle size distribution was measured.

In order to obtain relatively pure virus density gradient centrifugation was used to fractionate the sample.

Influenza infected EB66 cell supernatant was fractionated in a sucrose gradient. Heavy, medium and light sucrose was made up at a concentration of 55, 30 and 5% respectively. A 40ml Ultra-clear tube was partially filled manually with 10ml heavy density sucrose, overlaid with 10ml medium density sucrose, overlaid with 10ml low density sucrose, and left overnight at 4°C. 10ml of the supernatant sample was overlaid on the sucrose density gradient, and spun at 26000rpm for 2 hours, and subsequently the visibly identifiable virus fraction was removed manually.

Whole cell lysate of adenovirus infected HEK293 cells was fractionated in a caesium chloride (CsCl) gradient. Heavy and light CsCl was made up from 146g 10mM Tris-HCl buffer (pH 8.1) and 107.4 and 54g of CsCl (562602-1KG, Sigma Aldrich) respectively. The CsCl gradient was created manually. First 5.5ml of heavy CsCl

was pipetted into a 14ml ultra-clear tube (BECL344059, VWR international), and overlaid with 5.5ml of light CsCl. 200µl of the whole cell lysate was added to 1ml of 10mM Tris-HCl buffer (pH 8.1), and 1ml overlaid on the light CsCl in the centrifuge tube. A further 1ml of 10mM Tris-HCl buffer (pH 8.1) was overlaid on the sample. The tubes were spun at 20500rpm in an SW41 Ti rotor, and a Beckman Optima-L-100XP ultracentrifuge, for 2 hours at 4°C, and subsequently offloading was performed manually in 0.5ml fractions.

The fractions containing adenovirus were identified using the Nanosight, and combined and further concentrated (x10) using Vivaspin 500 centrifuge filters (VSO 111, Sartorius) before westernblots against adenovirus coat proteins were performed (see section 2.2.7.13).

In order to assess the impact of fractionation in a CsCl gradient, and compare to nanobeads fractionated in the PKII centrifuge, pre-sheared nanobeads were also fractionated at laboratory scale. A sucrose (04821713, MP Biomedicals, UK) gradient was prepared as for influenza, but in 14ml ultra-clear tube (BECL344059, VWR international). For sensitivities using a shallow density gradient, high and mid-range concentrations of 41.2 and 24% sucrose were used, and for a steeper density gradient a mid-range concentration of 34%. 2ml of sheared nanobead sample was added to each tube. All tubes were spun at 42000rpm for 1hour 27 minutes at 4°C using an SW 41Ti rotor and in a Beckman Optima-L-100XP ultracentrifuge. Offloading was performed manually in 0.5ml fractions using a standard laboratory pipette, from the top downwards.

2.2.1.5. Homogenisation

The two sets of operating conditions used on the APV lab 40 homogeniser (Gaulin GmbH, Germany) were 2 passes at a set pressure of 1200bar, and 3 passes at a set pressure of 500 bar. The homogeniser was used to stress test shear mimic candidates, with the aim of demonstrating that the assay techniques chosen / developed were capable of measuring damage to the shear mimics.

2.2.2. Cell Shear Mimic Candidates

2.2.2.1. Agarose

4% highly cross-linked agarose beads “superfine” with a mean diameter of 10μm dispersed in 20% ethanol were purchased from Agarose Bead Technologies (ABT). It was ensured that particles were uniformly distributed in the 5ml delivery container by inversing the container three times before removing a portion of the sample for testing.

For the initial test 88μl was extracted by pipette and dispersed in 40ml of PBS solution. A second test with a higher concentration of 500μl was extracted by pipette and dispersed in approximately 40ml of PBS solution, with the aim of generating a mixture whose particle size distribution could be accurately measured using the Mastersizer. Subsequent tests have been conducted with 330μl of agarose dispersed in 150ml of PBS solution, with the aim of creating a uniform initial concentration for the no shear, low shear and high shear cases.

A range of other agarose derived materials were tested, these include sepharose CL-4B (Amersham Biosciences, 17-0150-01), sepharose CL-6B (Amersham Biosciences, 17-0160-01), DEAE sepharose fast flow (Amersham Biosciences, 17-0709-01), 2% cross-linked agarose (Iberagar) and P6XL (origin unknown). The aim being to test whether the preparation of the beads and resultant properties, such as extent of cross-linking, had a significant impact upon the response to shear; following initial assays with agarose showing minimal shear impact.

2.2.2.2. Aluminium hydroxide

250ml of Alhydrogel was kindly donated by Brenntag Biosector. 8ml of aluminium hydroxide was diluted in 150ml of RO water, prior to shearing.

2.2.2.3. Aluminium Phosphate

Initially 250ml of Adj-Phos was kindly donated by Brenntag Biosector. 8ml of aluminium phosphate was diluted in 150ml of RO water, prior to shearing.

For later work 250ml bottles (Brenntag Nordic A/S, Frederikssund, Denmark, cat. no. 3471) were purchased, with concentration reduced to 1ml per 100ml PBS made up with milliq water. The work for which results are presented in chapter 4 is all based on this concentration. A sensitivity analysis was run at laboratory scale at

concentrations of 5ml Adju-Phos per 100ml PBS, and 15ml of Adju-Phos per 100ml PBS.

2.2.3. Virus Shear Mimic Candidates

2.2.3.1. Streptavidin Coated Polystyrene Nano-Beads

10ml of 0.109μm (adsorbed) streptavidin coated polystyrene beads at a concentration of 10mg beads/ml suspension were purchased from Bangs Laboratories. The quoted binding capacity of these beads is given as 7.66μg GFP-biotin/mg bead. The quoted material density was 1.06g/ml.

Nanobeads were allowed 10minutes out of the fridge to warm towards room temperature. To ensure uniform distribution the container was inverted three times and placed on a vortex shaker for 20 seconds. Nanobeads were added to PBS, using a pipette, at a concentration of 100μl of nanobeads for 100ml of PBS.

For some early initial trials nanobeads were washed before being suspended in PBS. If this is the case it is indicated in the method description. After vortexing 200μl of nanobeads were extracted by pipette and washed three times using a vivaspin-20 (with 300,000 MWCO filter) tube (Sartorium Stedim UK ltd) and an Eppendorf centrifuge 5810R at 3220 x g. Washed beads were added to PBS to give a total volume of 200ml. Use of vivaspins was discontinued as they appeared to strongly effect the apparent nanobead concentration, as measured by fluorescence assays and Nanosight. The latter, along with a substantial decrease in vivaspin water flux after use, was thought to imply that the nanobeads were sticking to the vivaspin filters.

2.2.4. Fluorescent Labels

0.1mg of anti-GFP labelled biotin was purchased from 2B Scientific ltd. 5ml of anti-GFP labelled biotin was added to 10ml PBS (milliq).

0.3mg of Green Fluorescent Protein (GFP) was purchased from Millipore UK ltd. The GFP in its original container was allowed approximately 10 minutes to reach room temperature then centrifuged at 5000rpm for 5 minutes in an Eppendorf 5415R centrifuge. In addition the contents was mixed using a pipette. Aliquots were then created, as advised on the manufacturer's instructions, by diluting 5μl in 1ml of a

PBS glycerol mixture. Initial work with GFP showed no promising results. The easier fluorescein system was therefore adopted for the majority of the project.

1mg of biotin (5-fluorescein) was purchased from sigma Aldrich ltd (53608 Sigma). As this was received in powder form a small amount (~1.4g/ml) was diluted in water to form a stock solution, and 1ml aliquots frozen at -20°C. Details of assay methodology are described in section 2.2.7.8.

2.2.5. Cells

2.2.5.1. UCL based cell work

CY0 CHO cells (Lonza, UK) were grown in 250ml working volume shake flasks at 37°C, 5%CO_2, in chemically defined media containing TMX (Life technologies, Paisley, UK). Cells were harvested on day 7 with a viability of 95% and cell density of $4x10^6$cells/ml. These cells were used to generate particle size distributions exemplifying the effects of shear on mammalian cells as measured on the casy counter and mastersizer.

HEK293 cells (85120602-1VL SIGMA293 Cell Line, European Cell Bank) were grown as adherent cell cultures in T-175 flasks (660160, greiner bio-one, UK), using defined DMEM media (21969-035, Gibco, life technologies, UK) with 10%FBS (10270-106, Gibco, life technologies, UK) and 5.5ml L-glutamine (25030-024, Gibco, life technologies, UK), and in a Sanyo incubator at 37°C and 5%CO_2. These cells were used in adenovirus production studies, to compare the shear sensitivity of virus infected and uninfected cells.

Virus infection stages are discussed in section 2.2.6.1.

For non-virus infected runs the cell culture conditions were similar in range to those seen in virus infected runs at the time of infection (see Table 2.2). For both virus infected and uninfected runs, in order to remove the samples from the T-flasks and prepare them for shearing the following steps were undertaken: (i) free liquid was removed from the T-flask, (ii) any remaining attached cells were washed with PBS, then trypsin added for a maximum of 3 minutes at 37°C, the trypsin neutralised by addition of fresh media and the cells spun down, and the pellet re-suspended in the free liquid removed in step (i).

2.2.5.2. GSK based cell work

15 litres of CHO and HEK cells were kindly provided by GSK Vaccines (Rixensart, Belgium) for analysis of separation in the PSC-5 (GEA, Milton Keynes, UK) centrifuge. CHO cells were grown in shake flasks over a 7 day period, and induced at low temperature to produce a recombinant product. The HEK cells by contrast were grown in a stirred bioreactor. Details of upstream processing were not considered relevant to this analysis. Total cell count was approximately 1.9 x 10^6 cells/ml for both, i.e. below the 2% wet w/v, which has been shown to require modification of the USD methodology (Tustian et al., 2007).

EB66 cells (Valneva, France) were produced by GSK Vaccines (Rixensart, Belgium) for trials and analysis of the influenza production process. The cells were grown to a concentration of approximately 10 x10^6cells/ml, and diluted in fresh media and other constituents for viral propagation, before infection. Infection Culture occurred in a 50L single use bioreactor. Sample volumes were taken at 4 and 5 days after infection, and subjected to the shear conditions of interest (within 2 hours), and then clarified, and OD measured (within the same day). For the non-virus infected culture a small volume was taken from the main bioreactor and diluted in the same material as for infection, except without the addition of the virus seed. As with the virus infected samples the non-virus infected sample volume was subjected to a range of shear conditions within 2 hours of being extracted from the bioreactor / diluted, and then clarified and OD measured within the same day.

2.2.6. Viruses

2.2.6.1. UCL based virus work

The Adenovirus kit used was supplied by the Clinical BioManufacturing Facility (Oxford, UK). It was an Ad5 control stock (D419, p53). HEK 293 cell cultures, grown as described in section 2.2.5.1, were used to propagate this virus. The aim was to infect HEK cells at a confluence of 70-80%. Actual confluence on infection is included in Table 2.2, which summarises the key parameters of the adenovirus culture.

Run#	Confluence[1]	Cell Count[1]	MOI[2]	TOI[3]	TOH[4]	Cell Passage #
	%	10^6/ml		hrs	hrs	
1	93.7+/-1.4	4.9+/-0.03	8	110	159	6
2	67.3+/-5.0	3.4+/-0.37	12	105	168	7
3	90.7+/-2.0	4.8+/-0.16	8	104	169	12
4	89.7+/-4.3	4.8+/-0.09	8	98	211	12
5	75.8+/-3.6	4.6+/-0.08	8	97	241	14
6	61.0+/-6.3	3.9+/-0.29	5	93	237	16
7	63.4+/-6.3	4.1+/-0.28	7	99	235	8
8	56.9+/-2.3	4.0+/-0.17	7	48	114	11
9	42.9+/-7.3	1.5+/-0.29	13	129	168	18
10	45.0+/-7.5	1.5+/-0.35	13	129	217	18

[1] On infection, measured by taking 5 images per T-175 flask and analysing using cell counting tool (referenced section 2.2.7.1)

[2] Multiplicity of Infection, based on a P2 stock virus count of 10^{10} measured using TEM. MOI is the ratio of virus count to cell count.

[3] Time of Infection, i.e. time from start of cell culture to seeding of the virus, in the same culture vessel

[4] Time of Harvest, i.e. time from start of cell culture to harvest, in the same culture vessel in which virus seeding occurred.

Table 2.2. Summary of culture conditions for adenovirus / HEK cell runs

2.2.6.2. GSK based virus work

The flu virus runs used four separate flu strains: A/Shanghai/2/2013 (H7N9), A/Gyrfalcon/Washington (H5N8) from the centre for disease control (CDC) and A/Duck/Bangladesh/19097/2013(H5N1) from St Jude Children's Research Hospital. EB66 cell cultures, as described in section 2.2.5.2, were used to propagate these viruses.

2.2.7. Analytics

2.2.7.1. Optical Microscope

The optical microscope can be used for automated cell count and size distribution evaluation. However here it was used to perform manual counts and look for any visibly distinguishable morphological changes to micro-particles.

For early work with micro-particles, whilst trying to identify whether any visible impact from shear could be distinguished a haemocytometer was used for number counting and a Leica microscope with camera was used to create a record of measurements.

A Haemocytometer was also used to count cells in virus free and adenovirus infected HEK cells, subjected to different shear levels, using an optical microscope. A number of runs were completed with Trypan blue used to distinguish between viable and non-viable cells.

An EVOS digital microscope was used to take photographs at representative points in the T-175 flasks and an in-house developed software (Asselborn et al., 2015) used to estimate cell count and confluence on infection.

2.2.7.2. Beta Galactosidase Staining Kit

Cells were washed with PBS, and stained with staining solution, from the β-Galactosidase Reporter Gene Staining Kit (GALS, Sigma Aldrich, Saint Louis, USA), prepared as per manufacturer's instructions. 0.5% gluteraldehyde was used for cell fixing. The infectivity assay protocol is described below.

2.2.7.3. BFU Infectivity assay

The blue forming units (BFU) assay was used to test for infectivity of the adenovirus by identifying cells which had been transfected with the LACz gene (Mittereder et al. (1996), Cell_Biolabs_Inc (2004b)). A 96 well plate was coated with Poly L Lysine (PLL) (P4832, Sigma) by incubating with 30µl per well for 5 minutes, removing the

PLL and leaving for a further 2 hours to dry, all at room temperature. 100µl of HEK293T cells at a concentration of 10^5cells/ml were added per well, and left overnight in an incubator (conditions in incubator as per section 2.2.5.1 throughout).

The frozen sample of sheared virus was thawed on ice, and dilutions, in cell media, prepared with dilution factors of $2x10^3$, $2.5x10^4$, $5.1x10^4$, $7.2x10^4$, $2.1x10^5$, $4.3x10^5$, $8.5x10^5$ and $1.7x10^6$. The media in each well was removed and replaced with 100µl of diluted sample. Each dilution was prepared in triplicate, with fresh media added to 3 of the columns, acting as a blank. The plate with infected sample was left in the incubator for 1 hour, then the adenovirus containing media was removed and replaced with 100µl of fresh media, and the plate incubated overnight.

Wells were washed twice with 30µl of PBS, left in 30 µl of fixation solution for 5minutes, washed twice again with 30µl of PBS, and left in the incubator overnight in 30µl of staining solution (see section 2.2.7.2 for reagent details).

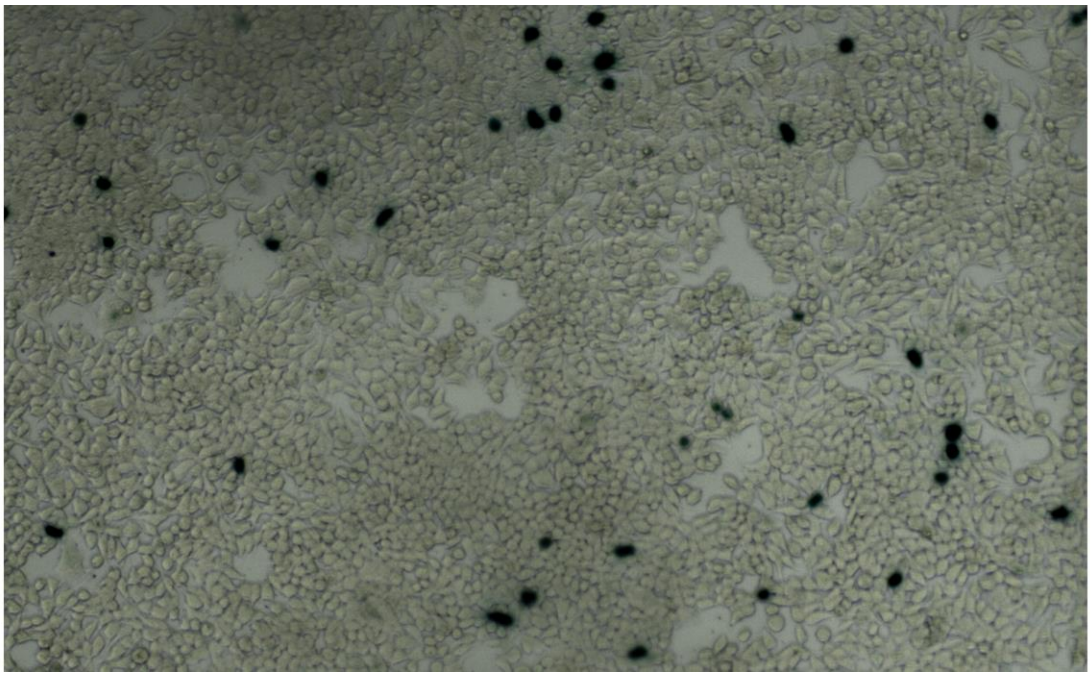

Figure 2.2-2. Illustrative image of HEK cells exposed to diluted adenovirus, fixed and stained (BFU assay)

The total number of cells which stain blue (see Figure 2.2-2) was counted for each well at a magnification of 5x and, where this number was between 50 and 200, corrected for dilution and averaged, to give the BFU/100µl.

The above describes an optimised BFU assay, developed by Jelena Ruscic and Bernice Wright (with the author locating and providing Cell_Biolabs_Inc (2004a)). An earlier iteration of the BFU assay was also used in a non-quantitative manner to confirm the presence of adenovirus, but did not allow the quantification of infective virus due, most likely, to overgrowth of cells and loss of transfected cells during washing. The problem with the original BFU assay was identified by the author when it was observed that there was a relationship, which should not have existed, between dilution and predicted BFU/ml. The original protocol used 24 well plates, not coated in PLL. 1ml of cells, at a concentration of $2.5x10^5$ cells/ml, was added to each well, and the plate left in the incubator for 1 hour, before 1ml of media diluted virus was added to each plate at dilutions of 1 in 2000, 1 in 20000 and 1 in 200000. After a further 48 hours in the incubator, the cells were fixed and stained as above (with correction for the larger volume), except that the Beta-galactosidase staining kit fixation solution was used instead of gluteraldehyde. The number of blue stained cells at 5 well spaced locations, was counted at a magnification of 10x and the total number of blue stained cells per well extrapolated. A count of between 50 and 200 at each of the 5 locations was taken as acceptable.

2.2.7.4. $TCID_{50}$ Infectivity assay

$TCID_{50}$ infectivity assays for influenza were performed at GSK, by members of the team at GSK. No further details are available.

The $TCID_{50}$ of adenovirus was measured in a 96 well plate, on HEK293 cells seeded at a density of 10^5cells/ml with 100µl cells per well. Cells were left a minimum of 2 hours to adhere before virus dilutions were added. Sheared adenovirus samples were thawed on ice and 8 different dilutions were used for each sample, with a dilution factor ranging from $1x10^5$ to $1x10^{12}$, with 10 replicates per plate used to estimate each $TCID_{50}$, and triplicate plates prepared for each sample, with the $TCID_{50}$ being estimated from the average, excluding any obvious outliers.

2.2.7.5. Transmission Electron Microscopy (TEM)

A model JEM-1010 transmission electron microscope (Joel, Japan) was used to look for morphological changes in sheared virus, to count virus particles, to look for morphological changes in sheared nanobead, and to count anti-biotin gold tags per nanobead on sheared nanobeads.

The TEM was used to estimate the virus count by mixing virus samples with a known amount and concentration of nanobeads, and counting both nanobeads and virus particles over a number of grid squares. 2ml of Whole cell lysate of HEK cells infected with adenovirus was spun down at a speed of 3krpm for 5minutes in an Eppendorf centrifuge, and 100ul of supernatant removed and frozen. Following thawing 100ul of glutoaldehyde was added to the sample. For the count the adenovirus samples were mixed with a nanobead suspension, of known concentration in a known ratio. The adenovirus and nanobeads were allowed to adhere to a copper grid over a period of 15minutes and blotted, followed by alternately blotting and washing in filtered buffer and distilled water for 20 seconds each, and staining with uranyl for 30 seconds. Both adenovirus and nanobead were counted simultaneously at a focus of x60k, with an aim to count a minimum of 100 nanobeads.

2.2.7.6. Particle Size Distribution

The following particle sizing equipment was used:

- Nanosight tracker LM10 (Nanosight Ltd, Malvern Instruments, Malvern, UK), with the software version 3.1 and camera type CCD. Nanosight uses a camera to track the Brownian motion of individual nanoparticles highlighted by a laser beam, and can be used to derive a particle size distribution and count. Typically for nanobeads the camera level used was 9, with a threshold of 9 in post processing. Typically for fractionated adenovirus (section 2.2.1.4), and HEK cells with and without adenovirus, the camera level used was 12 and the threshold approximately 3. A dilution of 1 in 10 was used for cell supernatant and lysate samples. The Nanosight was also used on Adju-Phos supernatant, but showed very low particle concentration.
- CPS Disc Centrifuge (CPS instruments, Europe). CPS uses a sucrose gradient between 4 and 18% inside a spinning disc, with samples injected at the centre, and the particle size inferred from the time taken to travel from the centre to the detectors. CPS was used for the particle size distribution of fractionated influenza virus (section 2.2.1.4).
- Mastersizer (Malvern Instruments, Malvern, UK). The mastersizer uses static light scattering, whereby the degree of laser scatter is greater for larger particles (Malvern_Website). The sample is pumped through an optical

window, through which a laser is shone, and the scattered light from which is detected on a semi-circular array of detectors. Both blue and red lasers are used to broaden the instruments measurement range. Dispersant used was milliq-PBS, to prevent a change in dispersant generating any agglomeration, destruction of cells etc. Early work was done with the Mastersizer 2000SM series, using Mastersizer 2000 5.53 software version. Later work was done using Mastersizer 3000 HydroMV and HydroSV dispersion units, and using v3.10 of the software. An obscuration target of 11% was used. The refractive index for agarose, polystyrene nanobeads, CHO, aluminium hydroxide and aluminium phosphate were 1.58, 1.6, 1.6, 1.57 and 1.5295 respectively, with an absorption of 0.1 for Adju-Phos and 0 for all other materials. Further details are given in Melinek (2013).

- Casy Counter and analyser, Model TTC (Scharf System GmbH, Reutlingen, Germany). The Casy Counter measures the change in electrical resistance across a constricted aperture as particles suspended in an electrolyte solution are pulled through a capillary. For agarose and CHO cells a capillary size of 150µm was used with a dilution of 50µl in 10ml (or as required). For aluminium phosphate the dilution factor was 10200 (100µl in 10ml, further diluted 100µl in 10ml of triple filtered casytone), and a 45µm capillary was used.
- Vi-Cell (XR Series) (Beckmann Coulter, UK) with software version 2.03. The Vi-Cell works as an automated haemocytometer, mixing a sample with trypan blue, and taking a series of images, which are analyses for individual objects of the appropriate circularity, brightness and size, all of which need to be calibrated for each cell line. Pre-prepared cell types for CHO, EB66 and EB66 post infection were used.
- Flow cytometer (XL, Beckmann Coulter, Expo32). Use of this machine was trialled for measurement of nanobeads, sheared and incubated with fluorescein and separately with GFP; neither showed a strong enough signal for detection against background.
- Zetasizer NanoZS (Malvern Instruments, Malvern, UK), using version 7.01 of the software. The Zetasizer uses dynamic light scattering, measuring the rate at which the intensity of scattered light generated by particles fluctuates as a result of their movement under Brownian motion. The Zetasizer was used to

measure nanobead particle size distribution but was not as repeatable as the Nanosight. It was also used on Adju-Phos supernatant, but showed no repeatable measurement due to low particle concentration.

2.2.7.7. Optical Density (OD) measurements

At UCL OD measurements were made using

- Biomate 3S Spectrophotometer (thermo scientific, UK) for CHO cells, and Lowry assays;
- And an InfiniTe 200 plate reader (Tecan, UK) for HEK cells and BCA assays. Readings in a translucent 96 well plate (82.1581, Sarstedt, UK).

At GSK OD measurements were made using:

- UltraSpec 2000 (Pharmacia Biotech, Uppsala, Sweden) for EB66 cells, influenza infected EB66 cells, and sucrose fractionated influenza virus
- SpectraMax 190 (Molecular Devices, UK) for Lowry assays.

2.2.7.8. Fluorescence measurements

An assay, based on immunoassays for protein concentration, was developed based on the interaction between the streptavidin on the streptavidin coated nanobeads (section 2.2.3.1) and the biotinylated fluorescein (section 2.2.4): The fluorescence of the fluorescein is quenched when the biotin is bound to streptavidin. Figure 2.2-3 shows a schematic summary of the steps involved in this simple assay. The concentration of nanobeads and fluorescein was optimised to give a clear curve, with initial concentrations being selected as discussed in section 2.1.3.1.

At UCL an InfiniTe 200 plate reader (Tecan, UK) was used for measurement of fluorescein fluorescence curves against nanobead concentration. At GSK a SpectraMax M2 (Molecular Devices, UK) was used for measurement of fluorescein fluorescence curves against nanobead concentration.

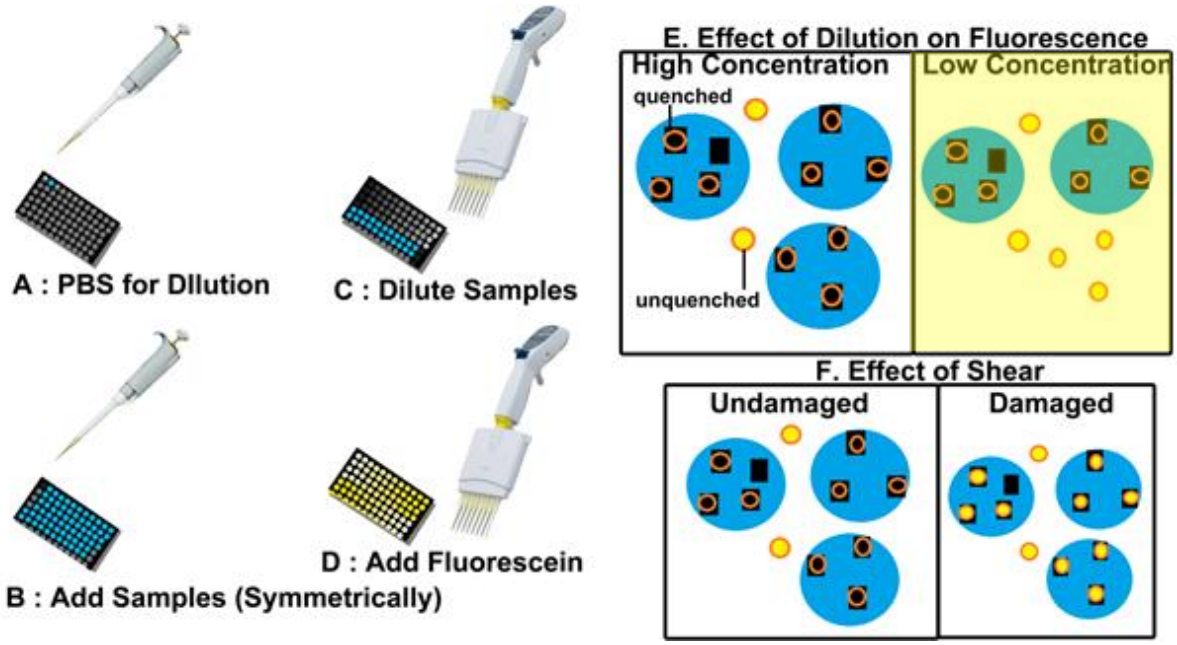

Figure 2.2-3. Schematic showing Stages of Fluorescence assay and principle by which it works. A. In a black well plate a fixed quantity of PBS is prepared in all but the first 4 wells of column 1 and last 4 wells of column 12. B. Duplicates of the sample are added to one of the first 4 wells in column 1, and the symmetrically opposite well in the last 4 wells of column 12. C. The sample is serially diluted across the plate, with the top 4 wells diluted, from left to right, and the bottom 4 wells diluted from right to left. D. A fixed quantity of fluorescein is added to all wells, as rapidly as possibly, and the plate left at least 15 minutes. Where the nanobead sample is in high concentration the biotinylated-fluorescein molecules will all be attached to streptavidin and the fluorescence quenched. At lower nanobead concentrations there will be a significant amount of free biotinylated-fluorescein, and the fluorescence will therefore increase. If the resulting fluorescence curve does not have a flat region at both extremes, and at least 5 points in the sloping region then the dilutions may need to be adjusted. E. Diagrammatic representation of fluorescence assay principle. Blue circles represent nanobeads, yellow circles fluorescein, black squares are streptavidin and orange-black circles are quenched fluorescein. F. Initially hypothesised impact of shear on nanobeads, which was disproved – clusters of nanobeads are broken down, but the attached streptavidin remains undamaged in the range of interest.

2.2.7.9. Density Gradient Concentration

The density of sucrose in fractionated density gradients was measured at GSK using a hand held BRIX device, pocket refractometer Pal-3 (atago, Japan). The density of sucrose and CsCl in fractionated density gradients was measured at UCL using a balance to measure the weight of 0.5 or 0.4ml removed by pipette.

2.2.7.10. UCL: Gel electrophoresis

Samples for gel electrophoresis were first suspended in NP40 (Appendix G) in a ratio of 1:1. The NP40 with sample was added in a ratio of 1:1 to Laemmli buffer (Appendix G).

Volumes to be added to each well were calculated such that the amounts of protein were equal, with the protein concentration being determined using the modified Lowry method (section 2.2.7.11) or BCA (section 2.2.7.12).

20x NuPAGE MES SDS running buffer (NP0002, novex, life technologies) was diluted to 1x in milliq water.

The gel used was a BOLT 4-12% bis-tris 10 well mini gel (Invitrogen, Thermo Fisher scientific, UK) using a mini gel tank (Invitrogen, Thermo Fisher scientific, UK) and PowerEase 90W unit (Thermo Fisher scientific, UK) run at 200V. Set-up and use of equipment was as per manufacturer's instructions (Lifesciences, 2014).

Molecular weight markers were SeeBlue pre-stained protein standard (LC5625, Thermo Fisher scientific, UK).

2.2.7.11. UCL: Modified Lowry

Where stated, the protein concentration was measured using the modified Lowry method (reagents 500-0114, 500-0113 and 500-0115, Bio-Rad, UK) in acrylic semi-micro cuvettes (67.740, Sarstedt, UK), with the OD at 750nm measured on a biomate3s spectrophotometer (thermo scientific, UK). A serial dilution of BSA (500-0007, bio-Rad, UK) was used as standards. The following were added sequentially to the cuvette: 10µl of sample or standard, 100µl of reagent A, 800µl of reagent B, mixed with a pipette between each addition. The samples were incubated at room temperature for a minimum of 15minutes and a maximum of 1 hour before being measured. Samples were prepared in triplicate. (Lowry et al., 1951)

2.2.7.12. UCL: BCA

The Pierce BCA protein Assay kit (233225, 23227, Thermo Scientific) was also used for some protein concentration assays at UCL for the purposes of the western blot, which used equal protein concentration in each lane. The standard protocol for use of this kit in 96 well plates was followed (Pierce_Biotechnology, 2015).

2.2.7.13. UCL: Western blot

The protein loaded per well was approximately 9µg, derived using the modified Lowry method (section 2.2.7.11), with the exception of the CsCl fractionated virus where the protein concentration was measured using BCA (section 2.2.7.12). The gel was prepared and run as per section 2.2.7.10. Proteins and molecular weight markers were transferred from the bis-tris gel to a PVDF membrane (IB24001, Invitrogen, Thermo Fisher scientific, UK) using the iBlot 2 Dry transfer (Thermo Fisher scientific, UK). The template method P0 was used, and manufacturers protocol was followed (Thermo_fisher_scientific, 2015).

5% milk (Marvel dried milk, Ireland) was used for blocking, and 2% milk was used when incubating first in primary and then secondary antibodies. Tris Base (Appendix G) was used to wash between primary and secondary antibody, for 3 x 5 minutes, and after secondary antibody, for 3 x 5minutes. The blot was incubated in the primary antibody, at 4°C without agitation overnight, and in the secondary anti-body at room temperature, under agitation for 2 hours.

Two primary anti-bodies were used: a 1 in 4000 diluted rabbit adeno coat proteins primary antibody (ab6982, abcam, Cambridge, UK) and a 1 in 5000 diluted mouse hexon antibody (10R-8460, fitzgerald, UK). The secondary anti-bodies used against these primary antibodies were respectively goat anti-rabbit HRP (ab6721, abcam, Cambridge, UK) diluted 1 in 8000, and rabbit anti-mouse HRP (ab6728, abcam, Cambridge, UK) diluted 1 in 5000.

The chemiluminescence substrate used was Supersignal West Pico (34080, Thermo scientific, UK), in which the blot was incubated at room temperature for 45 seconds.

Imaging was completed using a ChemiDoc MP (Bio-Rad, UK), and an exposure chosen which avoided saturation of all bands. Image Lab version 5.2.1. (Bio-Rad, UK) was used for band position and strength identification.

The final blot completed (adenovirus samples prepared as per the final paragraph of section 2.2.1.4) used the Amersham Imager 600 (GE, UK), with GelAnalyzer version 2010a (GelAnalyzer.com, Lazar and Lazar) was used for band position and strength identification.

2.2.7.14. UCL: SDS-Page

Silver staining was used for identification of protein bands, according to standard protocols. The amount of protein loaded per well was approximately 9µg, derived using the modified Lowry assay (section 2.2.7.11). The gel was prepared and run as per section 2.2.7.10. In summary the gel was stained as follows: agitated in fixing solution (Appendix G) for 1 hour, washed under agitation for 3 x 5 minutes in milliq water, left for 30 minutes under agitation in sensitising solution (Appendix G), washed under agitation for 3 x 10 minutes in milliq water, left for 20 minutes under agitation in silver stain solution (Appendix G), washed 3 times by manual rocking for 2-5 minutes in milliq water, left under agitation in developing solution (Appendix G)

(until it was judged that the fainter bands had started to show, or that the intense bands were becoming too smudged) then transferred to stopping solution (Appendix G), and left under agitation for a minimum of 30 minutes. Before imaging the gel was washed under agitation 3 times for 5 minutes in milliq water and left in preserving solution consisting of 5% acetic acid until ready to image. Imaging was completed using a standard scanner with a resolution of 600, in both colour and grey scale.

For Sypro Tangerine stained gels the amount of protein loaded per well was approximately 32µg. The gel was prepared and run as per section 2.2.7.10. Staining was conducted as per standard protocols (see Appendix G for solution recipes). Imaging was completed using a typhoon with an excitation / emission wavelength of 490/640nm

2.2.7.15. GSK: Gel electrophoresis

An in-house produced and optimised non-reducing sample buffer was used. The sample was boiled to denature the virus, for biosafety reasons. No further details available. MOPS (3-(N-morpholino) propane sulfonic acid) running buffer was used.

The gel used was a Criterion XT precast 4-12% bis-tris 18 well comb gel (Bio-Rad, Ca) using a Bio-Rad criterion cell gel tank and Bio-Rad Power PAC 200 unit run at 200V. Set-up and running were as per manufacturer's instructions (Bio-Rad(a)).

For western blots molecular weight markers were Precision Plus Protein WesternC Blotting Standards (161 0376, Bio-Rad, UK), with Precision Protein StrepTactin-HRP conjugate (161 0380, Bio-Rad, UK) used in parallel with the secondary anti-body to enable visualisation of these markers.

For gels molecular weight markers were Precision Plus Protein unstained Protein Standards, strep-tagged recombinant (161 0363, Bio-Rad, UK).

2.2.7.16. GSK: Modified Lowry

For the EB66 cells (infected with influenza, and uninfected) the sample was diluted to three different dilutions (x10, x20 and x40 dilution factor), and chemicals added to denatured and precipitate the protein. It was then spun down, and the supernatant removed, leaving the protein pellet. This procedure was followed for biosafety reasons and to remove interfering compounds. The protein concentration was then

measured in duplicates, using a Lowry reaction, with a maximum variance of 10% accepted across the three different dilutions. The exact protocol is confidential.

2.2.7.17. GSK: Western blot

Western blots were run in one of two ways, with equal volumes loaded per well or equal protein. Equal volumes of 6µl were loaded for blots against EB66. Equal volumes of 10µl were loaded following dilution 1 in 10 (approximately 1µg unsheared) of supernatant samples were loaded per well for blots against HA. Equal protein amounts of approximately 1.5µg of sucrose fractionated influenza virus was loaded per well for blots against HA, where the relative concentration of the virus was estimated based on peak Optical Density (OD) (see section 2.2.7.7).

Proteins and molecular weight markers were transferred from the bis-tris gel to a nitrocellulose membrane (162-0145, Bio-Rad, UK) using a wet blotting method, with a criterion blotter unit (Bio-Rad, UK), run using a Bio-Rad Power PAC 200 unit at 100V with a standard solid re-usable ice pack to prevent the system overheating. Set-up and running were as per manufacturer's instructions (Bio-Rad(b)). A methanol based transfer buffer was pre-prepared by members of the team at GSK.

Skim Milk (BD Worldwide, US) was used for blocking, and the same milk re-used at a lower concentration, which was used when incubating in primary and secondary antibodies.

Two primary anti-bodies were used: a rabbit anti-EB66 host cell primary protein antibody (GSK) and anti-HA uni 1. The secondary anti-bodies used against these primary antibodies were respectively Rabbit α-sheep IgG HRP conj (AP147P, Millipore) and Polyclonal goat α-rabbit IgG HRP (P0448, Dako).

The chemiluminescence substrate used was Supersignal West Pico (34080, Thermo scientific, UK), which was added dropwise across the membrane surface and left with minimal disturbance whilst imaging.

Imaging was completed using an Image Quant LAS4000 (GE), and an exposure chosen which avoided saturation of all bands. GelAnalyzer version 2010a (GelAnalyzer.com, Lazar and Lazar) was used for band position and strength identification on Tif files, convert from .gel format using Imagej software (Wayne Rasband, Research Services Branch, National Institute of Mental Health, USA).

Further details of the method are confidential.

2.2.7.18. GSK: SDS-Page

SDS-PAGEs were run in one of two ways, with equal volumes loaded or equal protein. Equal volumes of 10µl were loaded for most of the gels. Equal protein amounts of approximately 4µg of sucrose fractionated influenza virus was loaded per well, where the relative concentration of the virus was estimated based on peak Optical Density (OD) (see section 2.2.7.7).

Sypro ruby (S21900, Invitrogen) was used to stain the protein bands, as per the standard protocol (Molecular_Probes_Inc, 2007), with overnight agitation in sypro ruby stain.

Imaging was as per western blots (section 2.2.7.17)

2.2.8. Buffers

Buffer recipes and material vendors are given in Appendix G.

3. Mapping the Process Shear Environments using CFD

3.1. CFD Analysis – Continuous Centrifuge

The PSC-1 and PSC-5 are part of a series of centrifuge bowls by GEA Westfalia fitted within the same housing designed to offer equivalent performance at progressively larger scales. The PSC-1 has a bowl volume of 1litre and flowrate range of 15 to 30L/hr. The PSC-5 has a bowl size of 1.4litres and flowrate range of 100 to 200L/hr. The speed range of both machines is identical, 8000 to 13500rpm. Although there are differences in the inlet geometry as a result of this difference in bowl size fitted within the same frame, these differences are unlikely to have a material impact on the shear rate, which is believed to be dictated largely by the hermetic nature of the model, speed of rotation and disc diameter, all of which are identical.

3.2. Development Process

3.2.1. 2D-Axisymmetric

Early work on the continuous centrifuge Ultra Scale-Down (USD) model used Computational Fluid Dynamics (CFD) simulation to compare the environments within the rotating disc shear device and a continuous centrifuge model. This work, by Boychyn et al. (2001), used an axisymmetric methodology for the modelling of both the rotating disc shear device and the continuous centrifuge, and concentrated on the shape of the shear zone and the maximum shear rate within the liquid as points of comparison between the two systems. The authors show a maximum shear rate at the tip of the rotating shear device and at the furthest radial point of the centrifuge inlet zone, where the distributor branches open into the separation zone. This is where solids collect and fluid flows upwards through the discs. Boychyn et al. (2001), however, used a different simulation software, and this work was completed a number of years ago.

As a first pass, this modelling approach was replicated using COMSOL Multiphysics®, with the continuous centrifuge modelled by Boychyn et al. (2001) being replaced by the PSC-5 disc stack centrifuge which is of interest to this project.

The primary aim of replicating this earlier work was as an initial validation of the COMSOL model, and to explore in more detail the flow environment within the two systems. However, it was felt that an axisymmetric model could not reasonably be treated as a good representation of the continuous centrifuge, or at least needs to be evaluated, as the centrifuge geometry is not axisymmetric. The use of maximum shear rate as the primary point of comparison between the USD rotating disc shear device and the continuous centrifuge is also questionable. Unlike bioreactors, where the process material is exposed to the process environment over an extended period of time and where the design is intended to maximise mixing, the process material passes only once and rapidly through -or through the region proximate to- the highest shear zones in the continuous centrifuge feed. Use of maximum shear rate takes no account of the length of time for which particulates within the process stream are exposed to a given level of shear. In addition the maximum shear rate is found only in a narrow volume. Sections 3.2.1.1 and 3.2.2.1 touch on this issue in more detail. Other modelling approaches are therefore considered in this chapter in particular in section 3.2.2.2.

3.2.1.1. Comparison against Previous Studies

Although it may not be expected that maximum shear rate will correlate against experimental damage, previous studies have used this parameter. To confirm that the model build in Comsol matches these previous models the level of maximum shear was therefore used. For this it is easier to focus first on the rotating disc shear device. For both the continuous centrifuge and the rotating disc shear device the level of discretization used on the models was first validated by confirming the convergence of various parameters, but chiefly the maximum shear rate, as illustrated in Figure 3.2-1. The slight dip in maximum shear rate for the highest speed at the maximum discretization is considered likely to be numerical in origin. The level of maximum shear rate in the rotating disc shear device could then be compared to results previously published in the recent literature, as shown in Figure 3.2-2. This comparison shows a good level of agreement between this model and the published values, although it may be noted that these more recently published values do not agree with the values published by Boychyn et al. (2001). Finally the minimum Kolmogorov's scale is calculated based on these energy dissipation rates, showing minimum values of the same order as the size of a mammalian cell,

reflecting well the experimental observation that damage is seen to occur within this range of disc speeds within the rotating disc shear device.

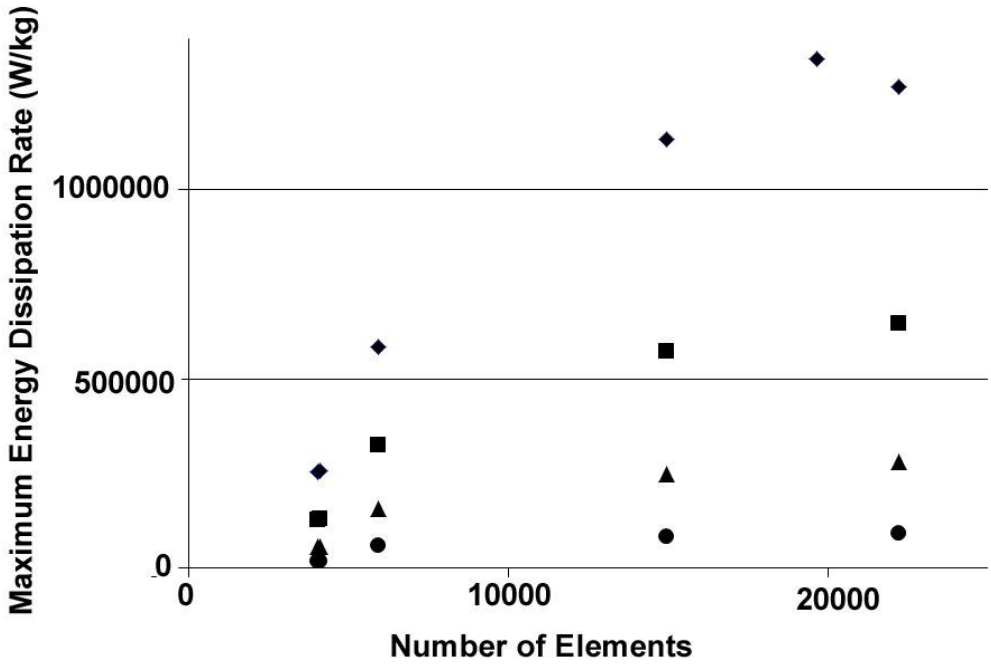

Figure 3.2-1. Maximum energy dissipation rate with number of mesh elements for the rotating disc shear device and over the full range of rotating disc shear device disc speeds presented in this thesis, from highest (◆) to lowest (●), with the remaining symbols (▲,■) representing intermediate disc speeds.

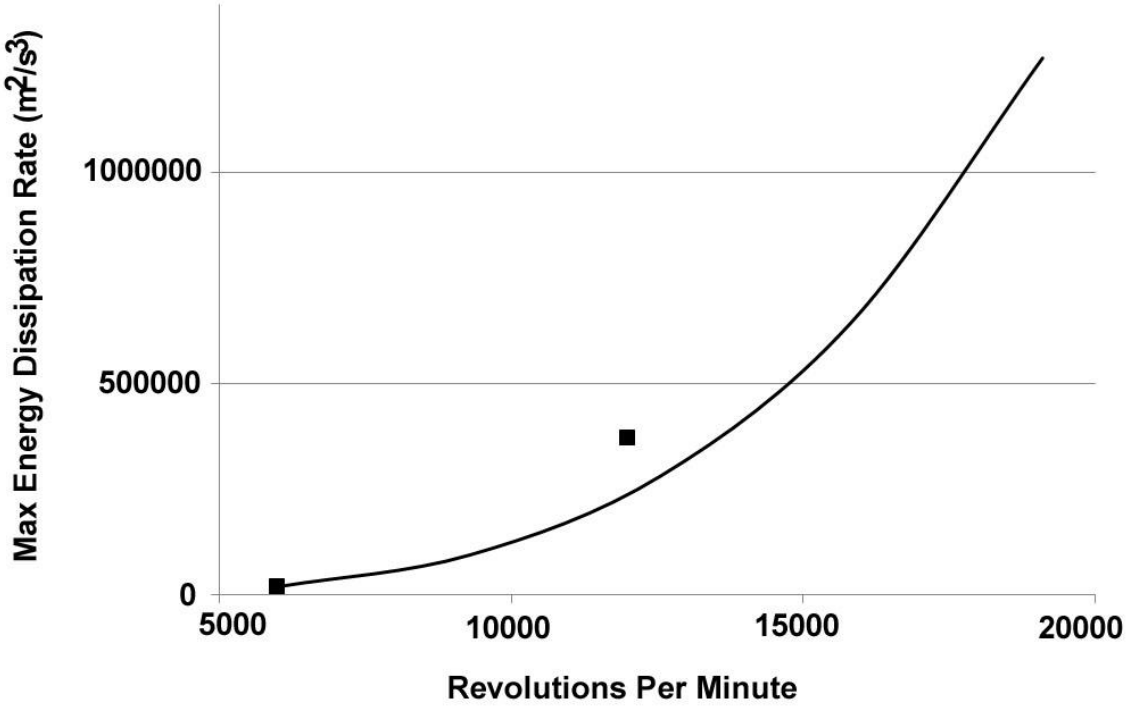

Figure 3.2-2. Maximum energy dissipation rate with increasing disc speed for the rotating disc shear device as modelled by CFD. Literature values from Lau et al. (2013) are also shown (■) for comparison.

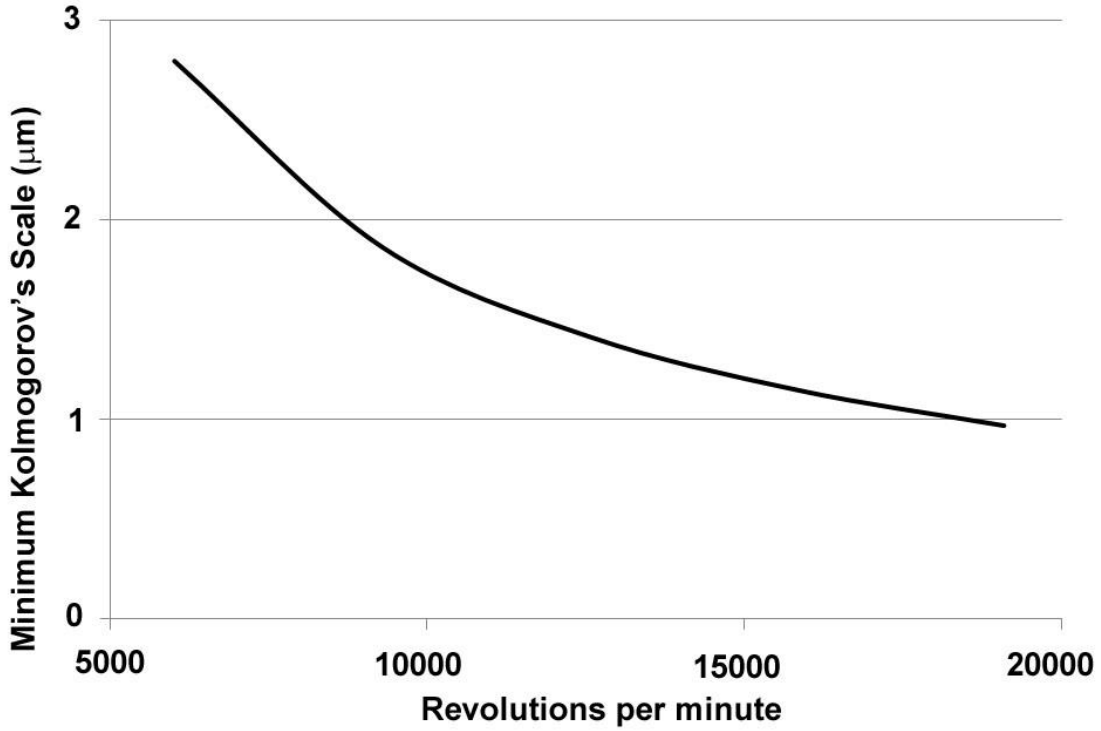

Figure 3.2-3. Minimum Kolmogorov's scale, derived from maximum energy dissipation rate, with increasing disc speed for the rotating disc shear device (based on Eqn. 4, section 1.1.3.1)

In order to further characterise the shear environment the shear tensor was broken down in to its three Eigen value components (section 2.1.1.2). The results for the rotating disc shear device (Figure 3.2-5 to Figure 3.2-8) and continuous centrifuge (Figure 3.2-9 and Figure 3.2-10) reflect well those reported by Boychyn et al. (2001), in that the maximum shear rates are experienced in the same narrow locations; in the rotating disc shear device at the disc tip (at a radial distance of 0.02m), and in the continuous centrifuge at the furthest radial point of the centrifuge feedzone (at a radial distance of 0.057m).

For clarity the eigen values for the rotating shear device are plotted along set flow paths, running in parralel to the rotating disc, as illustrated in Figure 3.2-4. In the rotating shear device the particles are expected to follow a path running parallel to the rotating disc due to the pumping motion set up by the rotation of the disc, discussed further in section 3.2.2.2. At the rotating shear device disc speeds used in this work the particles are expected to pass along this path at least once within a 20 second period. In addition the path along the disc passes through the zone of maximum shear within the shear device. It is for these reasons that it was decided to plot the results along these flow paths.

In the PSC-5 centrifuge the optimum presentation of the CFD derived shear rates is less obvious. The particles are expected to pass through the centrifuge feedzone only once, and be evenly distributed across the inlet branch. In addition the zone of highest shear appears to be less localised across the width of the inlet branch, whilst still remaining a function of the radial distance. For this reason the eigen values are presented in Figure 3.2-9 and Figure 3.2-10 as a scatter plot of all datapoints at a given radial position, ensuring that the maximum shear rate will be amongst those plotted.

It may be noted that the maximum shear rate in the rotating disc shear device and continous centrifuge is of a similar order of magnitude: compare the maximum eigen values in Figure 3.2-6 and Figure 3.2-8 to those in Figure 3.2-9 and Figure 3.2-10. As an hermetic low shear centrifuge, the PSC-5 is expected to be best modelled using a rotating disc shear device disc speed of the order of 6000rpm. This work, however, does not show any direct comparability of the maximum shear rate values in the centrifuge to that in the rotating disc shear device at a speed of 6000rpm (Figure 3.2-6), as oppose to a speed of 12000rpm (Figure 3.2-8). As stated above, this maximum shear rate was the basis of the justification given by Boychyn et al. (2001).

However, comparing Figure 3.2-5 to Figure 3.2-6 and Figure 3.2-7 to Figure 3.2-8 illustrates further the extreme narrowness of this maximum shear location: even at approximately a mammalian cell's width distance of 15μm from the disc surface the maximum shear rate at a radial distance of 0.02m has dropped dramatically, and is far closer to the maximum levels seen in the continuous centrifuge. The scatterplot, for which the density of points at a given shear will depend upon the areas of highest mesh density as oppose to volume, is not so useful in illustrating the degree of localisation for the maximum shear rates in the centrifuge. The heat map of shear rate, however, which can be viewed in Comsol®, shows a similarly narrow volume for the maximum shear rate in the PSC-5 centrifuge (results not shown). The issue of shear levels and spatial distribution is explored further in section 3.2.2.1 below.

The above illustrates the first of the difficulties in simply comparing the maximum shear rates in the two systems.

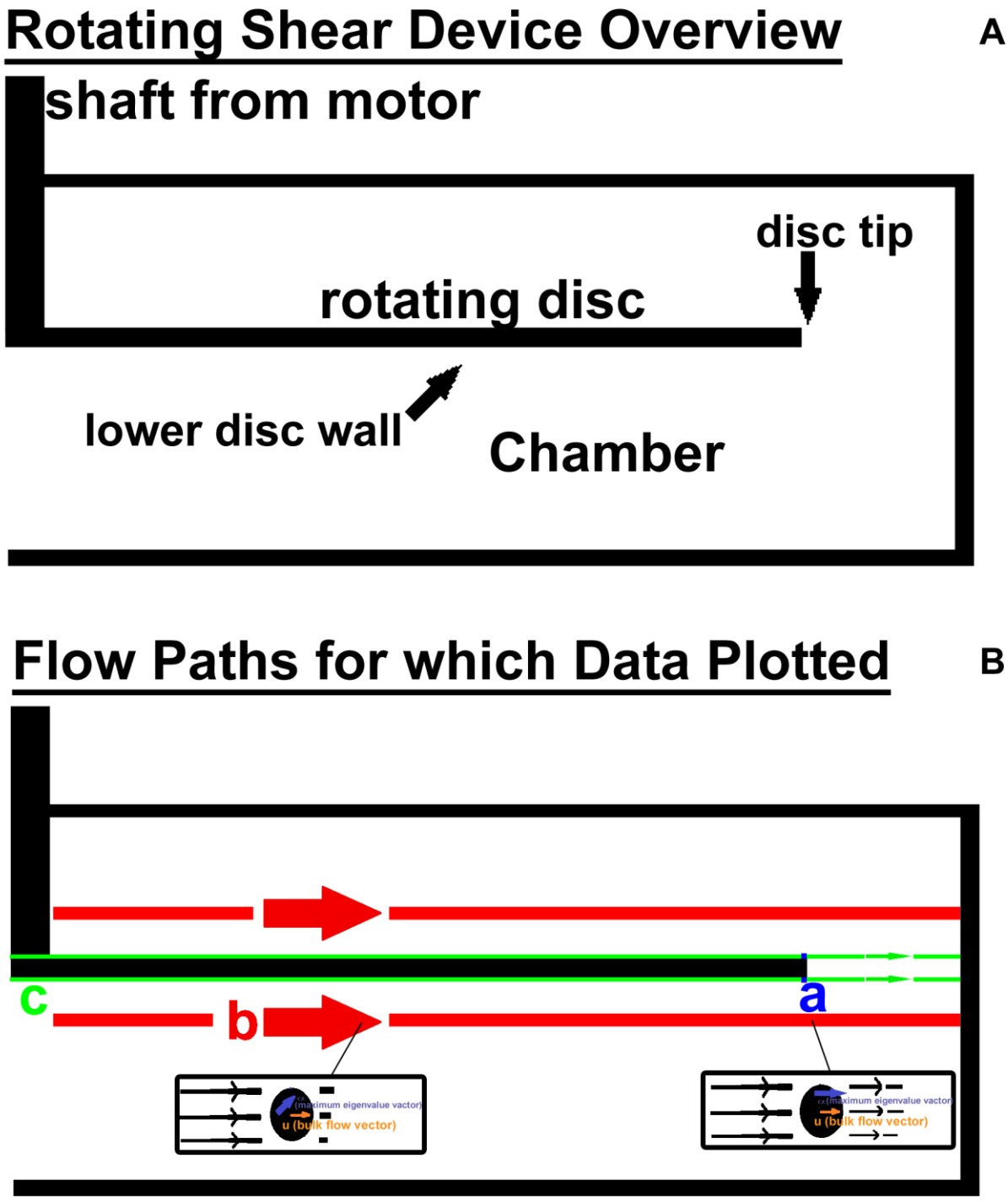

Figure 3.2-4. Schematics of the rotating disc device showing the axi-symmetric cross section (i.e. a cross section of half the device). A. An annotated schematic, designed to indicate the conventions adopted with respect to describing components of the rotating shear device. B. A schematic indicating the flow paths for which data is plotted in the figures in sections 3.2.1.2 and 3.2.1.1, where (a, brown) indicates the highest shear zones at the tip of the rotating disc, (b, red) is a flowpath, parallel to the lower surface of the rotating disc, but offset, in the vertical direction, by a distance of 15µm, representing the approximate diameter of a mammalian cell (n.b. not to scale), and (c, green) is a flowpath along (in very close proximity to) the surface of the rotating disc. The insets illustrate the predominant flow and shear stress vector components at two points along path b, where simple (left) and extensional (right) shear are present.

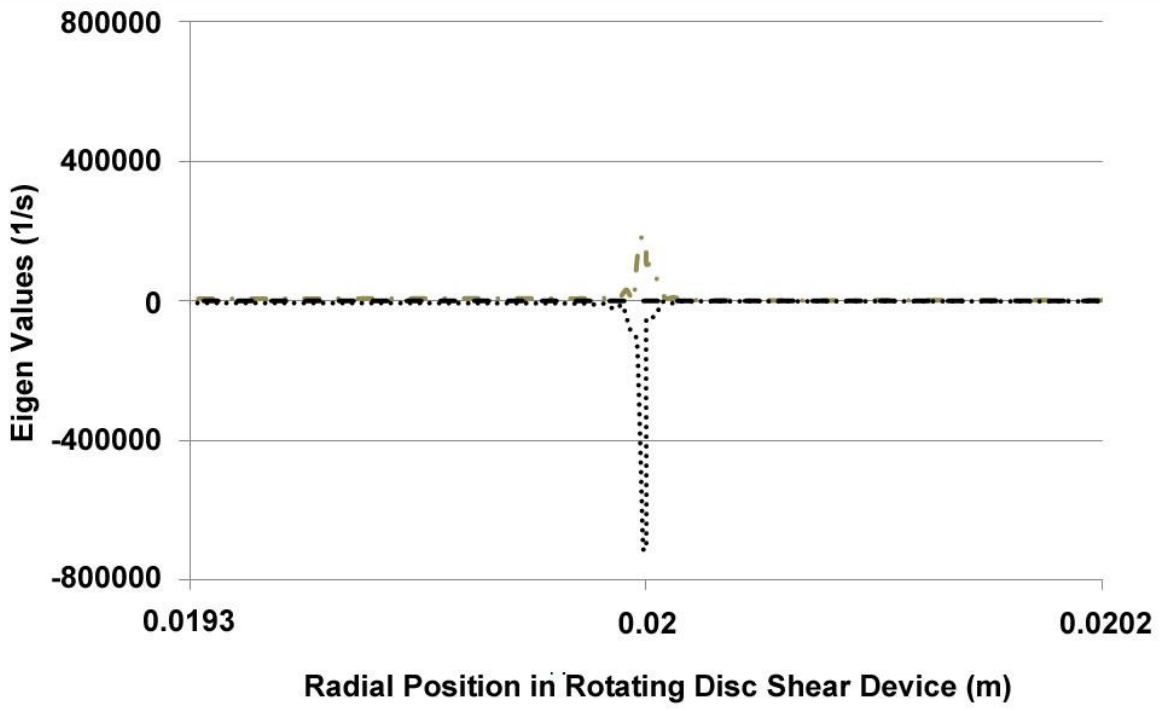

Figure 3.2-5. Eigen Values of the shear tensor along a path following the lower surface of the disc in the rotating disc shear device with increasing radial position, for a disc speed of 6000rpm

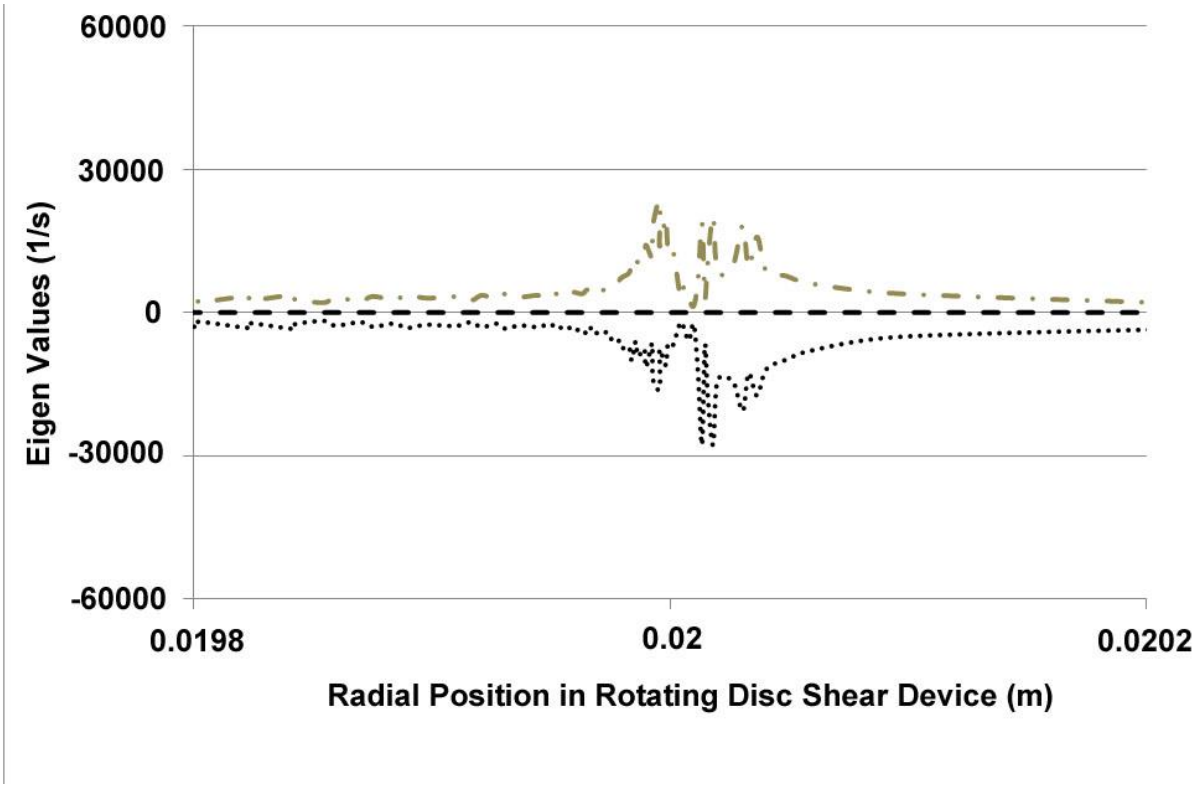

Figure 3.2-6. Eigen values of the shear tensor along a path parallel to the lower surface of the disc, at a distance of 15μm (approximate mammalian cell diameter) below, in the rotating disc shear device with increasing radial position, for a disc speed of 6000rpm. The position of the tip is 0.02m.

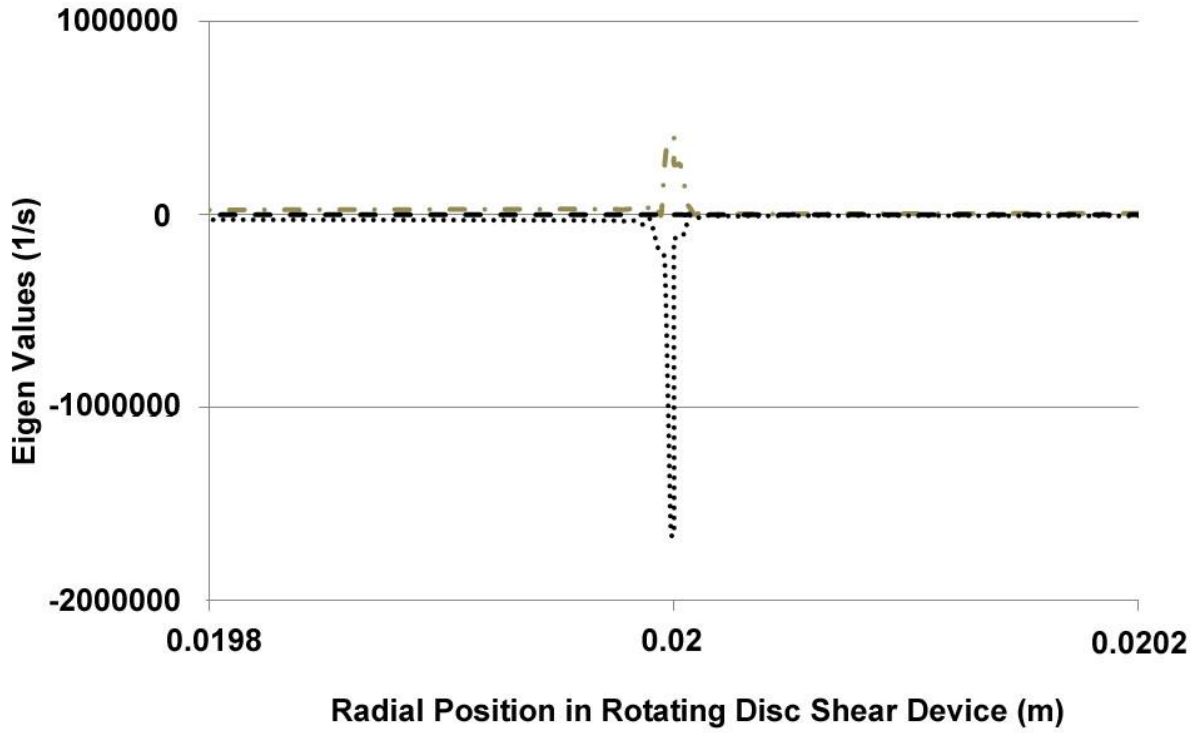

Figure 3.2-7. Eigen Values of the shear tensor along a path following the lower surface of the disc in the rotating disc shear device with increasing radial position, for a disc speed of 12000rpm

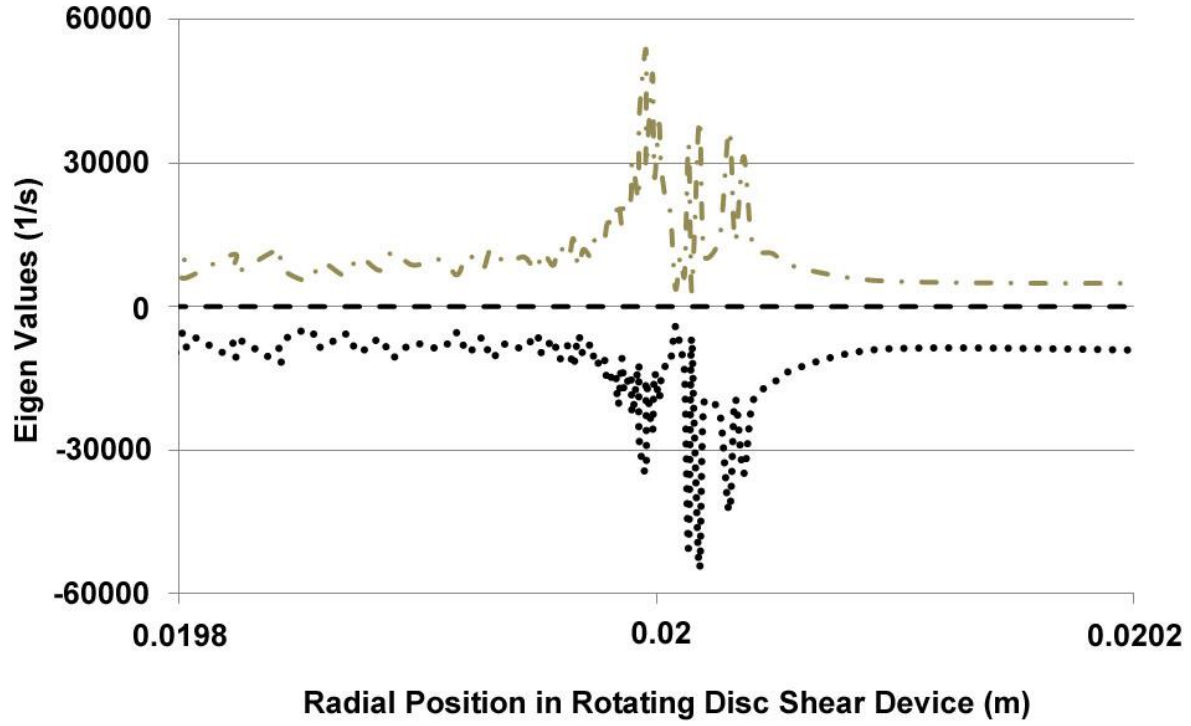

Figure 3.2-8. Eigen values of the shear tensor along a path parallel to the lower surface of the disc, at a distance of 15μm (approximate mammalian cell diameter) below, in the rotating disc shear device with increasing radial position, for a disc speed of 12000rpm. The position of the tip is 0.02m.

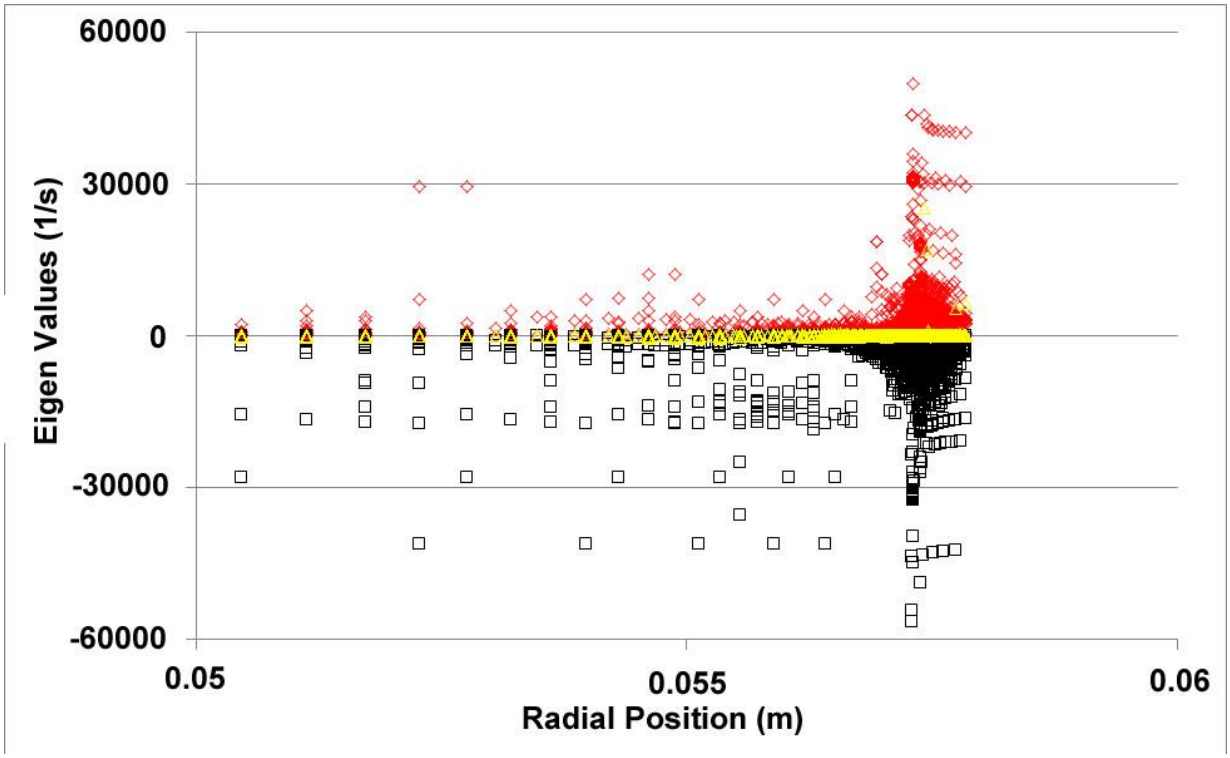

Figure 3.2-9. Eigen values of the shear tensor with increasing radial position in the PSC-5 centrifuge for a rotation speed of 8100rpm, using an axisymmetric model assumption. The three eigenvalues are shown using three different markers (◇, □, Δ).

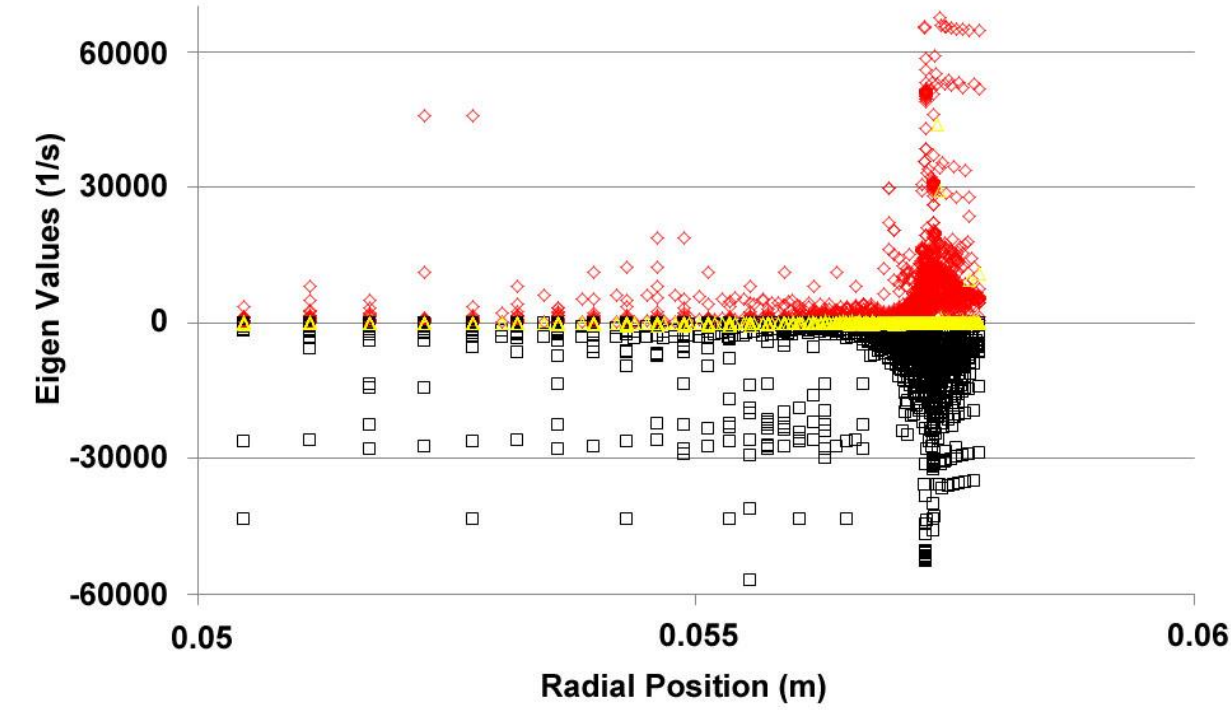

Figure 3.2-10. Eigen values of the shear tensor with increasing radial position in the PSC-5 centrifuge for a rotation speed of 13500rpm, using an axisymmetric model assumption. The three eigenvalues are shown using three different markers (◇, □, Δ).

3.2.1.2. The nature of the flow – Angle of the Eigenvectors

Further complicating the interpretation of the results is that normal and extensional shear stresses may have substantially different impacts (as described in sections 1.1.4 and 2.1.1.2). Understanding the nature of the shear, particularly in the regions where the shear rate is at its maximum magnitude, may therefore supplement our understanding of how these two systems compare. In addition to maximum shear rate, therefore, the angle between the maximum Eigen value vector and the flow field vector was also plotted for the rotating disc shear device (Figure 3.2-11 to Figure 3.2-14) and the continuous centrifuge (Figure 3.2-15 and Figure 3.2-16). This angle gives an indication of the nature of the shear, where an angle of 0° is associated with extensional shear and an angle of 45° indicates normal shear. The angle in the rotating shear device is plotted for the same flow paths, running in parallel to the rotating disc, as used in the preceding section for the eigen values and illustrated in Figure 3.2-4.

The results (Figure 3.2-11 to Figure 3.2-14) show that in the same region where the shear rate in the rotating disc shear device reaches its maximum, i.e. at the disc tip, at a radial distance of 0.02m, the angle drops to 0°, representing an extensional flow. This can be seen far more strongly as we move down (or up) into the chamber and away from the surface of the rotating disc (i.e. onto flowpath b as illustrated in Figure 3.2-4B), where the absolute shear rates are substantially reduced, but also potentially where more particles may pass through. Elsewhere, at radial distances less than 0.02m, in proximity to the rotating disc the shear is normal / simple shear, with an angle of 45°. These different shear types are illustrated in inset in Figure 3.2-4.

The centrifuge when modelled as axi-symmetric shows a similar pattern (Figure 3.2-15 and Figure 3.2-16), in that the angle drop towards 0°, representing an extensional flow, towards the region of highest shear rate, at a radial distance of approximately 0.054m, as seen in figure Figure 3.2-9 and Figure 3.2-10. Elsewhere, at radial distances less than 0.054m, simple shear predominates.

Thus in both the rotational shear device and centrifuge, at the region of maximum shear rate (a radial distance of 0.02 and 0.054m respectively) the shear is extensional, whilst elsewhere the shear is more likely to be simple / normal shear.

It might be inferred from the above that the shear in the rotating disc shear device is not only of a similar order of magnitude to that the continuous centrifuge, with a similarly narrow spatial concentration, but it is also of a similar nature. However, these conclusions are expected to be strongly dependent on the fact that the continuous centrifuge has been treated as axi-symmetric. To test the impact of this modelling simplification, this approach has been extended to make use of the 3-D rotating machinery function available in the COMSOL Multiphysics® package.

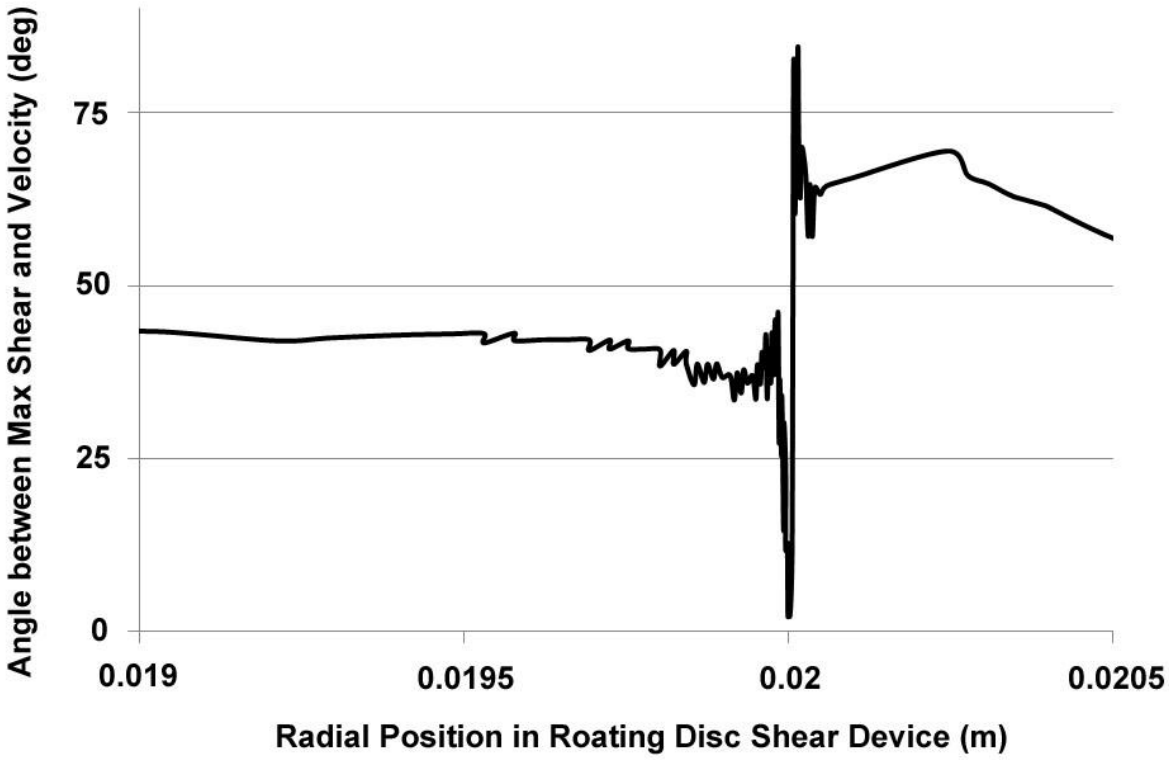

Figure 3.2-11. Angle between the direction of the maximum Eigen value vector and the flow field vector along a path running parallel to the lower surface of the disc, at a distance of 15μm (i.e. the approximate diameter of a mammalian cell) below in the rotating disc shear device with increasing radial position for a disc speed of 6000rpm. The position of the tip is 0.02m.

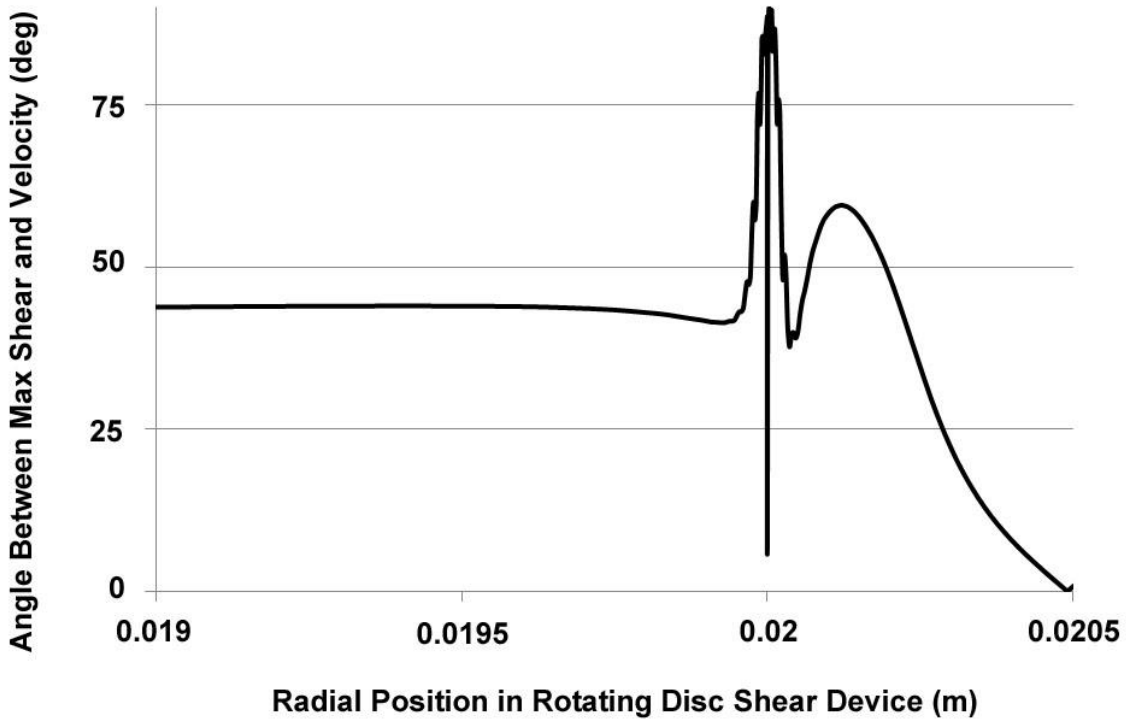

Figure 3.2-12. Angle between the direction of the maximum Eigen vector and the flow field vector following the lower surface of the disc in the rotating disc shear device with increasing radial position, for a disc speed of 6000rpm.

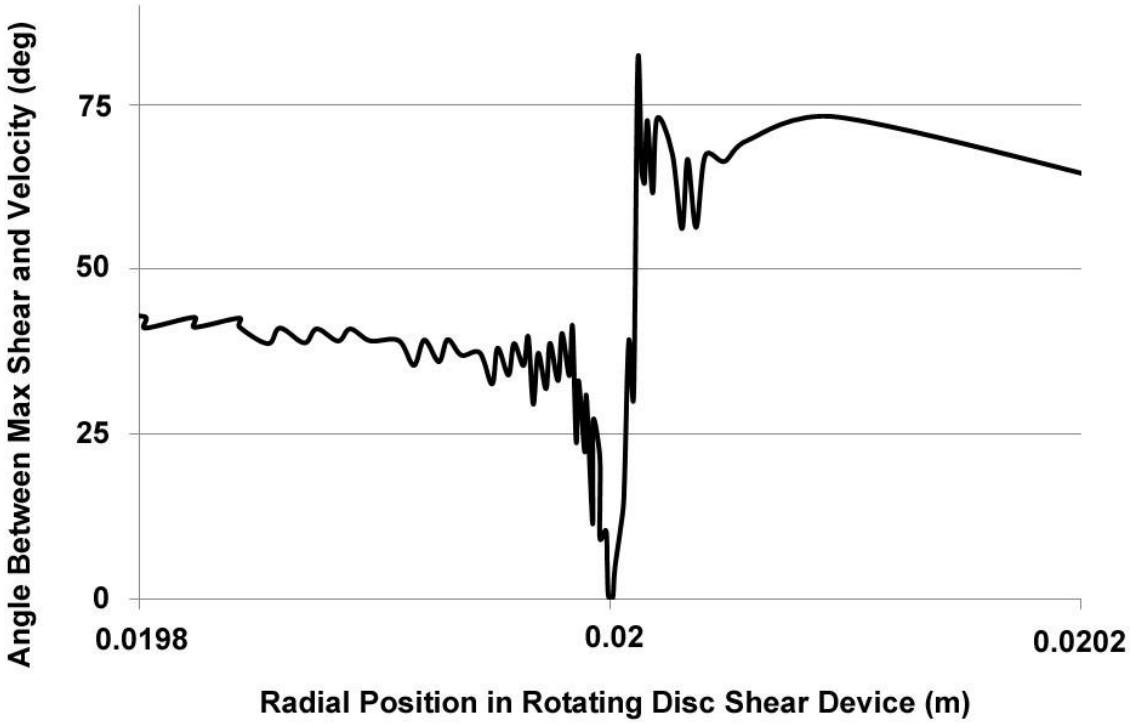

Figure 3.2-13. Angle between the direction of the maximum Eigen value vector and the flow field vector along a path running parallel to the lower surface of the disc, at a distance of 15μm (i.e. the approximate diameter of a mammalian cell) below in the rotating disc shear device with increasing radial position for a disc speed of 12000rpm. The position of the tip is 0.02m.

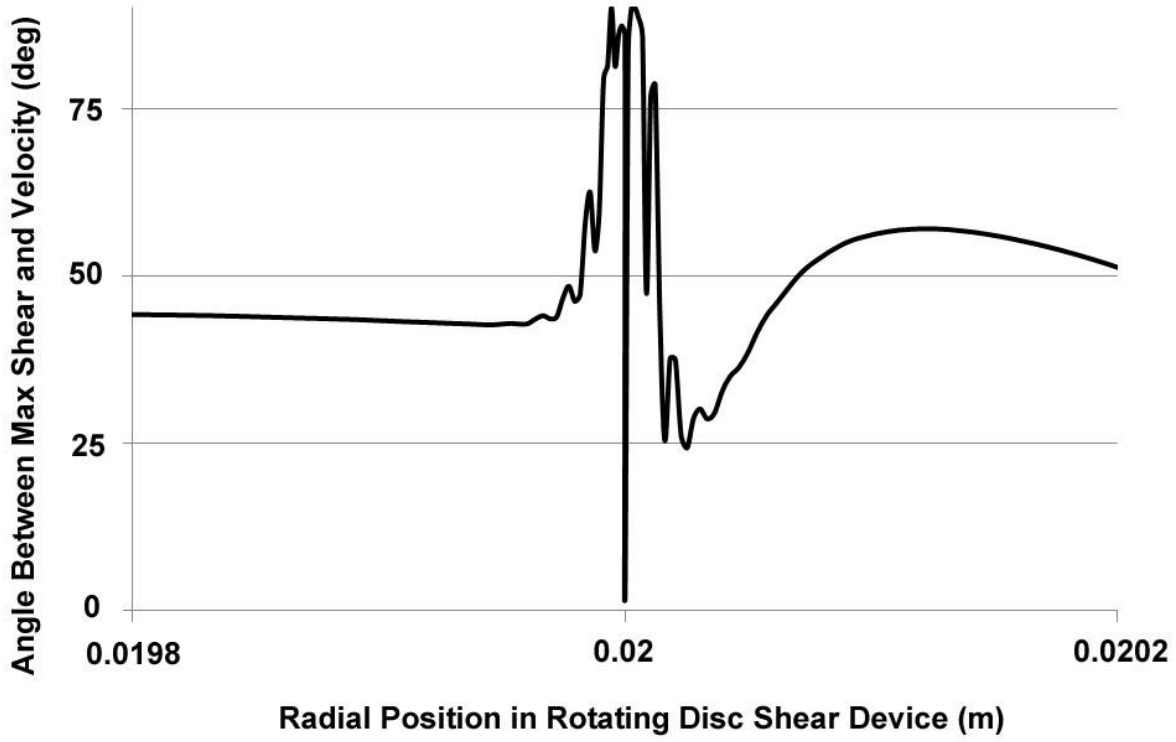

Figure 3.2-14. Angle between the direction of the maximum Eigen vector and the flow field vector following the lower surface of the disc in the rotating disc shear device with increasing radial position, for a disc speed of 12000rpm.

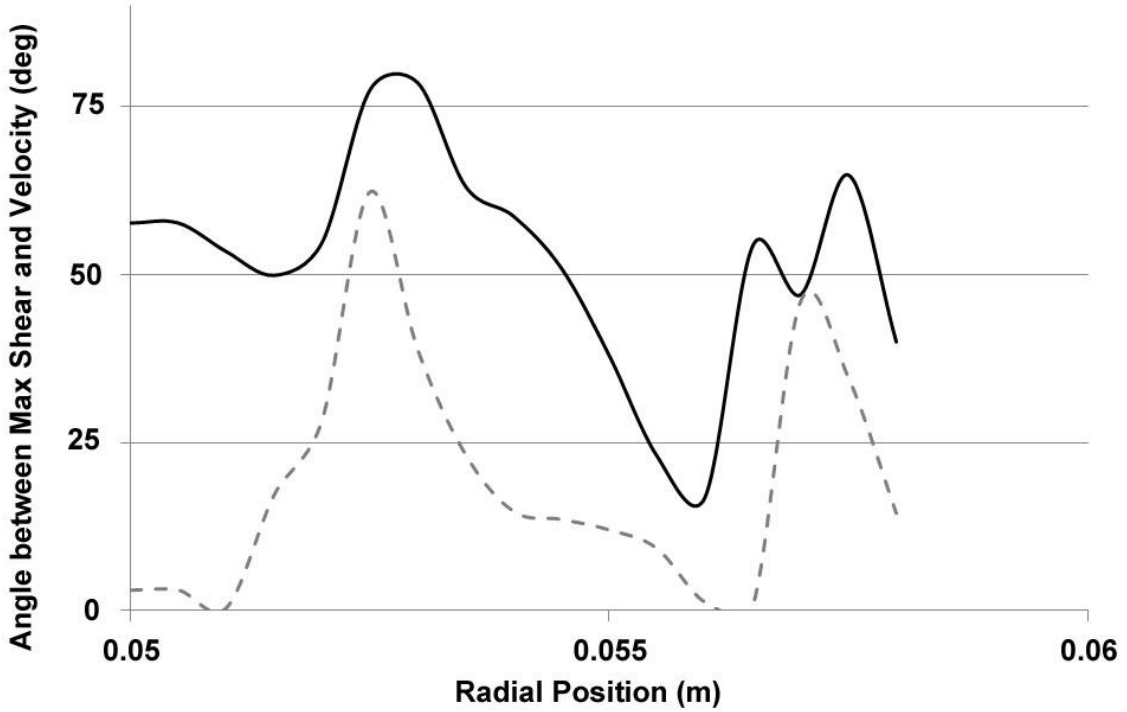

Figure 3.2-15. Angle between the direction of the maximum Eigen value vector and the flow field vector with increasing radial position in the PSC-5 centrifuge for a rotation speed of 8100rpm, using an axisymmetric model assumption. Lines indicate the upper and lower bound values across the width of the inlet branch.

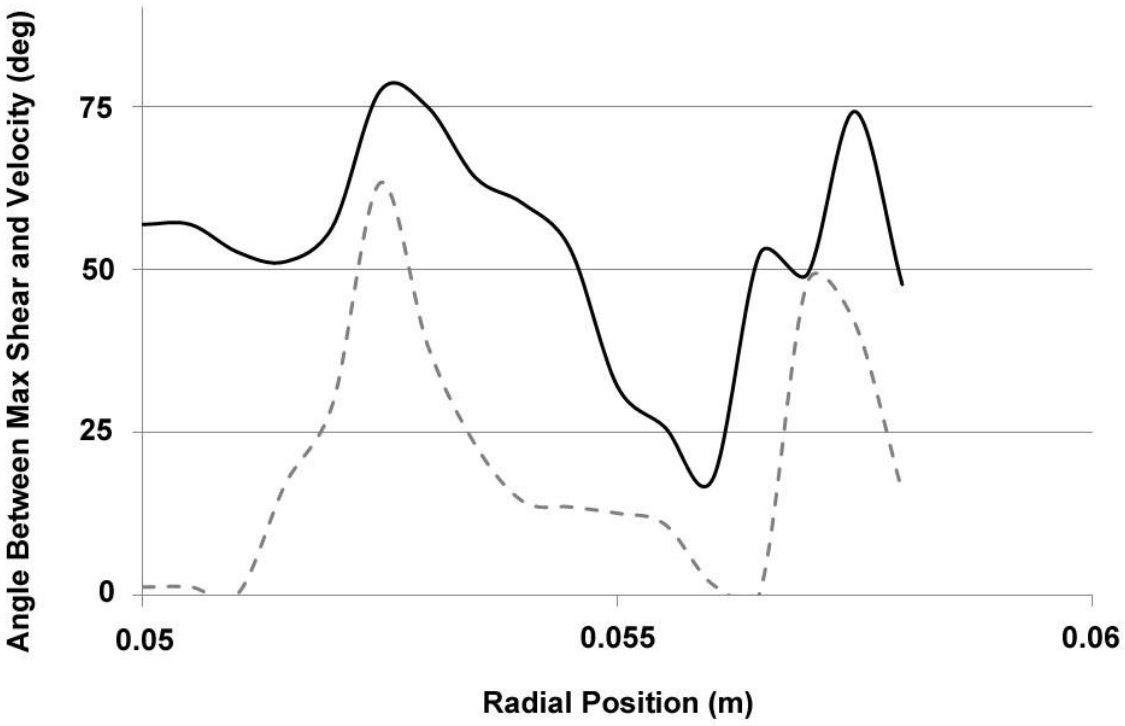

Figure 3.2-16. Angle between the direction of the maximum Eigen value vector and the flow field vector with increasing radial position in the PSC-5 centrifuge for a rotation speed of 13500rpm, using an axisymmetric model assumption. Lines indicate the upper and lower bound values across the width of the inlet branch.

3.2.2. Modelling the 3D-Rotating Machinery

3.2.2.1. Maximum Shear Rate

The continuous PSC-5 disc stack centrifuge was modelled in 3 dimensions, accounting for the division of the inlet into discrete sections or branches in the inlet distributor, using the rotating machinery function in COMSOL Multiphysics®. Comparing Figure 3.2-17 and Figure 3.2-9 the shear levels in the 3D model are highly comparable to those from the 2D axi-symmetric model. The data points shown in both Figure 3.2-17 and Figure 3.2-9 are as per the mesh point outputs, i.e. areas of denser meshing will contribute disproportionately to the points shown.

Intuitively, the time that particles spend in a given shear zone can be expected to be related to the size of that shear zone, and thus the probability of the particle being damaged by that given level of shear likewise. For this reason the analysis was extended further, as shown in Figure 3.2-18, to account for the proportion of the liquid within the system that is subjected to a given level of shear. It can be observed in both figures that the maximum shear rate in the rotating disc shear device is substantially higher than in the continuous centrifuge. However, as a

proportion of the volume the PSC-5 centrifuge shows a greater volume in which the shear rate is high as compared to the rotating disc shear device. It may be further argued that the exposure time will also be a function of the particle speed and flow path. This latter issue is explored in more detail in section 3.2.2.2 below.

Finally it may also be observed from Figure 3.2-18 that the level of shear in the ultracentrifuge is very much comparable to that seen in the PSC-5 centrifuge, suggesting that these two centrifuge types may cause a similar level of shear damage.

With respect to the angle the comparison to the axisymmetric model is less clear cut (compare Figure 3.2-19 and Figure 3.2-15). A mixture of extensional and normal shear can be seen along the length of the feed zone; however, there is no substantial move towards extensional shear toward the highest shear point, with a maximum shear rate in the sub 10 degrees angle range of the order $1x10^4$/s. This difference in the nature of the shear, in terms of normal versus extensional flow is accounted for in the population balance analysis described in section 3.2.2.2.

It should also be noted that there will be differences in the way the axi-symmetric and rotating machinery physics approximate to shear. It was intended to run additional simulations of the rotating disc shear device to confirm the significance of this, but there was insufficient time to debug and converge the model.

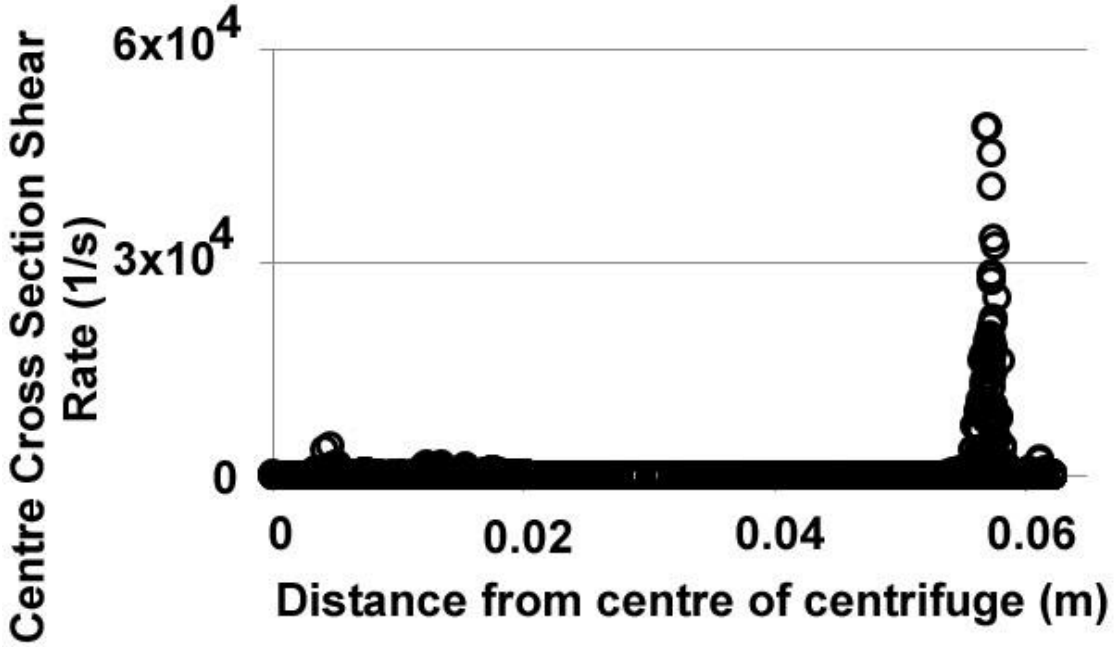

Figure 3.2-17. Shear rate in the PSC-5 as modelled using the 3-D rotating machinery method with increasing radial distance for a centrifuge rotatory speed of 8.1krpm.

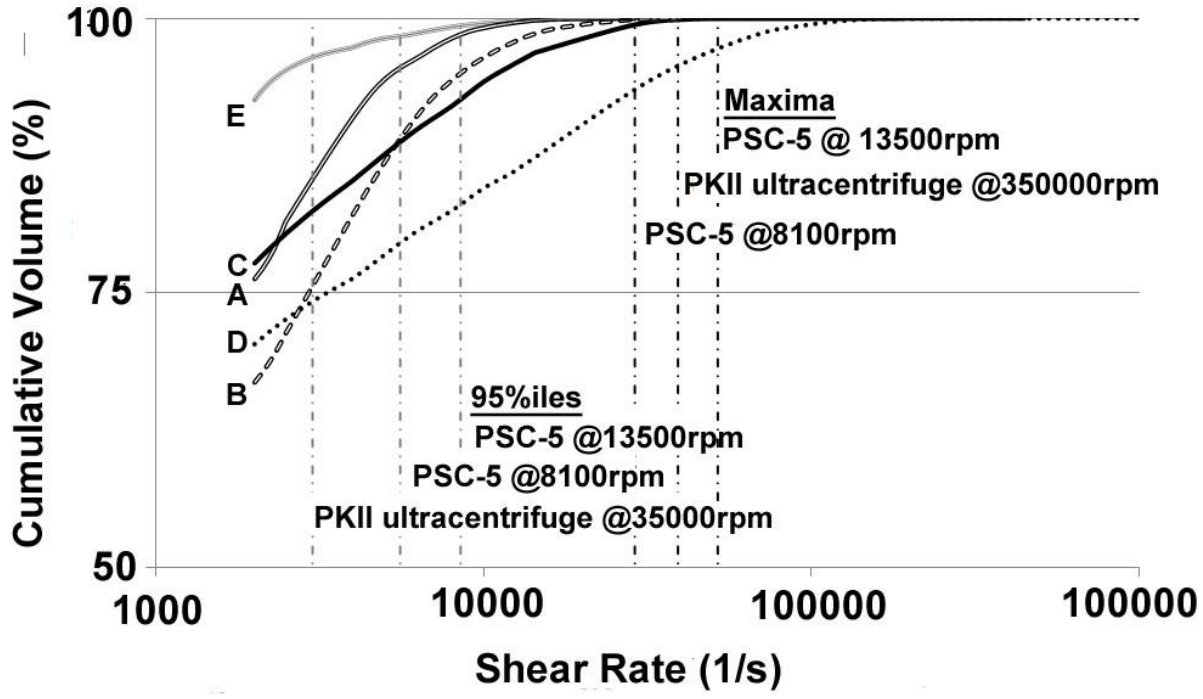

Figure 3.2-18. Cumulative % of volume for which the shear rate is below the value plotted on the x-axis. For the rotating disc shear device at a disc speed of 6krpm (A) and 12krpm (B), for the PSC-5 centrifuge modelled using the rotating machinery function for a rotating speed of 8.1krpm (C) and 13.5krpm (D) and for the PKII centrifuge for a rotating speed of 35krpm (E). Vertical lines are shown marking the 95%ile and maximum shear for the centrifuges.

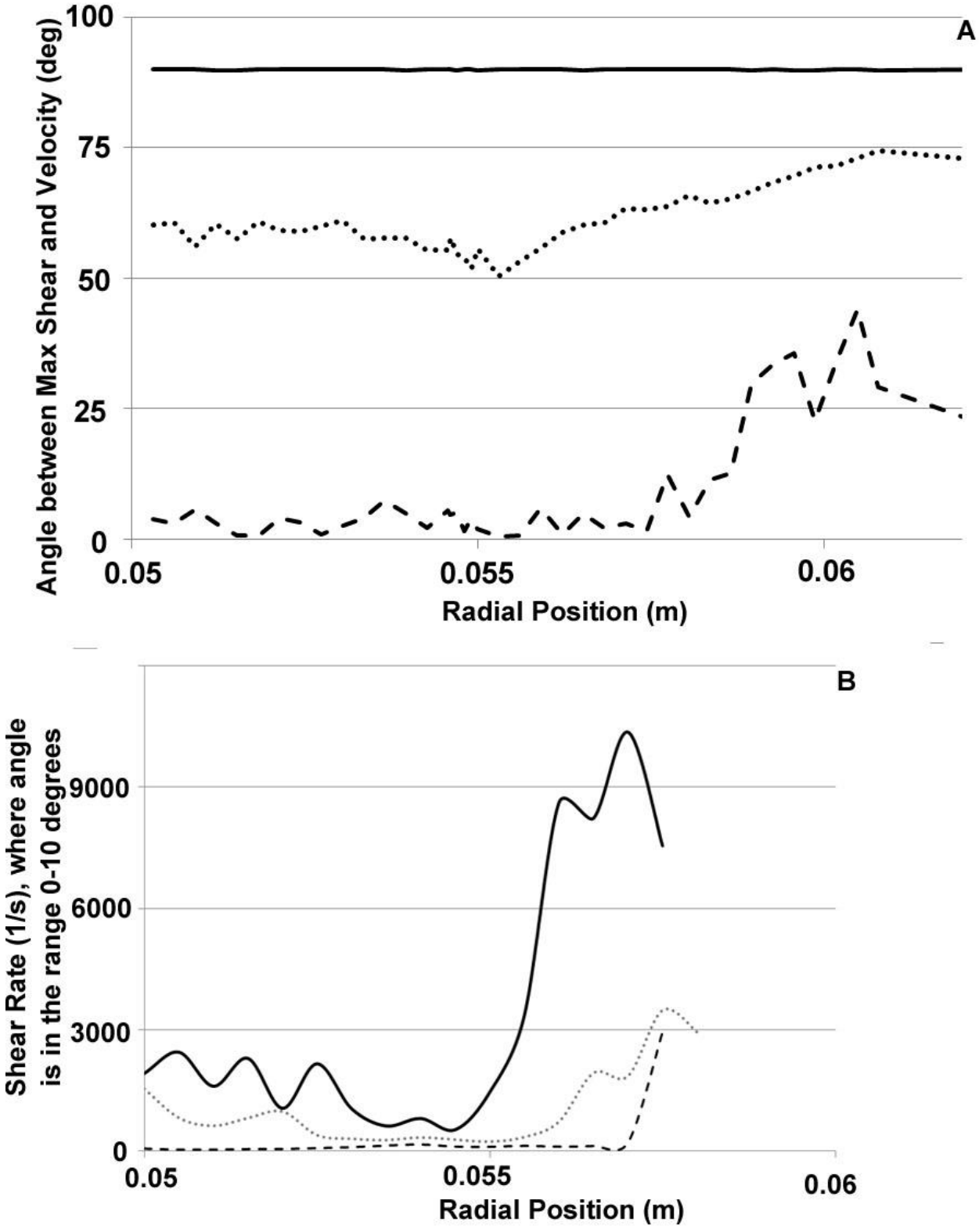

Figure 3.2-19. Angle between the direction of the maximum Eigen value vector and the flow field vector (A) and shear rate for angles below 10 degrees (B), with increasing radial position in the PSC-5 centrifuge for a rotation speed of 8100rpm, using the rotating machinery function. Lines indicate the upper, average and lower bound values across the width of the inlet branch.

3.2.2.2. Population Balance

As described in section 2.1.1.4 a simplified population balance analysis has been conducted with the aim of accounting for the shear level, time of exposure to a given shear rate level and nature of the shear. This simplified population balance involved applying an energy dissipation rate dependent breakage rate formula to particles traveling along set paths through the rotating disc shear device and industrial centrifuge feedzone.

In doing so it is necessary to consider the particle behaviour within the rotating disc shear device and continuous centrifuge. It is expect that this particle movement will be very different in these two systems. Specifically, as illustrated in Figure 3.2-20, the disc sets up a pumping action in the neighbouring fluid, thus the particles in the rotating disc shear device can be expected to pass through, or close to, the highest shear zone a number of times. Figure 3.2-21 further illustrates this, along with the narrowing and acceleration of the highest shear zone of liquid in proximity to the disc with increasing disc speed. It may also be noted that further from the disc tip there appear to be more stagnant zones, with particles which are less likely to enter into high shear zones during the running period. The particles in the PSC-5 centrifuge by contrast might reasonably be expected to travel parallel to the feed zone distributor branches' walls, at a speed approximately equal to that of the suspending liquid, and be evenly distributed across the channel. This assumption makes the exposure time of the particles to shear rates a strong function of the flow rate and the volumes over which different shear rates apply irrespective of precise position within the inlet zone.

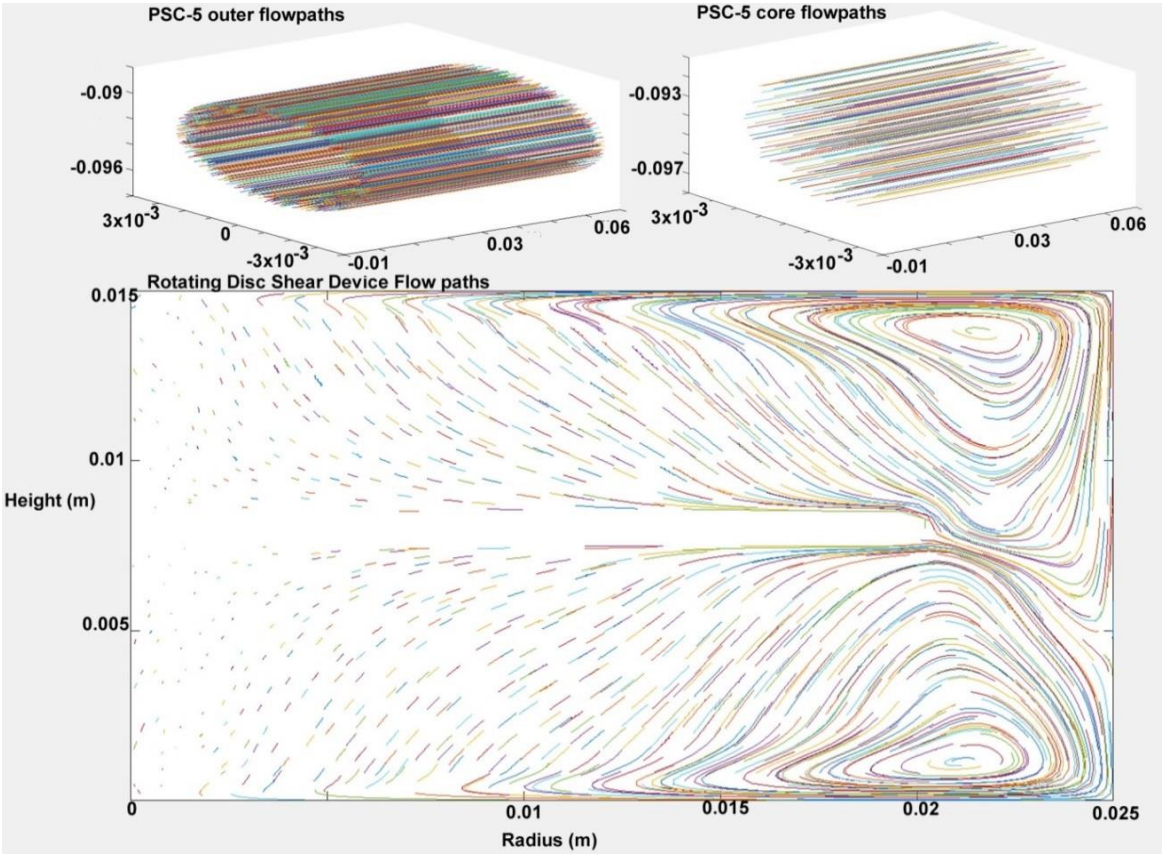

Figure 3.2-20. Particle paths assumed in the rotating disc shear device and PSC-5 centrifuge. The paths in the rotating disc shear device are based on output from the particle tracing model. The PSC-5 flow paths are parallel to the walls of the centrifuge inlet branches and for computational efficiency were modelled in two sections: the core and, in finer detail / greater concentration of particles, around the outer rim where the changes in shear are steeper.

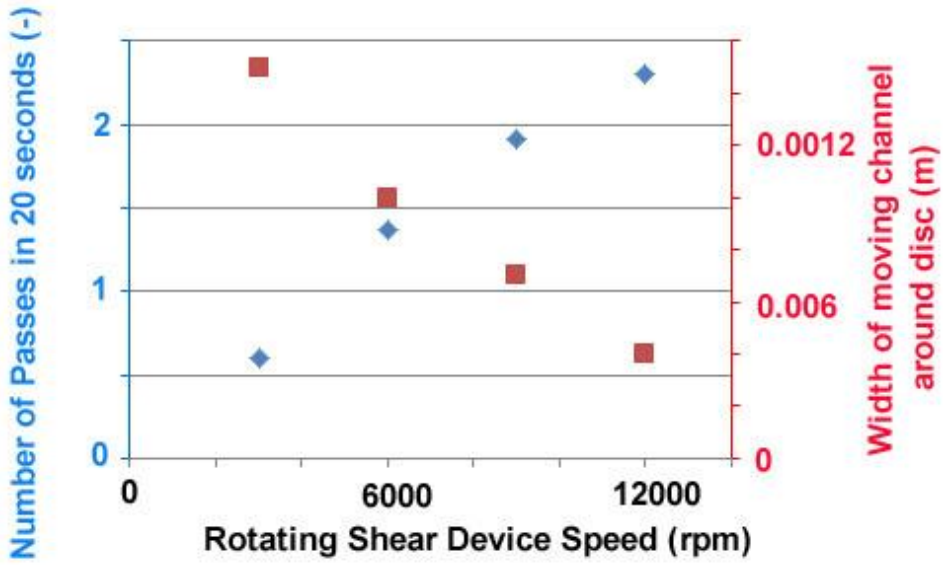

Figure 3.2-21. Average number of passes through the zone in proximity to the disc tip for a particle over a 20 second period in the rotating disc shear device with increasing disc speed (◆), and, on the right hand axis, the approximate width of the high speed boundary layer at the disc surface with increasing disc speed (■).

Figure 3.2-22 shows the predicted particles breakage for the PSC-5 centrifuge for rotating speeds of 8100rpm and 13500rpm at flow rates of 100, 200 and 350lph, i.e. over the range of centrifuge operation. The predictions produced by this methodology fall within the expected range, particularly towards the upper end. The slightly lower than expected predicted rotating shear device speed may be due to the need for further optimisation of the breakage kernel parameters (see supplementary material in Appendix C) or uncertainties in geometries measured, the impact of which is explored further in section 3.2.2.3. It could also be a result of the assumptions around flow path, particle distribution and particle speed, which may for example be slower in proximity to the centrifuge distributor walls where the shear rate is highest.

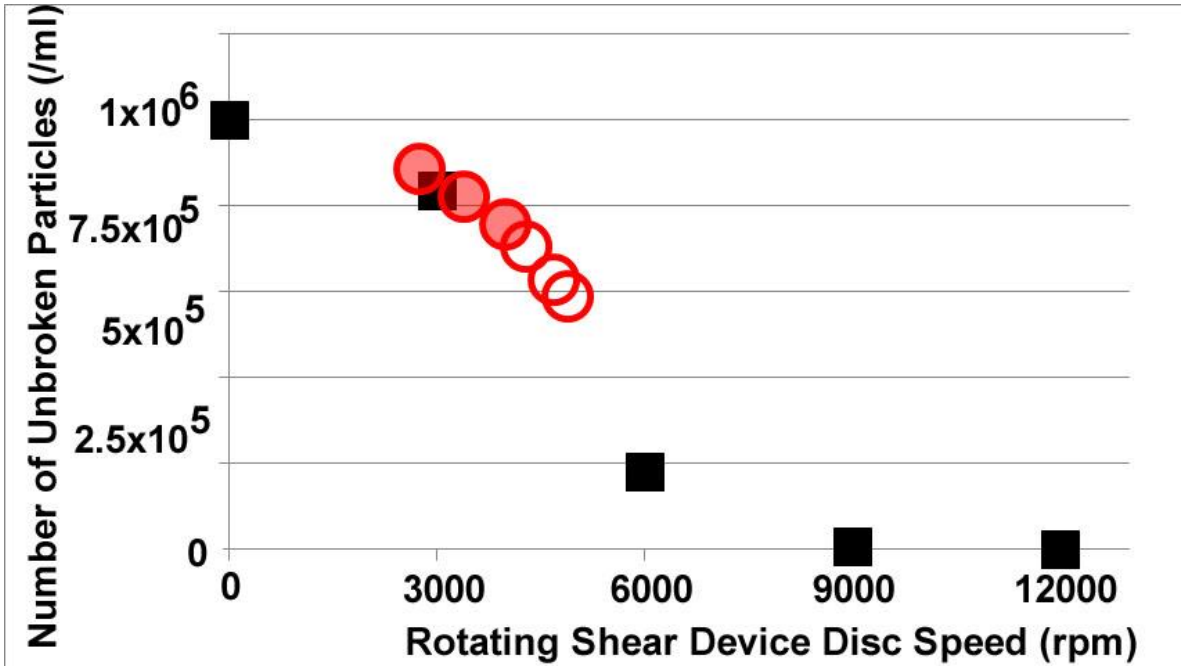

Figure 3.2-22. Predicted particle breakage for a selected set of particle breakage parameters (run 4), along the curve for the rotating disc shear device, indicating the equivalent disc speed for the given PSC-5 operating conditions. The operating conditions cover the full range of flows and rotational speeds. PSC-5 for three flowrates and two speeds (◯) and rotating disc shear device at 5 different speeds (■)

3.2.2.3. Model Sensitivity analysis using ANOVA

Sensitivities were conducted with two key aims. Firstly due to the difference in the geometry of the PSC-5 centrifuge used by GSK, and the PSC-1 centrifuge available at UCL for runs with the shear mimic; differences which are described in section 2.1.1.7. Secondly due to the uncertainties inherent in manual measurements. In addition, it is hoped that this analysis will provide some insight into the importance of

the various parameters when making predictions respecting the relative impact of shear that different centrifuge models are likely to suffer.

Design Expert 10 (Stat-Ease, Inc., Minneapolis) was used to analyse the impact outputs, as measured by rotating disc speed required to replicate particle breakage. The ANOVA gave a significant model as follows:

$$\%\ of\ Rotating\ Disc\ Speed\ for\ PSC-5@\ 13500rpm\ \&\ 350lph = 90.44 - 3.41 \times R_{outer} + 9.31 \times RPM - 12.19 \times Flow + 4.25 \times D_{branch} + 8.41 \times Angle - 1.91 \times R_{outer} \times D_{branch} + 2.09 \times R_{inner} \times RPM + 2.47 \times R_{outer} \times R_{inner} \times Angle - 2.66 \times R_{outer} \times RPM \times D_{branch} + 2.12 \times R_{inner} \times RPM \times Angle + 2.47 \times R_{outer} \times R_{inner} \times RPM \times Angle - 3.75 \times R_{outer} \times RPM \times D_{branch} \times Angle$$

[Eq. 13]

Where the terms of greatest significance (all above 99%ile) are the rotational speed (RPM), the flow (Flow), the diameter of the distributor channels (D_{branch}), and its angle from horizontal (Angle), followed by the outer radius of the inlet distributor (R_{outer}). Where the variables have been normalised to the ranges 57.7 to 67.7mm for outer radius, 8100 to 13500rpm for rotational speed, 100 to 350lph for inlet flow, -30 to +30degrees for angle, 6.36 to 8.36mm for channel diameter and 10.35 to 14.35mm for inner radius, such that the minimum values are coded as -1 and the maximum values are coded as +1. And where the equivalent rotating disc shear device speed for the PSC-5 operating at 13500rpm and 350lph was 5000rpm.

A reasonable match to the data is also achieved with a simpler formula, which will be used in later analysis:

$$\%\ of\ Rotating\ Disc\ Speed\ for\ PSC-5@\ 13500rpm\ \&\ 350lph = 90.44 - 3.41 \times R_{outer} + 9.31 \times RPM - 12.19 \times Flow + 4.25 \times D_{branch} + 8.41 \times Angle - 3.75 \times R_{outer} \times RPM \times D_{branch} \times Angle$$

[Eq. 14]

There is room for greater exploration of the impact of various parameters, in particular flow rate. The impact on the Computational Fluid Dynamics (CFD) output was not substantial within the range considered. However, the impact on particle breakage predictions is substantial; a fact inherent in the assumption which ties exposure time based on particle speed to flow rate.

3.3. Experimental corroboration of CFD analysis

The above, with its complexity, flexibility of interpretation, and the impact of modelling/analytical choices, demonstrates the difficulty of relying on Computational Fluid Dynamics (CFD) analysis alone and the need of experimental validation.

In addition to the validation described below in sections 3.3.1 and 3.3.2, a novel shear mimic material was used to validate the CFD predictions, as described in Chapter 4.

3.3.1. Testing using mammalian cell material

The PSC-5 disc stack centrifuge was used to centrifuge two different types of mammalian cell, one CHO and one of HEK cells (see section 2.2.1.2). The same cell batches were also sheared in the rotating disc shear device and centrifuged in a lab scale centrifuge using standard Ultra Scale-Down (USD) methodology, to give clarification versus Q/Σ relationships at different shear levels (see section 2.2.1.1 and 2.2.1.3). These results are shown in Figure 3.3-1.

As shown in previous work, the level of clarification decreases with increasing shear as more cells are broken up into finer debris, taking a longer centrifugation time or higher centrifugation speed to achieve equivalent clarification. The results also indicate a dependence of the clarification on specific culture conditions (shake flask versus stirred bioreactor) and/or cell type (CHO versus HEK). This upstream process dependence means that simply knowing the shear level in the industrial centrifuge, whilst essential, is insufficient for parameterisation of the process. The USD experimental procedure will still have value both in allowing this shear rate to be interpreted in terms of clarification, host cell protein release, and in determining the sensitivity of these parameters to the operating conditions. The process parameters of clarification and host cell protein release are selected as they are likely to impact substantially on the performance of subsequent downstream processing units, and are thus key to understanding the wider implications of the centrifuge operating conditions.

It should be noted that the CHO and HEK cells used were provided by a research facility at GSK and were originally produced for upstream process development studies. Production of large quantities of mammalian cells, particularly where

consistent properties are required, is not trivial. It can also be observed that despite nearly identical operating conditions in the centrifuge the apparent level of shear for these two cell types does not appear to be identical. This may be due to the assumption of a fixed value to account for non-idealities in the centrifuge, as discussed in section 1.1.3.1. The appropriate value can be expected to vary in reality with particle concentration, size, type and media properties such as viscosity.

In Figure 3.3-1 the large black circles, representing the clarification of the PSC-5 at the Q/Σ associated with these operating conditions (8500rpm, 200lph), sits more or less on the line representing laboratory scale clarification following shearing in the rotating shear device at 6000rpm (triangles). More precisely, by extrapolation from the clarification at various shear levels, the corresponding shear device speed was 6.1 and 4.6krpm for CHO and HEK cells respectively, whilst based on measurement of protein (Figure 3.3-2) the corresponding speed was 5.5krpm. This result appears to validate the assumption that the PSC-5 centrifuge is a low shear centrifuge model, whilst also demonstrating the variability which comes from working with biological process material. It may be noted from Figure 3.3-1 and Figure 3.3-2 that, with the exception of two outliers, the measured points match well to the lines fitted through them according to the standard methodology. The difference in corresponding shear device speed noted above is unlikely therefore to be due to experimental variability. Further repeats, however, would be required to confirm that these two processes / cell-lines will consistency give the same result.

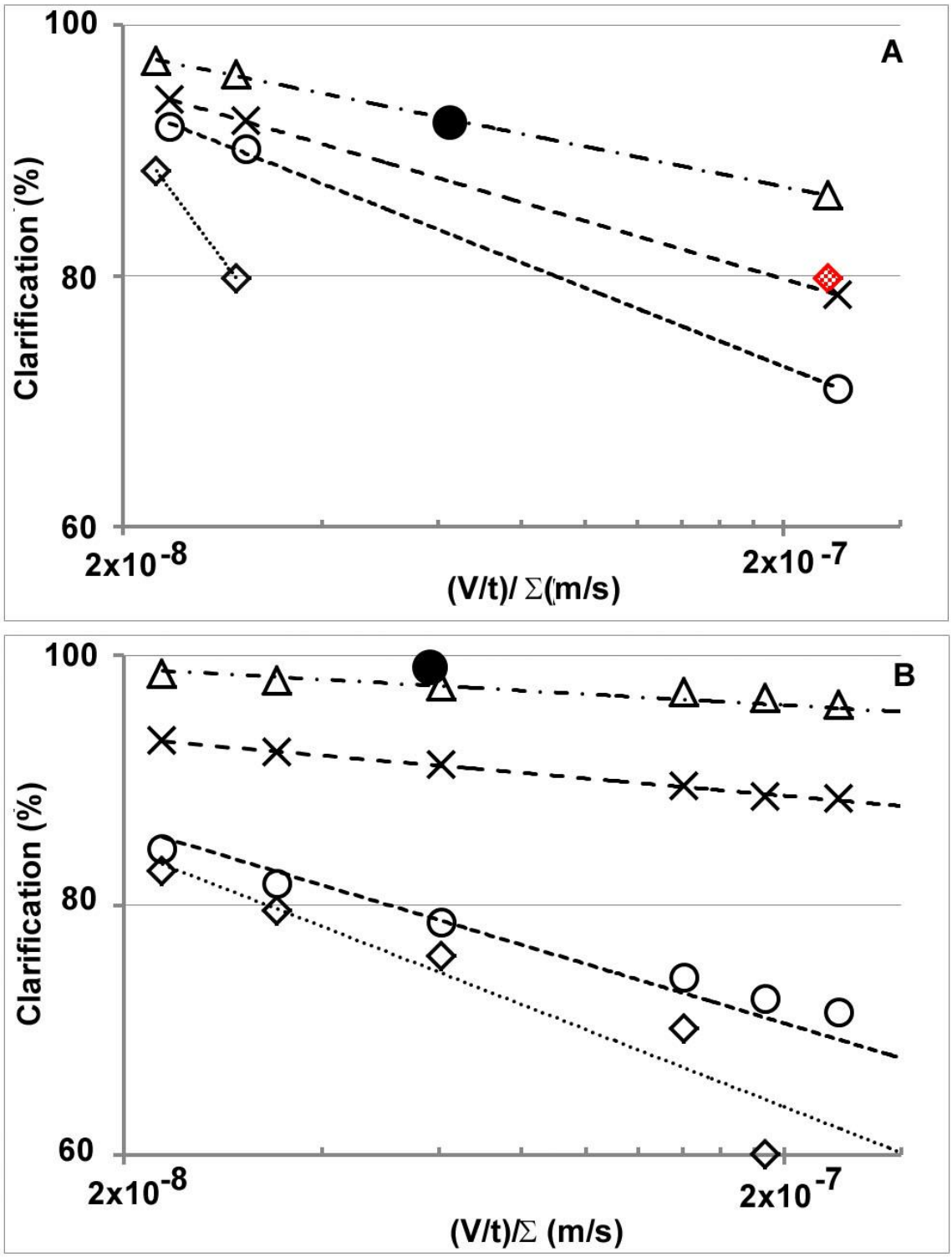

Figure 3.3-1. Clarification of mammalian cells with varying flow rate to settling area ratio (V/Σt) for CHO cells (A) and HEK cells (B). Samples were subject to different levels of shear in the rotating shear device and then processed using a laboratory centrifuge. Shear rates of 6krpm (△), 8krpm (✕), 10krpm (○) and 12krpm (◇) were used. The large filled circle (●) is the steady state industrial scale clarification in the PSC-5 centrifuge. The red point with hatched fill is an outlier.

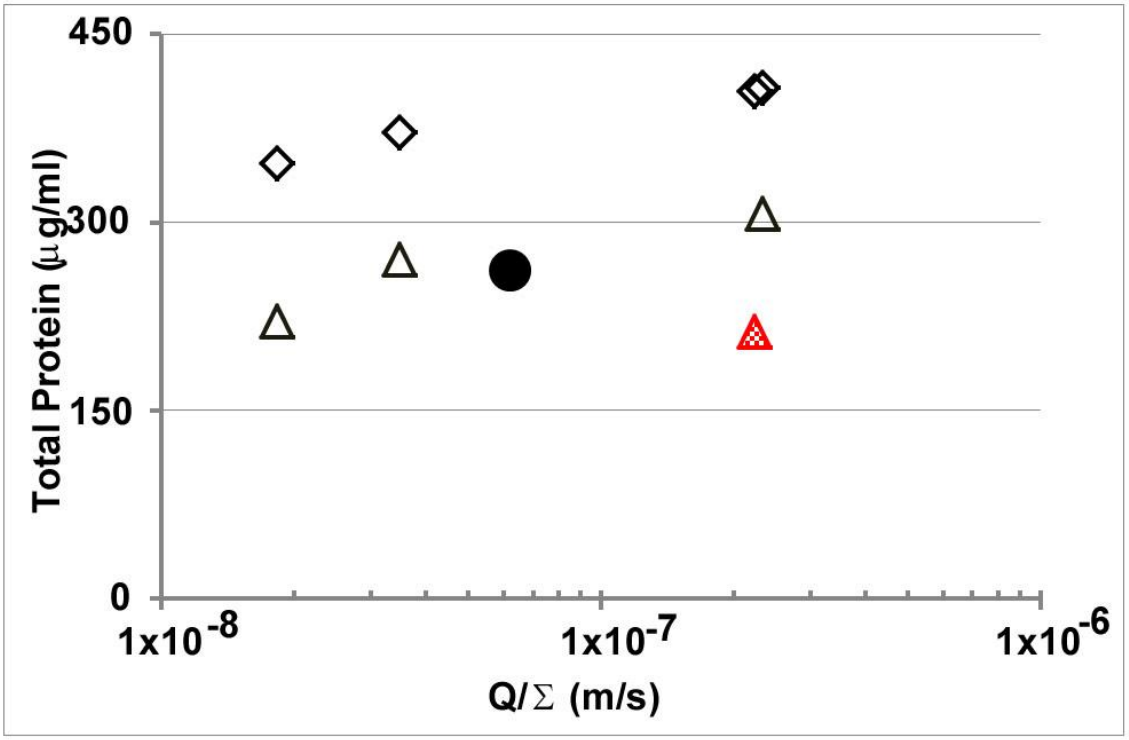

Figure 3.3-2. Supernatant protein concentration following clarification over varying flow rates to settling area ratio (V/Σt) for CHO cells. At laboratory scale the samples were subjected to two different levels of shear in the rotating shear device: 6krpm (△), 12krpm (◇). The large filled circle (●) is the protein concentration in the supernatant at steady state from the industrial scale PSC-5 centrifuge. The red point with hatched fill is an outlier for which a repeated was requested. Measurement provided by Emilie Boulanger at GSK, Rixensart.

3.3.2. Review against Data Available in Literature

Using Eqn. 14 (section 3.2.2.3), the formula from the sensitivity analysis, predictions can be derived for the centrifuges previously characterised in the literature. For example comparing to results presented by Boychyn et al. (2004) and assuming the branch diameter is matched to the PSC-5:

- The multi-chamber bowl would be expected to require a rotating disc speed of 5,900rpm to accurately model process unit. Using a rotating shear device speed of 6000rpm results in an over-prediction of the clarification by just 3%.
- The disc stack would be expected to require a rotating disc speed of 6030 to 6350 rpm for the highest and lowest flow rates respectively. At a disc speed of 6000rpm the clarification is under predicted by 3% and 12.5% respectively. It may be observed that the most under-predicted laboratory scale clarification are at the condition for which a higher rotating disc speed requirement is predicted by the CFD methodology – which would only make the accuracy worse. This may imply that at different flow rates, with different resultant

residence times, other factors than feed zone shear come into play. For example, it may be that the pump shear represents a significant proportion of the shear damage experienced by the cells.

- The production multi-chamber bowl would be expected to require a rotating disc speed of 3300rpm to accurately model the process unit. Using the standard 6000rpm results in an under prediction of the clarification by 16%; an inaccuracy which a lower disc speed might improve.

Further work to confirm the accuracy of and refine this prediction method is clearly required.

3.4. CFD Analysis – PKII Density gradient Ultracentrifuge

3.4.1. Computation Fluid Dynamics (CFD) Prediction

For the PKII ultracentrifuge a similar methodology was followed to that described above for the PSC-5, in that a 3D model was built from manual measurements, the rotating machinery function used and a simplified population balance approach used to predict the equivalent USD conditions required to mimic the shear levels seen.

Figure 3.4-1 shows the final results of this analysis, with a rotating disc shear device disc speed of approximately 8.5krpm over a 1 minute period required. The higher value predicted here makes sense in terms of the higher rotating speed, lower feed rate, and smaller inlet channel diameter, resulting in a greater proportion of the feed being exposed to the higher wall shear rates.

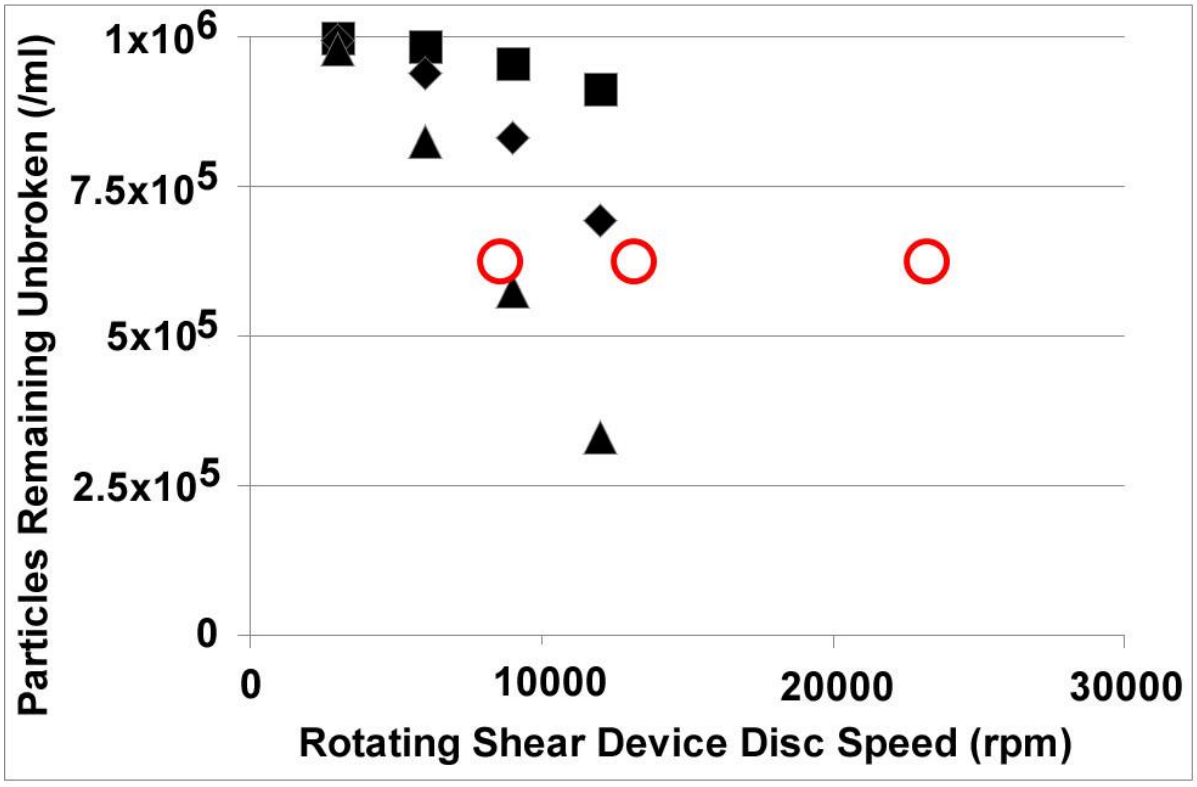

Figure 3.4-1. Predicted particle breakage for a selected set of particle breakage parameters in the rotating disc shear device, for a range of run times: 5seconds (■), 20seconds (◆) and 1 minute (▲). Particle diameters assumed uniform at 100nm. Red circles (○) are the predictions for the PKII centrifuge.

3.4.2. Validation using shear mimic

The development and use of the virus shear mimic is described in chapter 5.

3.5. Summary

In this chapter the development of the Computation Fluid Dynamics (CFD) methodology is described. Comsol multiphysics® was used, beginning with an axi-symmetric modelling approach, directly comparable to work previously published by Boychyn et al. (2001), and the rotating disc shear device maximum shear levels compared with the literature values. Both maximum shear stress and the narrow location of this high shear rate at the rotating shear device disc tip were consistent with the published literature.

The modelling approach was further extended to incorporate the 3-Dimensional nature of the continuous centrifuge system, by modelling using the rotating machinery function. In addition, by use of a simplified population balance model, the effect of the time of exposure to different shear levels and the nature of the shear (in terms of extensional versus normal) were also incorporated in to the final predictions of equivalent rotating shear device speed.

The PSC-5 centrifuge modelling results were consistent with published literature in that the highest shear rates were seen at the distributor feed zone tip. The equivalent rotating shear device speed was of the order 6krpm across the operating range of the centrifuge, as would be expected for an hermetically sealed, low shear centrifuge. These results were confirmed by measurement of clarification and protein release using the ultra-scale down laboratory mimic and at industrial scale. The PKII showed similar levels of predicted shear rate.

To further test the combined CFD and particle breakage modelling technique a cell shear mimic has been developed, which is described in chapter 4. This mimic was used to confirm equivalent shear levels across a range of operating conditions in the PSC-1 centrifuge, which belongs to the same Pathfinder series as the PSC-5. Possible errors in the manual centrifuge measurements and the geometric differences between the PSC-5 and PSC-1 were accounted for by a sensitivity analysis. The resulting formula can also potentially be used to predict scale down conditions over a range of centrifuge types and operating conditions as demonstrated by a comparison to experimental results previously presented in the literature.

In the following chapters (4 and 5) the development of cell and virus shear mimics is described. These were used to validate the CFD and population balance modelling approach described in this chapter. This understanding of the shear levels of interest was then applied to the interpretation of USD measurements on viral vaccine / vector producing processes (Chapter 6).

4. Development of a Shear Mimic for Mammalian Cells

4.1. The Objective

The objective of this phase of work was to identify a material which could be used as a shear mimic for cells. Shear has been shown, on a number of occasions, to be a key parameter in determining the impact of an industrial process unit on the process stream and cell based products (see Section 1.1.3). In addition in a number of industrial process units, such as centrifuges, shear rate is difficult or impossible to measure directly. Previously therefore, in developing ultra scale-down laboratory mimics tools and protocols for these industrial process units, computational fluid dynamics (CFD) has been used to equate the maximum energy dissipation rates in large scale and small scale systems; and the equivalence of response in biological materials used as validation. There are a number of disadvantages to this approach, including the heterogeneous nature of the biological material, effecting in particular the predictability of settling in industrial centrifuges, and the complexity and cost associated with continuous cell line culture.

The cell shear mimic therefore was intended for use in supplanting or supplementing biological material in the validation of CFD modelling. Additionally, as new unit operations are developed, the shear mimic could also be used to characterise new equipment prior to usage to define shear intensive operating parameters without the need of generating cell material or CFD models.

4.2. Development Methodology of the Cell Shear Mimic

4.2.1. Setting criteria

4.2.1.1. General

In developing the cell shear mimic the first step was development of a set of criteria to describe what that cell shear mimic might look like and what it was intended to achieve. The below summarised the original set of objectives. Although the final shear mimic produced did not fulfil all criteria identified, the process of developing the shear mimic and associated assays allowed these criteria to be stress tested, and compromises reached.

The criteria originally developed for this shear mimic were:

- To be a synthetic cell mimic, because biological products themselves are poorly characterised and highly variable, take considerable effort to produce, must be handled with due concern for biosafety issues and it may not be desirable to risk contamination of industrial process equipment with biological material.
- To be approximately the same size range as the biological product of interest. If Kolmogorov's theory is taken as physically representative – which fits with the rule of thumb identified for cells, that damage occurs to cells when the Kolmogorov's micro-scale and cell size are similar (section 1.1.4.1) – then the degree of damage to any material at any given energy dissipation level should be linked to the size of that material.
- To be approximately the same density as the biological product of interest. The qualities of the cell or biological particle which would be expected to impact on its separation and therefore flow path within a centrifuge include its hydraulic diameter and density (Boychyn et al., 2004). As such the size and density ranges of these materials are of particular relevance. If too dense the mimic would leave a centrifuge system, for example, only in the solids, if too light all the mimic material would not pass through the same areas of the centrifuge as the biological materials (e.g. cells) might potentially pass through and therefore may not be subject to the same forces. However, the significance of this may depend on where and when the most significant shear rate is seen: for example in the disk stack centrifuge the highest energy dissipation rate is predicted in the feed zone, where even material which was too light or dense might be expected to be fairly evenly distributed.
- To be an off the shelf, commercially available product. This will limit the development time, potential for unexpected variability, and additional variables introduced by a bespoke manufacturing process.

From which a number of potential acceptance criteria were developed, including:

- A faithful and tune-able mimic of the biological product. That is a material whose response to shear is in some way equivalent to that of the biological product of interest; e.g. if aiming to imitate a cell the size distribution of the

mimic particles would be impacted by shear, with a decreased volume/number at upper sizes and potentially creation of some fine debris.

- A probe which has some measurable response to shear, even if it is not analogous to the biological product being imitated. Hence the mimic can be used for the purpose of validating the equivalence of the maximum energy dissipation rate between the large and small scale.
- A probe or probes whose response can indicate the nature of the stress type (normal, perpendicular or elongational).
- A probe for which some quantifiable physical characteristic(s) is impacted by shear and for which some quantifiable relationship can be found between degree of physical change(s) and level of shear.

4.2.1.2. Response of cells to shear

CHO cells were grown, as described in section 2.2.5.1, and used to obtain illustrative results of the response of mammalian cells to shear in the rotating shear device.

Results for cell sample particle size distribution following shear are broadly in-line with previous results published in this area (e.g. Tait et al. (2009)), namely, as shear increases from low (6krpm, 26.8kW/kg) to high (12krpm, 417kW/kg), the amount of debris formed increases (Figure 4.2-1). The rotational speeds quoted here are the speeds of the rotational shear device, where 6krpm has been shown to correspond to the level of damage in the feed zone of a low shear centrifuge and 12krpm to that of a high shear centrifuge. The importance of this particles size distribution (PSD) is in the formation of fine debris and particulates, which do not settle so well, and are liable to carry through to subsequent process units. Readers interested in how this cell particle size distribution varies with cell viability/age are referred to work previous published by Tait et al. (2009) who gives the most complete analysis in this respect. There is scope for further work on the impact of growth condition and additives on the breakdown of mammalian cells.

At low shear whilst debris increases the number of cells (i.e. particles larger than 10μm) remains largely unchanged, indicating that few cells (in number terms) are actually destroyed at this lower rotational shear device speed. Whilst at high shear rates cell breakage occurs, indicated by a sharp spike at 2-3um. It can be seen how substantially the relative quantity of debris to intact cells changes as the shear rate

increases. This ratio of debris to whole cells appeared in this case to increase in an approximately linear manner (results not shown), however, there is no evidence that this is universally true for all cell types under all culture conditions, nor is it expected that it should be.

This shear rate range is therefore the range over which the cell shear mimic needed to show a response. This was considered the key selection criteria.

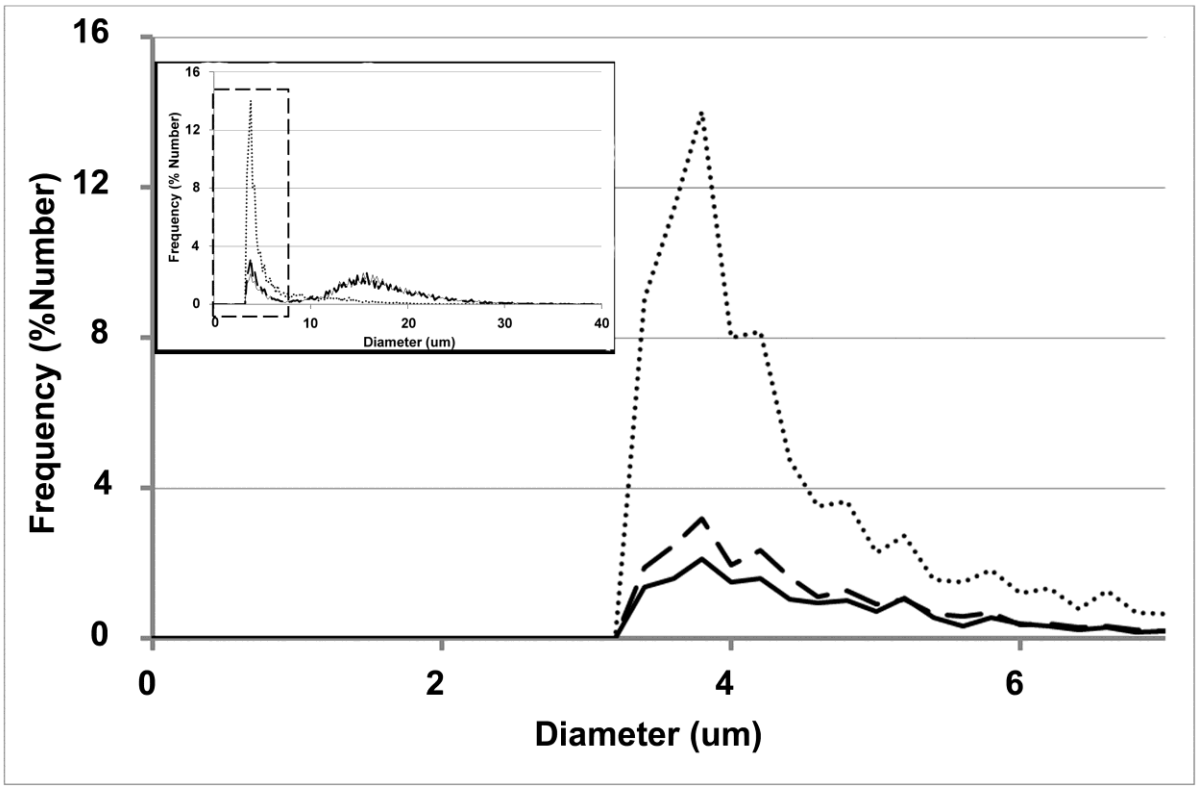

Figure 4.2-1. Effect of shear on the particle size distribution for a mammalian cell suspension by a USD rotational shear device at no shear (–), low shear of 6krpm (- - -) and high shear of 12krpm (·····), based on particle count (% number) using a Casy Counter. The particle size distribution and count for the debris is shown, with the full particle size distribution in inset.

4.2.2. Identifying potential Cell Shear Mimic Candidates

There are a large number of materials and structures available for synthetic materials at the nano and micro scale. However, as the initial aim of this study was to identify micro or nano-particles which are available commercially only these, or materials which can be manufactured from commercially available material relatively easily were considered.

Materials identified which are available in the desired density and size range include: polystyrene, silica or PMMA plain polymeric particles, streptavidin coated polymeric particles (Bangs Laboratories Inc. USA), metal coated polymeric beads

(Microparticles GmbH, Berlin, Germany), PLGA or chitosan polymeric micro-capsules with a dextran liquid core (Nanomi BV, Oldenzaal, Netherlands), Aggregates (of various compositions, such as glycerol-water and polystyrene-NaCl or chalk), agarose particles (Agarose Bead Technologies, Madrid, Spain), uni and multi-lamellar liposomes (Encapsula, Brentwood, USA) and yeast cell walls (Lesaffre, Marcq-en-Baroeul, France).

Types of micro-capsules mentioned by Mercade-Prieto and Zhang (2012) include polyelectrolyte multilayer systems to form microcapsules, which are potentially interesting as they 'self-assemble' in layers, melamine formaldehyde, yeast cells (and other microbial cells), proteoglycan gel, collagen fibrils, chromatographic particles (such as agarose), excipient powders, embolic agents etc. Caruso (2001), Ariga et al. (2012) and Chaudhuri and Paria (2012) give a number of potential materials which can be used in constructing micro-capsules and Goldberg et al. (2007) lists material used for polymeric micelles.

The first possible mimic identified for the cell was a polymeric micro-capsule, made from PLGA, chitosan, or both. Their key advantages are that their density, size and shell thickness can be controlled and that they are commercially available, although this appears to be chiefly through companies which offer research and development and custom products. There are a large number of possible customisations which can be applied including use of fluorescent materials in the shell or encapsulated material to ease the measurement of rupture. Goldberg et al. (2007) state that particles smaller than 100nm can be encapsulated, which may also be a useful feature of this technology. It is also possible to give them densities and diameters of the right order of magnitude. According to the supplier (Nanomi B.V.) they can produce micro-capsules with a density of approximately 0.9 g/ml, a diameter of 10μm and a shell thickness of 0.5μm with fluorescent material incorporated into the shell for ease of visualisation.

However, there are a number of issues in their construction in the size range of interest. Blaiszik (2012) stated that there are more issues forming capsules between 5 and 10μm in size and with a tight size distribution. Clumping is more of an issue at these small sizes. To generate the micro-capsules would require both mechanical mixing and homogenisation and a considerable amount of time and to gain an even

shell thickness might require another method altogether such as co-axial jetting. It can be noted that Lu et al. (1992) used a cell mimic system for which the size distribution was between approximately 20 and 300 μm, lending credence to the difficulties of working below 20 μm suggested by Blaiszik (2012). Furthermore although Mercade-Prieto et al. (2011) were able to separate their microcapsules into the ranges 8-20μm, less than 8μm and greater than 20μm, by using nucleo-pore track etched membranes from Whatman, the equipment for making the microparticles included a fusion turbine, heater, homogenizer and the time required was approximately 9 hours, excluding the filtration steps.

Possibly as a result of these technical difficulties the cost is considerable, with a quote, for example of €3000 (Euro) for 1 gram. The information currently available in the literature and from manufacturers does not appear to include the micro-capsules response to shear, neither is the sensitivity of this parameter to and likely variability in the shell thickness known. It cannot therefore be said for sure whether the micro-capsules would respond to shear at the right order of magnitude for this application.

Ariga et al. (2012) state that the layer-by-layer method can be used to construct a hollow microcapsule by using a chemically or thermally destructible central core. If this core is porous this can also be used to introduce dye to the microcapsule core (e.g. $CaCO_3$). Chaudhuri and Paria (2012) further describe how the layer-by-layer method can be used to produce micro-capsules with multiple core shapes, multiple small cores and moveable cores within a hollow shell material. Moveable cores are formed by coating the core in two types of layers the inner of which can be destroyed either chemically or thermally.

Liposomes are available from a company called Encapsula Nano Sciences in a multi-lamellar form, with an onion-like structure. These multi-lamellar liposomes are of a range of diameters from 60nm up to approximately 4μm, so a fraction of these are in the right size range. The density of these micro-capsules remains to be confirmed and is likely to vary depending on the size and number of layers of capsule inside, but for the moment is assumed likely to be approximately the same density as water. The shell chemistry and strength can be altered by the incorporation of a number of chemicals including fluorescent molecules, which can be either encapsulated or added to the bi-layer, and it is also possible to attach anti-

bodies to the surface. According to Goldberg et al. (2007) lipid stability is affected by temperature and osmolarity amongst other environmental factors and lipid polymer conjugate nanocapsules are more stable than lipid only.

Emptied yeast cell walls can also be used as capsule material, but were excluded in this case due to the risk of introducing biological material to the process.

Agarose micro-particles are available from ABT Beads with a reasonably narrow size range around 10μm, with a maximum size of less than 20μm and a minimum size of approximately 0.6μm. Again both the density and response to shear were unknown. Aluminium hydroxide and aluminium phosphate are available from Brenntag, with a minimum size of 0.3 μm and 0.7 μm respectively and a maximum size of 7 μm and 6 μm respectively. Response to shear rate had not been quantified.

On discussion with a commercial vaccine manufacturer it was decided that the project would focus on chromatographic beads, as materials which are already safely used within the context of the biopharmaceutical industry. A range of particles available at UCL were selected (see section 2.2.2), and assayed for their susceptibility to shear as described in section 2.2.1.1. None of these showed any response to shear, as illustrated in Figure 4.2-2. Further treatments gave the following results: acid treatment either completely destroyed or dissolved the beads, or did not result in any changes which made the beads more susceptible to shear. Homogenisation gave a substantial change in particle size distribution, implying that (i) the analytical methods selected should be capable of detecting any changes due to shear if they had occurred, (ii) the material itself is susceptible to breakage such as can be measured, but not under the shear conditions assayed. Further work with this material range was therefore discontinued.

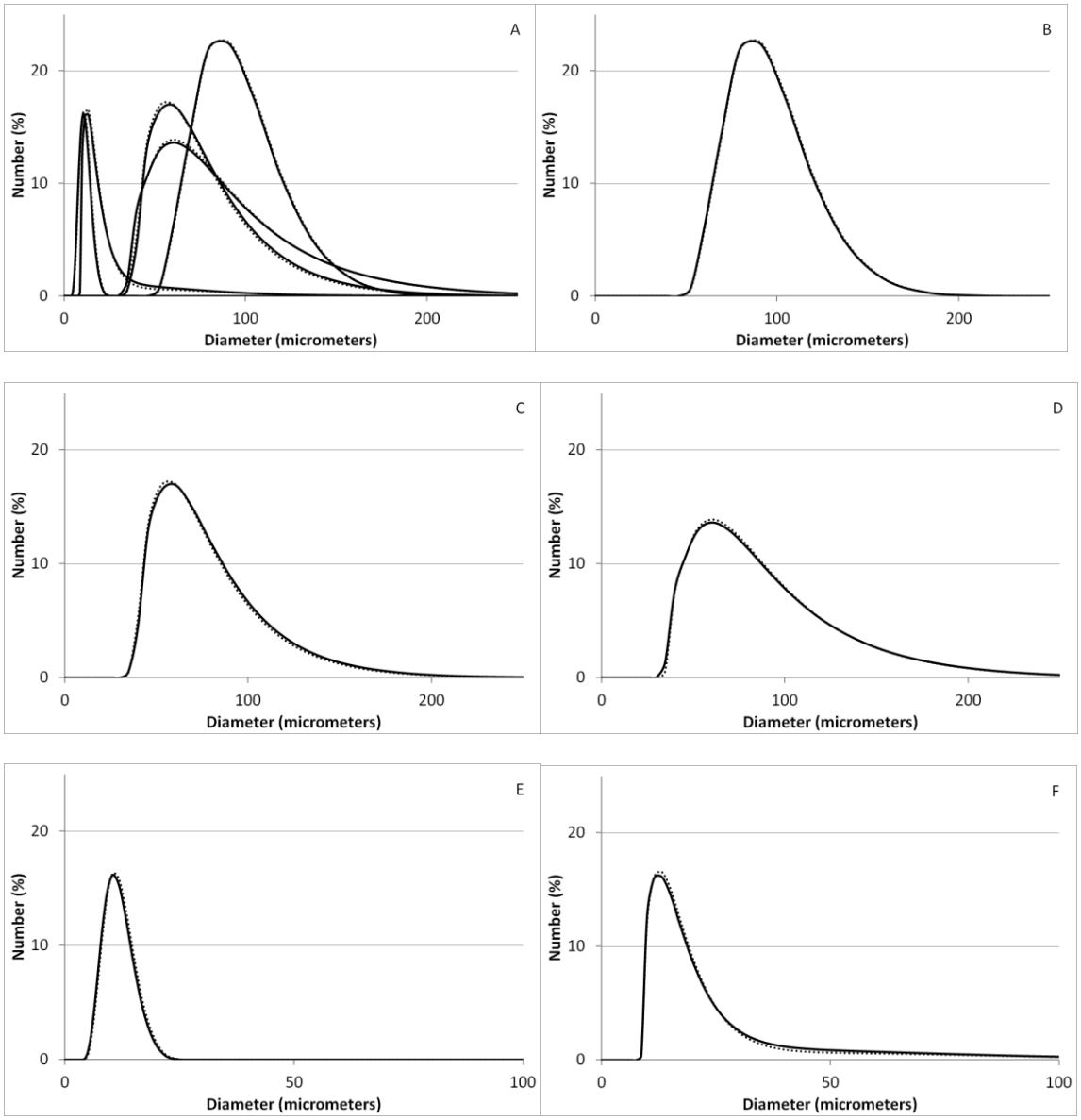

Figure 4.2-2. Particle size distributions (PSDs) of a range of chromatographic material. Unsheared material (unbroken line) was compared to sheared material (dashed line) in a rotating shear device at a speed equivalent to a high shear centrifuge (12krpm, 417kW/kg). Results include PSDs for all chromatographic materials (A), PSDs for P6XL (B), PSDs for Sepharose Fast Flow (C), PSDs for Iber Agar (D), PSDs for 10um Agarose beads (E), and PSDs for Sepharose CL4B (F).

Work by Kolade et al. (2015) showed an effect of shear on an aluminium phosphate adjuvant, which suggested that it would show a measurable impact from shear in the range of interest. Adju-Phos and Al-Hydrogel are used as adjuvants in injectable vaccination, and were therefore considered acceptable candidates in terms of biosafety profile, i.e. minimal risk from contamination. Initial examination of the samples indicated that the particle size was approximately the same as mammalian cells, but that the sample appeared to settle marginally quicker than mammalian

cells, implying a greater density. Al-Hydrogel showed no measureable response to shear, however Adju-Phos showed promising results, as described below.

Figure 4.2-3 compares side-by-side the particle size distributions of cells and Adju-Phos at no shear, low shear and high shear. The Particle Size Distributions (PSDs) for Adju-Phos and this representative mammalian cell follow a similar pattern in their response to shear in that the size distribution includes two peaks (located at 4 and 15μm diameters in Figure 4.2-3 A and 15 and 20μm diameters in Figure 4.2-3B), the relative size of which change with increasing shear. For rotating shear device speeds between 6krpm and 12krpm both cells and Adju-Phos show a decrease in the ratio of large particles to small particles with increasing shear, approximately linear for Adju-Phos. Whilst there is a similarity in the shapes of the PSDs, in that two peaks are present, there are also substantial differences. From the figure it may be observed that cells break down into very small constituent debris in response to shear, implying perhaps that cells are destroyed completely by shear, whilst Adju-Phos is 'chipped'. In addition it is clear, particularly at higher shears, that cells are more sensitive to shear. However, it is not necessary or expected that the shear mimic should give an identical response to shear, Adju-Phos and cells being very different materials. Equally the degree of the response being less than possible inter-culture or inter cell-line variability should not be of concern. The intention of the shear mimic is as a tool for measurement of shear in the same range as that which affects cells, not as a substitute for experimentation on mammalian cells, but with the aim of characterising the industrial system sufficiently to allow experiments on process material to be conducted at small scale, and/or at conditions representing a range of industrial process operating conditions. What is key in this result is that both cells and Adju-Phos respond to shear in the same range. Mastersizer measurements (Figure 4.2-4, Figure 4.2-5) corroborated these results: showing a shift in particle size distribution towards the left and a decrease in the particle size measured.

Before examining results further some discussion of different particle size distribution presentations is useful. The Casy Counter works by measuring the size of individual particles and counting the number which fall in to each size range. In the 'frequency (% Number)' distribution (e.g. Figure 4.2-3) the percentage of particles by number in each size bracket is plotted. The Mastersizer by contrast measures the degree of

scatter generated by particles passing through a laser beam, which is a direct function of the volume occupied by the particle. The Mastersizer therefore records the percentage of the total volume occupied by particles in each size bracket, referred to as 'frequency (%volume)' (Figure 4.2-6 B). The Mastersizer software, however, has the capacity to estimate to the number based distribution (e.g. Figure 4.2-4) using a number of assumptions. These particle size distributions can further be represented by a number of parameters, including (i) percentiles, giving the diameter below which a given percentage of the particles can be found, and (ii) the peak or median diameter at which the largest number of particles can be found, either of which may be derived from a particle size distribution on a number or volume basis.

The ease of measuring Adju-Phos on the Mastersizer and the greater reproducibility and flexibility of results analysis when compared to Casy Counter measurements, meant that this methodology was the preferred approach for later work on the shear mimic development. Figure 4.2-5 shows the peak diameter derived from the volume based particle size distribution. Error bars on this data indicate that the rotational shear device speed could be estimated using this mimic to within approximately 1000rpm. The breakage of Adju-Phos in response to shear is measurable and consistent, and falls within the same range as that for mammalian cells.

Preliminary experiments were conducted to explore the impact of Adju-Phos concentration (5%, 10% and 15%), shear period (at 10, 20 and 30 seconds) and shear rate (at 0krpm, 6krpm and 12krpm). The 90%ile (number basis) was a weak function of concentration and shear period (see supplementary data in Appendix D), but a strong function of the shear rate, whilst the peak (volume basis) was a strong function of shear rate only (see supplementary data in Appendix D). Previous work has shown that for shear periods greater than 5 seconds, cell response remains unchanged, indicating maximum damage has already been achieved for a given shear rate (Hutchinson et al., 2006). The Adju-phos cell mimic is therefore broadly in-line with this result.

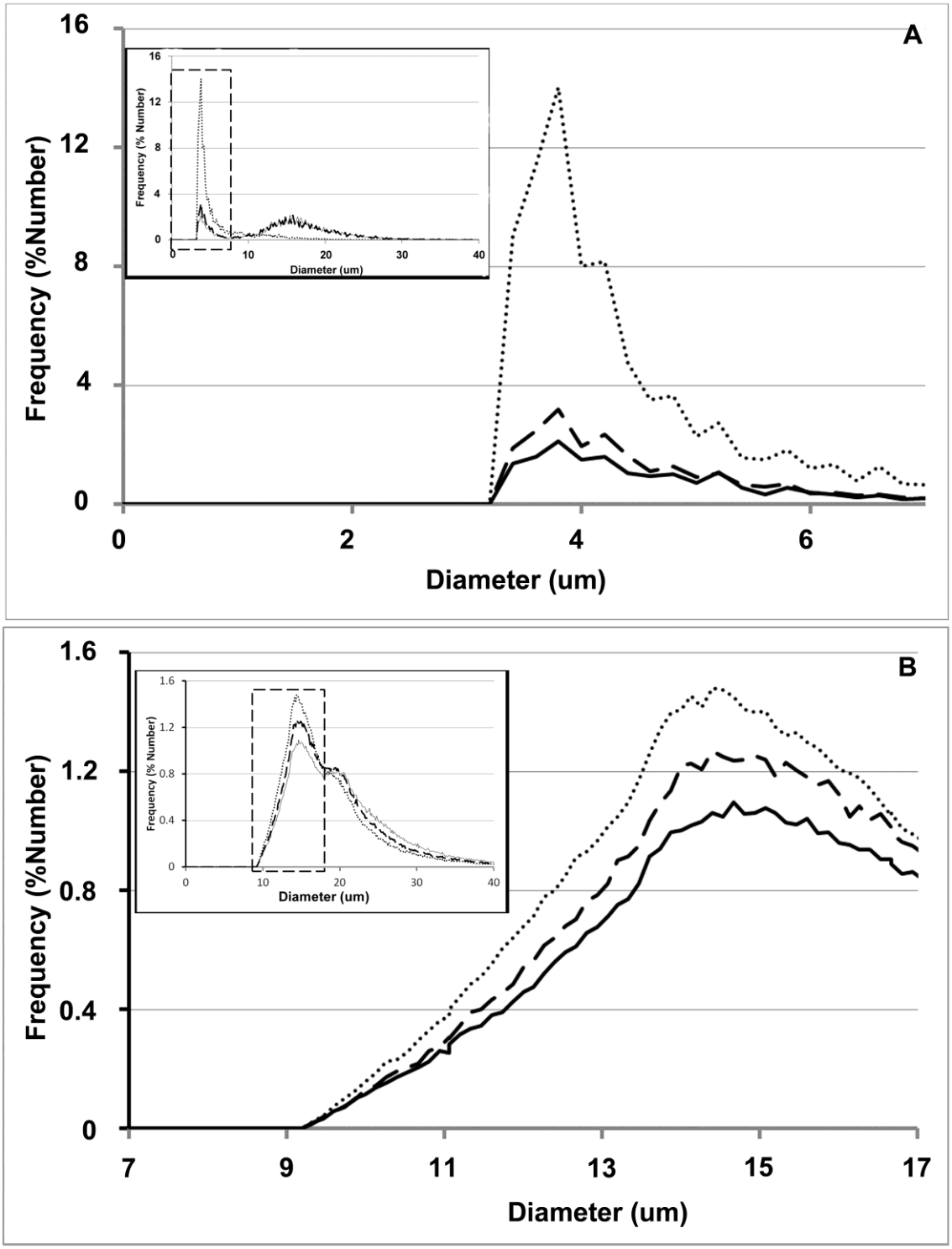

Figure 4.2-3. Effect of shear on the particle size distribution for a mammalian cell suspension (A) and Adju-Phos (B) by a USD rotational shear device at no shear (–), low shear of 6krpm (- - -) and high shear of 12krpm (·····), based on particle count (% number) using a Casy Counter. The particle size distribution and count for the debris is shown, with the full particle size distribution in inset. N.b. the diameter values and units for Adju-Phos will not be correct, as the Casy counter is calibrated for cell types, but not for this material.

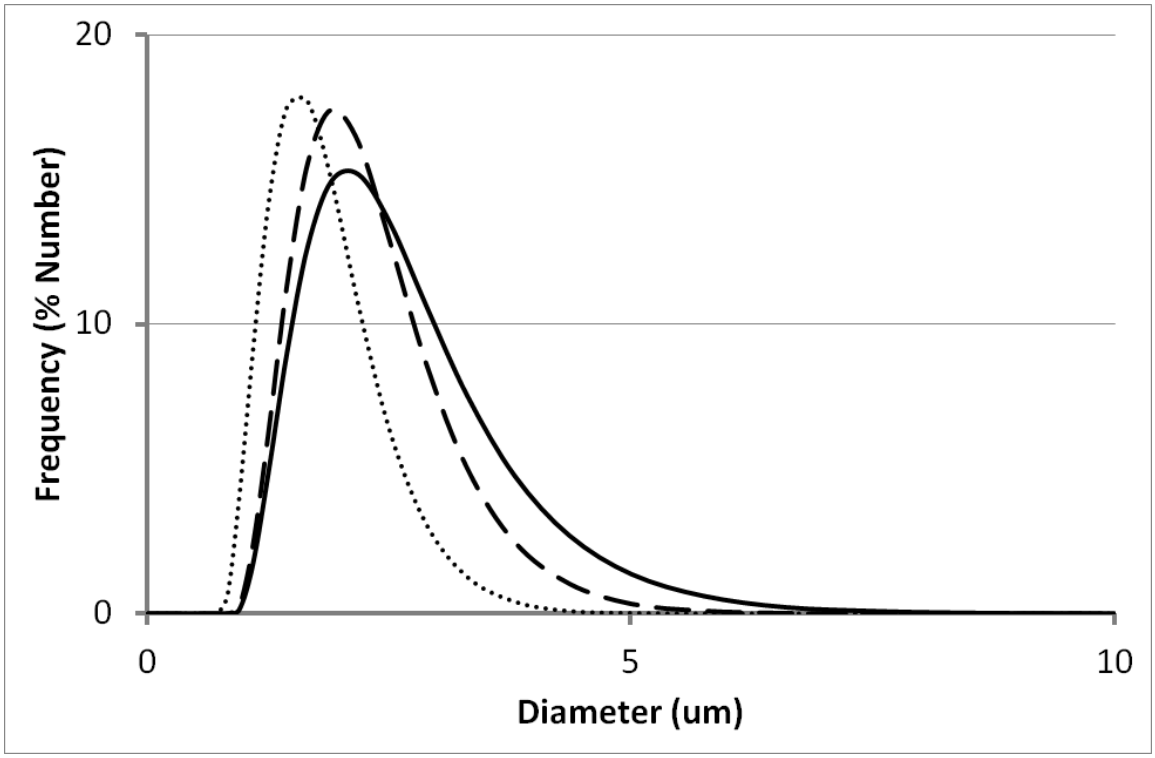

Figure 4.2-4. Effect of shear on the particle size distribution for 1%v/v Adju-Phos suspension by a USD rotational shear device at no shear (–), low shear at 6krpm (- - -) and high shear at 12krpm (·····) measured using the Mastersizer 2000.

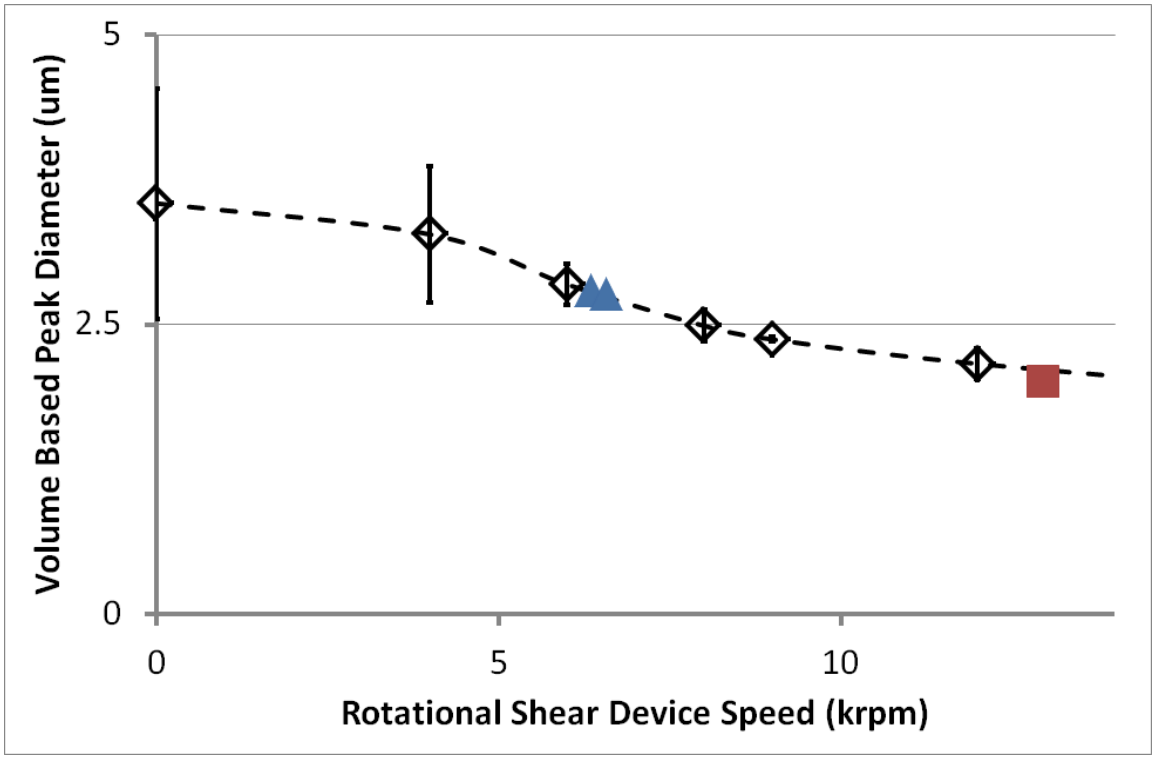

Figure 4.2-5. Effect of shear on a 1%v/v Adju-Phos suspension using the USD rotational shear device at varying shear rates, based on Mastersizer 2000 data. Error bars represent 95% confidence intervals using student t-test (n=4). Open diamonds (◇) represent Adju-phos runs on the rotating disc shear device, filled triangles (▲) are Adju-phos runs on the pilot scale disc stack centrifuge (CSA-1) with solids manually removed from the solids collection chamber within the centrifuge bowl. Filled square (■) is an Adju-phos run on a pilot scale tubular bowl centrifuge (CARR) with solids removed manually.

4.2.3. Evaluation of Adju-Phos in a low shear disc stack centrifuge (CSA-1 and PSC-1)

Adju-Phos had been shown to respond to shear in the same range as cells, and was of approximately the same size. However, the density of Adju-Phos is somewhat greater than that of cells, approximately 1.01-1.25 and 1.05–1.14 kg/m^3 respectively, and debris formed by Adju-Phos may not be as small. It was therefore necessary to validate robustly the use of Adju-Phos in centrifuge systems, and to develop a methodology to account for the extraction of accumulated cell mimic material from the solids collection areas of the centrifuge, and confirm whether this compaction adversely affected the measurability of impact from the feedzone shear.

Example particle size distributions are shown in Figure 4.2-6, as measured on the Mastersizer. Figure 4.2-6 shows that following exposure to the conditions in the CSA-1 the size distribution has shifted to the left; showing a measurable impact from the exposure to the process conditions. The difference between the bowl and discharge particle size distributions demonstrates the degree of additional damage caused by the solids discharge processing step in this pilot scale disc stack centrifuge.

The aim of running the shear mimic through the pilot scale CSA-1, which has previously been extensively characterised in work by UCL (Lau et al., 2013), was to confirm whether the shear mimic would return an accurate ‘prediction’ of the rotating shear device speed required to replicate this centrifuge. Figure 4.2-5 therefore shows where the samples from the CSA-1 sit on the curves measured at USD. As with previous work (Boychyn et al., 2004) it is assumed here that the main cause of damage to particles entering the disc stack centrifuge is shearing in the feed zone.

For a contrast it is worth observing the consistency of the two measurements made with Adju-Phos in the CSA-1 centrifuge (Figure 4.2-5), to that made using mammalian cells (Figure 3.3-1), although of course these are two different cells types, grown in different culture conditions.

Initially the count ratio measured on the Casy counter and the equivalent (number based) Mastersizer 90%ile parameter were used (see supplementary data in Appendix D). This gave a higher than expected prediction of shear; 8.3 to 9.5krpm instead of the expected 6krpm. It was speculated that this high prediction of shear

was due to the CSA-1 being run directly following a discharge, with air in the feed zone, potentially increasing the shear to which the material was exposed (Hutchinson et al., 2006). The run was therefore repeated with the feed to the CSA-1 switched directly from PBS to Adju-Phos suspended in PBS, ensuring that the feed zone was flooded from the beginning. The result from this run was not, however, substantially different from that obtained previously. This implies that the CSA-1 quickly becomes fully primed again following a discharge, and that another explanation was required for the disparity between expected and observed prediction of shear.

It was observed that the particle size distribution following shearing in the rotating shear device was much narrower than that measured following processing through the feed zone of the CSA-1 (compare Figure 4.2-4 and Figure 4.2-6). It is speculated that this may be due to differences in the exact mechanism of damage, or the relative importance of different mechanisms of damage, in the rotating disc shear device and in the pilot scale centrifuge. It may also be associated with re-aggregation of the sample between shearing and sample measurement, or phenomena in the solids collection chamber, such as particle-particle collisions. However, when the parameter against which the Adju-Phos damage measured was changed to the peak of the volume based particle size distribution curve (Figure 4.2-5) the estimated rotating shear device speed was approximately 6krpm (6.1 and 6.3krpm), which corresponds well to the expected value. The discrepancy between the conclusions drawn based on the number or volume based distributions may be due to the measurement method employed. The Mastersizer instrument measures more accurately the size of larger particles. As discussed below this is particularly true for the older instrument used in this earlier work, which did not detect fine debris which was evident on the particle size distribution as measured on the newer instrument. It is likely therefore that any differences in the particle size distribution, as discussed above, will show disproportionately in the number based distribution, whilst being less evident in the volume based distribution.

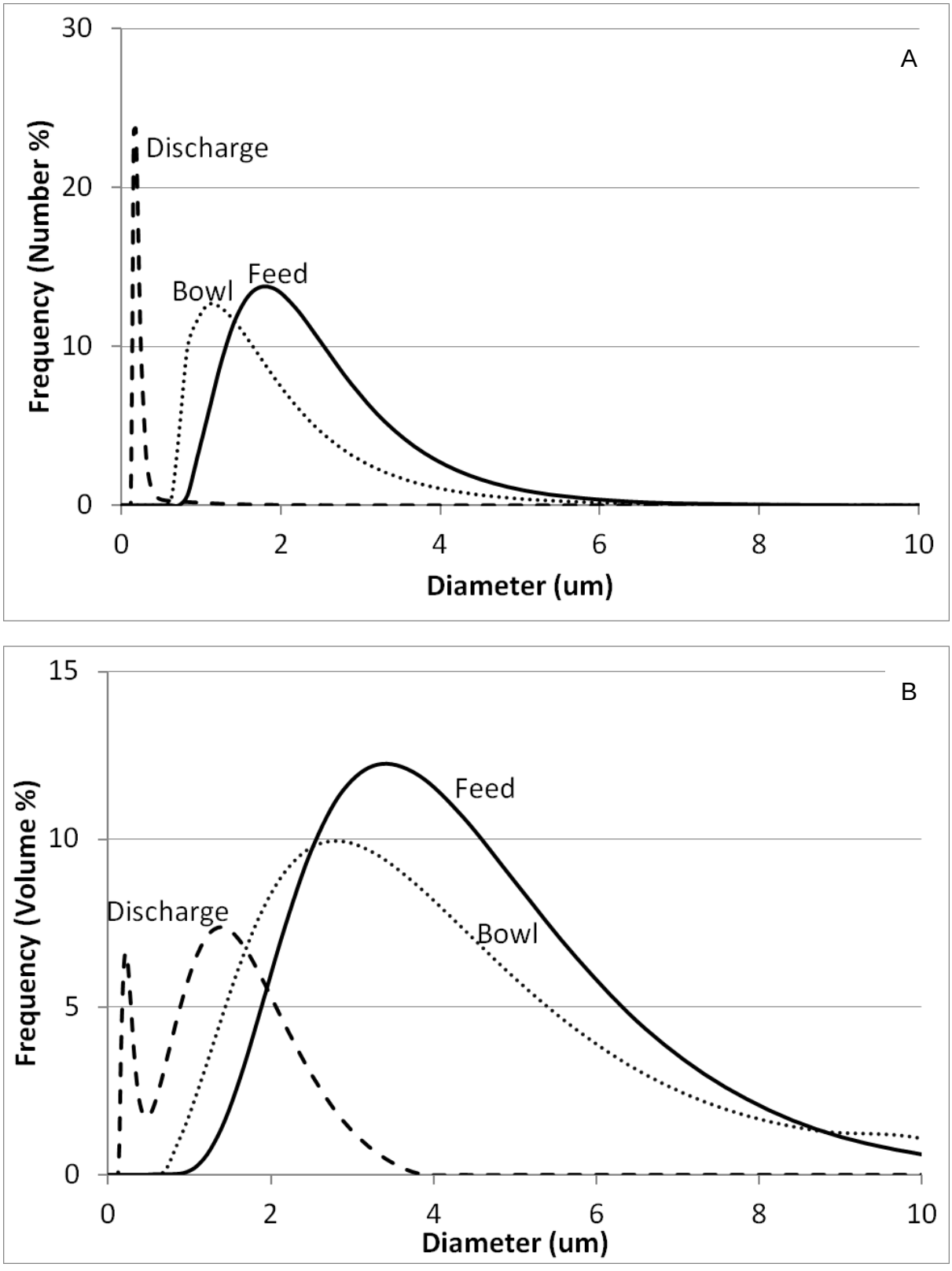

Figure 4.2-6. PSD by %number (A) and %volume (B) for a 1%v/v Adju-Phos suspension processed by a pilot scale disc stack centrifugation (CSA-1), including the feed (–) and solids discharge (- - -), and a bowl sample (·····), which was collected manually without a solids discharge. Samples were measured using a Mastersizer 2000.

4.2.4. Following manual solids discharge

The PSC-1 centrifuge, which the shear mimic was intended to characterise for the first time, presents the additional complication of automatically discharging when in use, or when the machine is stopped. As a result the quantity of solids available for evaluation is significantly reduced, and could not therefore be measured using the Mastersizer 2000 as previously.

Measurements for the runs on the PSC-1 were therefore conducted using the Mastersizer 3000 and the small volume dispersion unit. The resulting PSD can be seen in Figure 4.2-7. There is a clear difference in the appearance of the PSD in Figure 4.2-7 when compared to Figure 4.2-6. It may be anticipated that the newer model, and indeed newer Mastersizer instrument, would detect finer debris which the Mastersizer 2000 did not. There was also concern, however, that the nature of this solid might be fundamentally different, and no longer representative of the solids which had accumulated in the bowl prior to discharge. To mitigate these concerns the calibration curve was recreated by shearing Adju-Phos in the rotating shear device and measuring on the Mastersizer 3000; and the CSA-1 run was repeated, but with the solids manually discharged prior to stopping the centrifuge, in order to recreate the conditions which would be seen in the PSC-1 run.

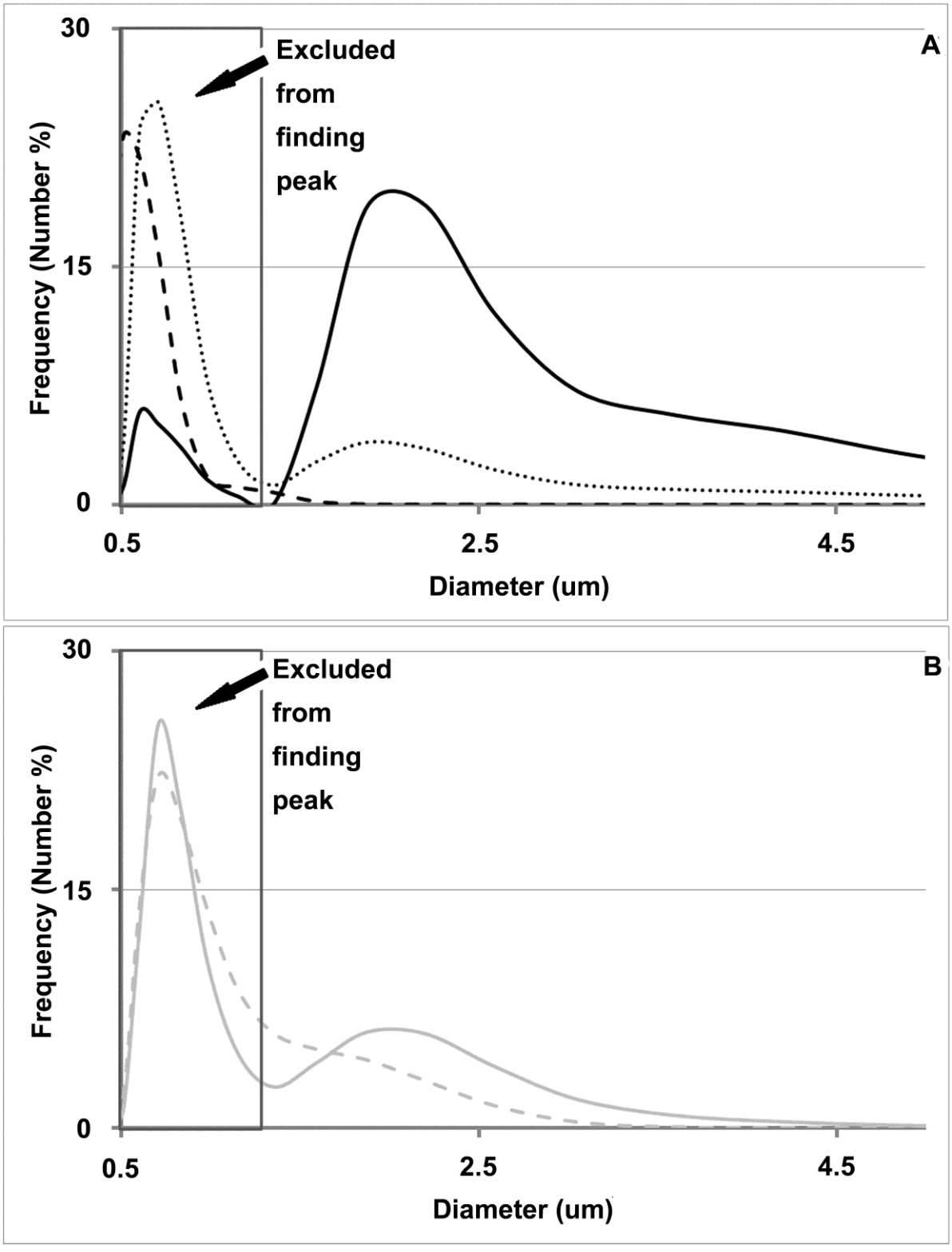

Figure 4.2-7. (A). PSD of a 1%v/v Adju-Phos suspension processed by CSA-1 centrifugation from the centrifuge bowl (–). Solids discharge (- - -) and bowl samples (·····) of 1% Adju-Phos suspension processed by PSC-1 centrifugation. (B). PSDs from the rotating shear device at low shear, 6krpm (–) and high shear, 12krpm (- - -) . Samples measured using Mastersizer 3000.

It was found for the CSA-1, using the Malvern 3000, that the volume based PSD peak no longer gave a prediction that fell within the expected range. However, switching to a number based PSD peak gave a good prediction using the low shear correlation of the USD shear device, shown in Figure 4.2-8. Although it cannot be said for sure that the fine debris may not present a correlation, either in size or relative quantity, to the degree of shear, the fine debris, shown in Figure 4.2-7 in the size range 0.5-1.2µm, were discounted, for a number of reasons. Firstly the larger particles are more directly comparable to those previous measured on the Mastersizer 2000, and should be detectable by a range of equipment types capable of detecting whole Adju-Phos particles. Secondly the Mastersizer is weighted towards accurate measurement of larger particles, and therefore the size distribution of the debris is likely to be far more sensitive to any changes in quantities of whole Adju-Phos particles, and/or aggregates resulting, in the case of the centrifuge, from the compaction following shear or the presence of contaminant particles. Finally, within the context of a centrifuge where the solids are discharged just before the machine stops, a significant amount of fine debris may be washed away by the rush of liquid leaving the bowl. This is likely to explain the substantial difference in amount of debris seen in the CSA-1 and PSC-1 (Figure 4.2-7 (A)).

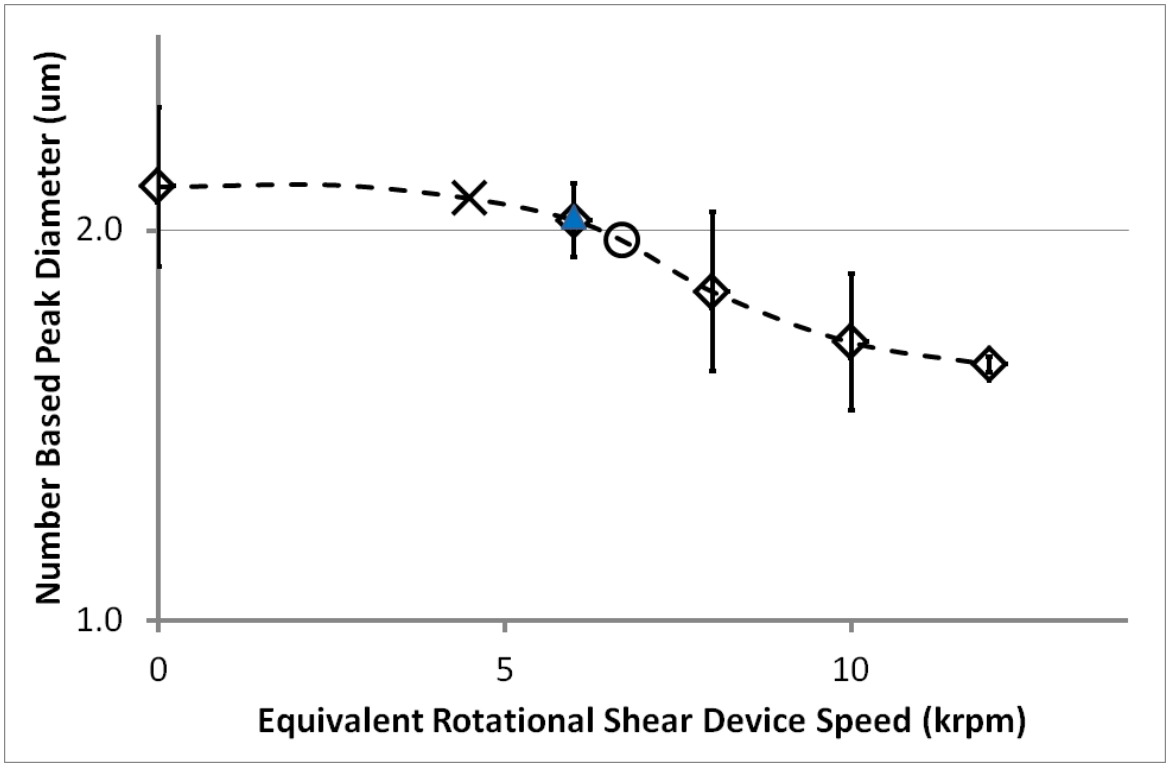

Figure 4.2-8. PSD of a 1%v/v Adju-Phos suspension processed by a USD rotational disc shear device over a range of shear rates. The number based peak diameter (µm) is generated using a single main peak identified from Figure 4.2-6 using the Mastersizer 3000 SV. Open diamonds (◇) represent Adju-phos sheared in the rotating shear device. Filed triangle (▲) is solids from the bowl from runs on the CSA-1 centrifuge where a solids discharge has been performed just before stopping. The open circle (◯) is a run at maximum rotational speed and minimum flow, and the cross (✕) a run at minimum rotational speed and maximum flow on the PSC-1, with solids removed manually. Error bars represent 95% confidence intervals using student t-test (n=3).

4.2.5. Evaluation of Adju-Phos in a high shear tubular bowl centrifuge (CARR)

Adju-Phos was also centrifuged in the CARR tubular bowl centrifuge. This was done in order to confirm the utility of the above described method of correlating shear at pilot scale against shear in the rotating shear device at USD scale, by using the peak of the volume based particle size distribution curve as measured on the Mastersizer 2000. As with the CSA-1 disc stack, the CARR bowl centrifuge has been substantially characterised and is expected to require a high rotating shear device speed of 12krpm to imitate the effects of the centrifuge feed zone (Lau et al., 2013, Boychyn et al., 2004).

Figure 4.2-5 shows where the samples from the CARR sit on the curves measured at USD. The predicted equivalent rotating shear device speed of approximately 12.5krpm corresponds very well with previously characterisation of this centrifuge.

4.2.6. Covering the operating range

The PSC-1 centrifuge is hermetically sealed, and is therefore expected to be a low shear centrifuge (Hutchinson et al., 2006). Beyond this no detailed characterisation of this centrifuge has previously been published.

Figure 4.2-8 also shows the results from two runs on the PSC-1 designed to indicate the range of shears over the operating range of this centrifuge, which showed an equivalent rotating shear device speed of between 4.5krpm and 6.5krpm as the machine moves from minimum speed and maximum flow rate to maximum rotating speed and minimum flowrate. In fact, using the volume based peak diameter for the PSC-1 runs gave the same equivalent rotational shear device speed as using the number based peak (see supplementary data in Appendix D). This result is consistent with previous studies, which have noted an impact of centrifuge speed on shear rate for other centrifuge models (Westoby et al., 2011, Zaman et al., 2009). The shear mimic appears therefore to be sensitive enough to detect relatively small variations in shear across the operating range of a hermetically sealed continuous disc stack centrifuge.

Results from the PSC-5 Computational Fluid Dynamics (CFD) model (Chapter 3), adjusted using the sensitivity analysis, gives a minimum of 4300rpm and maximum of 5500rpm for the same range of conditions. As expected this confirms the expectation that the PSC is a low shear centrifuge, that the CFD predictions are the right order of magnitude, and shows a good match across the range for the CFD model. The poorer match at the higher centrifuge speed may be due to the increasing importance of other shear/impact factors, or may imply a need for greater refinement in the CFD and / or breakage model.

The implication which may be drawn is that care is needed in selecting appropriate parameters to correlate shear using the shear mimic. But that even in a complicated process unit such as the continuous centrifuge good predictions of shear levels may be achieved. Although not able to imitate the full complexity of the biological process stream the cell shear mimic may produce useful initial information on the conditions in a process unit operation, is substantially cheaper than biological material to produce and working with it does not require the same level of forward planning, time, safety precautions or cleaning.

4.3. General Discussion

By combining Adju-Phos measurements and the Ultra Scale-Down (USD) protocol, it may be possible to predict the clarification for any given set of operating conditions, based on rotating speed and flow; or potentially for visualisation of windows of operation (Salte et al., 2006).

For example, for the two extremes of operation measured on the PSC-1 centrifuge (Figure 4.2.7), using the rotating shear device at the Adju-Phos derived predicted speed followed by clarification in a laboratory scale centrifuge, yields clarification predictions between 98.8 and 98.9% for the uninfected CHO cells, and 94.4 and 99.2% for the uninfected HEK cells (for which the measurements were presented in section 3.3.1). These results are derived based on the standard method of scaling for settling conditions between laboratory and industrial scale centrifuges (see section 1.1.3.1). Similar information can be derived for the virus production processes presented in chapter 6. These values may be derived using either Computational Fluid Dynamics (CFD) or Adju-Phos based measurements, but the costs in terms of time for the trials with Adju-Phos should be substantially less than those associated with CFD modelling; so that, long term, replacing CFD characterisation of equipment may be an attractive option presented by this technology.

Some work of this nature has previously been done in upstream processing (Lu et al., 1992), (Poncelet and Neufeld, 1989), (Henzler, 2000). However, the different conditions in downstream processing, in particular the higher shears over a shorter period, makes identifying a suitable mimic more challenging. There is also arguably a longer potential time frame between passing the mimic through the unit operation and measuring the resultant particle size distribution (Henzler, 2000). The proposed mammalian cell shear mimic, though slightly smaller, has a similar size to that of the mammalian cell, is of a similar density and responds to shear in the same range. However, the viscosity following breakdown is unlikely to be the same as that of a cell based process fluid, and it is possible that the relative susceptibility of the particle to hydrodynamic shear and the related interfacial phenomena (wall collisions/ air-liquid interfaces) may differ from that of actual cells; these factors may be significant in some cases. In addition the mimic does not micronize in the same

way as the mammalian cell, which forms submicron particles when sheared; it is not therefore suggested that the mimic can be used to replace mammalian cells experimentally, or that the solids or supernatant from the centrifuge be used further in interaction studies with USD models or subsequent processing steps. Until the model particle has been more fully characterised and its response to shear is more fully understood it is proposed to use it to verify CFD predictions of shear across single unit operations.

Given that one of the chief justifications for use of this material is reduced cost it is worth drawing a comparison between the costs involved in the large scale experiments with this material and the alternatives of using a range of process materials or CFD simulation. The cost of a 250ml bottle of Adju-Phos was 85Euros as of April 2014. A single large scale experiment requires approximately 60ml, to which may be added the cost of approximately 6 litres of PBS, which can be purchased at 10x concentration for 45.9GBP for 1 litre. More substantial are the costs associated with a day's use of an expert user or centrifuge manufacturer's engineer, in order that the centrifuge may be operated, dismantled and re-assembled safely, for which the cost is an estimated 1500GBP. Clearly a single cell culture will be substantially more expensive, with media alone for example likely to cost of the order 5000GBP for a pilot scale run, and with a greater risk of failure, substantial time and expertise required, and a longer lead time.

For adjuphos the centrifuge needs to be taken apart in order to extract the sheared and settled beads. For some centrifuges, such as the CARR Powerfuge, bowl centrifuge this is simple, and part of the standard operating procedure. For disc stack centrifuges such as the PSC-1 or PSC-5 this is more complicated, and would require a day of time from an expert user or GE engineer to be completed safely. This will also decrease the flexibility of using adjuphos, i.e. there will be a certain lead time associated with confirming availability of an engineer or expert user to coincide with equipment availability.

4.4. Summary

The aim was to develop or find a material which could be used in place of biological material, which would be cheap to produce, safe to use, not introduce a problematic contaminant, and provide greater consistency than the biological equivalent. This material, dubbed a 'shear mimic' could then be used to validate the Computational Fluid Dynamics (CFD) predictions, or provide a better prediction of shear in the centrifuge under a given set of operating conditions.

A shear mimic, Adju-Phos, was identified which has a number of similarities to mammalian cells:

i. It is sensitive to shear in the same range.

ii. It has a particle size distribution with two peaks.

iii. In response to shear the number of larger particles decreases and the number of smaller particles increases. Large particles clustered around a certain size range break down in to smaller particles also predominately of a certain size range.

However Adju-Phos is far from perfect, in that it differs from mammalian cells as follows:

i. It exhibits overlapping peaks, with a smaller difference between the particle size at the large and small particle peaks.

ii. The predominant size is smaller than the typical mammalian cell.

iii. Its density is slightly greater than that of mammalian cells.

The fact that Adju-Phos responds to shear in the same range as mammalian cells, however, was considered of predominant importance.

As the shear mimic is a novel concept use of the shear mimic for this application needed to be validated first. This was done by running the shear mimic through low and high shear centrifuge models which have already been well validated (see sections 4.2.3 to 4.2.5). Thus having demonstrated that the shear mimic provides a

good prediction of shear levels in the centrifuge, the same procedure was followed in the PSC-1 centrifuge (section 4.2.6).

The predicted shear levels derived for the PSC-1 match well those that the CFD predicts, presented in the previous chapter, and serve to validate the modelling methodology used and predictions made for the PSC-5 centrifuge.

5. Development of a Shear Mimic for virus particles

Contradicting views exist on the likely impact of shear on viral products, such as vaccines or gene therapy vectors. On the one hand, they are small relative to cells, and thus unlikely to be caught in velocity gradients from shear vortices. However, they are relatively large (compared to, for example, therapeutic proteins), enormously complicated biopharmaceutical products, whose exact mechanism of action, and thus critical quality attributes, are rarely understood. Moreover, they are evolved to disassemble or lose elements of their structure to deliver genetic material. In this chapter a technique is presented for measuring the impact of shear on particulates of a similar scale to viruses, which demonstrates that an impact from shear can indeed be seen. The streptavidin coated nanobeads used here are available off-the-shelf, and are considerably easier and cheaper to measure and quantify than viral particles. The virus shear mimic has been successfully used to predict levels of shear in the continuous feed pilot scale density gradient centrifuge, a common and powerful technique in viral purification. This chapter can be read with reference to results in Chapter 6, where corresponding results are presented for the impact of shear on two virus types: influenza for viral vaccines and adenovirus for gene therapy.

5.1. Objectives

The objective of this phase of work was to identify a material which could be used as a virus shear mimic. A single candidate, a streptavidin coated 100nm bead, has been investigated.

As with the shear mimic for mammalian cells one of the key arguments for its use is the reduced costs associated. Streptavidin coated nanobeads cost 894 Ultra Scale-Down (USD) for a 10ml container in October 2014. A single USD run requires approximately 250µl and a single large scale run requires approximately 6ml. The beads were suspended in PBS, which can be purchased at a cost of 45.9GBP for 1L at 10x concentration. This would be more than sufficient for a USD and a large scale

run. For a virus production, culture media costs alone, for a total of approximately 60L of media, would be approximately 4740 USD, based on purchasing 3 x 20L bags of liquid media HyClone^{TM} CDM4Avian Media, which is produced by GE healthcare specifically for viral production using EB66 cells (excl. tax and shipping). For experiments with the virus shear mimic preparation is extremely simple, involving as it does simply suspension and dispersion of the beads in the appropriate volume of PBS, as described in section 2.2.3.1. This compares to the complexity, long lead time, and facility requirements to meet biosafety concerns, associated with viral vaccine production.

The impact of shear on viral products, such as attenuated viral vaccines and gene therapies, and the processes producing them has not previously been explored. For this reason the impact of shear on virus infected cells is explored further in sections 6.2.4 to 6.2.6, and the impact on virus in section 6.3. Measuring the impact of shear on a viral particle is particularly challenging (section 5.2.1.2), whilst both the measurement and production of viral material is costly, time consuming and requires specialist skills. For this reason it was deemed desirable to develop a virus shear mimic. The results and process for this development are discussed in the following chapter, along with the application of the technology to verification of shear level in a PKII ultracentrifuge, where the challenges are similar to those already discussed for pilot scale centrifugation (section 4.1).

5.2. Development methodology of the virus shear mimic

5.2.1. Setting criteria

5.2.1.1. General

As with the cell shear mimic (section 4.1) virus production involves a long, complicated and failure prone process. Additional biosafety requirements can make experimentation and process characterisation of virus infected material very difficult. In addition the measurement of the impact of shear on a virus particle is particularly challenging. Thus the objective of producing a virus shear mimic is as with the cell shear mimic, but with additional emphasis being placed on the ease with which the impact of shear might be measured.

5.2.1.2. Measuring the response of virus to shear

Viruses are incredibly complicated biopharmaceutical products, the assays for which show a wide range of variance and limited sensitivity. Standard approaches to measuring the quality of a viral product might include cell based infectivity assays, particle size measurement, intrinsic fluorescence, morphological assays such as transmission electron microscopy (TEM), gels, blots and proteomics all of which attempt to be surrogates to predict interaction with the end user. (Jawetz et al., 2013)

Results from the work on the impact of shear on virus particles is presented in section 6.3 and relies on infectivity assays, TEM and particle size distributions. Assays were selected based on cost, time and availability.

The virus shear mimic presented in this chapter successfully uses simple and quantifiable assay techniques.

5.2.2. Identification of potential virus mimic candidates

Fewer candidates were identified for the virus shear mimic than for the cell shear mimic, with fewer off the shelf materials available within the size and density range of interest. A number of methods of production are listed by Goldberg et al. (2007) for construction of nano-particles including sonication and vortexing.

As a first stage in the development of the shear mimic the criteria were set that the material should have the properties of being of a similar size to typical viruses and similar density. The mimic should have a measurable response to shear within the range of shears likely to be encountered in downstream processing units, and up to the shears, which show an impact on the virus product themselves. However, as discussed above, measuring the impact of shear on viruses is itself extremely challenging. The material was therefore subjected to disruption in a rotating shear device at varying speeds, over the range previously shown to match shears in a low and high shear continuous centrifuge: i.e. at speeds of between 6 and 12krpm. As it was anticipated that a particle as small as these nanobeads (~100nm) is unlikely to be impacted by shear in this range, a higher shear of 18krpm was also used. The rule of thumb (section 1.1.4) commonly applied in bioprocessing is that a particle (cell, virus, biomolecule) will not be impacted by shear if it is smaller than the Kolmogorov's microscale of turbulence. Computational Fluid Dynamics (CFD) simulations put this at approximately 1μm even for the highest shear device speed

used in these experiments (18krpm). However, Vo and Papavassiliou (2016) show an impact on adsorbed molecules around nanoparticles at much lower shear rates, giving rise to the possibility of rearrangement and detachment of molecules associated with structures as small as a nanobead or virus.

5.2.3. Analytics development: Measuring the response of the shear mimic

Initial work with the virus shear mimic candidate was done with material which had been diluted in PBS and sheared. On which assays were then conducted to try to identify any impact from the shear (section 5.2.3.1). As the aim was to use the virus shear mimic in density gradient ultracentrifugation to verify the level of shear in this industrial process, an additional step of laboratory scale density gradient fractionation was applied (section 5.2.3.2) after the initial work had been conducted showing an indication of the material responding to shear.

5.2.3.1. Without ultracentrifugation

The virus shear mimic candidate consists of a 100nm polystyrene bead, with a coating of streptavidin molecules. The initial hypothesis was that the impact of shear might be visible in damage to this streptavidin layer, in a manner analogous to damage to virus proteins on a capsid or membrane layer. What can be seen in Figure 5.2-1, however, is that the nanobeads were never mono-dispersed, but clumped, mostly in groups of 2 or 3, giving a peak nanobead size of approximately 200nm. This particle size distribution was not significantly effected by sonication or use of Tween-20. However, by exposing the sample to high shear rates, the nanobead clumps began to break up and gave rise to a changing particle size distribution. This changing particle size distribution could be characterised by a number of simple parameters, expressing a general trend for decreased aggregate size, and increased count, as some nanobead aggregates break down. The change in size is particularly noticeable in the upper size ranges of the particle size distribution and in the 95%ile diameter (Figure 5.2-2). The 5%ile diameter changes very little if at all, perhaps due to the limitation at the lower size range dictated by the size of a single nanobead. Comparing the decrease in the 50%ile diameter to that in the 95%ile diameter shows that the latter begins to fall at a lower shear rate, with a greater overall decrease. This is consistent with shear having a greater impact on larger molecules and with larger aggregates being weaker on average.

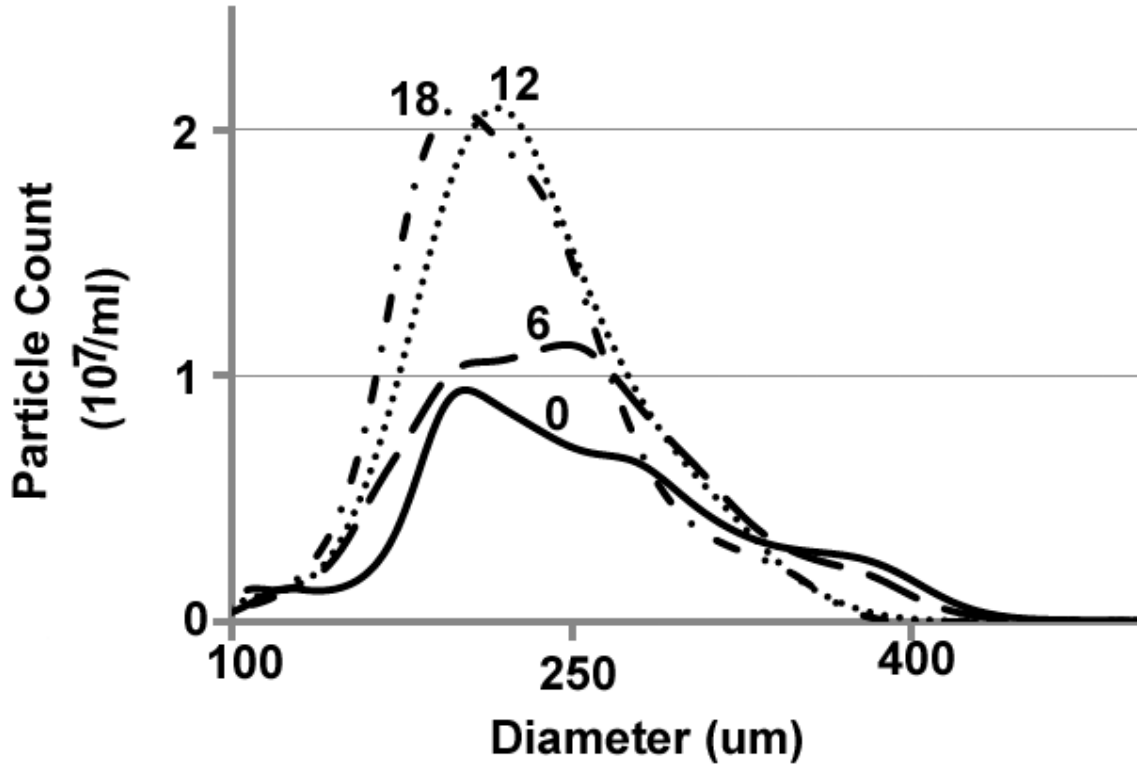

Figure 5.2-1. PSDs for nanobeads subjected to disruption by a rotating shear device at varying shear rates. No shear (solid line), low shear at 6krpm (long dashes), medium shear at 12krpm (dots) and high shear at 18krpm (dot-dash) are measured using Nanosight.

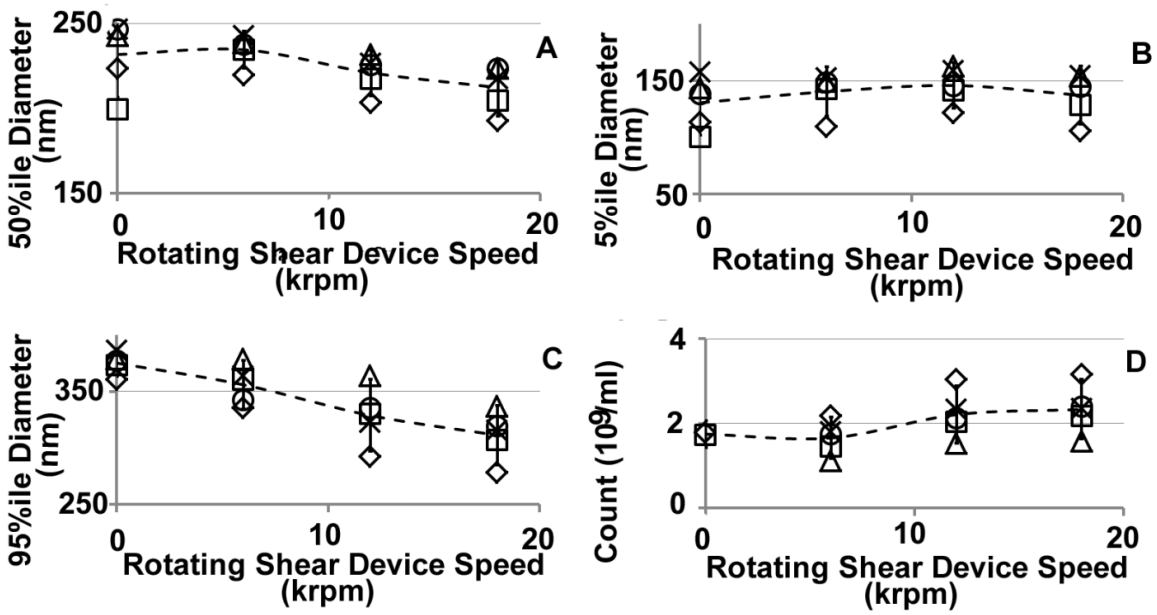

Figure 5.2-2. PSD parameters for sheared nanobeads. The 50%ile (A), 5%ile (B) and 95%ile (C) diameters, and total count (D) of nanobeads subjected to disruption by a rotating disc shear device at varying shear rates. Each symbol represents repeat data sets. Lines are plotted through average of the repeats shown. Error bars represent 95% confidence interval using student t-test (n=5)

To test the original hypothesis that the streptavidin layer would be damaged by shear a biotinylated fluorescein was used in a dilution assay. Binding to undamaged streptavidin quenches the fluorescence observed. As shown in Figure 5.2-3 A, there

is perhaps a slight increase in fluorescence assay corrected count at the highest shear compared to the previous shear levels, representing a very slightly lower dilution at which the fluorescence begins to increase. The minimum fluorescence reached, and which it might be expected would show an increase in fluorescence, indicating a poorer bond between biotin and streptavidin, if the streptavidin were damaged, shows no consistent increase for the highest shear level (results not shown).

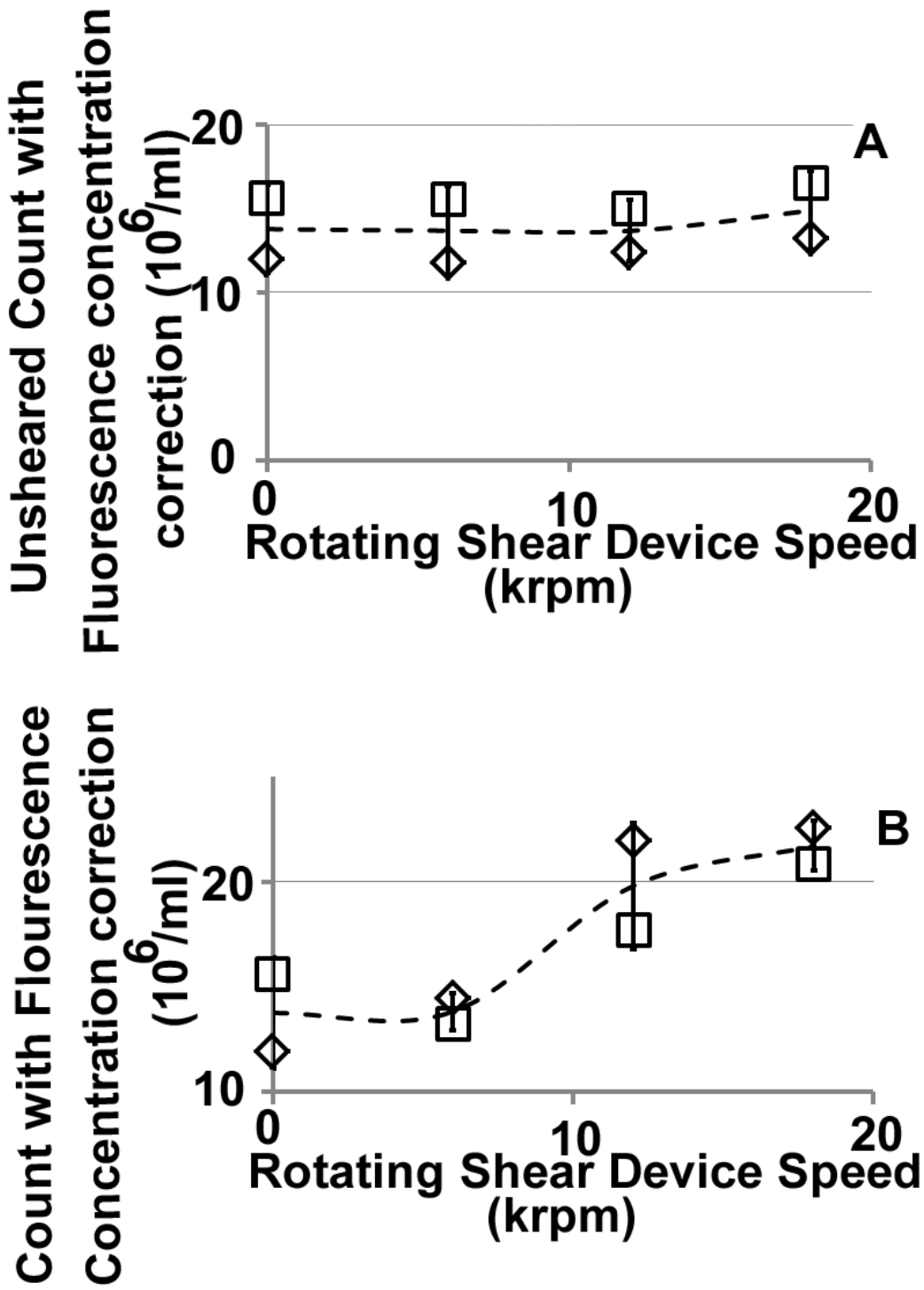

Figure 5.2-3. Fluorescence assay results of sheared nanobeads. Nanobeads have been subjected to disruption by a rotating shear device at varying shear rates. Samples were then serially diluted in a 96-well plate and a fixed volume of fluorescein added to each well. The curve of increasing fluorescence with decreasing nanobead concentration was fitted to a 4 parameter logistic fit curve, and the concentration, is plotted in figures A and B. Where (A) represents counts using unsheared nanobeads as the 100% value, and (B) where the Nanosight count for each shear level is used to set the 100% nanobead concentration in the fluorescence assay. The line is plotted through the average of duplicate measurements. Error bars represent standard deviation of the sample (n=2).

A further assay was therefore conducted to confirm whether the streptavidin was affected by shear. Sheared nanobeads were incubated with anti-biotinylated gold

tags, which will bind to streptavidin, and the number of tags per nanobead recorded using TEM. The results (Figure 5.2-4) showed a wide variability and, an apparent difference between unsheared and sheared nanobeads which is not significant due to the large error on the sheared nanobead measurements. There is no indication of a difference between shear levels. It might be hypothesised that any difference between sheared and unsheared nanobeads is due to the removal of adsorbed particles (Vo and Papavassiliou, 2016), which, when present, might hinder the binding of large particles such as the gold-tags, but not the biotinylated fluorescein.

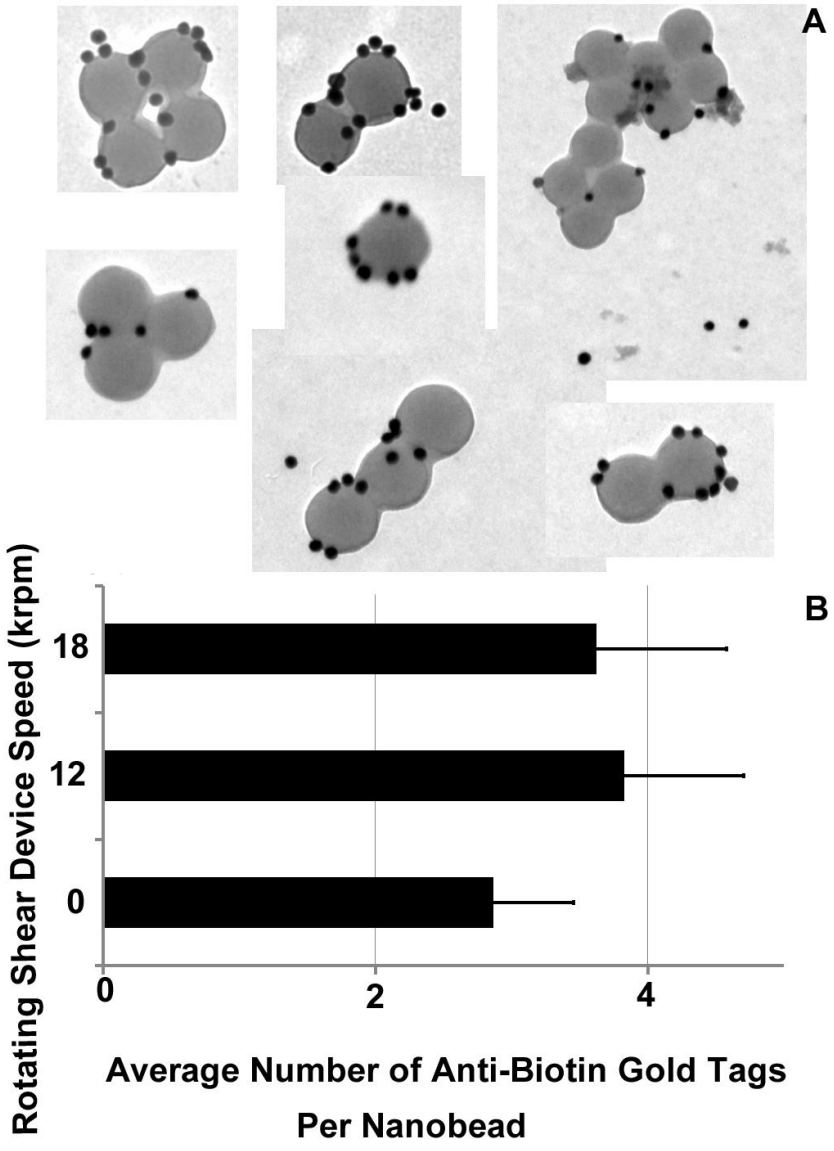

Figure 5.2-4. Transmission electron microscope (TEM) measurements for sheared nanobeads. Nanobeads have been subjected to disruption by a rotating shear device at varying shear rates, then incubated with anti-biotin gold-tags, before imaging on TEM. Some sample TEM images are shown (A), along with a bar chart (B) of the average number of gold tags per nanobead. Error bars represent 95% confidence intervals using student t-test, where the number of individual nanobeads identified ranged from 550 to 1288.

Taken together the above assays indicate that there is probably no substantial damage to the streptavidin layer in this virus shear mimic, and that measurement of the particle size distribution may give a stronger tool for tracking shear levels. The particle size distribution, however, does not always give a very clean, repeatable measurement. In addition, as will be discussed later, a good measure of particle size distribution is not always possible. An alternative measure was therefore developed by combining the two assays (Figure 5.2-3B) (for calculation see supplementary data in Appendix E). This should also show any damage to the streptavidin layer as an increase in the 'count' parameter potentially extending the range of the shear mimic, although this remains to be demonstrated. This parameter showed an impact of shear on the nanobeads at shear device speeds greater than 6krpm, therefore within the range likely to be experienced in industrial equipment. The result, although surprising given the small size of the nanobeads, raises the possibility of shear having an impact on smaller particles, such as viruses. This will be examined in more detail in section 6.3.

5.2.3.2. Assessment of the nanobeads in density gradient centrifugation

One of the most effective methods of concentrating and purifying viruses, which allows them to be separated from particles of a similar size or mass is density gradient centrifugation (Reimer et al. (1967), Duffy et al. (2005)). Although generally considered a low impact technique the industrial scale continuous feed version has the potential to introduce shear, particularly in the feed zone (Figure 3.4-1), in a manner analogous to that demonstrated with continuous centrifugation for cell harvest (Boychyn et al., 2001). The PKII was selected therefore as a large scale application for this shear measurement technique. First, the effect on the nanobeads during concentration in a density gradient needed to be assessed, which was done at laboratory scale, in batch density gradient centrifugation.

The measurement of particle size distribution following density gradient fractionation became considerable poorer, with variability in average density and nanobead concentration in the density gradient layers probably responsible. There is still a general trend for increasing nanobead count with shear, although this will be dependent on which fraction is measured, and the degree to which the nanobeads have concentrated within the gradient, or been disrupted during harvesting of the fractions. It may be possible to infer from the general trends in Figure 5.2-5 that

diameter at a given concentration is still lower for nanobeads that have been subjected to a higher level of shear, but this can only be seen on a number of repeated measurements over a range of concentrations. Measurement of the particle size distribution on the nanosight is no longer therefore a reliable assay for the impact of shear on the nanobeads.

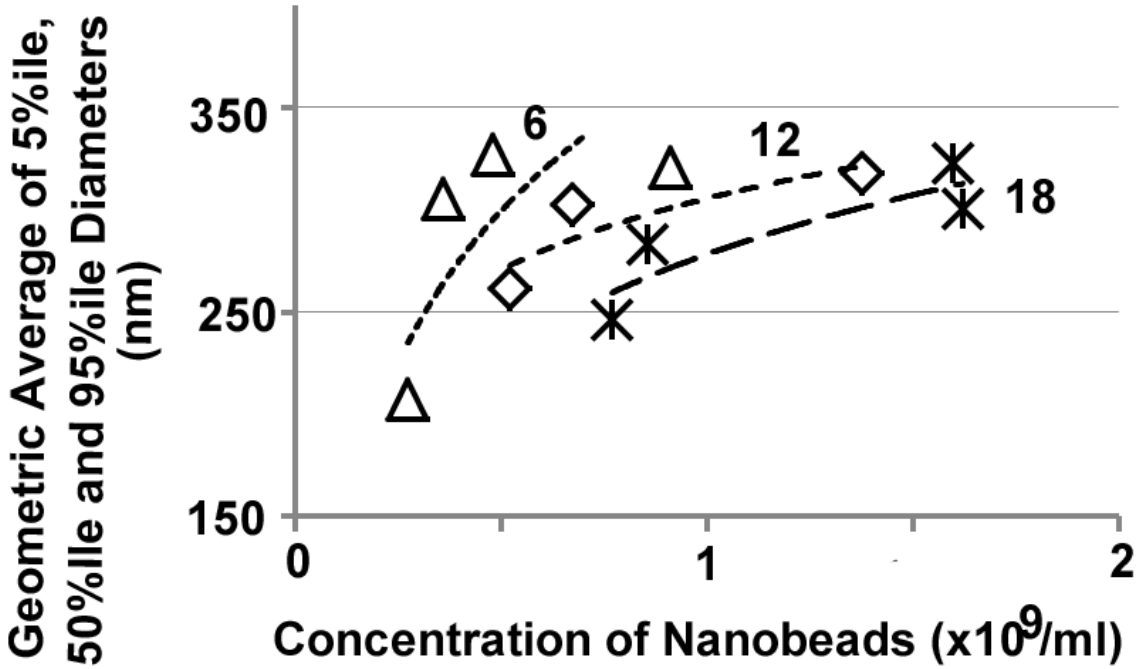

Figure 5.2-5. PSDs for nanobeads which have been subjected to disruption by a rotating shear device at varying shear rates prior to fractionation in a laboratory density gradient centrifuge. Geometric average of 5%ile, 50%ile and 95%ile diameters, with rotating shear device speeds of 6krpm (△), 12krpm (◇) and 18krpm (✳), plotted against concentration of nanobeads. The particle size distribution was measured and averaged over the three highest concentration fractions (selected based on minimum fluorescence).

The method adopted therefore was that described in Figure 5.2-3B, of combining particle count and fluorescence assay, giving a clear trend with shear for the density gradient purified sample (Figure 5.2-6). Indeed the level of change seen with shear is greater following purification in the density gradient than before (compare Figure 5.2-3B and Figure 5.2-6), showing a difference between unsheared and low shear levels. This is likely to be due to removal of loose streptavidin, and therefore a cleaner reading of the nanobead associated streptavidin concentration.

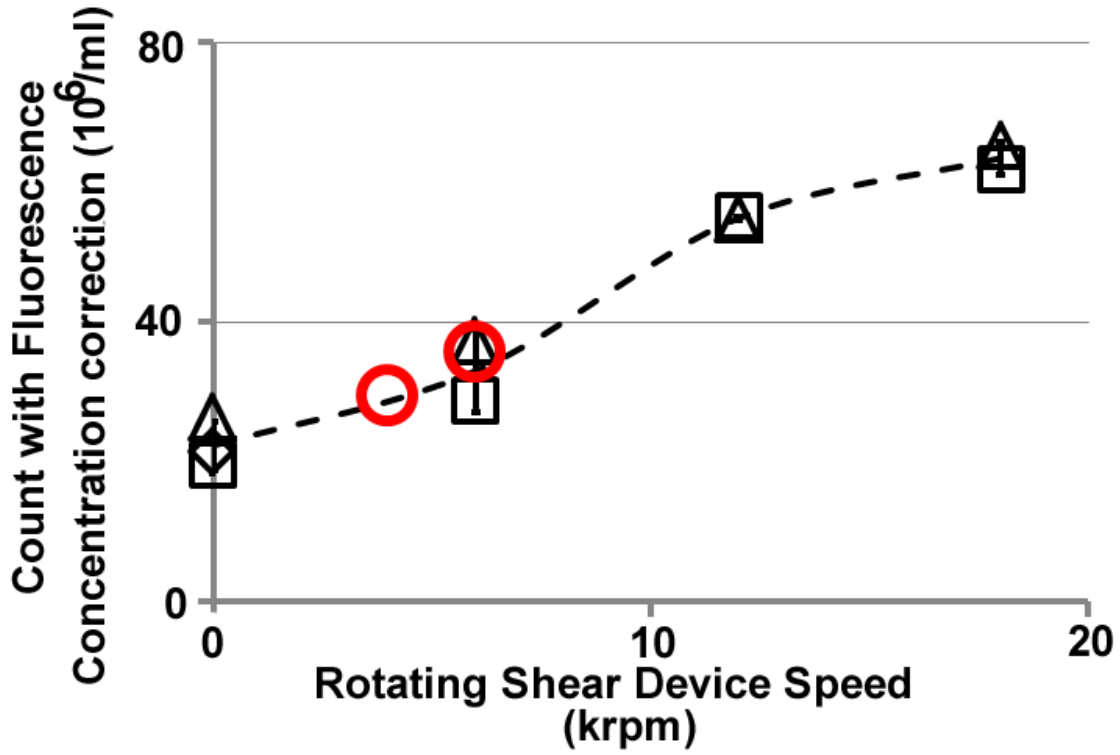

Figure 5.2-6. Fluorescence assay results for sheared nanobeads which have been subjected to disruption by a rotating shear device at varying shear rates prior to fractionation in a laboratory density gradient centrifuge. The nanosight-fluorescence assay derived concentration for duplicate runs (□, Δ) is plotted against the shear device speed to which the sample was subjected. Error bars represent standard deviation of the duplicate sample. The two large red circles (◯) are duplicate runs for nanobeads separated using the PKII continuous feed ultracentrifuge.

5.2.4. Understanding the impact of density gradient and shear level on nanobead particles

Sensitivities were conducted on shear level and duration, and on the density gradient used to fractionate the nanobeads. Although increasing shear time showed a small increase in particle count, the more substantial impact was seen from changes in the density gradient (Figure 5.2-7). Count changes with steeper and shallower density gradient, particularly at higher shear levels. The density gradient for the data points shown in Figure 5.2-6 are equivalent to that used in the PKII centrifuge (detailed in section 5.2.5), where the measurement of density was based on a curve fitted to multiple points along the density gradient. It is further suggested that, although the density of the layer itself appears to show a clearer correlation against count, both the density and the integral of the density up to that point be taken, as co-correlates to improve precision. Although this adds complexity to the use of this shear mimic for the prediction of shear at large scale, it does present an interesting finding in terms of the combined effect of pre-shearing and fractionation in a density gradient on nanoscale particulates.

It seems unlikely that this is due to shear from the density gradient itself, or anything similar. Although it is conceivable that loosely held together aggregates disintegrate further, or that binding of biotinylated fluorescein to damaged streptavidin is inhibited in the presence of a more viscous solution. It may also possibly be a measurement artefact. Further investigation is required to better understand this phenomenon.

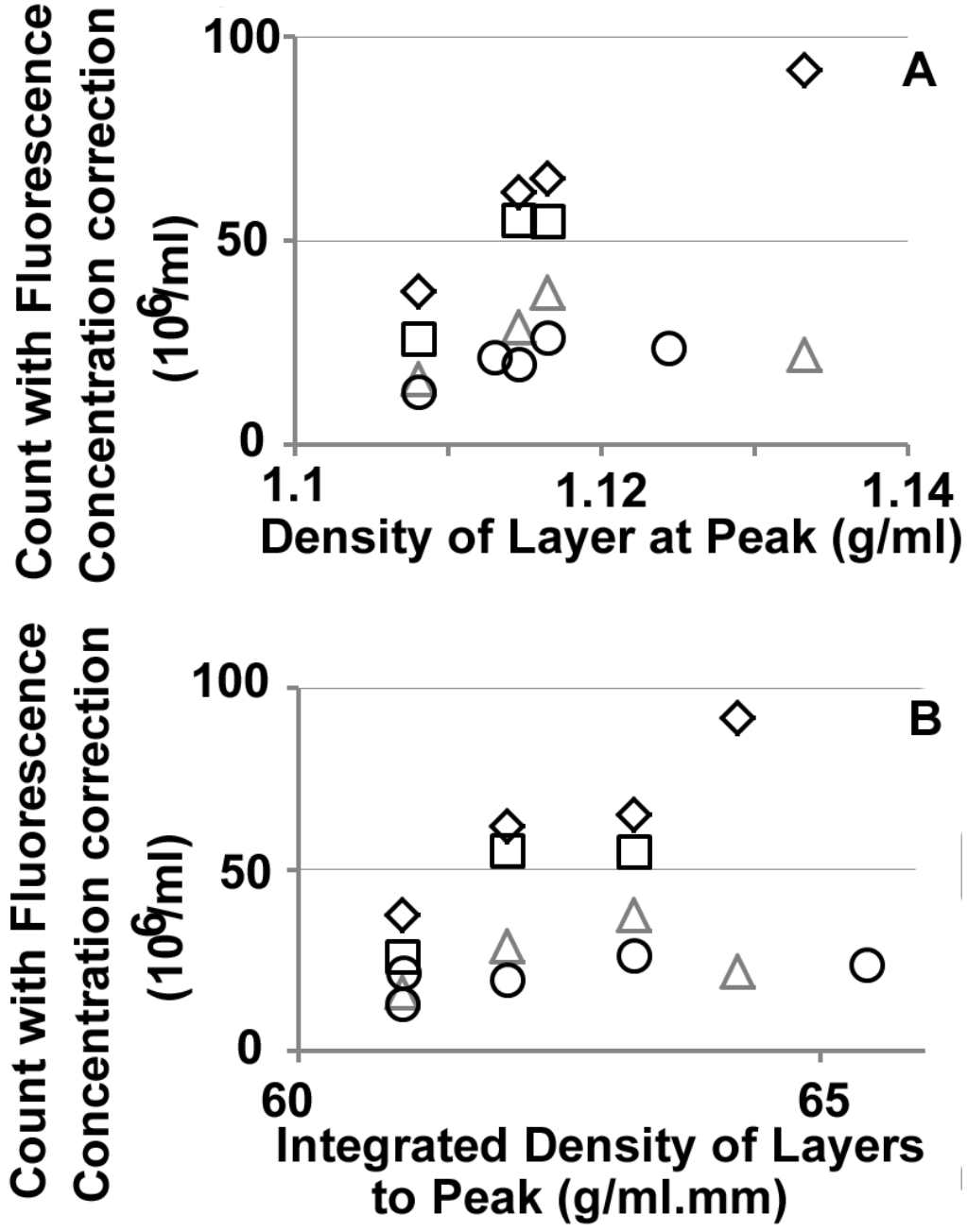

Figure 5.2-7. Combined nanosight and Fluorescence assay results for sheared nanobeads which have been subjected to disruption by a rotating shear device at varying shear rates prior to fractionation in a laboratory density gradient centrifuge. The data points are for rotating shear device speeds of 0 (○), 6 (Δ), 12 (□), and 18 (◇) krpm, in different sucrose density gradients as measured by the density at the layers selected (A) and the integral of the density up to that layer (B).

5.2.5. Shear and density gradient: Applying the lessons to a real process

Having established the technique for laboratory scale batch density gradient centrifugation, the pilot scale continuous feed density gradient PKII centrifuge was used to fractionate nanobeads. The resulting change in count is plotted on Figure 5.2-6 (open circles), where the density gradient is comparable to that used at laboratory scale. The rotating speed and spin-down time at laboratory scale were chosen to match the $\omega^2 t$ at large scale, and the density gradient modified to give approximately the same head at the expected position of the nanobeads, i.e. to account for the fact that the PKII density gradient only starts at 110mm from the centre of rotation, with PBS or process fluid filling the inlet feed zone and passing close to the central rotor to the centrifuge outlet. It can be seen in Figure 5.2-8 that the nanobeads settle at the same position in both pilot and laboratory scale centrifuges. The measure of fluorescence for each layer is a quick and easy way to identify the layer containing the nanobeads at both scales (Figure 5.2-8 A). The reduced fluorescence at low density for laboratory scale, is not seen in the pilot scale centrifuges. This is likely to be due to loose streptavidin, which in the continuous feed (pilot) centrifuge will be washed through in the flow-through. This interpretation is further supported by the particle count measurement in Figure 5.2-8 B, which shows no detectible particulates in the low density fractions for the laboratory centrifuges.

The predicted level of shear for the PKII continuous feed density gradient centrifuge corresponds to a rotating disc shear device speed of approximately 5krpm. This is the level of shear seen in a low shear industrial disc stack centrifuge such as might be used during the harvest stage of a cell culture process. Although industrial density gradient centrifuges are generally assumed to be low shear processes, it is not altogether surprising that the level of shear should be comparable to that in a disc stack centrifuge, given the substantially higher rotational speeds mitigated by smaller feed diameter. The results therefore indicate that the virus shear mimic is capable of giving a good prediction of shear at large scale conditions. The implications of these levels of shear for viruses are explored more fully in section 6.3.

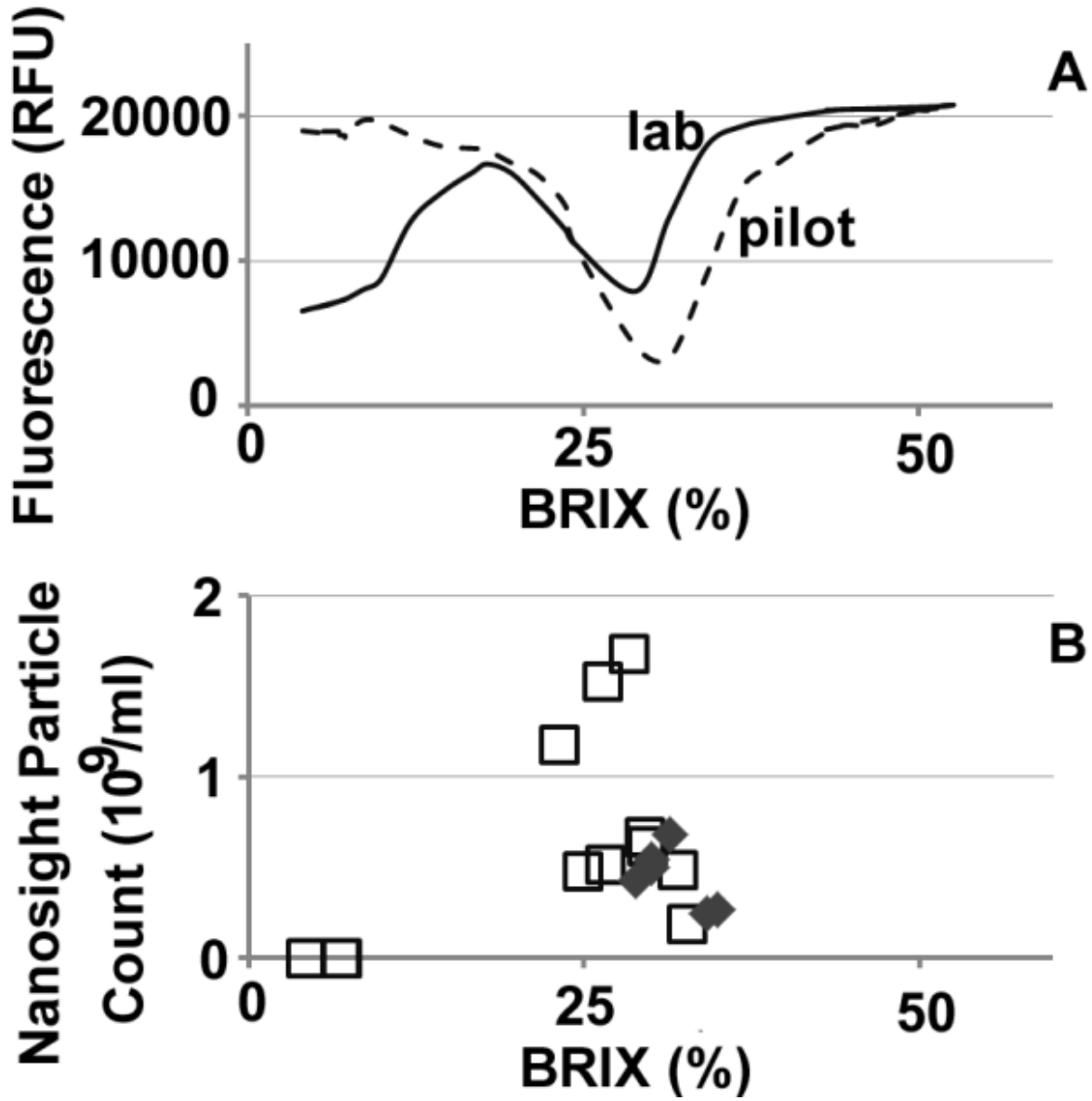

Figure 5.2-8. Fractionation of the nanobeads in the laboratory density gradient centrifuge and in the PKII centrifuge over a sucrose gradient, (calculated in BRIX), as measured by (A) fluorescence quenching at lab scale and pilot scale density gradient centrifugation and (B) particle count using Nanosight. Squares (□) are average of measurements from the laboratory density gradient centrifuge, and diamonds (◆) are average of measurements from the PKII continuous feed centrifuge.

5.3. Computational Fluid Dynamics (CFD) Validation

The predicted rotating disc shear device disc speed required to imitate the level of shear in the PKII based on the shear mimic is approximately 5krpm (section 5.2.5), which is the same order of magnitude of that from the CFD derived prediction of approximately 8.5krpm (Section 3.4.1).

5.4. Summary

Streptavidin coated nanobeads are proposed as a shear mimic for viral products, in order to quantify shear levels in process units which may be relevant to the downstream purification of viral vaccines or vectors.

A fluorescence assay was developed using a biotinylated fluorescein that quenches on binding to the streptavidin coat on the nanobeads. However, results indicate that the shear does not substantially damage the streptavidin layer. Therefore the fluorescence assay could not be used to measure the impact of shear.

Nanosight measurements of the nanobead particle size distribution revealed that the nanobeads clump, forming aggregates of multiple nanobeads. These aggregates are broken down by shear, showing a decrease in particle diameter, and a corresponding increase in particle count.

Sheared beads were applied to both lab and pilot scale density gradient centrifugation. By combining the fluorescence assay and nanosight count measurement for the most concentrated layers the correlation between pre-shearing of the nanobeads and particle count was still in evidence.

The methodology is further complicated, however, by the apparent dependence of this measurement on the density gradient conditions - the steepness of the gradient, head, $\omega^2 t$ – which needed to be accounted for.

The virus shear mimic has been used to measure the shear in the PKII density gradient centrifuge, more or less confirming the predictions made using CFD (section 3.4.1).

This shear level can be used in combination with measurements of the impact of shear on viral products in chapter 6, to infer the likely impact of process conditions.

Despite the complexity of the analytical methods derived to measure the impact of shear for this viral shear mimic it may still be simpler and more consistent than measurements made on viral products themselves. This question will also be explored in more depth in chapter 6.

6. Use of Ultra-Scale Down tool for Continuous Centrifugation Harvest of virus process materials

6.1. Objective & Summary

The centrifuge ultra scale-down (USD) model has previously been used successfully to predict the performance of various centrifuges for mammalian cell cultures (Hutchinson et al. (2006), Zaman et al. (2009)), protein precipitates (Boychyn et al., 2004) and flocculants (Berrill et al., 2008), including comparison to large scale of clarification (Boychyn et al., 2004), solids remaining, fragment antibody recovery and process impurity concentrations (Lau et al., 2013), and impact on subsequent filtration performance (Zaman et al., 2009). No literature has been published, however, on the use of the ultra scale-down mimic in predicting the performance on virus infected cell harvests. Nor is the author aware of any literature on the effects of shear on virus infected cells or on the virus product itself. This chapter therefore aims to redress this and gain insights into the performance of these important processes using this well characterised and already successfully demonstrated laboratory mimic.

It may be assumed that the time frame is more or less equal for both large and small scale, on the basis that a comparable experiment would require the cells to be passaged an equal number of times. Assuming 5 passages before bioreactor, this equates to a total lead time of approximately 4 weeks for both large and small scale. However, the effort and time working at a smaller scale may not be as significant, and a single failure at large scale is far more costly than at small scale. Small scale experiments with cell culture would also be constrained by the required stage of cell culture, in terms of timing the experiment, but availability of equipment and operators should be less of a constraint (e.g. no requirement for pilot scale centrifuge and operator to be made available). For viral vaccine production the complexity and costs are increased by biosafety concerns. So therefore are the benefits of using USD technologies.

Studies were conducted on the impact of shear on HEK and EB66 cells before and after infection with adenovirus and influenza respectively. The interest of these studies was in the implications for the harvest and subsequent processing of adenovirus and influenza for therapeutic and prophylactic viral vaccines. These are both areas of major importance, in which continuous cell line production of a viral product is involved and where scale plays a major role in cost and availability of sufficient product.

The starting hypothesis was that virus infection would make cells more “fragile” and prone to damage by shear. This was assessed by measuring clarification, protein release and cell count following shearing in the rotating disc shear device for both virus infected and uninfected cells. Although it cannot be said definitively from the data that virus infected cells are not more sensitive to shear at some point in the infection process, the evidence strongly suggests that cells used to propagate enveloped influenza virus in cell culture may be more shear sensitive and more difficult to clarify in comparison to non-enveloped adenovirus. The clarification may be worse for cells where the virus produces a significant amount of lysis debris, and unchanged, or even improved, for cells where the virus leaves the cell structure largely intact. Further work is required before any definite patterns can be drawn for clarification and shear sensitivity for different cell types, virus types and culture conditions.

With respect to the impact of shear on viral products the starting premise was that the viral particle’s small size would reduce the chances of its being caught in a vortex of small enough size for hydrodynamic shear alone to cause damage. However, initial experimental work with streptavidin coated nanobeads (Chapter 5), indicated that even particles in the 100 nanometer size range may show a measurable change within a relatively low shear environment. Indeed, although infectivity assays show no significant impact on the viruses from shear, there does appear to be some measureable changes in the virus particles with respect to the average particle size distribution and proteomic make-up. The significance of these changes, if any, remains to be fully explored. There is the possibility based on these results that, whilst the impact of shear appears subtle and the whole particle count may not be effected, other aspects of product quality may be influenced.

6.2. Impact of Virus Infection on Cells

6.2.1. Impact of shear on HEK cells used to produce Adenovirus

With increasing time post-infection HEK cells show no decrease in clarification, with clarification of sheared cells improving with later harvests (section 6.2.4.1). This contrasts with the hypothesis. It is interesting that the cell lysis by this virus does not appear to significantly decrease the clarification. Cell count combined with the trypan blue viability assay appear to suggest that the explanation is related to cell death under this mechanism of virus lysis which leaves the cell structure largely intact (section 6.2.5.1).

This has implications for the best approach to harvesting of adenovirus at large scale, because so much of the virus is inside the cell. Thus, a detergent lysis step or homogenisation is conducted to release the adenovirus from the cell mass. Bench scale processes, which rely on low shear pelleting followed by freeze-thaw to lyse cells and release the virus product will not accurately reflect what happens in large scale processes, and therefore will give limited insight into the challenges and opportunities. In particular, the addition of a higher-shear disc stack centrifugation step prior to lysis will clearly have implications for the product location and yield, and potentially for the relative importance placed on the processing of the supernatant. This is further complicated by the uncertainty respecting the relative quality of viral particles in the supernatant and in the cells which would also need to be investigated and taken into account (Altaras et al., 2005).

Although these results would need to be confirmed for suspension cultures they potentially provide some valuable insights for the numerous large scale production processes being developed, particularly with respect to harvest windows and decisions regarding harvesting product from the supernatant, cell mass, or both.

6.2.2. Impact of shear on EB66 cells used to produce Influenza virus

EB66 cells infected with influenza show a distinctly different clarification to uninfected EB66 cells. In contrast to the above result, with HEK cells infected with adenovirus the clarification of influenza infected EB66 cells decreases with increasing time post infection (section 6.2.4.2).

Again, as for HEK cells and adenovirus, the cell count was measured for different shear levels, for both influenza virus infected and uninfected EB66 cells. And as with HEK cells it was shown that after infection the cell count decreased less noticeably with shear than for uninfected cells (section 6.2.5.2). Application of the same explanation, of a greater number of dead cells, is supported by the decrease in viability.

The laboratory scale and pilot scale results were compared in terms of clarification (section 6.2.4.3) and protein release (section 6.2.6.2), where a good comparability was found at the expected level of shear.

6.2.3. Summary of cultures

6.2.3.1. Adenovirus

Cell culture and virus replication conditions for adenovirus in HEK cells are summarised in Table 2.2, and described in section 2.2.5.1.

6.2.3.2. Influenza

Cell culture and virus replication conditions for influenza virus in EB66 cells are summarised in section 2.2.5.2, and are as per the GSK pilot scale process in development.

6.2.4. Clarification of virus infected cell material via centrifugation

6.2.4.1. Adenovirus: The impact of infection period

HEK cells grown in an adherent culture were sheared either four to six days following infection, two to three following infection, or without being infected with adenovirus, and clarification measured at lab scale. It was anticipated that the cells might show increased sensitivity to shear following infection that could lead to the generation of fine debris which might impact on clarification (Silva et al., 2010), but as can be seen in Figure 6.2-1 this was not the case. No significant decrease in clarification was seen in the first 3 days following infection, and following longer infection periods the clarification improved significantly. In fact, cells that had been infected by virus for longer periods of time became less shear sensitive by this measure.

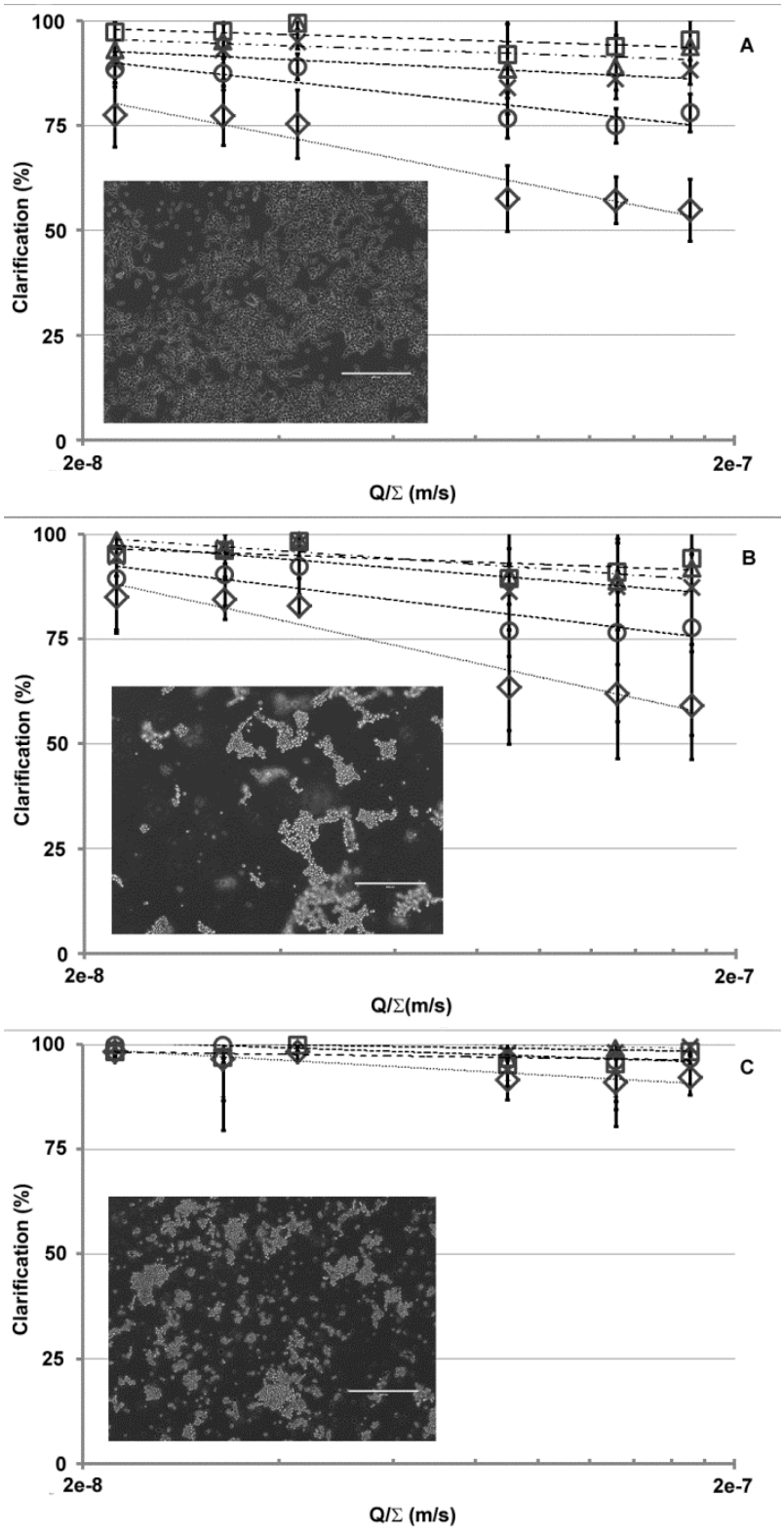

Figure 6.2-1. Clarification of (A) uninfected HEK cells, (B) infected HEK cells with adenovirus for less than 3 days, and (C) infected HEK cells with adenovirus for between 4 and 6 days. Cells have been subjected to disruption by a rotating shear device at varying shear rates prior to clarification in a laboratory centrifuge, with rotating shear device speeds of 0krpm (□), 6krpm (Δ), 8krpm (X), 10krpm (○) and 12krpm (◇) respectively. Error bars represent 95% confidence intervals using student t-test (n=6).

6.2.4.2. Influenza: The impact of infection period

Figure 6.2-2 shows that the clarification efficiency for influenza virus infected cells is significantly lower than that of non-virus infected cells based on a 95% confidence interval (n=3). It also appears to show an increase in the impact of shear. As shear increases, the clarification efficiency decreases and is worsened with increased viral infection duration.

It may be noted that whilst the slope of the curves in Figure 6.2-2 increase with virus infection, the distance between the slopes, representing different shear levels, only shows a clear visible increase after 5 days of infection. This may represent a combined effect of the impact of virus infection on the cells and the subsequent increasing sensitivity of the clarification to shear.

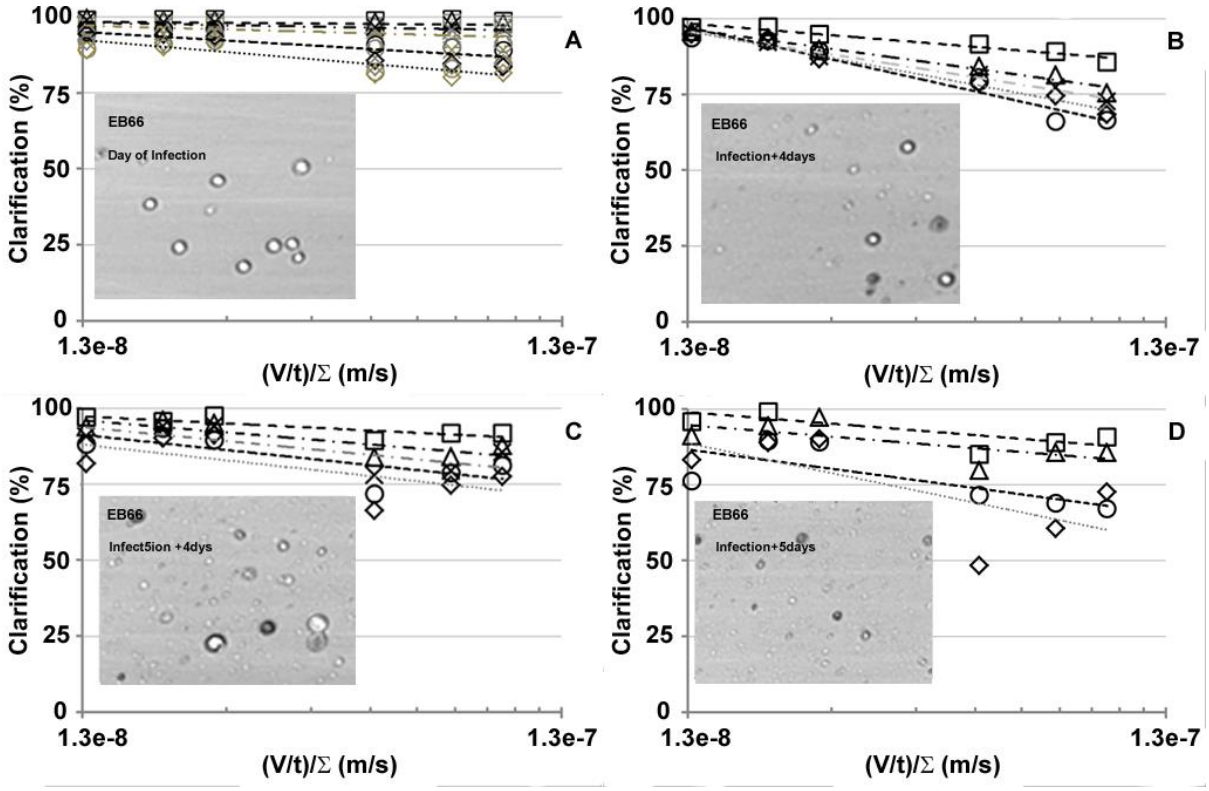

Figure 6.2-2. Clarification of EB66 cells, (A) uninfected with influenza virus, (B,C) infected with influenza virus for 4 days (n.b. strains used in B and C were not identical) and (D) infected with influenza virus for 5 days (same strain as in B). Cells have been subjected to disruption by a rotating shear device at varying shear rates prior to clarification in a laboratory centrifuge, with rotating shear device speeds of 0krpm (□), 6krpm (Δ), 8krpm (X), 10krpm (◯) and 12krpm (◇) respectively. Measurements shown are for a single representative run with the exception of (A), where n=3.

6.2.4.3. Influenza: Small versus large laboratory centrifuges

The influenza virus was cultured at pilot scale (50litres), and clarified using a disc stack centrifuge (PSC-5). Prior to these influenza based studies this disc stack

centrifuge was run with both HEK and CHO cells at the same flow rate and rotational speed as used for the clarification of the influenza harvest. The clarification of these HEK and CHO cell cultures were measured both for the disc stack centrifuge and using the ultra scale-down mimic (consisting of rotating disc and laboratory centrifuge), which has been used extensively for the prediction of clarification in mammalian cell cultures. This work (see section 3.3.1) confirmed that the centrifuge in question is a low shear centrifuge, with rotating shear device speeds of the order of 4.6 krpm and 6 krpm for HEK and CHO respectively giving a good prediction of clarification and protein release levels (Melinek et al., 2017). As this scale-down mimic has not yet been validated for use with virus infected continuous cell line harvest it was deemed important to include validation at scale, in discussing the implications of the presented results.

Figure 6.2-3 therefore includes the clarification as measured for the disc stack supernatant. The equivalent rotating shear device speed required to accurately match the disc stack centrifuge clarification, overall protein release and relative concentration for a number of host cell proteins (Figure 6.2-9 and Figure 6.2-10) is approximately 4.5krpm. This result is therefore consistent with expectations.

It was noted that there was an unexpected discrepancy between the small and large lab scale centrifuges (compare Figure 6.2-2D and Figure 6.2-3). Clarification from the larger lab scale centrifuge was consistently below that of the smaller lab scale centrifuge. Given the costs and industrial setting of this work it was not possible to complete sufficient repeats to verify the significance of this difference. However, it was noted that this effect was less visible in the non-infected EB66 cells. It has been hypothesised that this difference may be due to differences in the g-forces or head present in these different systems, but again it was not possible to fully verify this hypothesis. It may also be observed that the infected EBB66 cells give a less consistent measure of clarification. This may be due to (i) differences in the way the debris or cells pellet, or (ii) difference in the supernatant make up, such that there is a tendency to form solid impurities, which manifest as a floating ‘scum-film layer’ following virus infection, or (iii) differences in methodology, as noted in the materials and methods, clarification section.

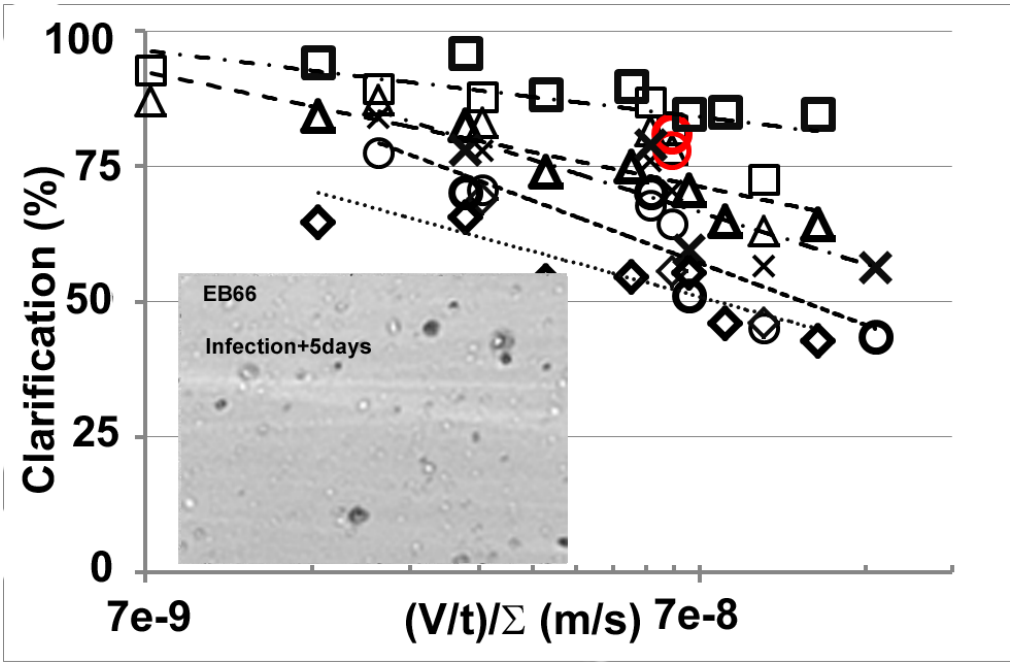

Figure 6.2-3. Clarification of EB66 cells, infected with influenza virus for 5 days. Cells have been subjected to disruption by a rotating shear device at varying shear rates prior to clarification in a Beckmann laboratory centrifuge, using 15ml falcon tubes, with rotating shear device speeds of 0krpm (□), 6krpm (Δ), 8krpm (X), 10krpm (◯) and 12krpm (◇) respectively. Measurements shown are for two separate runs, each using a different viral strain of influenza. In addition red circles (◯) give the clarification measured on the PSC-5 centrifuge.

6.2.5. Cell count

6.2.5.1. Adenovirus: The impact of infection period

Figure 6.2-4 shows no difference in the decrease in cell count relative to initial cell numbers for the first 3 days following infection, and no impact of shear on cell count following a longer period of infection. In fact, cells became less shear sensitive as infection time increased. Trypan blue was used to demonstrate that this change is likely to be due to cell death which occurs somewhere between the 3rd and 4th day of infection.

It has been shown elsewhere (Tait et al., 2009) that older or dead cells in non-virus infected cultures may be less shear sensitive, possibly due to the flaccid and weakened cell structure of the dead cell in the shear velocity gradients. This hypothesis is supported by cell count and viability assays and clarification (section 6.2.4.1) which show (i) that cell counts for sheared infected cells follow the same trend as for uninfected cells during the first 2 days of infection, whilst after longer infection periods the cell count no longer decreases with shear, and (ii) there is a decrease in viability of cells after 3 days of infection. As the cells die and become

more flexible they have less tendency to break-down or form the micro-debris (Figure 6.2-5) which decreases clarification efficiency.

For biosafety reasons, adenovirus infected cells could not be removed from the virus lab, and particle size distributions could not therefore be measured on a particle analyser such as the Mastersizer or Casy, for comparison to similar work with the continuous centrifuge ultra-scale down system. A combination of Nanosight and haemocytometer were therefore used, to measure the impact of shear in terms of the break down of whole cells into debris, as illustrated in Figure 6.2-5.

Visually the cells appear to remain largely whole and intact, with the population increasing substantially over the post-infection period. The debris count, as measured in the size range ~60 to 600nm, does not appear to increase substantially, reinforcing the impression given by visual inspection. The virus induced lysis takes the form of an increased permeable cell membrane, as oppose to the absolute destruction of the cell, under these culture conditions. It may be that the fact that these are adherent cell cultures plays to the morphology of the cells and their shear sensitivity, i.e. if these cells were grown as a HEK suspension the result would be different. This remains to be confirmed.

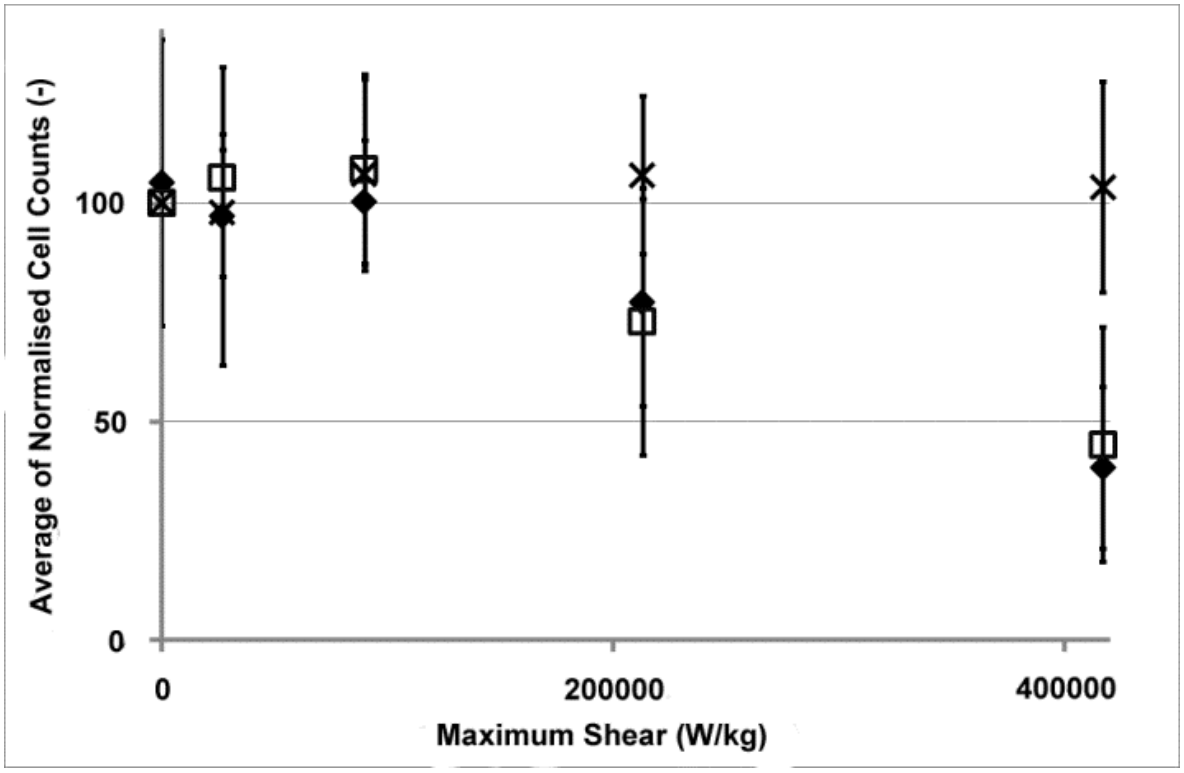

Figure 6.2-4. Normalised cell counts for HEK cells, not infected with adenovirus (◆), infected with adenovirus for less than 3 days (□) and infected with adenovirus for between 4 and 6 days (X). Cells have been subjected to disruption by a rotating shear device at varying shear rates, and then counted using a haemocytometer. Cell count has been normalised against unsheared cell count. Error bars represent 95% confidence intervals using student t-test (n=4).

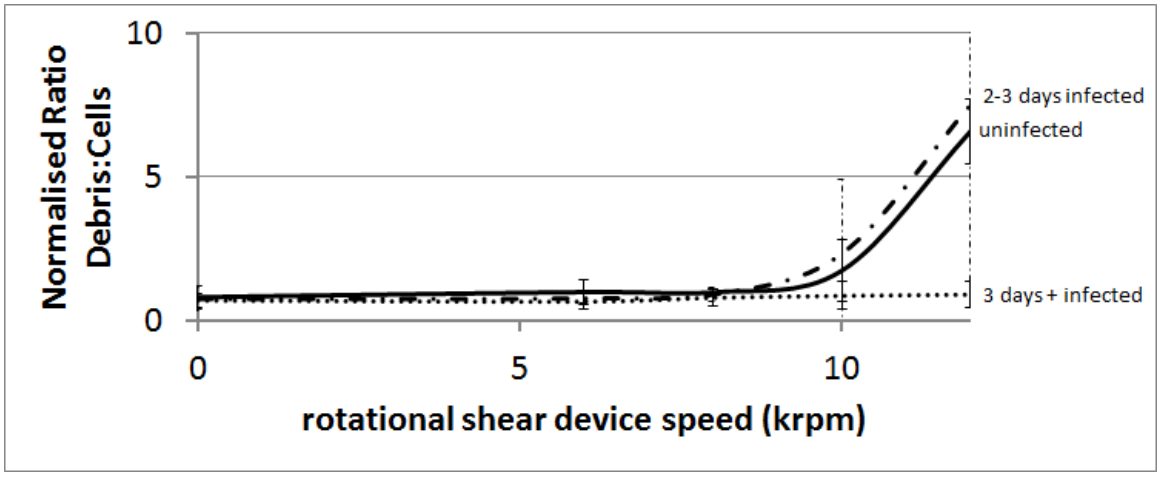

Figure 6.2-5. Ratio of debris to whole cells as measured by Nanosight (debris) and haemocytometer (cells). The ratio has been normalised to give a value of 1 for unsheared cells. Nanosight measurements were completed for the supernatant. Measurements shown are for uninfected HEK cell, cells, infected with adenovirus for less than 3 days and cells infected with adenovirus for more than 3 days.

6.2.5.2. Influenza: The impact of infection period

Figure 6.2-6 , shows a similar pattern to that seen in adenovirus infected HEK: the proportion of cells destroyed by shear in influenza infected cells decreases following infection, particularly for the highest shear level.

It was noted that the following infection the proportion of remaining cells which are viable increased with shear, whilst for uninfected cells it decreased. This may imply that cells deemed to be non-viable are marginally more likely to be destroyed by shear, possibly including infected cells. This could not be confirmed by infectivity assays, as with adenovirus, because influenza virus released by shear would not be enveloped, and therefore not mature, viable or infective.

The viability of sheared cells is marginally, but consistently, greater than for unsheared cells in the virus infected cells, whilst in the non-virus infected cells it is less. For unsheared cells the viability was 96+/-4.5% (95% CI, student t-test, n=3), to 73+/-9.2% and 77+/-10.8% (95% CI, student t-tests, n=2) for uninfected EB66 cells, and 4 and 5 days post infection respectively. For cells subjected to shear in the rotating shear device at a speed of 12krpm, for example, the viabilities of the uninfected EB66 cells was 92%, and cell viabilities of influenza infected cell at 4 and 5 days post infection were 78% and 81% respectively. As a percentage of the original number in the sample therefore the non-viable cell count decreased more than the viable cell count.

Taken together the decrease in clarification between uninfected and virus infected cells (Figure 6.2-2), and the increasing shear insensibility indicated by the cell count (Figure 6.2-6), implies that clarification is being impacted by the debris formed by virus induced cell lysis during or following viral egress from the cell. The Vi-Cell images certainly show a noisier background after a number of days of infection which may be membrane components which form during virus egress from the cell.

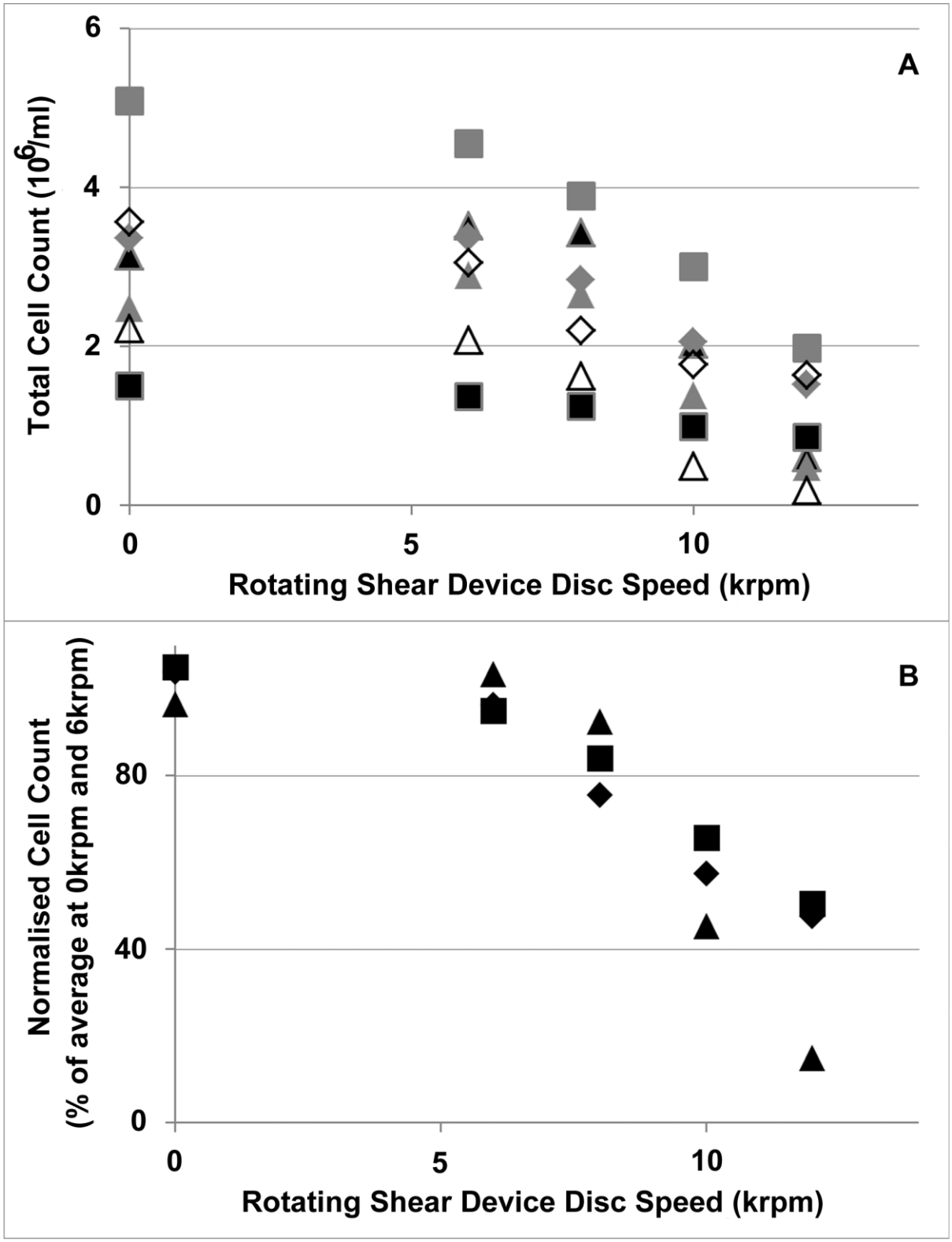

Figure 6.2-6. Cell counts for EB66 cells, not infected with influenza virus (Δ, ▲, ▲), infected with influenza virus for 4 days (■, ■) and infected with influenza virus for 5 days (◊, ◆, ◆). Cell have been subjected to disruption by a rotating shear device at varying shear rates, and then counted using a Vi-Cell. In (A) measurements shown are for three separate runs each using various influenza A viral strains. In (B) average normalised measurements are shown for pre-infection and the two post-infection time points

6.2.6. Proteins

6.2.6.1. Adenovirus: Protein release

Within the first 3 days following infection there is evidence that shear may cause release of virus from cells. Immunoblots (see supplementary data in Appendix F) were conducted showing that the viral protein concentrations in the supernatant increase with increasing shear, as shown in Figure 6.2-7. Although the proteins selected are nominally identified, it should be noted that these identifications are designed for illustrative purposes only. Overall measures of protein concentration in the supernatant show an increase with increasing shear, with each lane on the Western blots run at equal protein concentration. From which it appears that viral proteins are released at a greater rate than host cell proteins. This is supported by an increase of more than a log in infective units in the supernatant (Figure 6.3-2), based on a duplicate measurement using a blue forming units assay for quantification of virus by counting transfected cells.

From section 6.2.4.1 and 6.2.5.1 infected cells appear no more likely to be destroyed by shear than uninfected cells. This implies that the virus production processes are efficient, with cells producing more protein as virus production factories than they do for normal metabolic activities. Indeed this agrees well with evidence that adenovirus production is highly metabolically demanding (Silva et al., 2010), and with the high burst volumes shown for adenovirus in HEK (Xu et al., 2015a), and also with evidence that adenoviruses may induce autophagy (Balvers et al., 2011).

It may also be noted that the evidence gathered to date does not preclude the possibility that the additional virus release is due to detachment of virus which was bound to the external cell membrane, or disaggregation of virus aggregates (Slater, 2018), as oppose to destruction of virus infected cells. Further work is required to verify the source of the additional virus in the supernatant following shear.

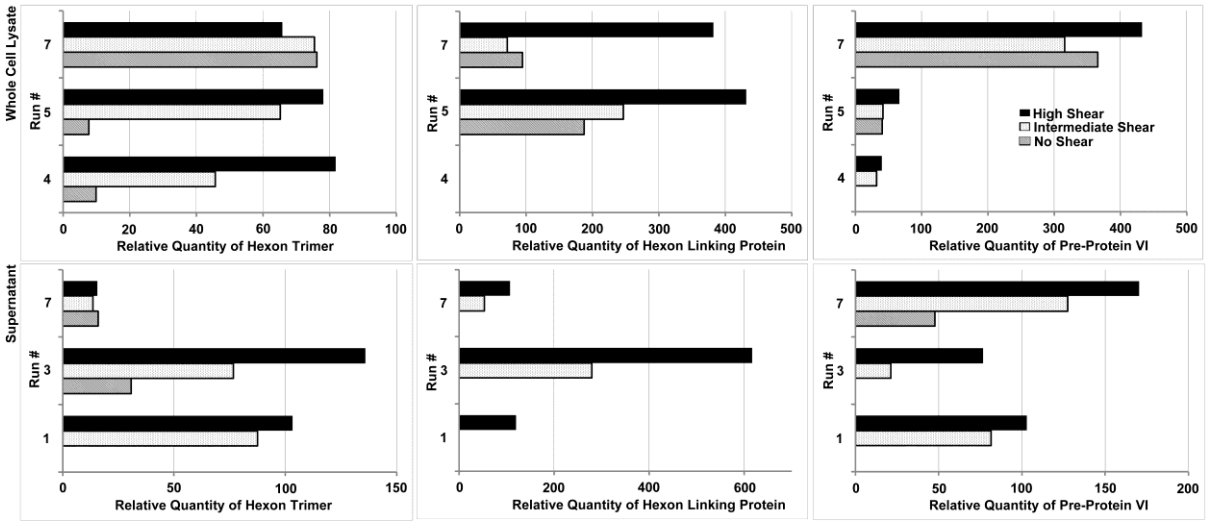

Figure 6.2-7. Graphs show relative concentrations for selected viral proteins (identified on the immunoblot in Appendix F supplementary data). Graphs on the top are of lysate concentrations, and on the bottom are of concentration in the supernatant. Striped is unsheared, dotted has been subjected to an intermediate level of shear (12krpm in the rotating shear device) and filled has been subjected to a high level of shear (18krpm in the rotating shear device). In the lysate plot results from three replicate runs are shown, and in the supernatant plots two replicate runs (1, 3) harvested 2 to 3 days post infection and one run (7) harvested approximately 5 days post infection. The concentrations for all runs have been normalised against the same reference sample.

6.2.6.2. Influenza: Protein release

With increasing shear more proteins are released from EB66 cells, as shown in Figure 6.2-8, with an immunoblot against EB66 host cell proteins shown in Figure 6.2-9 and with a number of individual protein levels quantified in Figure 6.2-10, showing significant increases in the concentration of various proteins with shear.

It would be valuable to future similar work to complete (see supplementary data, Appendix F) an immunoblot of the influenza virus proteins, as it is potentially informative with respect to demonstrating the relative shear induced release of viral protein from cells as compared to host cell proteins. It may be for example that viral protein release would be more problematic than that of host cell proteins for downstream purification, in particular chromatography.

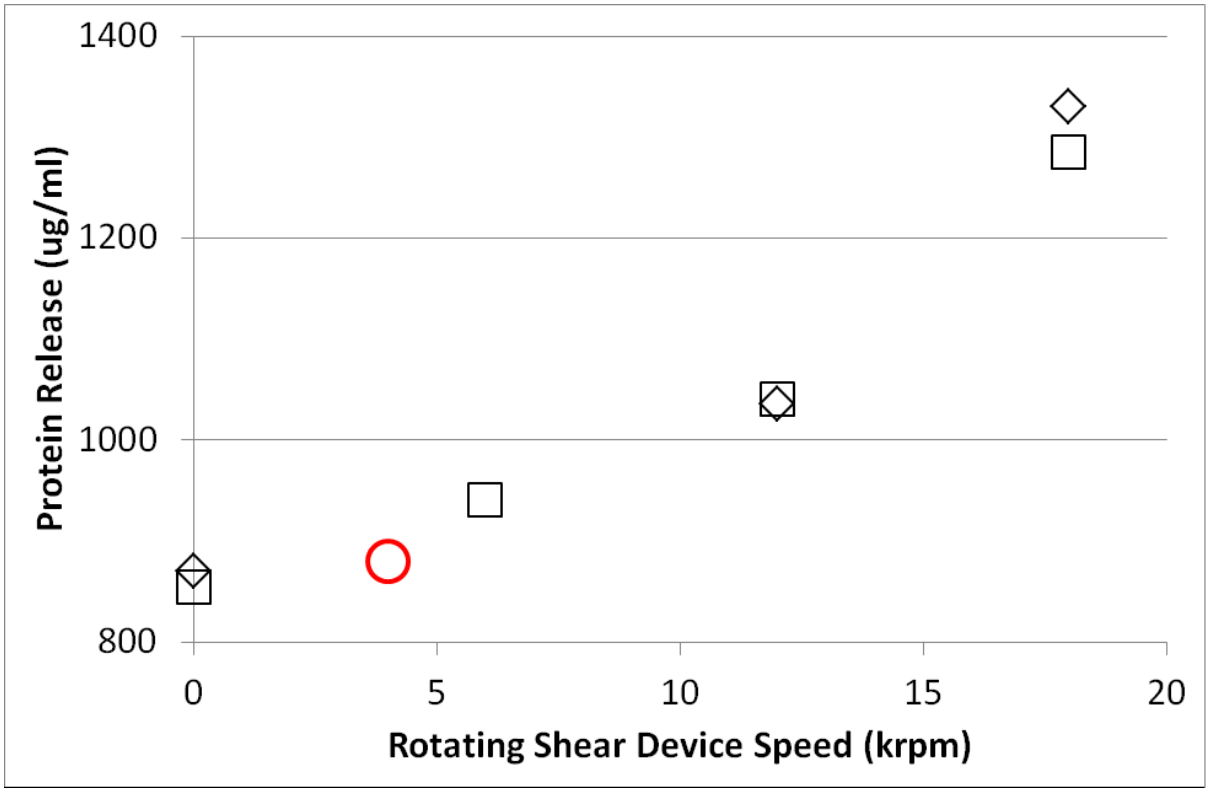

Figure 6.2-8. Total protein concentration for EB66 cells infected with influenza virus for 5 days. Cells have been subjected to disruption by rotating disc shear device at varying shear rates prior to clarification in a Beckmann laboratory centrifuge, using 15ml falcon tubes. Measured using modified Lowry method. Two measurements shown at laboratory scale (□,◊), using influenza A strains. In addition the red circle (◯) gives the clarification measured on the PSC-5 centrifuge

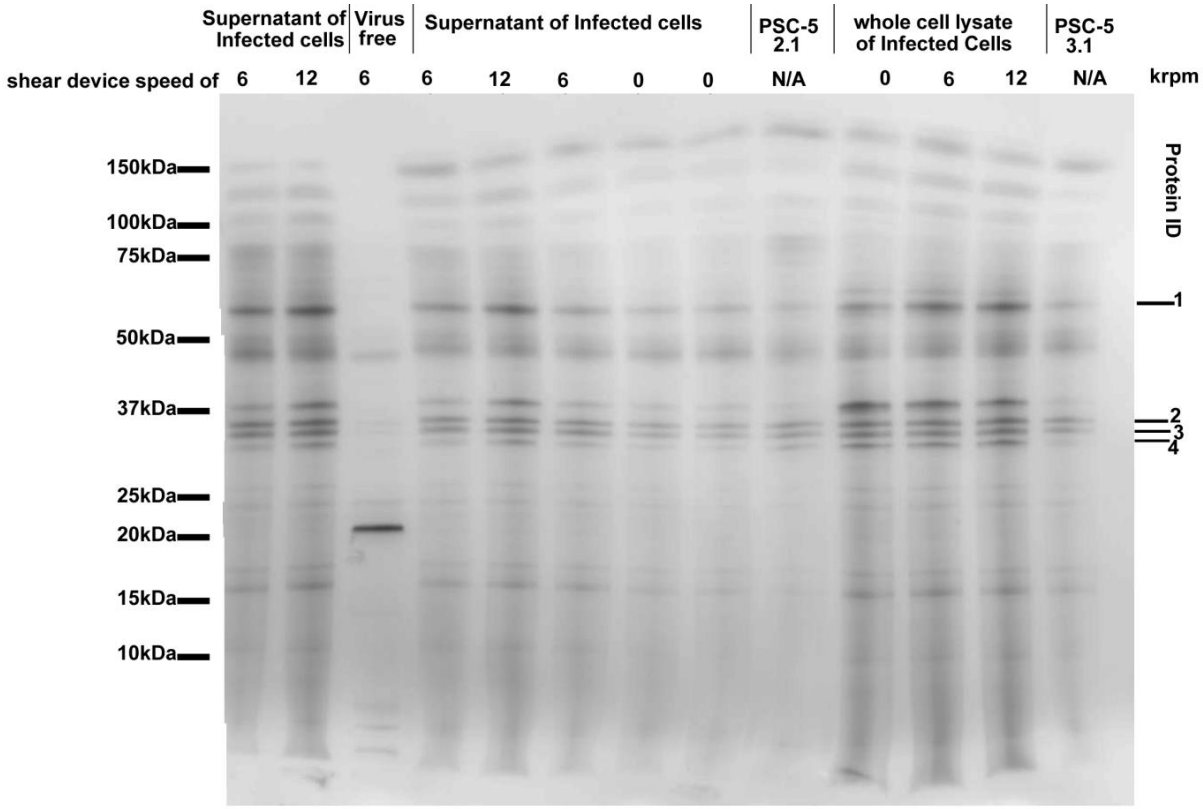

Figure 6.2-9. Sample Immunoblot, tagged with antibodies against EB66 host cell proteins. Lanes are supernatant of influenza virus infected EB66 cells subjected to rotating shear device speeds of 6 and 12krpm respectively, supernatant of EB66 cells not infected with virus subjected to a rotating shear device speed of 6krpm, supernatant of influenza virus infected EB66 cells subjected to rotating shear device speeds of 6, 12, 6, 0 and 0krpm, the supernatant from PSC-5 and the same virus run as in the other lanes, lysate from influenza virus infected EB66 cells subjected to rotating shear device speeds of 0, 6 and 12krpm and a reference virus infected supernatant sample (the supernatant from the PSC-5 on the first virus run). Equal volume of sample was loaded in each lane.

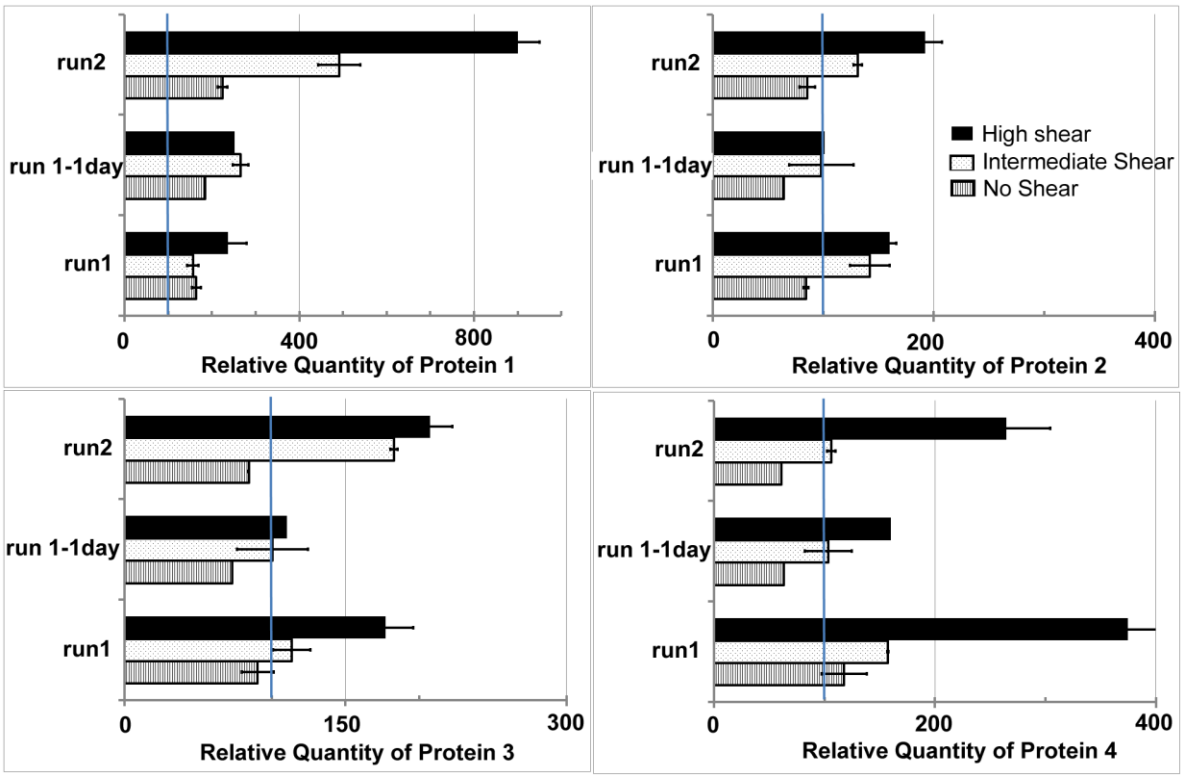

Figure 6.2-10. Graphs show relative concentrations for selected host cell proteins (identified on the immunoblot in Figure 6.2-9). Graphs show average concentrations for two separate run (with different viral strains) and from the day before harvest for the second run. Cells have been subjected to disruption by a rotating shear device at varying shear rates prior to clarification in a Beckmann laboratory centrifuge, using 15ml falcon tubes. The protein concentrations for each run have been normalised such that the concentration for the PSC-5 centrifuge supernatant for that run is 100. In the bar charts striped is unsheared, dotted has been subjected to a low level of shear (6krpm in the rotating shear device) and filled has been subjected to a high level of shear (12krpm in the rotating shear device). Error bars are sample standard deviation of duplicate measurement (n.b. 'run 1 – 1 day' has duplicates for the mid shear level only).

6.3. Impact of Shear on Viruses

A virus is an extremely complicated and heterogeneous biological agent, large on a molecular scale, with multiple component and structural levels involved in the many stages of its life cycle and interaction with its host. As a result there remain many questions regarding that life cycle, the role of the different structural components of the virus, and how the virus interacts with the cell and the wider host organism. In bioengineering terms, the critical quality attributes remain to be fully elucidated (Rathore and Winkle (2009), Vandercammen et al. (2012), Metz et al. (2009)). For cost, time and resource reasons only a limited number of carefully selected assays could be performed.

Cell based infectivity assays are of primary importance, demonstrating a likely subsistence of the basic functional features of the virus structure. Results based on infectivity assays alone support the original hypothesis that virus will be too small to be significantly effected by shear at the levels tested, i.e. within the range likely to be seen in industrial equipment.

However, previous stress experiments on viruses, focused on the impact of temperature and pH, showed substantial changes in other measures, before any change in infectivity was evident (Rexroad et al., 2003). This may be partly due to the high variability or low accuracy in infectivity outputs, such as $TCID_{50}$ assays. However, it may also reflect a certain robustness in the virus, that it retains the ability to transfect and infect even after undergoing a number of morphological changes. Evidence for such morphological changes, in measurement of particulate size and protein composition of isolated, post sheared virus, was therefore sought, to confirm the degree of impact from shear, if any.

6.3.1. Impact of shear on adenovirus infectivity

Figure 6.3-1 shows the $TCID_{50}$ infectivity assay results for adenovirus at a range of shear levels. Even at the highest shear level assayed no significant change in the infectivity of the virus is seen. The largest difference between the minimum and maximum infective titre based on this assay, for a given run, was 0.4 log_{10}/ml, not an unacceptable range for this assay type. This result was confirmed by use of a plaque assay quantified using Blue Forming Units (BFU), which showed no

significant change in the number of cells transfected by the sheared adenovirus (Figure 6.3-2). The BFU assay did, however, show an increase in the number of infective units in the supernatant with shear, showing infective virus being released from virus infected cells. For the whole cell lysate the largest difference between the minimum and maximum infective titre based on the plaque assay was 0.2 log_{10}/ml, again indicating a reasonable level of accuracy, and with no outliers. The maximum increase in the number of infective virus in the supernatant by contrast was 1.7 log_{10}/ml. The number of infective units per ml was in good agreement between the $TCID_{50}$ and BFU assays.

It may be noted that the results graphed in Figure 6.3-1 to Figure 6.3-4 are normalised, in order to improve the presentation, given the large differences in virus titres seen between replicate runs. The measurements were normalised separately for each replicate run by dividing by the average titre across all shear levels.

Rotating Shear Device Speed (krpm)	Unnormalised $TCID_{50}$ ifu/ml				
0 (unsheared)	2.0E+08	4.3E+07	5.0E+07	2.7E+08	1.5E+08
12 (high shear)	2.7E+08	4.8E+07	2.3E+07	2.6E+08	1.7E+08
18 (high-high shear)	2.0E+08	9.4E+07	2.1E+07	2.3E+08	2.0E+08

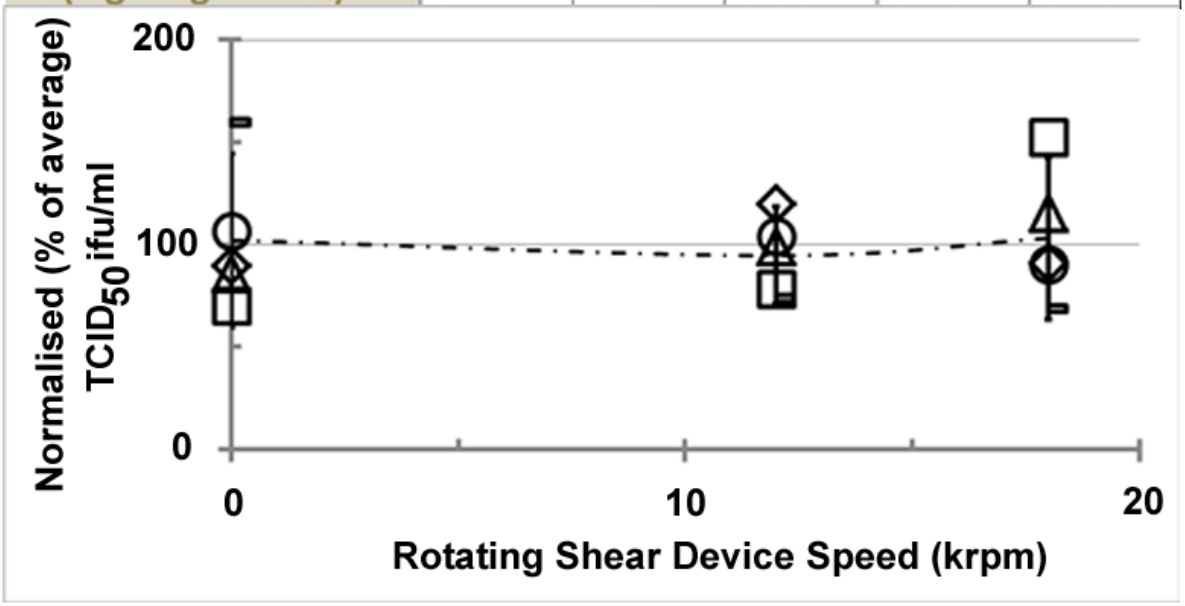

Figure 6.3-1. $TCID_{50}$ infectivity assay for adenovirus subjected to varying shear rates. The virus count is plotted as a percentage of the average virus count across all shears for each run. Five replicate results are shown (each represented by a different symbol- ◊, ○, Δ, □). Error bars represent 95% confidence intervals using student t-test (n=5). Samples were subjected to shear at 0 and 12krpm for 20 seconds, and 18krpm for 1 minute.

Rotating Shear Device Speed (krpm)	Unnormalised BFU/ml				
0 (unsheared)	4.2E+07	1.0E+08	7.0E+07	*2E+06	*4E+06
12 (high shear)	3.1E+07	1.1E+08	1.1E+08	*8E+07	*4E+07
18 (high-high shear)	4.3E+07	9.1E+07	9.4E+07	*9E+07	*9E+07

*Using supernatant from spun down cell lysate

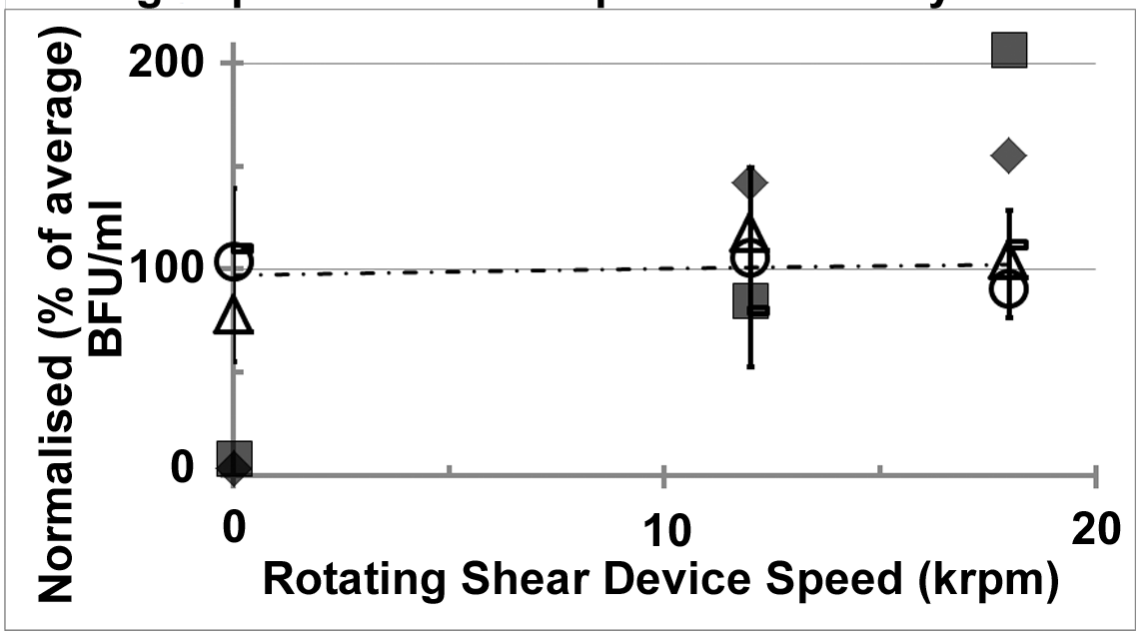

Figure 6.3-2. Infectivity assay for adenovirus subjected to varying shear rates. The virus count is plotted as a percentage of the average virus count across all shears. Three replicate results are shown (each represented by a different symbol- Δ, ○, ▫). Error bars represent 95% confidence intervals using student t-test (n=3). Samples were subjected to shear at 0 and 12krpm for 20 seconds, and 18krpm for 1 minute. In addition duplicate results (■, ◆) are shown for samples which were subjected to disruption by a rotating shear device at varying speeds, as above, and then centrifuged. Following spin-down the supernatant was removed, frozen, thawed and the infectivity measured using the BFU assay.

6.3.2. Influenza: Infectivity

Influenza virus, being enveloped, and forming at the cell cytosolic membrane, is not released in its infective form by shear induced lysis of the infected cells. This is demonstrated by the results in Figure 6.3-3. As seen above for adenovirus no significant change in the number of infective units is seen with shear. The largest difference between the minimum and maximum infective titre based on this assay, for a given run, was 0.75 $\log_{10}$/ml.

Rotating Shear Device Speed (krpm)	Unnormalised $TCID_{50}$ ifu/ml			
	Day 4		Day 5	
Cell lysate				
0 (unsheared)	4.4E+07	NR	NR	NR
6 (low shear)	7.6E+07	NR	NR	NR
12 (high shear)	5.5E+07	NR	NR	NR
18 (high-high shear)	5.5E+07	NR	NR	NR
Cell Supernatant				
$V/(t\Sigma)$ in m/s =	$4.58x10^{-7}$	$6.3x10^{-8}$	$6.3x10^{-8}$	$6.7x10^{-8}$
0 (unsheared)	1.9E+07	6.3E+07	1.0E+08	1.3E+07
6 (low shear)	1.1E+08	1.3E+08	5.0E+07	1.6E+07
12 (high shear)	4.2E+07	2.5E+08	4.0E+07	1.0E+07
18 (high-high shear)	NR	1.3E+08	1.0E+08	2.5E+07

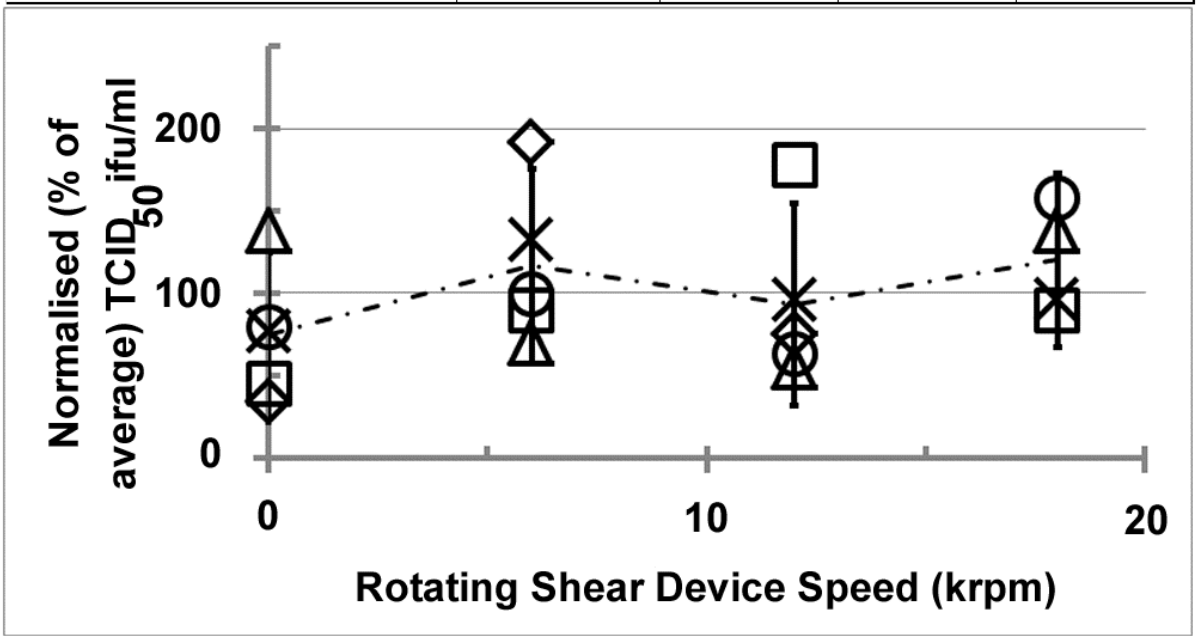

Figure 6.3-3. $TCID_{50}$ infectivity assay for influenza virus subjected to varying shear rates. The virus count is plotted as a percentage of the average virus count across all shears. Samples were subjected to shear at 0, 6 and 12krpm for 20 seconds, and 18krpm for 1 minute. Four replicate results (each represented by a different symbol- ○, Δ, □, ◊) are shown for supernatant from spin-down of the sample after shearing, with one assay result shown for the unspun cell lysate following shear (X). Error bars represent 95% confidence intervals using student t-test (n=5).

6.3.3. Fractionated Adenovirus: Particle Size

To confirm that no increase could be seen in the number of obviously damaged adenoviruses with shear Transmission Electron Microscope (TEM) was used. Although involving only a very limited sample size, there was no sign of any increase in the number of obviously damaged particles, or morphological changes which could be detected by TEM. Further the number of particles which could be identified as adenovirus did not change significantly (Figure 6.3-4). It may be noted that the count from TEM is an order of magnitude greater than that measured using infectivity assay techniques. This may reflect a large number of non-infective virus, indicating a very high P:I (particle to infectivity) ratio of the sample. It may be noted, however, that TEM measurements were performed on supernatant from spun-down samples, not whole cell lysate. And therefore an increase in count might have been expected. The absence of this increase may reflect a substantial number of non-infective virus already in the supernatant before shearing of the cells. If so this non-infective virus shows no more propensity to be destroyed by shear than infective virus. Despite the large error bars on the normalised count the largest difference between the minimum and maximum count, for a given run, using TEM was 0.5 $\log_{10}$/ml. This is not substantially greater than that seen above for adenovirus infectivity assays. TEM, however, is clearly not a very accurate or easily quantifiable measure of virus morphology.

Particle size distribution is one measure that can change significantly in response to certain stresses before any impact is seen on the virus infectivity (Rexroad et al. (2003)). Figure 6.3-5A shows the particle size distribution of adenovirus, which has been fractionated in a CsCl density gradient following shear, where measurements were conducted on the fractions that had been identified as containing adenovirus and showed the highest concentration of virus. The shift in the position of the peak is shown in Figure 6.3-5B. The change in modal diameter, although small, is significant for this substantial level of shear. The shear level used here is likely to be far higher than any shear seen in industrial process equipment, but the duration of shear may also be shorter. The presence of adenovirus in the particle size distribution samples, was confirmed by both silver staining and western blot against Ad5 coat proteins (data not shown).

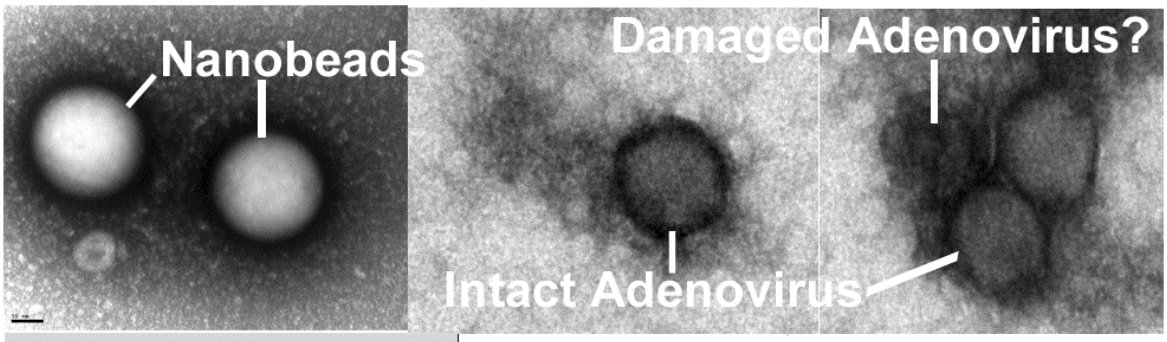

Rotating Shear Device Speed (krpm)	Unnormalised TEM count (viral particles/ml)			
0 (unsheared)	3.6E+09	7.7E+08	8.0E+09	2.6E+10
12 (high shear)	5.1E+09	8.3E+08	1.5E+10	4.7E+10
18 (high-high shear)	9.4E+09	1.9E+09	9.7E+09	1.5E+10

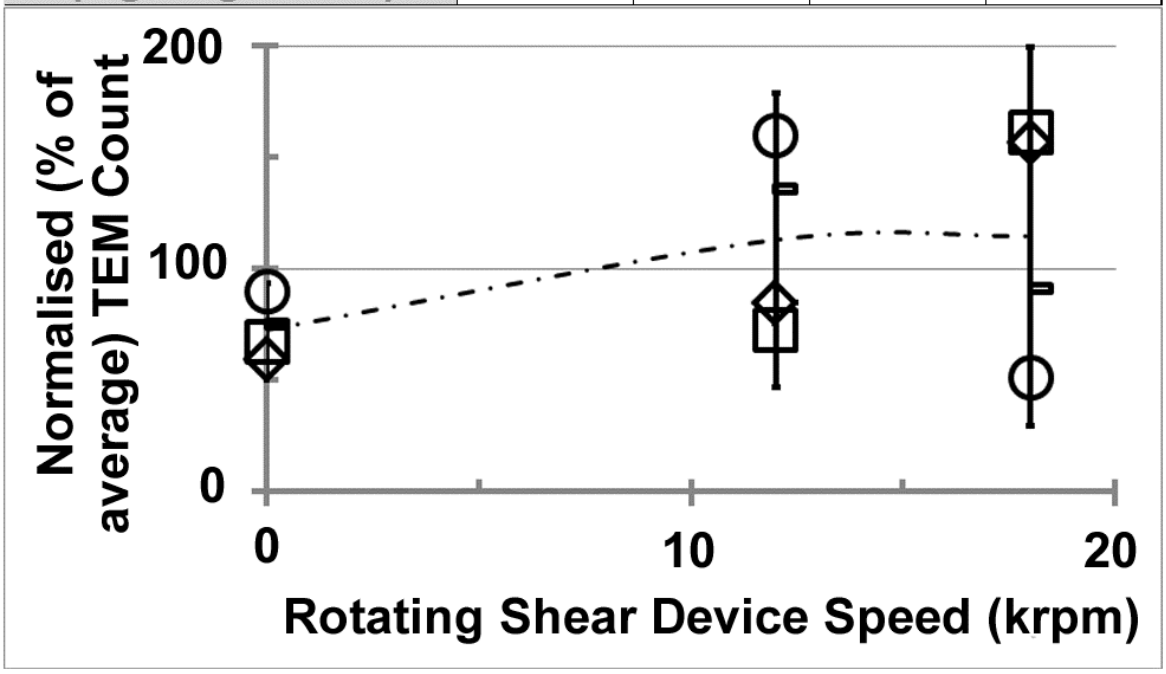

Figure 6.3-4. TEM adenovirus particle count following disruption using a rotating shear device at varying shear rates, prior to centrifugation. Supernatant following spin down was frozen, and later thawed, mixed with a known nanobead concentration and counted using TEM. Images show examples of virions as seen on TEM, and nanobeads, based on whose concentration the virus count was determined (see section 2.2.7.5). An average of 243+/-59 (95% confidence interval, student t-test, n= 13) nanobeads was counted for each replicate at each shear rate. The virus count is plotted as a percentage of the average virus count across all shears. Results are shown for four replicate runs (each represented by a different symbol- ○, ◊, □, ▫). Error bars represent 95% confidence intervals using student t-test (n=4). Samples were subjected to shear at 0 and 12krpm for 20 seconds, and 18krpm for 1 minute.

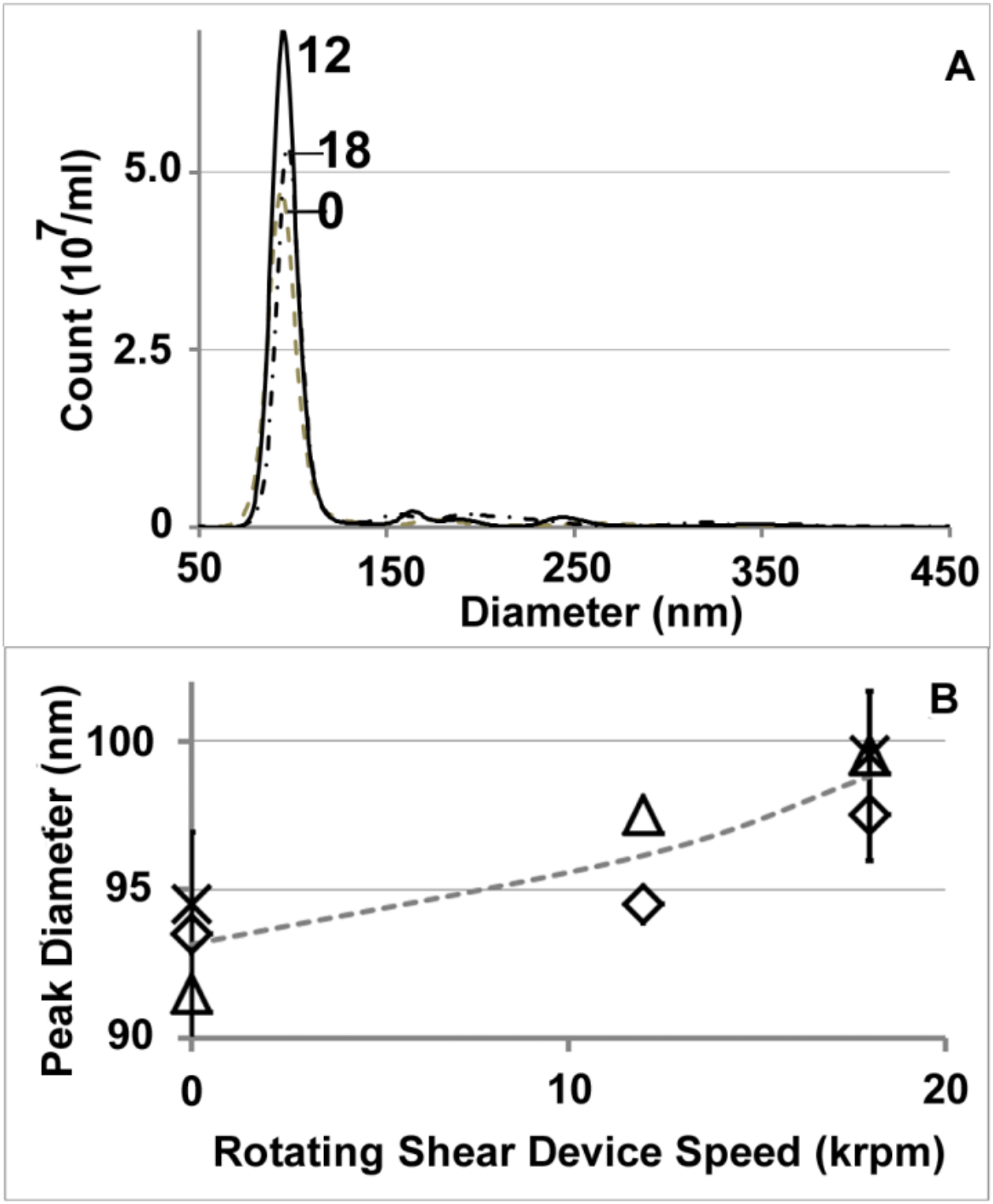

Figure 6.3-5. (A) Sample PSD for adenovirus fractionated using CsCl density gradient centrifugation, measured on the Nanosight. Lines are labelled with the relevant rotating shear device speeds in krpm. (B) Changing peak diameter as measured on the Nanosight for adenovirus subjected to varying shear rates. Samples were subjected to disruption by shear in a rotating shear device at 0 and 12krpm for 20 seconds, and 18krpm for 1 minute. Triplicate results are shown, for each of which a different symbol (Δ, ◊, X) is used. Errors bars represent 95% confidence intervals using student t-test (n=3).

6.3.4. Fractionated Influenza: Particle Size

Similarly, Figure 6.3-6 shows the particle size distribution for influenza virus, showing what may be an increased range of diameters at the peak of the particle size distribution. The repeat measurements of the 0krpm sample indicate that the peak (modal value) and width of the curve at the peak remain consistent for this measurement technique. Further repeats would be required to confirm the significance of this results, but the change appears, visually, to be more substantial than that seen for adenovirus at a similar shear level. This would support the notion that enveloped viruses may be more shear sensitive than unenveloped viruses. The presence of influenza virus in these samples was confirmed by Western blot against Haemagglutinin (HA) antigens (see Appendix F).

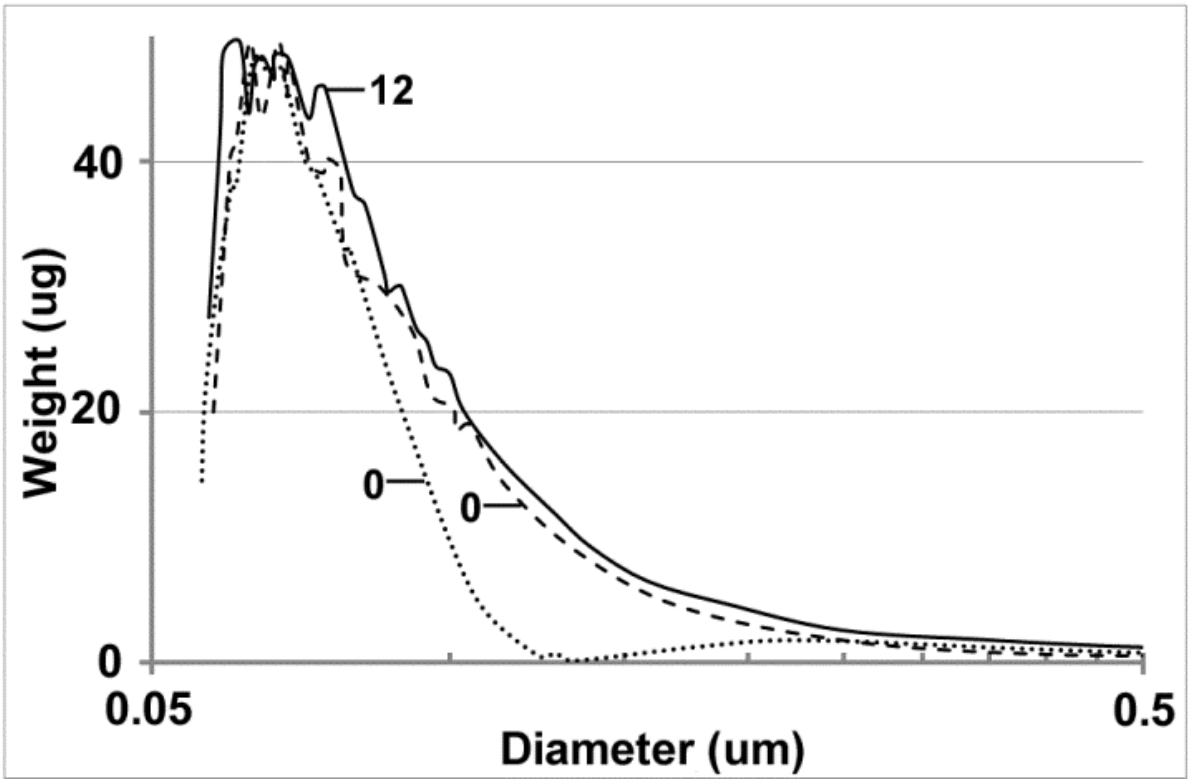

Figure 6.3-6. Sample PSD for influenza virus supernatant fractionated using sucrose density gradient centrifugation, measured on the CPS Disc Centrifuge. Samples were subjected to disruption by shear in a rotating shear device at 0 and 12krpm for 20 seconds. A single run was completed, with replicate measurements at 0krpm, to indicate the repeatability of the measurement method. Lines are labelled with the relevant rotating shear device speeds in krpm.

6.3.5. Fractionated Influenza: SDS-Page & Western blot

Sypro Ruby staining was used to assess the isolated influenza virus samples for any change in overall protein levels, which might be caused by loss of envelope proteins, or a greater propensity to aggregation or destruction of viruses with a given protein

makeup. An attempt was also made to use a Western blot against HA proteins (Supplementary data, Appendix F), but the quality was poor. This immunoblot does however, serve to demonstrate definitively that the sucrose fractionated samples do contain influenza virus. Figure 6.3-7 shows a stained gel from a single virus run, with protein composition for each shear level measured in triplicate. Some protein levels can clearly be seen to be changing consistently across the triplicate measurements. Proteins at molecular weights of 218, 122, 66, and 58kDa appear to show a decrease between low shear (0 and 6krpm) and high shear levels (12 and 18krpm). Of these 122 and 66kDa are not readily identifiable as viral proteins, and 122kDa may be an identified EB66 protein. By contrast the relative concentration of proteins in the range 30 to 50kDa, which may be identified as trypsinised Polymerase Acidic (PA) protein (an influenza core protein), appear to increase. The overall impression is that influenza virus may encounter a tipping point somewhere between 6 and 12krpm in the rotating shear device, above which changes in the prevalence of some proteins changes. The significance of these changes would need to be confirmed by further replicates, but it does indicate that the virus may be impacted by shear even in the range encountered in the process environment. An additional possible explanation for these changes is that cellular proteins from destroyed or damaged cells become associated with the virus particle or that proteases are released by sheared cells. The PSC-5 clarified sample gives some indication of the impact that these proteases might have, as this sample was left overnight unfrozen and could have been exposed to proteases for a longer period of time. The protein make-up of this sample appears roughly in line with a sample exposed to a low shear level, as would be expected for a low shear centrifuge such as the PSC-5.

The impact of shear on viruses has been very little investigated to date, due possibly to the relatively small size of the virus particles, putting them below the range which hydrodynamic shear might be anticipated to impact, and the complicated nature of the particles and substantial uncertainty in the assays required to monitor that impact. Despite shear showing no significant impact on infectivity for both adenovirus and influenza, evidence has been found of a slight change in average particle size, and, for influenza, a modification in the proteomic make-up. Further work is required to confirm these initial findings and elucidate their significance.

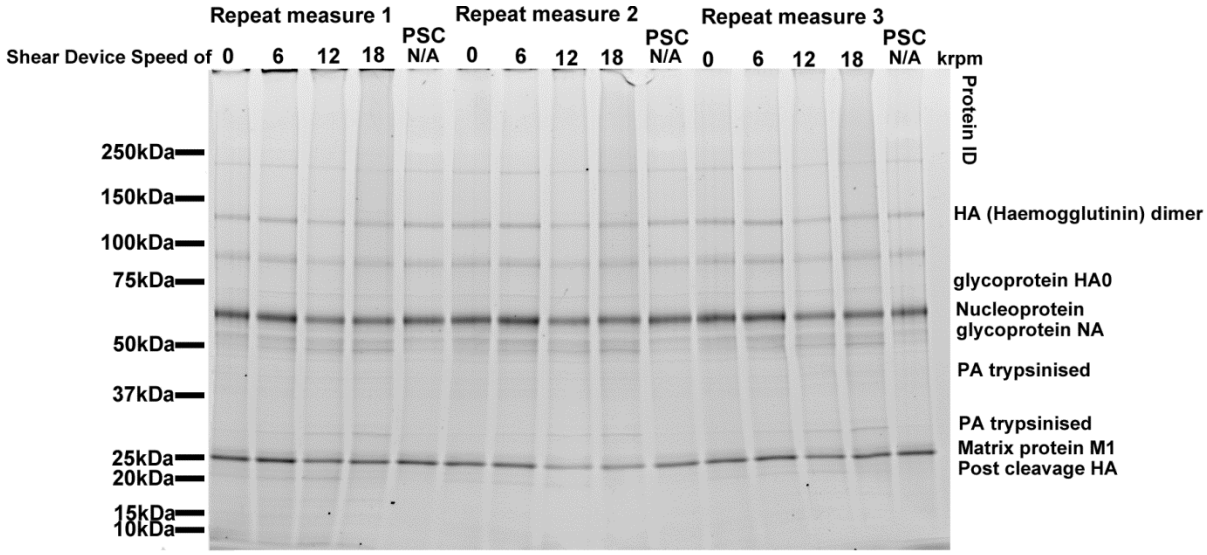

Figure 6.3-7. Sypro Ruby Gel for influenza virus. Supernatant of samples subjected to disruption by shear in a rotating shear device at 0, 6 and 12krpm for 20 seconds and 18krpm for 1 minute. The sample clarified in the PSC-5 centrifuge was left overnight without freezing. Influenza viruses in all the samples have been isolated by fractionation using a sucrose density gradient. A single run was completed, with triplicate measurements on a single sypro ruby gel. The OD of the samples for all wells is identical, at the peak absorbance wavelength of 290nm.

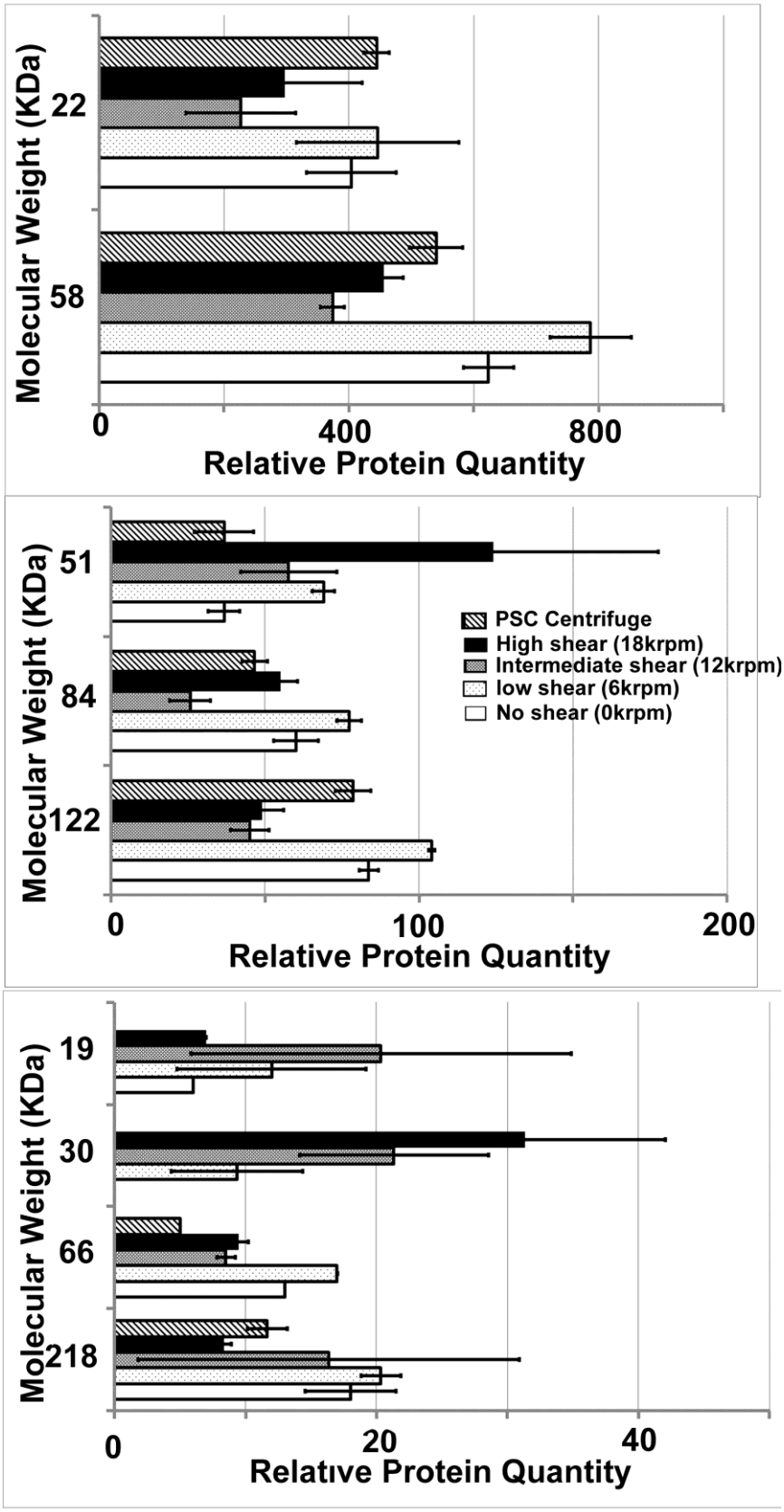

Figure 6.3-8 Graphs indicating the relative quantity of protein, for no shear at 0krpm (unfilled), low shear at 6krpm (light dotted), intermediate shear at 12krpm (dense dotted), high shear at 18krpm (filled) and PSC-5 clarified (stripped), as measured on a protein gel (Figure 6.3-7), for influenza which has been sheared, frozen overnight, and fractionated by sucrose density gradient. Error bars are standard deviation of triplicate measurements.

6.4. Operating windows for Influenza production in EB66 cells

As discussed in the introduction (section 1.1.3) the aim of USD modelling is to produce usable results, which should therefore be presented in a form that can quickly be translated to process changes. Figure 6.4-1 is therefore included to illustrate how such an operating window might look for the PSC-5 centrifuge in the influenza process under investigation. The data in Figure 6.4-1 is derived from the curves in Figure 6.2-2A and Figure 6.2-3 for uninfected EB66 cells and harvest respectively. The shear imposed by the continuous centrifuge at a given set of operating conditions was derived from the formula in section 3.2.2.3. Results imply that considerable improvements in clarification could be achieved, from the current value of approximately 75% to approximately 92%, by altering centrifuge speed and flow rate. However, the best possible clarifications are only achieved at the highest rotating speeds and lowest flowrates in a very narrow window which could result in greater variability. On this basis it is suggested that the current operating conditions be retained, or that flowrate be increased by about 100l/hr, which may allow an improvement of order 4% in clarification without substantially increasing variability. This result would need to be confirmed experimentally. Clearly selection of an alternative operating condition is open to interpretation and better clarification might well be possible. The operating windows allow these possibilities to be explored.

Figure 6.4-1 also illustrates the differences between uninfected and influenza producing cell cultures at harvest. The pre-infection culture clarifies far better for the majority of the operating space. Although it may be noted that according to this predicted operating window the influenza producing culture will clarify better than the pre-infection culture at the lowest rotational speed-highest flow. The change of clarification across the operating window for the influenza producing culture is also more complicated. For the pre-infection culture, as we move towards the top right corner the decrease in shear as the machine is operated more slowly appears to be offset by the decrease in clarification efficiency. For the influenza producing culture by contrast the effects of rotational speed and flow rate on shear and settling efficiency appear to compete across the operating window, resulting in minimum clarification towards the middle of the operating window.

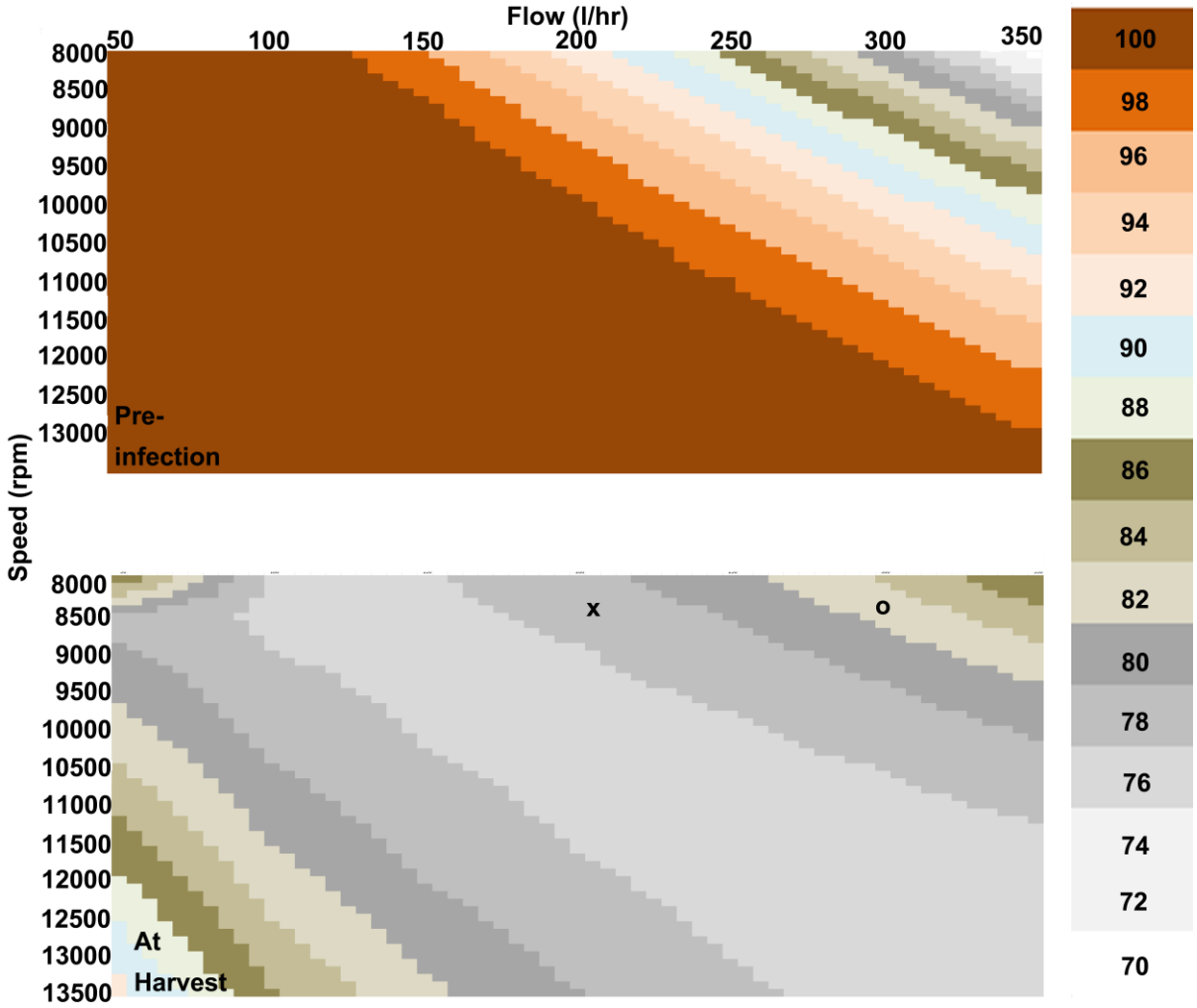

Figure 6.4-1. Operating windows for clarification in the PSC-5 disc stack centrifuge for EB66 cells pre-infection and 5 days post infection with influenza virus (i.e. the standard day of harvest). The range of PSC-5 centrifuge operating parameters of speed and inlet flow rate are covered, with predicted clarification based on CFD predictions of equivalent rotating shear device speed, and clarification based on the experimental outputs from the large laboratory scale centrifuge. The current operating conditions are marked with an X, and possible adjusted operating conditions are marked with a ○.

6.5. Summary of main findings

Little has previously been published regarding the impact of shear on virus producing processes. It is assumed that virus infection increases the fragility of cells, and thus their susceptibility to shear. It is further assumed that the virus products themselves are two small to be damaged by shear. The aim of this section of work was to begin examining these hypotheses.

Contrary to expectations the clarification for adenovirus infected HEK cells, grown as an adherent culture, improved following infection, and showed less susceptibility to shear. This result was consistent with evidence showing a less pronounced decrease in cell count with shear in cells which have been infected with adenovirus.

The implication being that virus infection results in cells which are less susceptible to damage by shear.

For adenovirus the infectivity may not change with increasing shear – although this is hard to establish, as the infectivity assay may not have sufficient resolution. However, the particle size distribution does change – and becomes increasingly noisy at higher shear levels. This may indicate that some shear effect is occurring, possible clipping of hexon proteins, – but nothing that significantly effects its overall biological activity.

The impact of shear on EB66 cells, grown as a suspension culture, before and after infection with influenza virus was also examined. Contrary to adenovirus infection of HEK cells, the influenza infected EB66 cells showed a significant decrease in clarification. However, it is not clear that virus infected cells are more susceptible to shear. Evidence from cell count changes with shear pre and post infection with influenza appear to support this result. The decrease in clarification seems to be due to the debris formed by viral egress. This indicates that budding virus types may have a substantial negative impact on downstream processing when compared to lytic virus types, which may give rise to improved clarification.

As for adenovirus the infectivity assays do not show any indication of a negative impact from shear on the influenza virus itself. However, particle size distribution does appear to be impacted more substantially than in adenovirus. This result would need to be confirmed, but might be indicative of greater shear sensitivity in enveloped viruses.

Further it has been demonstrated that the ultra scale-down laboratory mimic previously developed for use with mammalian cells gives a good prediction on a range of parameters for the harvest by continuous centrifugation of EB66 cells producing influenza virus. Particularly with respect to viral vectors, where substantial expense, expertise and biosafety issues may also play a role, this represents demonstration of a highly promising tool for timely and robust process development.

7. Summary & Future Works

The subject of this thesis was ultra-scale down tools for viral vaccine harvest and early purification steps. The focus of the work has been on two centrifuge unit operations: harvest by continuous centrifugation, and virus purification and concentration by density gradient ultra centrifugation. To this end the Computational Fluid Dynamics (CFD) modelling was extended to include a simulation in 3 dimensions and population balance modelling to gain further insight in to the shear environments in both centrifuge types, with a novel validation approach using synthetic shear mimics. Further the existing ultra-scale down method was applied for the first time to the centrifugal harvest of a viral vaccine production process, to investigate the impact of various viral production process parameters on cell shear sensitivity, and to investigate the impact of shear on virus particles themselves.

Previous CFD work modelling the shear in continuous centrifuges and in the rotating shear device, which was designed to replicate the effects of shear in the feedzone of the centrifuge, appears to draw a comparison between the two based on peak shear and a 2D axi-symmetric assumption. This work sought to increase the understanding of the centrifuge and rotating shear device shear environments by comparing them in three additional ways: in terms of the nature of the shear (normal versus extensional), the volumetric distribution of shear levels, and by applying a simple population model to account for the level of shear and the time of exposure to that shear. The hypothesis being that the two environments would be comparable, adding weight to the existing evidence from scale-down studies on cell culture harvests. The results show comparability not in terms of maximum shear but with the magnitude of shear over the majority of the modelled volumes. The extensional shear in both modelled volumes was similar, including in or near the highest shear zones. Most of the shear in the modelled volumes was simple shear. A reasonable prediction of shear was achieved by the population balance analysis method as validated against shear mimic and cell samples. Interestingly, this work identified that ultracentrifugation introduced a small amount of shear, which has not been previously identified. However, work remains to be completed on debugging the methodology and increasing accuracy for which I would propose the first step would be to analyse the sensitivity of outputs to the assumptions made.

It is a recognised requirement of CFD modelling to validate experimentally. However, the typical experimental validation methods are not applicable to a pilot scale centrifuge processing virus infected materials. It was therefore proposed to develop a shear mimic for mammalian cells. This approach has a number of clear advantages over use of mammalian cells: it avoids the cost, time and resources to grow sufficient volumes of mammalian cell culture, the biosafety and cleaning burdens are considerably reduced, and it broadens the evidence base for comparability between the scale-down model and industrial unit operation. The rotating shear device was used to test the susceptibility of microparticle material to shear, and Adju-Phos was identified, which showed a measurable response to shear over the same range as mammalian cells. The hypothesis was that a material of approximately the same size and density of a mammalian cell, and which responds to shear in the same range, when subjected to shear by the rotating shear device, will also respond to shear in the pilot / industrial scale continuous centrifuge in an equivalent manner. Centrifuges which have already been well characterised using both CFD and the ultra-scale down approaches were used first to test this hypothesis. Good 'predictions' of equivalent Ultra Scale-Down (USD) rotating shear device speed were demonstrated for Adju-Phos in both a high and low shear centrifuge.

However, the slightly greater density of Adju-Phos when compared to mammalian cells, and the larger size of the debris formed by shear induced break-down, meant that the material settled very well in the centrifuge, with negligible particulates in the supernatant. It was therefore necessary to take the centrifuge apart to extract sample, which had been subjected to shear in the centrifuge feed zone. This was not possible with the centrifuge of interest located at a GMP research facility owned by GSK. UCL had recently purchased a PSC-1 centrifuge, which is, according to the manufacturer, comparable to the PSC-5, however opening up the centrifuge revealed a substantial difference in geometric layout in the feed zone, the significance of which could not be determined based on existing knowledge. The CFD modelling approach was therefore expanded to incorporate geometric as well as operating condition sensitivities, and the PSC-1 run with Adju-Phos at two extreme operating conditions to add confidence to the validation of the CFD modelling approach, and by extension the predictions made for the PSC-5

centrifuge. Two mammalian cell cultures were also used giving an order of magnitude shear level for the PSC-5 centrifuge.

The existing ultra-scale down tool was used to compare the clarification, protein release and impurity profile for the influenza viral vaccine production process to that from the PSC-5 disc stack centrifuge harvest. It was also used to investigate the impact of virus infection on the shear sensitivity of HEK293 and EB66 by adenovirus and influenza respectively. It was hypothesised that the USD tools would give good predictions for viral vaccine production processes, and that infection with virus would have a negative impact on the clarification and shear sensitivity of the cells. Results of the experiments appear to demonstrate that the USD tool does indeed give a good prediction of the centrifuge harvest, but that virus infection does not necessarily increase the shear sensitivity of cells, or indeed decrease the clarification in all cases, with stark differences observed between enveloped and non-enveloped viral propagation. The latter may depend more strongly on the virus release mechanism and the amount of debris resulting, than on the process conditions.

It was speculated that an ultra-scale down system could be developed for the KII/PKII semi-continuous density gradient ultra centrifuges, which is analogous to the existing ultra-scale down method for centrifugal harvest: subjecting the sample to representative shear using the rotating shear device, followed by fractionation in a laboratory-scale ultra centrifuge with the scaling factor being related to the $\omega^2 t$. Work presented in this thesis, including CFD combined with population balance modelling, and use of a synthetic virus shear mimic, may provide insights that are valuable to the development of such a scale down model, including the apparent importance of hydrodynamic head or the profile of the density gradient. However, it was not possible to complete the requested assays on the viral vaccine process material and future work requires further experimentation. These experiments could take some post filtration process material, shear it in the rotating shear device and fractionate it using the laboratory scale density gradient ultracentrifuge, with the idea of identifying, (i) whether the results would be comparable to those in the PKII and (ii) whether any comparable semi-solid impurity might form at laboratory scale.

Some initial work was completed on the impact of shear on the viral product, but further work is needed to allow more definite interpretation of these results and

further repeats, and development of the proteomic approaches for measuring the impact of shear on viruses. It was initially hypothesised, given that the CFD analysis showed a Kolmogorov scale of 1μm even at a high rotational speed of 18krpm (in the rotating disc shear device), that neither nanobeads nor viruses would be impacted at all by this level of shear. The streptavidin coated nanobeads did in fact show an impact from shear at much lower shear rates. For the both influenza virus and adenovirus the infectivity showed negligible impact from shear, whilst the measurement of the particle size distribution and virus protein make-up showed an apparent relationship to shear, but one which is much harder to interpret definitively. It does, however, indicate an effect which warrants greater investigation, starting with additional replicate runs on influenza to confirm the significance of the differences seen, and optimisation of the Western blot work for adenovirus to confirm the extent of any proteomic changes which may be seen for this virus type.

There is also room for significant additional work on interaction studies at ultra-scale down for a continuous cell-line viral production process and to further develop the windows of operation and experimentally validate the models generated.

The original project proposal included interaction studies for the downstream harvest and purification steps up to and including the ultracentrifuge. It is speculated that including the filtration steps might reveal more about the original motivation for the project: the formation of semi-solid impurities. The work completed here has shown no evidence of these as a result of shear alone. It is therefore speculated that cumulative shear across the steps of harvest centrifugation, filtration and ultracentrifugation gives rise to the phenomenon. The work in this thesis provides evidence that the existing USD system could be a good representation of the disc stack centrifuge for virus producing processes, although further measurements, for example particle size distributions and concentration of lipids and other host cell components, might add to this. With respect to filtration there are a number of options for scale down. For microfiltration this includes chiefly laboratory scale using of the order 10-100s of ml of material and well plate based filtration systems which use Tecan robots and vacuum to create a transmembrane pressure drop. For tangential flow ultrafiltration there is a USD device which aims to mimic the shear in the filtration system using a rotating disc, and laboratory scale systems for which the shear-time multiple could potentially be used as a scaling factor. Filter and piping

material would need to be kept consistent between scales, though pump type would almost certain be different for practical reasons. Other relevant scaling factors are likely to include the concentration gradient at the filter surface, as it may be that this too has relevance to the solid impurity formation. Future interaction studies might look for any indication of the relative importance of shear and concentration, and any indication of whether shear at a given stage is of more or less importance, for a given process stream.

Finally it was suggested by Sandrine Dessoy that a larger version of the shear device would be valuable, allowing greater quantities of material for further scale down work up to and including chromatography optimisation, based on the quantities of material that in house GSK scale down models require. This might take the form of a reactor like vessel with a stirring / shearing impeller, or a continuous circulation, flow through or automated batch flow through version of the existing USD shear device.

8. Validation

My sponsoring company (GSK Vaccines) produces a vaccine for seasonal flu based on an inactivated virus. This is a relatively high volume market with a large (and growing) number of suppliers and a recognised demand based on national health authority policies for provision of flu vaccine to at risk sections of society. As with many vaccine products there is pressure from these large-volume purchasers to lower Cost Of Goods (CoGs). There is, however, also a recognised need for influenza vaccines, particularly rapid production, in case of a pandemic. (VWP, 2013)

The seasonal nature of flu, and the evolution of different strains, means that each year process development, troubleshooting and clinical safety trails must be completed, all within very tight timeframes. This is also likely to limit the amount of material, expert personnel and resources available for any new or alternative process developments which may be occurring in parallel with annual production. (Proctor, 2012)

Any new process developed would need to go through full regulatory approval. Knowledge may be gleaned from previous work with the flu vaccine produced using legacy processes, though there is likely to have been limited characterisation conducted during this preceding period of production. It is likely that any radical change in the flu vaccine production process may require submission for approval following the tenets of the modern regulatory procedures, i.e. Quality by Design (QbD), though regulators do recognize the need to maintain elements of the previous regime in order to handle legacy products. The company would therefore need to be in discussion with regulators from a very early stage to understand the requirements for their submission. (Rathore and Winkle, 2009)

In order to make use of a Ultra Scale-Down (USD) model in a regulatory submission the user needs to be able to demonstrate that USD is ‘qualified’ and/or the performance (in terms of Critical Quality Attributes, Key Process Parameters etc.) scales correctly and predictably throughout the design space. (Rathore and Winkle, 2009)

In the case of a viral vaccine (or indeed any vaccine) identification of the Critical Quality Attributes (CQAs) is in itself challenging: these are complex, often

heterogeneous and often legacy products whose mechanism of action may not be understood. In terms of high level characteristics efficacy and safety are the priority for a vaccine, but these cannot always be linked directly to an easily measurable physicochemical characteristic. Cell based assays and animal models are available, though time consuming, of limited accuracy in transfer to humans and costly, while product variability at clinical trial will obviously be limited by safety concerns. Ideally critical quality parameters should be selected, based on a risk based approach, but the uncertainties make it difficult to narrow down. This may therefore require measurement of a very broad range of parameters in order to identify acceptable performance surrogates; which would make high throughput testing and large numbers of scale down runs usefully feasible. (Rathore and Winkle, 2009, Vandercammen et al., 2012, Metz et al., 2009)

Selection and validation of assays and product attributes to be measured is therefore likely to be a major challenge in characterising and qualifying the USD model. Multivariate analysis and centre point repeats will be needed to characterise likely complex interactions and variability in the process outcomes.

VWP (2013) do provide guidelines for measuring flu vaccine quality including the following:

- Hemagglutinin (HA) antigen identification against a central calibration strain, for which an immunodiffusion assay is suggested;
- HA physicochemical properties;
- Neuraminidase (NA) antigen identification (measured enzymatically);
- NA levels, where the ratio of NA to HA is required to remain consistent for any given strain;
- Purity: removal of exogenous agents, ratio Hemagglutinin to total proteins, concentration of cellular DNA, detergents, organic solvents, inactivating agents, ovalbumin, endotoxin etc.
- Aggregates' size, make-up and dissolution kinetics;

Other process parameters to be monitored might include yield, stability, adsorption to adjuvant etc.

Typically on and off-line process testing is used for continuous process validation at the large scale, which can then be used for continued validation of USD models and design spaces derived from them (Phillips et al., 2009). The nature of historic data already collected for the disk stack and Density Gradient-Ultra Centrifugation (DG-UCF) may also therefore impact upon which parameters / qualities are selected to compare between the scales.

Parameters useful for linking to up/downstream processes may also need to be considered, for example nature and degree of solids in a centrifuge supernatant stream which may cause clogging of downstream filters (Chhatre et al., 2011). Challenge studies are also suggested as a way to understand the relationship between consecutive stages; taking conditions to extremes at one stage and evaluating the outcome from the subsequent processing stage (Banerjee et al., 2010). The purpose of a particular stage should also be considered in selecting parameters to monitor / prioritise. DG-UCF for example could be expected to have a significant impact on impurity levels, whilst equally the degree of shear, time exposed to shear and final degree of concentration might have detrimental effects on the product. (Aldington, 2014)

Alfa Wassermann have previously developed a laboratory scale version of their DG-UCF, the patent for which claims comparable performance based upon the gradient and distribution of virus versus impurities (Meriño, 2013).

Whatever the final set of qualities selected for monitoring and USD validation subsequent process stream preparation and assays should be identical at both scales for optimal comparability. These will therefore need to be planned carefully. (Tsang et al., 2014)

A USD model should also ideally have the same control capacities as its large scale equivalent and take into account constraints in large scale manufacturing, such as increased hold times or mixing scale (Tsang et al., 2014).

In the case of disc stack centrifugation process parameters which may vary include bowl speed and flow-rate which are scaled using Q/Sigma (Maybury et al., 2000, Boychyn et al., 2004) and centrifuge model which will impact upon the degree of shear encountered in the feed zone. However, the USD model is still being adjusted

to account for factors such as solids sedimentation and enhanced settling which may vary with solids concentration or character. (Tustian et al., 2007)

For DG-UCF variables to be examined might include the density gradient media and centrifuge model (impact on shear), rotor type, sample load, density gradient media concentration and preparation, bowl speed, residence time, feed flow rate etc. (Merino et al., 2003) The aim would be to create a USD which allowed for adjustments to match the range of conditions which might occur at large scale. The existing disk stack centrifuge USD exemplifies the possibilities and difficulties this may involve.

Shear is frequently cited as a key concern in scale-up (Garcia et al., 2012). It is thus hoped that using the shear mimic and CFD modelling can allow sufficient verification of the range of shear expected at large scale and the comparability of shear at the different scales and under different conditions. Ideally the range of shears will thus be explored at reduced cost and with a more easily controlled variability in the input material and assays. In the spirit of QbD both the CFD and shear mimic development were themselves systematised: As a first approach to confirm the repeatability of results with the shear mimic the response to variations in concentration, shear rate and shear period were explored using a Design of Experiments (DoE) factorial model; The CFD models for the disk stack centrifuge was benchmarked against previous models, input data, and modelling approach (including explicit and implicit assumptions) fully documented (although checking remains to be completed) and meshing sweeps were performed to confirm that the model has been sufficiently discretized.

9. Bibliography

British pharmacopoeia, London : Published for the General Medical Council by Constable & Co.

NF Official Compendia of Standards, Rockville, Md., United States Pharmacopeial Convention.

ALDINGTON, S. Quality by Design (QbD) Applied to purification Process Development, Characterisation, Qualitification and Validation. MBI Quality by Design for Effective Bioprocess Design and Validation, 2014 UCL. Lonza.

ALTARAS, N. E., AUNINS, J. G., EVANS, R. K., KAMEN, A., KONZ, J. O. & WOLF, J. J. 2005. Production and formulation of adenovirus vectors. *Gene Therapy and Gene Delivery Systems,* 99**,** 193-260.

ANDERSON, E. C., PETERSEN, D. F. & TOBEY, R. A. 1970. Density Invariance of Cultured Chinese Hamster Cells with Stage of Mitotic Cycle. *Biophysical Journal,* 10**,** 630-645.

ANDREADIS, S. T., ROTH, C. M., LE DOUX, J. M., MORGAN, J. R. & YARMUSH, M. L. 1999. Large-scale processing of recombinant retroviruses for gene therapy. *Biotechnol Prog,* 15**,** 1-11.

ARIGA, K., JI, Q., RICHARDS, G. J. & HILL, J. P. 2012. Soft Capsules, Hard Capsules, and Hybrid Capsules. *Soft Materials,* 10**,** 387-412.

ASSELBORN, T., SUPER, A. & N, J. 2015. Manual for software allowing non invasive quantification of cell density in adherent cell cultures. Department of Biochemical Engineering, University College London.

BALVERS, R., JIANG, H., PIYA, S., GOMEZ-MANZANO, C. & FUEYO, J. 2011. Adenovirus, autophagy and lysis: ecstasies and agonies. *Future Virology,* 6**,** 1161-1164.

BANERJEE, A., MA, N. N. & RAMASUBRAMANYAN, N. 2010. Designing in Quality: Approaches to Defining the Design Space for a Monoclonal Antibody Process. *Biopharm International,* 23**,** 26-40.

BEKARD, I. B., ASIMAKIS, P., BERTOLINI, J. & DUNSTAN, D. E. 2011. The Effects of Shear Flow on Protein Structure and Function. *Biopolymers,* 95**,** 733-745.

BERRILL, A., HO, S. V. & BRACEWELL, D. G. 2008. Ultra scale-down to define and improve the relationship between Flocculation and disc-stack centrifugation. *Biotechnology Progress,* 24**,** 426-431.

BIDDLECOMBE, J. G., CRAIG, A. V., ZHANG, H., UDDIN, S., MULOT, S., FISH, B. C. & BRACEWELL, D. G. 2007. Determining antibody stability: Creation of solid-liquid interfacial effects within a high shear environment. *Biotechnology Progress,* 23**,** 1218-1222.

BIO-RAD(A) CriterionXT Precast Gel Instruction Guide. Rev F ed.

BIO-RAD(B) Criterion Blotter Instruction Manual. Rev B ed.

BLAISZIK. 20/11/2012 2012. *RE: email: micro-capsules.*

BOULDING, N., YIM, S. S. S., KESHAVARZ-MOORE, E., SHAMLOU, P. A. & BERRY, M. 2002. Ultra scaledown to predict filtering centrifugation of secreted antibody fragments from fungal broth. *Biotechnology and Bioengineering,* 79**,** 381-388.

BOYCHYN, M., DOYLE, W., BULMER, M., MORE, J. & HOARE, M. 2000. Laboratory scaledown of protein purification processes involving fractional precipitation and centrifugal recovery. *Biotechnology and Bioengineering,* 69**,** 1-10.

BOYCHYN, M., YIM, S. S. S., BULMER, M., MORE, J., BRACEWELL, D. G. & HOARE, M. 2004. Performance prediction of industrial centrifuges using scale-down models. *Bioprocess and Biosystems Engineering,* 26**,** 385-391.
BOYCHYN, M., YIM, S. S. S., SHAMLOU, P. A., BULMER, M., MORE, J. & HOARE, A. 2001. Characterization of flow intensity in continuous centrifuges for the development of laboratory mimics. *Chemical Engineering Science,* 56**,** 4759-4770.
BRYAN, A. K., GORANOV, A., AMON, A. & MANALIS, S. R. 2010. Measurement of mass, density, and volume during the cell cycle of yeast. *Proceedings of the National Academy of Sciences of the United States of America,* 107**,** 999-1004.
CAMPOS, S. K. & BARRY, M. A. 2006. Comparison of adenovirus fiber, protein IX, and hexon capsomeres as scaffolds for vector purification and cell targeting. *Virology,* 349**,** 453-462.
CARR, D. R. & BRADSHAW, S. E. 2016. Gene therapies: the challenge of super-high-cost treatments and how to pay for them. *Regenerative Medicine,* 11**,** 381-393.
CARUSO, F. 2001. Nanoengineering of particle surfaces. *Advanced Materials,* 13**,** 11-74.
CASTELLANOS, M., PEREZ, R., CARRILLO, P. J., DE PABLO, P. J. & MATEU, M. G. 2012. Mechanical disassembly of single virus particles reveals kinetic intermediates predicted by theory. *Biophysical Journal,* 102**,** 2615-24.
CELL_BIOLABS_INC 2004a. Product Manual: QuickTiter Adenovirus Titer Immunoassay Kit. *Catalog Number VPK-109.*
CELL_BIOLABS_INC 2004b. Product Manual: B-Galactosidase Staining Kit. *Catalog Number AKR-100.*
CHAN, G., BOOTH, A. J., MANNWEILER, K. & HOARE, M. 2006. Ultra scale-down studies of the effect of flow and impact conditions during E-coli cell processing. *Biotechnology and Bioengineering,* 95**,** 671-683.
CHANG, S. H., SUN, D. P., LIANG, H. H., WANG, J., LI, J., GUO, L., WANG, X. L., GUAN, C. C., BORUAH, B. M., YUAN, L. M., FENG, F., YANG, M. R., WANG, L. L., WANG, Y., WOJDYLA, J., LI, L. J., WANG, J. W., WANG, M. T., CHENG, G. H., WANG, H. W. & LIU, Y. F. 2015. Cryo-EM Structure of Influenza Virus RNA Polymerase Complex at 4.3 angstrom Resolution. *Molecular Cell,* 57**,** 925-935.
CHAUDHURI, R. G. & PARIA, S. 2012. Core/Shell Nanoparticles: Classes, Properties, Synthesis Mechanisms, Characterization, and Applications. *Chemical Reviews,* 112**,** 2373-2433.
CHHATRE, S., PAMPEL, L. & TITCHENER-HOOKER, N. J. 2011. Integrated Use of Ultra Scale-Down and Financial Modeling to Identify Optimal Conditions for the Precipitation and Centrifugal Recovery of Milk Proteins. *Biotechnology Progress,* 27**,** 998-1008.
CHRISTENSEN, J. B., BYRD, S. A., WALKER, A. K., STRAHLER, J. R., ANDREWS, P. C. & IMPERIALE, M. J. 2008. Presence of the adenovirus IVa2 protein at a single vertex of the mature virion. *J Virol,* 82**,** 9086-9093.
CHUA, J. V. & CHEN, W. H. 2010. Bench-to-bedside review: vaccine protection strategies during pandemic flu outbreaks. *Crit Care,* 14**,** 218.
DE NEVERS, N. 1991. *Fluid mechanics for chemical engineers*, McGraw-Hill.
DIMITROV, D. S. 2004. Virus entry: Molecular mechanisms and biomedical applications. *Nature Reviews Microbiology,* 2**,** 109-122.

DORAN, P. M. 2013. *Bioprocess engineering principles,* Waltham, MA, Focal Press.
DOSHI, N., ZAHR, A. S., BHASKAR, S., LAHANN, J. & MITRAGOTRI, S. 2009. Red blood cell-mimicking synthetic biomaterial particles. *Proceedings of the National Academy of Sciences of the United States of America,* 106**,** 21495-21499.
DUFFY, A. M., O'DOHERTY, A. M., O'BRIEN, T. & STRAPPE, P. M. 2005. Purification of adenovirus and adeno-associated virus: comparison of novel membrane-based technology to conventional techniques. *Gene Therapy,* 12 Suppl 1**,** S62-72.
EDELSTEIN 2016. Vectors Used in Gene Therapy Clinical Trials. *Journal of Gene Medicine.* February 2016 ed.
ENCAPSULA. Available: http://www.encapsula.com/products_01.html.
FENG, S. Z., JIAO, P. R., QI, W. B., FAN, H. Y. & LIAO, M. 2011. Development and strategies of cell-culture technology for influenza vaccine. *Appl Microbiol Biotechnol,* 89**,** 893-902.
FISCHER, H., POLIKARPOV, I. & CRAIEVICH, A. F. 2004. Average protein density is a molecular-weight-dependent function. *Protein Science,* 13**,** 2825-2828.
FLICKINGER, M. C. & DREW, S. W. 1999. *The encyclopedia of bioprocess technology : fermentation, biocatalysis, and bioseparation,* New York, Wiley.
FREI, M. 2011. Centrifugation Separations - Differential Centrifugation. *BioFiles* [Online], 6. Available: http://www.sigmaaldrich.com/content/dam/sigma-aldrich/articles/biofiles/biofiles-pdf/biofiles_v6_n5.pdf.
GARCIA, T., MCCURDY, V., WATSON, T. N. J., ENDE, M. A., BUTTERELL, P., VUKOVINSKY, K., CHUEH, A., COFFMAN, J., COOPER, S. & SCHUEMMELFEDER, B. 2012. Verification of Design Spaces Developed at Subscale. *Journal of Pharmaceutical Innovation,* 7**,** 13-18.
GAROFF, H., HEWSON, R. & OPSTELTEN, D. J. 1998. Virus maturation by budding. *Microbiol Mol Biol Rev,* 62**,** 1171-90.
GENZEL, Y. 2015. Designing cell lines for viral vaccine production: Where do we stand? *Biotechnology Journal,* 10**,** 728-U115.
GENZEL, Y. & REICHL, U. 2009. Continuous cell lines as a production system for influenza vaccines. *Expert Review of Vaccines,* 8**,** 1681-1692.
GOLDBERG, M., LANGER, R. & JIA, X. Q. 2007. Nanostructured materials for applications in drug delivery and tissue engineering. *Journal of Biomaterials Science-Polymer Edition,* 18**,** 241-268.
GROS, A. & GUEDAN, S. 2010. Adenovirus Release from the Infected Cell as a Key Factor for Adenovirus Oncolysis. *The Open Gene Therapy Journal,* 3**,** 24-30.
GÜRTLER, L. 2006. Influenza Report 2006. *In:* KAMPS, S., HOFFMANN, C. & PREISER, W. (eds.) *Influenza Report 2006.* Flying Publisher.
GUU, T. S. Y., DONG, L. P., WITTUNG-STAFSHEDE, P. & TAO, Y. J. Z. 2008. Mapping the domain structure of the influenza A virus polymerase acidic protein (PA) and its interaction with the basic protein 1 (PB1) subunit. *Virology,* 379**,** 135-142.
HANDEL, A., AKIN, V., PILYUGIN, S. S., ZARNITSYNA, V. & ANTIA, R. 2014. How sticky should a virus be? The impact of virus binding and release on transmission fitness using influenza as an example. *Journal of the Royal Society Interface,* 11.
HARRISON, S. C. 2010. Virology. Looking inside adenovirus. *Science,* 329**,** 1026-7.

HARSHE, Y. M., LATTUADA, M. & SOOS, M. 2011. Experimental and Modeling Study of Breakage and Restructuring of Open and Dense Colloidal Aggregates. *Langmuir,* 27**,** 5739-5752.
HARUKI, H., GYURCSIK, B., OKUWAKI, M. & NAGATA, K. 2003. Ternary complex formation between DNA-adenovirus core protein VII and TAF-I beta/SET, an acidic molecular chaperone. *Febs Letters,* 555**,** 521-527.
HEDLUND, M., LARSON, J. L. & FANG, F. 2010. Antiviral Strategies for Pandemic and Seasonal Influenza. *Viruses-Basel,* 2**,** 1766-1781.
HENNING, P., LUNDGREN, E., CARLSSON, M., FRYKHOLM, K., JOHANNISSON, J., MAGNUSSON, M. K., TANG, E., FRANQUEVILLE, L., HONG, S. S., LINDHOLM, L. & BOULANGER, P. 2006. Adenovirus type 5 fiber knob domain has a critical role in fiber protein synthesis and encapsidation. *Journal of General Virology,* 87**,** 3151-3160.
HENZLER, H. J. 2000. Particle stress in bioreactors. *Adv Biochem Eng Biotechnol,* 67**,** 35-82.
HSU, H.-W. & PERRY, E. S. 1981. *Separations by centrifugal phenomena,* New York ; Chichester, Wiley.
HU, W. W., BERDUGO, C. & CHALMERS, J. J. 2011. The potential of hydrodynamic damage to animal cells of industrial relevance: current understanding. *Cytotechnology,* 63**,** 445-460.
HULO, CASTRO, D., MASSON, BOUGUELERET, BARIOCH, XENARIOS & MERCIER, L. 2011. *Cell lysis* [Online]. Available: http://viralzone.expasy.org/all_by_species/1077.html 2016].
HUTCHINSON, N., BINGHAM, N., MURRELL, N., FARID, S. & HOARE, M. 2006. Shear stress analysis of mammalian cell suspensions for prediction of industrial centrifugation and its verification. *Biotechnology and Bioengineering,* 95**,** 483-491.
J. MAYBURY, M. H., P. DUNNILL 1999. The use of laborartory Centrifugation Studies to Predict Performance of Industrial Machines: Studies of Shear-Insensitive and Shear-Sensitive Materials. *Biotechnology & Bioengineering,* 67**,** 265-273.
JAWETZ, E., MELNICK, J. L. & ADELBERG, E. A. 2013. Review of medical microbiology. Norwalk, Conn.: Appleton & Lange.
JOSEFSBERG, J. O. & BUCKLAND, B. 2012. Vaccine process technology. *Biotechnology and Bioengineering,* 109**,** 1443-1460.
KADA, FALK & GRUBER 1999. Accurate measurement of avidin and streptavidin in crude biofluids with a new, optimized biotin fluorescein conjugate. *Biochimica et Biophysica Acta 1427*.
KAMPS, HOFFMANN & PREISER 2006. Influenza Report 2006. Flying Publisher.
KASALA, D., YOON, A. R., HONG, J., KIM, S. W. & YUN, C. O. 2016. Evolving lessons on nanomaterial-coated viral vectors for local and systemic gene therapy. *Nanomedicine,* 11**,** 1689-1713.
KOLADE, O. O., JIN, W. B., TENGROTH, C., GREEN, K. D. & BRACEWELL, D. G. 2015. Shear Effects on Aluminum Phosphate Adjuvant Particle Properties in Vaccine Drug Products. *Journal of Pharmaceutical Sciences,* 104**,** 378-387.
KOLEWE, M. E., HENSON, M. A. & ROBERTS, S. C. 2010. Characterization of aggregate size in Taxus suspension cell culture. *Plant Cell Reports,* 29**,** 485-494.

KOTTERMAN, M. A., CHALBERG, T. W. & SCHAFFER, D. V. 2015. Viral Vectors for Gene Therapy: Translational and Clinical Outlook. *Annual Review of Biomedical Engineering, Vol 17,* 17**,** 63-89.
KUMAR, G. B. S., GANAPATHI, T. R., REVATHI, C. J., PRASAD, K. S. N. & BAPAT, V. A. 2003. Expression of hepatitis B surface antigen in tobacco cell suspension cultures. *Protein Expression and Purification,* 32**,** 10-17.
LACKIE, J. M. & BLACKSHAW, S. E. 2007. *The dictionary of cell and molecular biology,* Amsterdam ; Boston, Academic Press.
LAMB, R. A., HOLSINGER, L. J. & PINTO, L. H. 1994. The Influenza-a Virus M2 Ion Channel Protein and Its Role in the Influenza Virus Life Cycle. *Cellular Receptors for Animal Viruses***,** 303-321.
LAU, E. C., KONG, S., MCNULTY, S., ENTWISLE, C., MCILGORM, A., DALTON, K. A. & HOARE, M. 2013. An ultra scale-down characterization of low shear stress primary recovery stages to enhance selectivity of fusion protein recovery from its molecular variants. *Biotechnology and Bioengineering,* 110**,** 1973-1983.
LEUNG, W. W.-F. 1998. *Industrial centrifugation technology,* New York, McGraw-Hill.
LEVY, M. S., COLLINS, I. J., YIM, S. S., WARD, J. M., TITCHENER-HOOKER, N., SHAMLOU, P. A. & DUNNILL, P. 1999. Effect of shear on plasmid DNA in solution. *Bioprocess Engineering,* 20**,** 7-13.
LI, M. & QIU, Y. X. 2013. A review on current downstream bio-processing technology of vaccine products. *Vaccine,* 31**,** 1264-1267.
LIFESCIENCES 2014. User Guide: Mini Gel Tank. *For protein electrophoresis of Novex, NuPAGE, and Bolt Mini Gels.* A.0 ed.
LIU, H., JIN, L., KOH, S. B., ATANASOV, I., SCHEIN, S., WU, L. & ZHOU, Z. H. 2010. Atomic structure of human adenovirus by cryo-EM reveals interactions among protein networks. *Science,* 329**,** 1038-43.
LOPES & KESHAVARZ-MOORE, E. 2012. Prediction and Verification of Centrifugal Dewatering of P. pastoris Fermentation Cultures Using An Ultra Scale-Down Approach. *Biotechology and Bioengineering,* 109**,** 2039-2047.
LOTFIAN, P., LEVY, M. S., COFFIN, R., WARD, J. & SHAMLOU, P. A. 2003a. Shear-induced release of disabled herpes simplex virus from baby-hamster kidney cells. *Biotechnology and Applied Biochemistry,* 38**,** 271-281.
LOTFIAN, P., LEVY, M. S., COFFIN, R. S., FEARN, T. & AYAZI-SHAMLOU, P. 2003b. Impact of process conditions on the centrifugal recovery of a disabled herpes simplex virus. *Biotechnology Progress,* 19**,** 209-215.
LOWRY, O. H., ROSEBROUGH, N. J., FARR, A. L. & RANDALL, R. J. 1951. Protein measurement with the Folin phenol reagent. *Journal of Biological Chemistry,* 193**,** 265-75.
LU, G. Z., THOMPSON, B. G. & GRAY, M. R. 1992. Physical Modeling of Animal-Cell Damage by Hydrodynamic-Forces in Suspension-Cultures. *Biotechnology and Bioengineering,* 40**,** 1277-1281.
LUISI, P. L. & STANO, P. 2011. Synthetic biology: minimal cell mimicry. *Nat Chem,* 3**,** 755-6.
LYNCH, J. P., FISHBEIN, M. & ECHAVARRIA, M. 2011. Adenovirus. *Seminars in Respiratory and Critical Care Medicine,* 32**,** 494-511.
MALVERN_WEBSITE. *Static Light Scattering (SLS)* [Online]. Available: http://www.malvern.com/en/products/technology/static-light-scattering/.

MANNWEILER, K. & HOARE, M. 1992. The Scale-down of an Industrial Disk Stack Centrifuge. *Bioprocess Engineering,* 8**,** 19-25.
MAYBURY, J. P., HOARE, M. & DUNNILL, P. 2000. The use of laboratory centrifugation studies to predict performance of industrial machines: Studies of shear-insensitive and shear-sensitive materials. *Biotechnology and Bioengineering,* 67**,** 265-273.
MCCOY, R., HOARE, M. & WARD, S. 2009. Ultra Scale-Down Studies of the Effect of Shear on Cell Quality; Processing of a Human Cell Line for Cancer Vaccine Therapy. *Biotechnology Progress,* 25**,** 1448-1458.
MCCREATH, G. & SHIVHARE, M. 2011. Drawn to Scale. *European Biopharmaceutical Review***,** 62-28.
MCLEAN, J. E., RUCK, A., SHIRAZIAN, A., POOYAEI-MEHR, F. & ZAKERI, Z. F. 2008. Viral manipulation of cell death. *Current Pharmaceutical Design,* 14**,** 198-220.
MELINEK, B. 2013. MRes Submission: Development of Synthetic Shear Tracer Particles for Scale-Down Models of Continuous Centrifugation and Density Gradient Ultra-Centrifugation as a Mimic of Various Vaccine Candidates. UCL.
MELINEK, B., DESSOY, S., MANNALL, G., BRACEWELL, D. G. & MUKHOPADHYAY, T. 2017. The Creation and Investigation of a Synthetic Shear Mimic for Mammalian Cells in Industrial Processes *Under review before submission to Biotechnolgy Progress*.
MERCADE-PRIETO, R., NGUYEN, B., ALLEN, R., YORK, D., PREECE, J. A., GOODWIN, T. E. & ZHANG, Z. B. 2011. Determination of the elastic properties of single microcapsules using micromanipulation and finite element modeling. *Chemical Engineering Science,* 66**,** 2042-2049.
MERCADE-PRIETO, R. & ZHANG, Z. B. 2012. Mechanical characterization of microspheres - capsules, cells and beads: a review. *Journal of Microencapsulation,* 29**,** 277-285.
MERIÑO, S. 15/03/2013 10:27 2013. *RE: Alfa Wassermann Ultracentrifuge.* Type to MELINEK, B.
MERINO, S. P., WOERDEN, DALESSIO, S. J., HOPATCONG, OTTEN, R. R. L. R. & MONTFOORT. 2003. *Centrifuge with removable core for scalable centrifugation*. US 2003/0114289 A1.
METZ, B., VAN DEN DOBBELSTEEN, G., VAN ELS, C., VAN DER GUN, J., LEVELS, L., VAN DER POL, L., ROTS, N. & KERSTEN, G. 2009. Quality-control issues and approaches in vaccine development. *Expert Review of Vaccines,* 8**,** 227-238.
MICHALSKY, R., PFROMM, P. H., CZERMAK, P., SORENSEN, C. M. & PASSARELLI, A. L. 2008. Effects of temperature and shear force on infectivity of the baculovirus Autographa californica M nucleopolyhedrovirus. *Journal of Virological Methods,* 153**,** 90-6.
MILO, R., JORGENSEN, P., MORAN, U., WEBER, G. & SPRINGER, M. 2010. *BioNumbers - the database of key numbers in molecular and cell biology* [Online]. Nucleic Acids Red. (D750-D753). Available: http://kirschner.med.harvard.edu/files/bionumbers/fundamentalBioNumbersHandout.pdf.
MITTEREDER, N., MARCH, K. L. & TRAPNELL, B. C. 1996. Evaluation of the concentration and bioactivity of adenovirus vectors for gene therapy. *J Virol,* 70**,** 7498-7509.

MOLECULAR_PROBES_INC 2007. Sypro Ruby Protein Gel Stain.
MORENWEISER, R. 2005. Downstream processing of viral vectors and vaccines. *Gene Therapy,* 12**,** S103-S110.
MORSHED, K. N., BARK, D., JR., FORLEO, M. & DASI, L. P. 2014. Theory to predict shear stress on cells in turbulent blood flow. *Plos One,* 9**,** e105357.
MOYER, C. L. & NEMEROW, G. R. 2012. Disulfide-bond formation by a single cysteine mutation in adenovirus protein VI impairs capsid release and membrane lysis. *Virology,* 428**,** 41-7.
MUENNIG, P. A. & KHAN, K. 2001. Cost-effectiveness of vaccination versus treatment of influenza in healthy adolescents and adults. *Clinical Infectious Diseases,* 33**,** 1879-1885.
MUKHOPADHYAY, T. Vaccines Future. MBI Vaccine Development and Commercialisation, 2012 UCL. UCL.
MYBIOSOURCE.COM. 2016. *PV recombinant protein :: Minor core protein (PV) Recombinant Protein* [Online]. Available: http://www.mybiosource.com/prods/Recombinant-Protein/Minor-core-protein-PV/PV/datasheet.php?products_id=1083513.
NESBETH, D. Cell Engineering to Ease Primary Recovery. MBI Downstream Processing: From Cell to Column, 2012 UCL. UCL.
OSTERHAUS, A., FOUCHIER, R. & RIMMELZWAAN, G. 2011. Towards universal influenza vaccines? *Philos Trans R Soc Lond B Biol Sci,* 366**,** 2766-73.
PAMPEL, L. W., BOUSHABA, R. & TITCHENER-HOOKER, N. J. 2008. A methodical approach to ultra-scale-down of process sequences: Application to casein removal from the milk of transgenic animals. *Biotechnology Progress,* 24**,** 192-201.
PEIXOTO, C., SOUSA, M. F., SILVA, A. C., CARRONDO, M. J. & ALVES, P. M. 2007. Downstream processing of triple layered rotavirus like particles. *J Biotechnol,* 127**,** 452-61.
PEREZ-BERNA, A. J., MARABINI, R., SCHERES, S. H. W., MENENDEZ-CONEJERO, R., DMITRIEV, I. P., CURIEL, D. T., MANGEL, W. F., FLINT, S. J. & MARTIN, C. S. 2009. Structure and Uncoating of Immature Adenovirus. *Journal of Molecular Biology,* 392**,** 547-557.
PETTITT, D., SMITH, J., FUERSTENAU-SHARP, M., BURE, K., HOLLANDER, G., PEREDKI, P., SLADE, A., JONES, P., MITROPHANOUS, K. & DAVID, B. 2016. Emerging Platform Bioprocesses for Viral Vectors and Gene Therapies. *Bioprocess International*.
PFLUG, A., GUILLIGAY, D., REICH, S. & CUSACK, S. 2014. Structure of influenza A polymerase bound to the viral RNA promoter. *Nature,* 516**,** 355-360.
PHEASEY, N., JOHN, J., LOVE, C., COFFIN, R., WARD, J. M., BOUSHABA, R., HOARE, M. & LEVY, M. S. 2006. A capillary cytometer method to quantitate viable virus particles based on early detection of viral antigens and cellular events within single cells. *Journal of Virological Methods,* 137**,** 213-218.
PHILLIPS, J., ERICSON, L., KARUNATILAKE, C., KUHN, B., RATHORE, A., LUNDELL, E., KRAUSE, H., RINN, C., SIEDLER, M., SIMON, S., WEBER, C., WITHERS, B., VINCI, V., DEFELIPPIS, M., DOBBINS, J., HILTON, M., MEIKLEJOHN, B., MIROQUESADA, G., KRUMMEN, L., TATICEK, R., MARTIN-MOE, S., KELLEY, B., BLUMENTALS, I., ERICKSON, J., GARDNER, A., PAOLELLA, D., PATEL, P., RINELLA, J., STAWICKI, M., STOCKDALE, G., SCHENERMAN, M., WASSERMAN, G., OLIVER, C., RAM, K., KELLIHER, L., ROBBINS, D., ANDERSON, J., AHUJA, S., CRAIGHEAD,

N., NIEDZIELSKI, A., SCHARF, O., BLOOM, L., BANERJEE, A., KIRCHHOFF, C., LAMBERT, W., SINGH, S., BERRIDGE, J., SEAMON, K. & VENUGOPAL, S. 2009. A-Mab: a Case Study in Bioprocess Development. *CMC Biotech Working Group,* 2.

PIERCE_BIOTECHNOLOGY 2015. Instructions. Pierce BCA Protein Assay Kit. *In:* SCIENTIFIC, T. (ed.).

PLOTKIN, S. A. & PLOTKIN, S. L. 2011. The development of vaccines: how the past led to the future. *Nat Rev Microbiol,* 9**,** 889-93.

PONCELET, D. & NEUFELD, R. J. 1989. Shear breakage of nylon membrane microcapsules in a turbine reactor. *Biotechnology and Bioengineering,* 33**,** 95-103.

PROCTOR, M. Vaccine Commercialisation and Project Management. MBI Vaccine Development and Commercialisation, 2012 UCL. medImmune.

RAPPUOLI 2006. Cell-Culture-Based Vaccine Production: Technological Options. *The Bridge,* 36**,** 25-31.

RATHORE, A. S. & SOFER, G. K. 2005. Process validation in manufacturing of biopharmaceuticals : guidelines, current practices, and industrial case studies. *Biotechnology and bioprocessing series.* Boca Raton: Taylor & Francis.

RATHORE, A. S. & WINKLE, H. 2009. Quality by design for biopharmaceuticals. *Nature Biotechnology,* 27**,** 26-34.

REIMER, C. B., BAKER, R. S., VAN FRANK, R. M., NEWLIN, T. E., CLINE, G. B. & ANDERSON, N. G. 1967. Purification of large quantities of influenza virus by density gradient centrifugation. *J Virol,* 1**,** 1207-16.

REITER, M., PORTSMOUTH, D. & BARRETT, P. N. 2014. Avian Suspension Culture Cell Lines for Production of Vaccines and Other Biologicals. *In:* MEYER, H.-P. & SCHMIDHALTER, D. R. (eds.) *Industrial scale suspension culture of living cells.* Wiley-VCH Verlag GmbH & Co.

REXROAD, J., WIETHOFF, C. M., GREEN, A. P., KIERSTEAD, T. D., SCOTT, M. O. & MIDDAUGH, C. R. 2003. Structural stability of adenovirus type 5. *J Pharm Sci,* 92**,** 665-78.

ROLDAO, A., MELLADO, M. C. M., CASTILHO, L. R., CARRONDO, M. J. T. & ALVES, P. M. 2010. Virus-like particles in vaccine development. *Expert Review of Vaccines,* 9**,** 1149-1176.

RUSSELL, W. C. 2009. Adenoviruses: update on structure and function. *Journal of General Virology,* 90**,** 1-20.

SALOMON, R. & WEBSTER, R. G. 2009. The Influenza Virus Enigma. *Cell,* 136**,** 402-410.

SALTE, KING, BAGANZ, HOARE & TITCHENER-HOOKER, N. 2006. A Methodology for Centrifuge Selection for the Separation of High Solids Density Cell Broths by Visualisation of Performance Using Windows of Operation. *Wiley Periodicals*.

SAXENA, A., TRIPATHI, B. P., KUMAR, M. & SHAHI, V. K. 2009. Membrane-based techniques for the separation and purification of proteins: an overview. *Adv Colloid Interface Sci,* 145**,** 1-22.

SCHAAP, I. A. T., EGHIAIAN, F., DES GEORGES, A. & VEIGEL, C. 2012. Effect of Envelope Proteins on the Mechanical Properties of Influenza Virus. *Journal of Biological Chemistry,* 287**,** 41078-41088.

SCHERMAN, D. E. O. C. 2014. *Advanced textbook on gene transfer, gene therapy and genetic pharmacology : principles, delivery and pharmacological and biomedical applications of nucleotide-based therapies*.

SHARMA, C., MALHOTRA, D. & RATHORE, A. S. 2011. Review of Computational fluid dynamics applications in biotechnology processes. *Biotechnology Progress,* 27**,** 1497-1510.
SHAW, M. L., STONE, K. L., COLANGELO, C. M., GULCICEK, E. E. & PALESE, P. 2008. Cellular proteins in influenza virus particles. *Plos Pathogens,* 4.
SHIGEMATSU, S., DUBLINEAU, A., SAWOO, O., BATEJAT, C., MATSUYAMA, T., LECLERCQ, I. & MANUGUERRA, J. C. 2014. Influenza A virus survival in water is influenced by the origin species of the host cell. *Influenza and Other Respiratory Viruses,* 8**,** 123-130.
SILVA, A. C., PEIXOTO, C., LUCAS, T., KUPPERS, C., CRUZ, P. E., ALVES, P. M. & KOCHANEK, S. 2010. Adenovirus vector production and purification. *Curr Gene Ther,* 10**,** 437-55.
SILVESTRY, M., LINDERT, S., SMITH, J. G., MAIER, O., WIETHOFF, C. M., NEMEROW, G. R. & STEWART, P. L. 2009. Cryo-Electron Microscopy Structure of Adenovirus Type 2 Temperature-Sensitive Mutant 1 Reveals Insight into the Cell Entry Defect. *J Virol,* 83**,** 7375-7383.
SINOBIOLOGICALINC Influenza A H1N1 Nucleoprotein / NP Protein (His Tag). Sino Biological Inc.
SLATER, N. 2018. Viva Examination.
SRIVASTAVA. Analytical Tools for Characterization of 21st Century Vaccines. MBI Vaccine Development and Commercialisation, 2012 UCL. Protein Sciences Corporation.
SVIBEN, D., FORCIC, D., KURTOVIC, T., HALASSY, B. & BRGLES, M. 2016. Stability, biophysical properties and effect of ultracentrifugation and diafiltration on measles virus and mumps virus. *Archives of Virology,* 161**,** 1455-67.
TAIT, AUCAMP & HOARE 2009. Ultra Scale-Down prediction using microwell technology of the industrial scale clarification characteristics by centrifugation of mammalian cell broths. *biotechnology & Bioengineering,* 104**,** 321-31.
THE RAPID REFERENCE TO INFLUENZA RESOURCE CENTER TEAM. ADAPTED FROM WILSCHUT, M. A. P. 2006. *The Influenza Virus: Structure and Replication* [Online]. Elsevier. Available: http://www.rapidreferenceinfluenza.com/chapter/B978-0-7234-3433-7.50009-8/aim/influenza-virus-structure.
THERMO. 2006. *Basics of Centrifugation* [Online]. Cole Parmer Technical Library. Available: http://www.coleparmer.co.uk/TechLibraryArticle/30.
THERMO_FISHER_SCIENTIFIC 2015. User guide: iBlot 2 Dry Blotting system. *For dry, electroblotting of proteins from mini-, midi-, and E PAGE gels.* C.0 ed.
THOMAS, C. R. & GEER, D. 2011. Effects of shear on proteins in solution. *Biotechnology Letters,* 33**,** 443-456.
TITCHENER-HOOKER, N. J., DUNNILL, P. & HOARE, M. 2008. Micro biochemical engineering to accelerate the design of industrial-scale downstream processes for biopharmaceutical proteins. *Biotechnology and Bioengineering,* 100**,** 473-487.
TSANG, V. L., WANG, A. X., YUSUF-MAKAGIANSAR, H. & RYLL, T. 2014. Development of a scale down cell culture model using multivariate analysis as a qualification tool. *Biotechnol Prog,* 30**,** 152-60.
TUSTIAN, A. D., SALTE, H., WILLOUGHBY, N. A., HASSAN, I., ROSE, M. H., BAGANZ, F., HOARE, M. & TITCHENER-HOOKER, N. J. 2007. Adapted ultra

scale-down approach for predicting the centrifugal separation behavior of high cell density cultures. *Biotechnology Progress,* 23**,** 1404-1410.
UNIPROT. 2015. *UniProtKB - Q2KS10 (COR10_ADE05)* [Online]. Available: http://www.uniprot.org/uniprot/Q2KS10.
UNIPROT. 2016a. *UniProtKB - P0C0U1 (PB1F2_I34A1)* [Online]. Available: http://www.uniprot.org/uniprot/P0C0U1.
UNIPROT. 2016b. *UniProtKB - P68951 (NP_ADE05)* [Online]. Available: http://www.uniprot.org/uniprot/P68951.
VANDERCAMMEN, A., PONSAR, C., MAINIL, R., VIGANO-WOLFF, C., CHAUBARD, J., LE-TALLEC, D., CALIARO, G., CHAMPLUVIER, B., KRAMER, L., PARKER, M., SCHWARTZ, M., CAUWENBERGHS, N., OUZAMA, N., DESSOY, S., SCHOFIELD, T., LA BRAS, V., FERRIS, B., YANG, H., FINKBOHNER, J., LIU, J., SCHENERMAN, M., THOMPSON, M., WASHABAUGH, M., RANJIT, D., JUNKER, B., MARALDO, D., ABRAHAM, D., BLUE, J., WARREN, J., SCHALLER, J., MIKOLA, M., RETZLAFF, M., KOSINSKI, M., NILESH, M., THORNTON, R., SITRIN, R., LORENZ, T., BANERJEE, A., GHOSH, B., STEENO, G., KHANDKE, L., BLOOM, L., PHELAN, L., RUPPEN, M., ROHLFING, P., REPETTO, R., RODRIGUEZ, R., NEMA, S., GHIGLIERI, C., KLOCK, C., JAIPERSAD, D., ZABLACKIS, E., ALBANESI, G., CHOUVENC, P., HALSTEAD, R., GEVIER, R., PUVANESARAJAH, V., AWAFO, V., GOMEZ, P., VENUGOPAL, S., DESHPANDE, S. & DURST, T. 2012. A-Vax: Applying Quality by Design to Vaccines. *CMC-Vaccines Working Group*.
VANREIS, R., GADAM, S., FRAUTSCHY, L. N., ORLANDO, S., GOODRICH, E. M., SAKSENA, S., KURIYEL, R., SIMPSON, C. M., PEARL, S. & ZYDNEY, A. L. 1997. High performance tangential flow filtration. *Biotechnology and Bioengineering,* 56**,** 71-82.
VELLINGA, J., VAN DER HEIJDT, S. & HOEBEN, R. C. 2005. The adenovirus capsid: major progress in minor proteins. *Journal of General Virology,* 86**,** 1581-1588.
VO, M. & PAPAVASSILIOU, D. 2016. The effects of shear and particle shape on the physical adsorption of polyvinyl pyrrolidone on carbon nanoparticles. *Nanotechnology,* 27.
VWP 2013. Guideline on Influenza Vaccines - Quality Module. *In:* AGENCY, E. M. (ed.). London: European Union.
WAEHLER, R., RUSSELL, S. J. & CURIEL, D. T. 2007. Engineering targeted viral vectors for gene therapy. *Nature Reviews Genetics,* 8**,** 573-87.
WESTOBY, M., ROGERS, J. K., HAVERSTOCK, R., ROMERO, J. & PIERACCI, J. 2011. Modeling Industrial Centrifugation of Mammalian Cell Culture Using a Capillary Based Scale-Down System. *Biotechnology and Bioengineering,* 108**,** 989-998.
WHITFORD, W. & FAIRBANK, A. 2011. Considerations in Scale-up of Viral Vaccine Production. *BioProcess International,* 9**,** 16-28.
WHO. 2014. *Influenza (Seasonal). Fact Sheet No. 211* [Online]. Available: http://www.who.int/mediacentre/factsheets/fs211/en/ [Accessed 17-10-2016 2016].
WIETHOFF, C. M., WODRICH, H., GERACE, L. & NEMEROW, G. R. 2005. Adenovirus protein VI mediates membrane disruption following capsid disassembly. *J Virol,* 79**,** 1992-2000.

WISNIEWSKI, J. R., HEIN, M. Y., COX, J. & MANN, M. 2014. A "Proteomic Ruler" for Protein Copy Number and Concentration Estimation without Spike-in Standards. *Molecular & Cellular Proteomics,* 13**,** 3497-3506.
WOLFF, M. W. & REICHL, U. 2011. Downstream processing of cell culture-derived virus particles. *Expert Review of Vaccines,* 10**,** 1451-1475.
XU, F., ZHAO, C., LI, Y. H., LI, J., DENG, Y. P. & SHI, T. L. 2011. Exploring virus relationships based on virus-host protein-protein interaction network. *Bmc Systems Biology,* 5.
XU, W., NEILL, T., YANG, Y., HU, Z., CLEVELAND, E., WU, Y., HUTTEN, R., XIAO, X., STOCK, S. R., SHEVRIN, D., KAUL, K., BRENDLER, C., IOZZO, R. V. & SETH, P. 2015a. The systemic delivery of an oncolytic adenovirus expressing decorin inhibits bone metastasis in a mouse model of human prostate cancer. *Gene Therapy,* 22**,** 247-56.
XU, Y., MILLEDGE, J., ABUBAKAR, A., SWAMY, R., BAILEY, D. & HARVEY, P. 2015b. Effects of centrifugal stress on cell disruption and glycerol leakage from Dunaliella salina. *De Gruyter Open,* 1**,** 20-27.
YARMUSH, M. L. 2003. *Biotechnology for biomedical engineers,* Boca Raton, Fla., CRC Press.
YEOH, G. H., CHEUNG, C. P. & TU, J. 2014. *Multiphase flow analysis using population balance modeling : bubbles, drops, and particles*.
YIM, S. S. & SHAMLOU, P. A. 2000. The engineering effects of fluids flow on freely suspended biological macro-materials and macromolecules. *Adv Biochem Eng Biotechnol,* 67**,** 83-122.
ZAMAN, ALLAN & HO 2009. Ultra scale-down approaches for clarification of mammalian cell culture broths in disc-stack centrifuges. *Biotechnology Progress,* 25**,** 1709-16.
ZHANG, H., KONG, S., BOOTH, A., BOUSHABA, R., LEVY, M. S. & HOARE, M. 2007. Prediction of shear damage of plasmid DNA in pump and centrifuge operations using an ultra scale-down device. *Biotechnology Progress,* 23**,** 858-865.
ZHANG, X. & GODBEY, W. T. 2006. Viral vectors for gene delivery in tissue engineering. *Adv Drug Deliv Rev,* 58**,** 515-34.
ZHIRNOV, O. P., IKIZLER, M. R. & WRIGHT, P. F. 2002. Cleavage of influenza A virus hemagglutinin in human respiratory epithelium is cell associated and sensitive to exogenous antiproteases. *J Virol,* 76**,** 8682-8689.

Appendix A: PSC-5 Comsol model setup

1. Global Definitions

Date	Oct 6, 2014 10:29:25 AM

Global settings	
Name	PCS5 - 9 (fpt 2 Fixed Rotor moving wall) - MesH 2 (13500-6500RPM - 200lph) solveV5 RB modified mesh.mph
Path	D:\Users\Beatrice\Documents\work\PSC-5\rotating equipment version\PCS5 - 9 (fpt 2 _ Fixed Rotor _ moving wall) - MesH 2 (13500-6500RPM - 200lph)_solveV5_RB_modified mesh.mph
COMSOL version	COMSOL 5.0 (Build: 244)
Unit system	SI

Used products
COMSOL Multiphysics
CFD Module
Particle Tracing Module

1.1. Parameters 1

Parameters			
Name	**Expression**	**Value**	**Description**
omega	Speed*2*pi[rad]	1413.7 rad/s	angular velocity
Speed	13500[rpm]*Para	225 1/s	rotational speed
Mesh	0.85	0.85	mesh size ratioing
partsize	15[um]	1.5E−5 m	size of particle
partdens	1010[kg/m^3]	1010 kg/m³	density of particle
TIME	0[s]	0 s	
visc	1	1	multiplication factor for viscosity for initial solution
Para	1	1	

2. Component 1

Date	Oct 6, 2014 10:29:26 AM

Component settings	
Unit system	SI
Geometry shape order	automatic

2.1. Definitions

2.1.1. Coordinate Systems

Boundary System 1

Coordinate system type	Boundary system
Tag	sys1

Coordinate names		
First	**Second**	**Third**
t1	t2	n

2.2. Geometry 1

Units	
Length unit	m
Angular unit	deg

Geometry statistics	
Description	**Value**
Space dimension	3
Number of domains	8
Number of boundaries	76
Number of edges	155
Number of vertices	100

2.2.1. Entry (Cyl1)

Position	
Description	**Value**
Position	{0, 0, 0}

Axis	
Description	**Value**
Axis type	z - axis

Size and shape	
Description	**Value**
Radius	9.89[mm]/2
Height	114[mm]

2.2.2. Distributor 1 (Cyl2)

Position	
Description	**Value**
Position	{0, 0, -3.4[cm]}

Axis	
Description	**Value**
Axis type	z - axis

Size and shape	
Description	**Value**
Radius	40.28[mm]/2
Height	3.4[cm]

2.2.3. Distributor 2 (Cone1)

Position	
Description	**Value**
Position	{0, 0, -5.9[cm]}

Axis	
Description	**Value**
Axis type	z - axis

Size and shape	
Description	**Value**
Bottom radius	24.7[mm]/2
Height	2.5[cm]
Specify top size using	Radius
Top radius	40.28[mm]/2

2.2.4. Distributor 3 (Cyl3)

Position	
Description	**Value**
Position	{0, 0, -9.5[cm]}

Axis	
Description	**Value**
Axis type	z - axis

Size and shape	
Description	**Value**
Radius	24.7[mm]/2
Height	3.6[cm]

2.2.5. Distributor - to Exclude 1 (Cyl4)

Position	
Description	**Value**
Position	{0, 0, -9.5[cm]}

Axis	
Description	**Value**
Axis type	z - axis

Size and shape	
Description	**Value**
Radius	13.93[mm]/2
Height	1.2[cm]

2.2.6. Distributor - to Exclude 2 (Cyl5)

Position	
Description	**Value**
Position	{0, 0, -8.3[cm]}

Axis	
Description	**Value**
Axis type	z - axis

Size and shape	
Description	**Value**
Radius	10.29[mm]/2
Height	0.5[cm]

2.2.7. Distributor - to Exclude 3 (Cone2)

Position	
Description	**Value**
Position	{0, 0, -7.8[cm]}

Axis	
Description	**Value**
Axis type	z - axis

Size and shape	
Description	**Value**

Bottom radius	10.29[mm]/2
Height	0.2[cm]
Specify top size using	Radius
Top radius	6.65[mm]/2

2.2.8. Distributor - to Exclude 4 (Blk1)

Position	
Description	**Value**
Position	{13.93[mm]/2, 0, -9.5[cm] + 1.2[cm] - 0.79[cm]}

Rotation angle	
Description	**Value**
Rotation	90

Axis	
Description	**Value**
Axis type	x - axis

Size and shape	
Description	**Value**
Width	0.2[cm]
Depth	0.79[cm]
Height	0.5[cm]

2.2.9. Distributor Flow Area 1 (Dif1)

Compose	
Description	**Value**
Keep interior boundaries	Off

2.2.10. Entry to Channel 1-1 (Blk2)

Position	
Description	**Value**
Position	{-7.36[mm]/2, 12.3[mm] - 0.8[mm], -9.5[cm] - 3.68[mm]/2}

Axis	
Description	**Value**
Axis type	z - axis

Size and shape	
Description	**Value**
Width	7.36[mm]
Depth	7.935[mm]*3/4
Height	3.68[mm]/2

2.2.11. Entry to Channel 1-2 (Cyl6)

Position	
Description	**Value**
Position	{-7.36[mm]/2 + 7.36[mm]/2, 12.3[mm] - 0.8[mm], -9.5[cm] + 3.68[mm]/2}

Axis	
Description	**Value**
Axis type	y - axis

Size and shape	
Description	**Value**

Radius	7.36[mm]/2
Height	44.99[mm] + 0.8[mm]

2.2.12. Entry to Channel 1-4 (Cone4)

Position	
Description	**Value**
Position	{-7.36[mm]/2 + 7.36[mm]/2, 12.3[mm] - 0.6[mm] + 44.99[mm] + 0.6[mm], -9.5[cm] + 7.36[mm]/2 - 3.68[mm]/2}

Axis	
Description	**Value**
Axis type	y - axis

Size and shape	
Description	**Value**
Bottom radius	7.36[mm]/2
Height	0.5[cm]
Specify top size using	Radius
Top radius	11.51[mm]/2

2.2.13. Block 3 (Blk3)

Position

Description	Value
Position	{-7.36[mm]/2 + 7.36[mm]/2 - 11.51[mm]/2, 12.3[mm] - 0.6[mm] + 44.99[mm] + 0.6[mm], -9.5[cm] + 7.36[mm]/2 - 3.68[mm]/2 + 11.51[mm]/3}

Rotation angle

Description	Value
Rotation	40

Axis

Description	Value
Axis type	x - axis

Size and shape

Description	Value
Width	11.51[mm]
Depth	11.51[mm]
Height	11.51[mm]

2.2.14. Entry to Channel Union (Uni1)

Compose	
Description	**Value**
Keep interior boundaries	Off

2.2.15. Entry to Channel Extrude 2 (Ext3)

Settings	
Description	**Value**
Extrude from	Faces
Input object handling	Keep

Distances
Distances (m)
1.983[mm]

Distances	
Description	**Value**
Keep cross-sectional faces	Off

Scales	
Scales xw	**Scales yw**
1	1

Displacements	
Displacements xw (m)	**Displacements yw (m)**
0	0

Twist angles

Twist angles (deg)
0

2.2.16. Entry to Channel Extrude (Ext1)

Settings	
Description	**Value**
Extrude from	Faces
Input object handling	Keep

Distances
Distances (m)
1.983[mm]

Distances	
Description	**Value**
Keep cross-sectional faces	Off

Scales	
Scales xw	**Scales yw**
1	1

Displacements	
Displacements xw (m)	**Displacements yw (m)**
0	0

Twist angles
Twist angles (deg)
0

2.2.17. Entry to Channel 1-3 (Cone3)

Position	
Description	**Value**
Position	{-7.36[mm]/2 + 7.36[mm]/2, 12.3[mm] - 0.6[mm], -9.5[cm] + 7.36[mm]/2}

Axis	
Description	**Value**
Axis type	y - axis

Size and shape	
Description	**Value**
Bottom radius	7.36[mm]*1.3
Height	7.936[mm]
Specify top size using	Radius
Top radius	7.36[mm]/2

2.2.18. Entry to Channel Intersection (Int1)

Compose	
Description	**Value**
Keep interior boundaries	Off

2.2.19. Entry to Channel 1-3.2 (Cone7)

Position

Description	Value
Position	{-7.36[mm]/2 + 7.36[mm]/2, 12.3[mm] - 0.6[mm], -9.5[cm] + 7.36[mm]/2}

Axis

Description	Value
Axis type	y - axis

Size and shape

Description	Value
Bottom radius	7.36[mm]*1.3
Height	7.936[mm]
Specify top size using	Radius
Top radius	7.36[mm]/2

2.2.20. Entry to Channel Intersection 1 (Int2)

Compose

Description	Value
Keep interior boundaries	Off

2.2.21. Channel 2 (Rot1)

Settings	
Description	**Value**
Keep input objects	On
Rotation	45
Point on axis of rotation	{0, 0, 0}
Axis type	z - axis

2.2.22. Channel 3 (Rot2)

Settings	
Description	**Value**
Keep input objects	On
Rotation	90
Point on axis of rotation	{0, 0, 0}
Axis type	z - axis

2.2.23. Channel 4 (Rot3)

Settings	
Description	**Value**
Keep input objects	On
Rotation	135
Point on axis of rotation	{0, 0, 0}
Axis type	z - axis

2.2.24. Channel 5 (Rot4)

Settings	
Description	**Value**
Keep input objects	On
Rotation	-90
Point on axis of rotation	{0, 0, 0}
Axis type	z - axis

2.2.25. Channel 6 (Rot5)

Settings	
Description	**Value**
Keep input objects	On
Rotation	-45
Point on axis of rotation	{0, 0, 0}
Axis type	z - axis

2.2.26. Channel 7 (Rot6)

Settings	
Description	**Value**
Keep input objects	On
Rotation	-135
Point on axis of rotation	{0, 0, 0}
Axis type	z - axis

2.2.27. Channel 8 (Rot7)

Settings	
Description	**Value**
Keep input objects	On
Rotation	-180
Point on axis of rotation	{0, 0, 0}
Axis type	z - axis

2.2.28. Discs Stack 1-1 (Cone5)

Position	
Description	**Value**
Position	{-10[cm], -10[cm], 0}

Axis	
Description	**Value**
Axis type	z - axis

Size and shape	
Description	**Value**
Bottom radius	126.96[mm]/2
Height	36.2[mm]
Specify top size using	Radius
Top radius	67.32[mm]/2

2.2.29. Disc Stack 1-2 (Cyl7)

Position	
Description	**Value**
Position	{-10[cm], -10[cm], 36.2[mm]}

Axis	
Description	**Value**
Axis type	z - axis

Size and shape	
Description	**Value**

Radius	60.8[mm]/2
Height	115[mm] - 36.2[mm]

2.2.30. Disc Stack 1-3 (Cone6)

Position	
Description	**Value**
Position	{-10[cm], -10[cm], 115[mm] - 36.2[mm]}

Axis	
Description	**Value**
Axis type	z - axis

Size and shape	
Description	**Value**
Bottom radius	126.96[mm]/2
Height	36.2[mm]
Specify top size using	Radius
Top radius	67.32[mm]/2

2.2.31. Disc Stack 1-4 (Ext2)

Settings	
Description	**Value**
Extrude from	Faces
Input object handling	Keep

Distances

Distances (m)
115[mm]-36.2[mm]

Distances	
Description	**Value**
Reverse direction	On

Scales	
Scales xw	**Scales yw**
1	1

Displacements	
Displacements xw (m)	**Displacements yw (m)**
0	0

Twist angles
Twist angles (deg)
0

2.2.32. Cut Through Discs 1 (Cyl8)

Position	
Description	**Value**
Position	{-10[cm] + 126.96[mm]/3, -10[cm] + 126.96[mm]/3, 0}

Axis	
Description	**Value**
Axis type	z - axis

Size and shape	
Description	**Value**
Radius	11.51[mm]/2
Height	115[mm]

2.2.33. Cut Through Discs 2 (Rot8)

Settings	
Description	**Value**
Keep input objects	On
Rotation	180
Point on axis of rotation	{-10[cm], -10[cm], 0}
Axis type	z - axis

2.2.34. Cut Through Discs 3 (Rot9)

Settings	
Description	**Value**
Keep input objects	On
Rotation	90
Point on axis of rotation	{-10[cm], -10[cm], 0}
Axis type	z - axis

2.2.35. Cut Through Discs 4 (Rot10)

Settings	
Description	**Value**
Keep input objects	On
Rotation	-90
Point on axis of rotation	{-10[cm], -10[cm], 0}
Axis type	z - axis

2.2.36. Cut Through Discs 5 (Rot11)

Settings	
Description	**Value**
Keep input objects	On
Rotation	45
Point on axis of rotation	{-10[cm], -10[cm], 0}
Axis type	z - axis

2.2.37. Cut Through Discs 6 (Rot12)

Settings	
Description	**Value**
Keep input objects	On
Rotation	-45
Point on axis of rotation	{-10[cm], -10[cm], 0}
Axis type	z - axis

2.2.38. Cut Through Discs 7 (Rot13)

Settings	
Description	**Value**
Keep input objects	On
Rotation	135
Point on axis of rotation	{-10[cm], -10[cm], 0}
Axis type	z - axis

2.2.39. Cut Through Discs 8 (Rot14)

Settings	
Description	**Value**
Keep input objects	On
Rotation	225
Point on axis of rotation	{-10[cm], -10[cm], 0}
Axis type	z - axis

2.2.40. Move 1 (Mov1)

Settings	
Description	**Value**
x	0.1
y	0.1
z	-0.095

2.2.41. Union 3 (Uni3)

Compose	
Description	**Value**
Keep interior boundaries	Off

2.2.42. Work Plane 1 (Wp1)

Settings	
Description	**Value**
Plane	yz - plane

Unite objects	
Description	**Value**
Unite objects	On

Visualization	
Description	**Value**
Projection (light blue)	Off

Plane Geometry (Sequence2D)

2.3. Materials

2.3.1. Water

Selection	
Geometric entity level	Domain
Selection	Domains 1–8

Material parameters		
Name	**Value**	**Unit**
Dynamic viscosity	visc*eta(T[1/K])[Pa*s]	Pa·s
Density	rho(T[1/K])[kg/m^3]	kg/m³

Basic Settings	
Description	**Value**
Dynamic viscosity	visc*eta(T[1/K])[Pa*s]
Ratio of specific heats	1.0
Electrical conductivity	{{5.5e-6[S/m], 0, 0}, {0, 5.5e-6[S/m], 0}, {0, 0, 5.5e-6[S/m]}}
Heat capacity at constant pressure	Cp(T[1/K])[J/(kg*K)]
Density	rho(T[1/K])[kg/m^3]
Thermal conductivity	{{k(T[1/K])[W/(m*K)], 0, 0}, {0, k(T[1/K])[W/(m*K)], 0}, {0, 0, k(T[1/K])[W/(m*K)]}}
Speed of sound	cs(T[1/K])[m/s]

Functions	
Function name	**Type**
eta	Piecewise
Cp	Piecewise
rho	Piecewise
k	Piecewise
cs	Interpolation

2.7. Mesh 4

Mesh statistics	
Description	**Value**
Minimum element quality	0.0
Average element quality	0.0

2.7.1. Size (Size)

Settings	
Description	**Value**
Calibrate for	Fluid dynamics
Maximum element size	0.0066
Minimum element size	0.00125
Curvature factor	0.5
Resolution of narrow regions	0.8
Maximum element growth rate	1.13
Predefined size	Fine

2.7.2. Size 1 (Size1)

Selection	
Geometric entity level	Boundary
Selection	Boundaries 1–4, 6, 8–11, 13–22, 24, 26–29, 32–36, 39–40, 42, 44, 46–54, 56, 59–63, 65–73, 75

Settings	
Description	**Value**
Calibrate for	Fluid dynamics
Maximum element size	0.00461*Mesh
Minimum element size	4.98E-4*Mesh
Curvature factor	0.4
Curvature factor	Off

Resolution of narrow regions	0.9
Resolution of narrow regions	Off
Maximum element growth rate	Off
Predefined size	Finer
Custom element size	Custom

2.7.3. Size 2 (Size2)

Selection	
Geometric entity level	Edge
Selection	Edges 4, 10, 12, 48, 51, 66, 116, 145, 147, 153

Settings

Description	Value
Maximum element size	10[um]
Minimum element size	1[um]
Curvature factor	0.2
Curvature factor	Off
Resolution of narrow regions	Off
Maximum element growth rate	1.3
Maximum element growth rate	Off
Predefined size	Extremely fine
Custom element size	Custom

2.7.4. Corner Refinement 1 (Cr1)

Selection	
Geometric entity level	Domain
Selection	Domains 1–8

2.7.5. Free Tetrahedral 1 (Ftet1)

Selection	
Geometric entity level	Domain
Selection	Domains 1–8

Settings	
Description	**Value**
Method	Delaunay (legacy version)

2.7.6. Boundary Layers 1 (Bl1)

Selection	
Geometric entity level	Domain
Selection	Domains 1–8

Settings	
Description	**Value**
Handling of sharp edges	Trimming
Maximum angle for trimming	20

Boundary Layer Properties 1 (Blp1)

Selection

Geometric entity level	Boundary
Selection	Boundaries 3, 8–11, 13–18, 20–21, 26–29, 32–36, 40, 42, 44, 46–49, 51–54, 56, 59–62, 65–70

Settings

Description	Value
Number of boundary layers	5
Thickness adjustment factor	2.5

2.7.7. Free Tetrahedral 2 (Ftet2)

Selection

Geometric entity level	Remaining

Settings

Description	Value
Method	Delaunay (legacy version)

Appendix B: PKII Comsol model setup

1. Global Definitions

Date	Jun 18, 2015 10:11:24 AM

Global settings	
Name	Pre-geometry details KII K3 v4 mod channelwidth v3 geometrycorrection.mph
Path	D:\Users\Beatrice\Documents\work\ultracentrifuge\pre-geometry details KII_K3_v4_mod_channelwidth_v3_geometrycorrection.mph
COMSOL version	COMSOL 5.2a (Build: 262)
Unit system	SI

Used products
COMSOL Multiphysics
CFD Module

1.1. Parameters 1

Parameters

Name	Expression	Value	Description
TIME	0[s]	0 s	
Param	1	1	ramp up the speed(stability)
Mesh	1	1	to test the effects of the mesh fineness
P2	1	1	ramping down the flow

2. Component 1

Date	Apr 13, 2015 3:05:09 PM

Component settings	
Unit system	SI
Geometry shape order	automatic

2.1. Definitions

2.1.1. Selections

Explicit 1

Selection type
Explicit

Selection
Boundary 19

2.1.2. Coordinate Systems

Boundary System 1

Coordinate system type	Boundary system
Tag	sys1

Coordinate names		
First	**Second**	**Third**
t1	t2	n

2.2. Geometry 1

Units	
Length unit	m
Angular unit	deg

Geometry statistics	
Description	**Value**
Space dimension	3
Number of domains	2
Number of boundaries	19
Number of edges	43
Number of vertices	27

2.2.1. Cylinder 1 (Cyl1)

Position	
Description	**Value**
Position	{0, 0, 0}

Axis	
Description	**Value**
Axis type	z - axis

Size and shape	
Description	**Value**
Radius	130[mm]/2
Height	0.42[m]

2.2.2. Cylinder 2 (Cyl2)

Position	
Description	**Value**
Position	{0, 0, 0}

Axis	
Description	**Value**
Axis type	z - axis

Size and shape	
Description	**Value**
Radius	110[mm]/2
Height	0.42[m]

2.2.3. Block 1 (Blk1)

Position	
Description	**Value**
Position	{109[mm]/2, 0, 0}

Axis	
Description	**Value**
Axis type	z - axis

Size and shape	
Description	**Value**

Width	21[mm]*2
Depth	0.173[cm]
Height	0.42[m]

2.2.4. Block 4 (Blk4)

Position	
Description	**Value**
Position	{109[mm]*2, 0, 0}

Rotation angle	
Description	**Value**
Rotation	0.85

Axis	
Description	**Value**
Axis type	z - axis

Size and shape	
Description	**Value**
Width	21[mm]*2
Depth	0.173[cm]/2
Height	0.42[m]

2.2.5. Block 5 (Blk5)

Position	
Description	**Value**

Position	{109[mm]*2, 0.173[cm]/2, 0}

Rotation angle	
Description	**Value**
Rotation	-0.85

Axis	
Description	**Value**
Axis type	z - axis

Size and shape	
Description	**Value**
Width	21[mm]*2
Depth	0.173[cm]/2
Height	0.42[m]

2.2.6. Rotate 1 (Rot1)

Settings	
Description	**Value**
Keep input objects	On
Rotation	60
Point on axis of rotation	{0, 0, 0}
Axis type	z - axis

2.2.7. Rotate 2 (Rot2)

Settings	
Description	**Value**
Keep input objects	On
Rotation	120
Point on axis of rotation	{0, 0, 0}
Axis type	z - axis

2.2.8. Rotate 3 (Rot3)

Settings	
Description	**Value**
Keep input objects	On
Rotation	180
Point on axis of rotation	{0, 0, 0}
Axis type	z - axis

2.2.9. Rotate 4 (Rot4)

Settings	
Description	**Value**
Keep input objects	On
Rotation	240
Point on axis of rotation	{0, 0, 0}
Axis type	z - axis

2.2.10. Rotate 5 (Rot5)

Settings	
Description	**Value**
Keep input objects	On
Rotation	300
Point on axis of rotation	{0, 0, 0}
Axis type	z - axis

2.2.11. Union 1 (Uni1)

Compose	
Description	**Value**
Keep interior boundaries	Off

2.2.12. Difference 1 (Dif1)

Compose	
Description	**Value**
Keep interior boundaries	Off

2.2.13. Cone 1 (Cone1)

Position	
Description	**Value**
Position	{0, 0, 0.42 - 1.5[mm]}

Axis

Description	Value
Axis type	z - axis

Size and shape

Description	Value
Bottom radius	1[cm]
Height	0.1[cm] + 1.5[mm]

2.2.14. Block 2 (Blk2)

Position

Description	Value
Position	{-1.5[mm]/2, 0, 0.42 - 1.5[mm]}

Size and shape

Description	Value
Width	1.5[mm]
Depth	129[mm]/2 - 38[mm]/4
Height	1.5[mm]

Axis

Description	Value
Axis type	z - axis

2.2.15. Rotate 6 (Rot6)

Settings

Description	Value
Keep input objects	On

Rotation	60
Point on axis of rotation	{0, 0, 0}
Axis type	z - axis

2.2.16. Rotate 7 (Rot7)

Settings	
Description	**Value**
Keep input objects	On
Rotation	120
Point on axis of rotation	{0, 0, 0}
Axis type	z - axis

2.2.17. Rotate 8 (Rot8)

Settings	
Description	**Value**
Keep input objects	On
Rotation	180
Point on axis of rotation	{0, 0, 0}
Axis type	z - axis

2.2.18. Rotate 9 (Rot9)

Settings	
Description	**Value**
Keep input objects	On
Rotation	240
Point on axis of rotation	{0, 0, 0}
Axis type	z - axis

2.2.19. Rotate 10 (Rot10)

Settings	
Description	**Value**
Keep input objects	On
Rotation	300
Point on axis of rotation	{0, 0, 0}
Axis type	z - axis

2.2.20. Union 2 (Uni2)

Compose	
Description	**Value**
Keep interior boundaries	Off

2.2.21. Mirror 1 (Mir1)

Settings	
Description	**Value**
Keep input objects	On

Point on plane of reflection	
Description	**Value**
Point in plane	{0, 0, 0}

Normal vector to plane of reflection	
Description	**Value**
Plane normal	{0, 0, 1}

2.2.22. Move 1 (Mov1)

Settings	
Description	**Value**
x	0
y	0
z	0.42

2.2.23. Union 3 (Uni3)

Compose	
Description	**Value**
Keep interior boundaries	Off

2.2.24. Block 3 (Blk3)

Position	
Description	**Value**
Position	{0, 0, -5[mm]}

Axis	
Description	**Value**
Axis type	z - axis

Size and shape	
Description	**Value**
Width	130[mm]/2
Depth	130[mm]/2
Height	0.42[m] + 10[mm]

2.2.25. Rotate 11 (Rot11)

Settings	
Description	**Value**
Keep input objects	On
Rotation	30
Point on axis of rotation	{0, 0, 0}
Axis type	z - axis

2.2.26. Rotate 12 (Rot12)

Settings	
Description	**Value**
Rotation	-60
Point on axis of rotation	{0, 0, 0}
Axis type	z - axis

2.2.27. Rotate 13 (Rot13)

Settings	
Description	**Value**
Keep input objects	On
Rotation	-60

Point on axis of rotation	{0, 0, 0}
Axis type	z - axis

2.2.28. Rotate 14 (Rot14)

Settings	
Description	**Value**
Keep input objects	On
Rotation	-60
Point on axis of rotation	{0, 0, 0}
Axis type	z - axis

2.2.29. Block 6 (Blk6)

Position	
Description	**Value**
Position	{-0.4, -0.1, -0.01}

Axis	
Description	**Value**
Axis type	z - axis

Size and shape	
Description	**Value**
Width	0.4
Depth	0.4
Height	0.3

2.2.30. Cylinder 3 (Cyl3)

Position	
Description	**Value**
Position	{0, 0, 0}

Axis	
Description	**Value**
Axis type	z - axis

Size and shape	
Description	**Value**
Radius	110[mm]/2 + 11[mm]/2
Height	0.42[m] + 1[cm]

2.2.31. Intersection 1 (Int1)

Settings	
Description	**Value**
Keep input objects	On

2.3. Materials

2.3.1. Water

Selection	
Geometric entity level	Domain
Selection	Domains 1–2

Material parameters		
Name	**Value**	**Unit**
Dynamic viscosity	eta(T[1/K])[Pa*s]	Pa·s
Density	rho(T[1/K])[kg/m^3]	kg/m³

Basic Settings	
Description	**Value**
Dynamic viscosity	eta(T[1/K])[Pa*s]
Ratio of specific heats	1.0
Electrical conductivity	{{5.5e-6[S/m], 0, 0}, {0, 5.5e-6[S/m], 0}, {0, 0, 5.5e-6[S/m]}}
Heat capacity at constant pressure	Cp(T[1/K])[J/(kg*K)]
Density	rho(T[1/K])[kg/m^3]
Thermal conductivity	{{k(T[1/K])[W/(m*K)], 0, 0}, {0, k(T[1/K])[W/(m*K)], 0}, {0, 0, k(T[1/K])[W/(m*K)]}}
Speed of sound	cs(T[1/K])[m/s]

Functions	
Function name	**Type**
eta	Piecewise
Cp	Piecewise
rho	Piecewise
k	Piecewise
cs	Interpolation

2.4. Rotating Machinery, Turbulent Flow, k-ε

Used products
COMSOL Multiphysics
CFD Module

Selection	
Geometric entity level	Domain
Selection	Domains 1–2

2.5. Mesh 1

Mesh statistics	
Description	**Value**
Minimum element quality	0.002189
Average element quality	0.381
Tetrahedral elements	25016
Pyramid elements	232
Prism elements	21537
Triangular elements	6124
Quadrilateral elements	831
Edge elements	557
Vertex elements	27

2.5.1. Size (Size)

Settings	
Description	**Value**
Calibrate for	Fluid dynamics
Maximum element size	0.00908*Mesh
Minimum element size	0.00171
Curvature factor	0.5
Resolution of narrow regions	0.8
Maximum element growth rate	1.13
Predefined size	Fine
Custom element size	Custom

2.5.2. Size 1 (Size1)

Selection	
Geometric entity level	Boundary
Selection	Boundaries 1–2, 4–5, 8–16

Settings	
Description	**Value**
Calibrate for	Fluid dynamics
Maximum element size	0.00394*Mesh
Minimum element size	2.57E-4
Minimum element size	Off
Curvature factor	0.3

Curvature factor	Off
Resolution of narrow regions	0.95
Resolution of narrow regions	Off
Maximum element growth rate	1.08
Maximum element growth rate	Off
Predefined size	Extra fine
Custom element size	Custom

2.5.3. Size 2 (Size2)

Selection	
Geometric entity level	Edge
Selection	Edges 16, 18, 21, 23

Settings	
Description	**Value**
Maximum element size	0.0052*Mesh
Minimum element size	5.2E-5
Minimum element size	Off
Curvature factor	0.2
Curvature factor	Off
Resolution of narrow regions	Off
Maximum element growth rate	1.3
Maximum element growth rate	Off
Predefined size	Extremely fine

Custom element size	Custom

2.5.4. Corner Refinement 1 (Cr1)

Selection	
Geometric entity level	Domain
Selection	Domains 1–2

2.5.5. Free Tetrahedral 1 (Ftet1)

Selection	
Geometric entity level	Domain
Selection	Domains 1–2

Settings	
Description	**Value**
Method	Delaunay (legacy version)

2.5.6. Boundary Layers 1 (Bl1)

Selection	
Geometric entity level	Domain
Selection	Domains 1–2

Settings	
Description	**Value**
Handling of sharp edges	Trimming
Maximum angle for trimming	20

Boundary Layer Properties 1 (Blp1)

Selection	
Geometric entity level	Boundary
Selection	Boundaries 1–2, 4–5, 8–16

Settings

Description	Value
Number of boundary layers	5
Thickness adjustment factor	2.5

Appendix C: Chapter 3 Supplementary Data

Figure(C) 1 C to F shows the shear level in the rotating disc shear device on the same basis, for reference. These results are based on raw data output from the CFD model, which doesn't allow for a clear understanding of the spatial distribution of the shear, such as the relative sizes of high shear zones. It may also be observed from Figure(C) 1 G and H that the level of shear in the ultracentrifuge is very much comparable to that seen in the PSC-5 centrifuge, suggesting that these two centrifuge types may cause a similar level of shear damage.

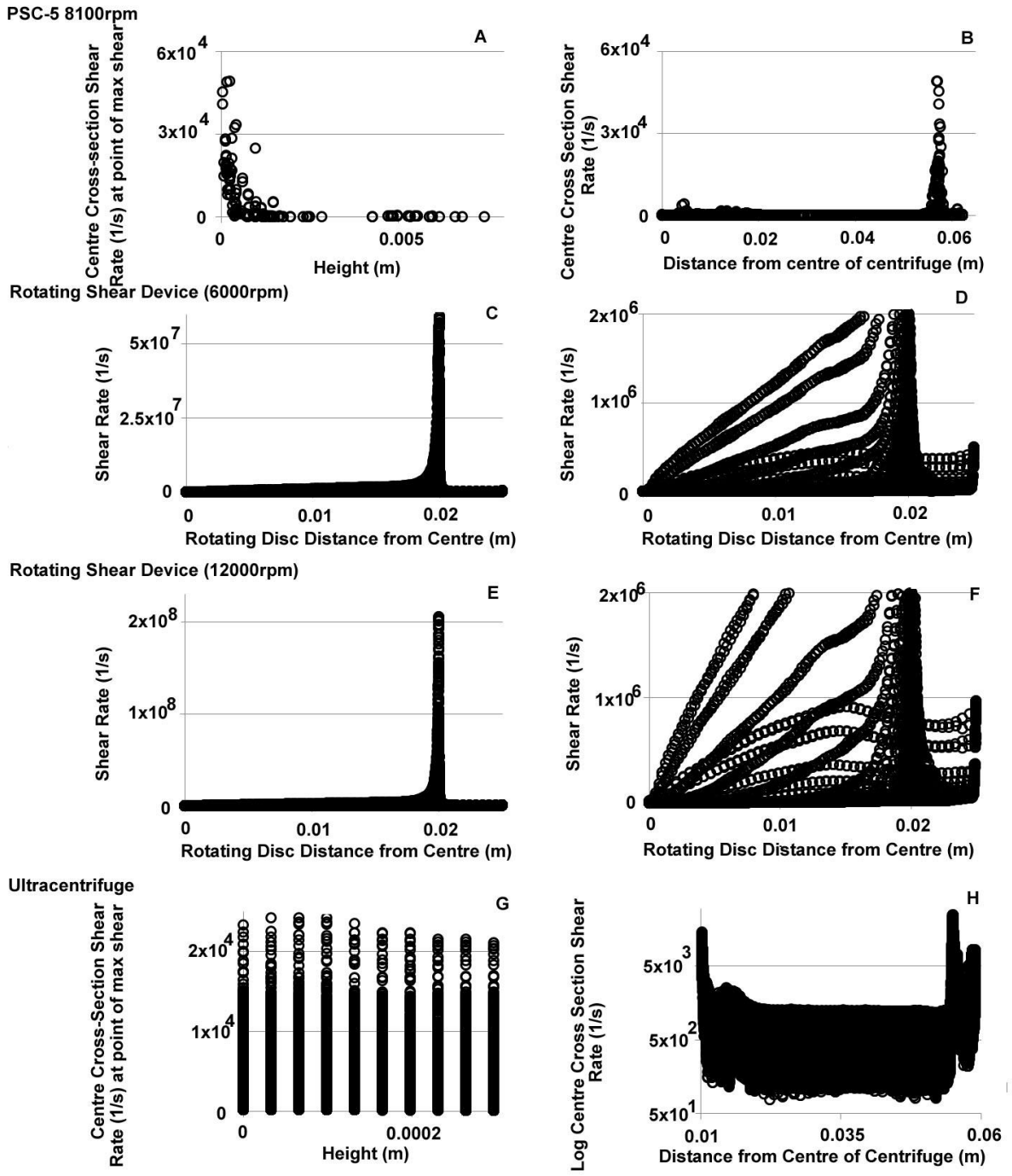

Figure(C) 1. Juxtaposed images showing the spatial distribution of shear rate values in the PSC-5, and PKII centrifuges and in the rotating disc shear device. The data points shown are as per the mesh point outputs, i.e. areas of denser meshing will contribute disproportionately to the points shown. A and B show shear rate for the PSC-5 centrifuge, modelled using the rotating machinery function, across the height of a cross-section at the radial point of highest shear (A) and with increasing radial distance (B). C and D show shear rates for the rotating disc shear device for a disc speed of 6000rpm with increasing radial distance, similarly E and F are for a disc speed of 12000rpm. G and H show shear rate for the PKII ultracentrifuge, modelled using the rotating machinery function, across the height of a cross-section at the radial point of highest shear (G) and with increasing radial distance (H).

Key variables are introduced by the use of a breakage model, in the form of the parameters of the power law breakage kernel (Eqn. 11, section 2.1.1.4). The impact of breakage kernel parameter selection is illustrated in Figure(C) 2 for the PSC-5 and Figure(C) 3 for the PKII. The breakage kernel parameters selected for use at large scale were those in sensitivity run #4, on the basis of similarities to the shear impact seen for cells and AdjuPhos, where damage is seen at shears greater than approximately 6000rpm, and substantial particle destruction is evident at 12000rpm, where the difference between the damage after 5 seconds and that after 20 seconds is not substantial, and where the increasing shear damage follows a roughly linear route. It should be noted that the results presented in Figure 3.2-22 are dependent on the breakage kernel parameters used, and that further optimisation of these parameters to more closely approach the experimental observed breakage trend is possible. The result presented here is the best that could be achieved within the time available.

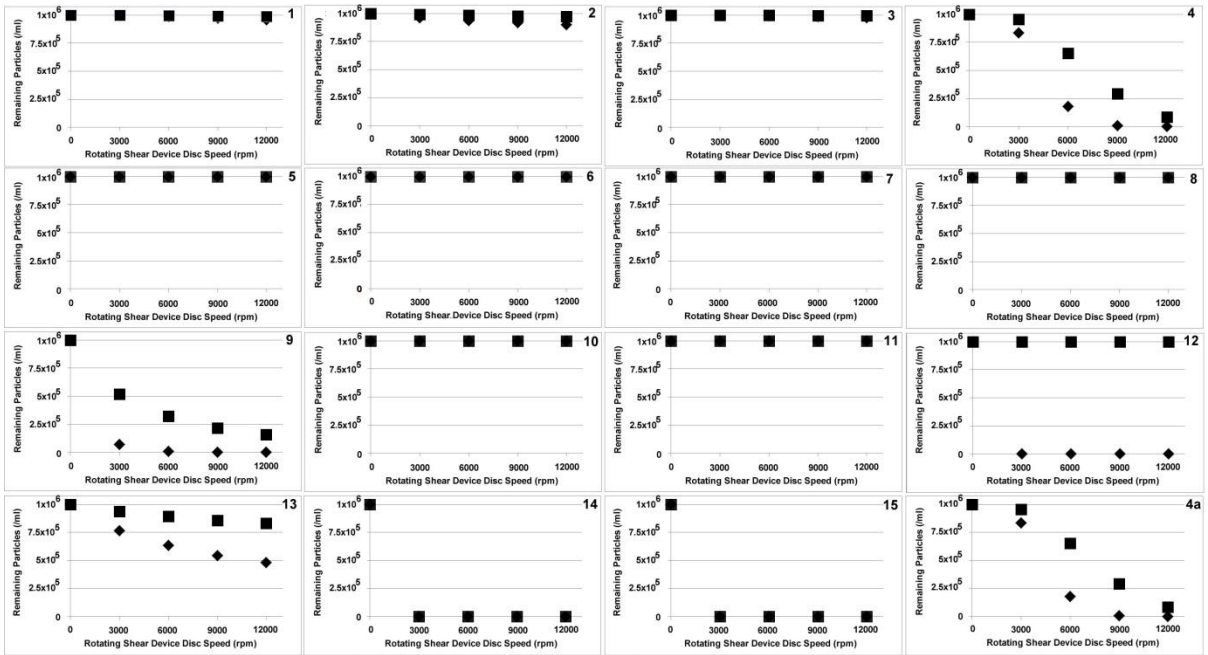

	1	2	3	4	5	6	7	8	9	10	11	12	13	14	15
C4	$1x10^{-3}$	$1x10^{-3}$	$1x10^{-3}$	$1x10^{-3}$	$1x10^{-3}$	$1x10^{-3}$	$1x10^{-3}$	$1x10^{-3}$	$1x10^{-3}$	$1x10^{-3}$	$1x10^{-3}$	$1x10^{-4}$	$1x10^{-4}$	$1x10^{-4}$	$1x10^{-4}$
alpha	1.25	1.25	1.25	1.25	1.25	0.5	2	0.5	2	0.5	0.5	2	2	2	2
beta	0.5	0.25	0.75	0.75	0.25	0.5	0.9	0.75	0.25	0.25	0.9	0.75	0.25	0.25	0.75
gamma	0.5	0.25	0.75	0.25	0.75	0.25	3	0.25	0.75	0.75	3	0.25	0.75	0.25	0.75

Figure(C) 2. Decrease in particle count in rotating shear device with different particle breakage parameters, and an assumed particle size of 5µm, after a shear period of 5 secs (■) and 20 secs (◆). Where the path by the disc is within 0.001m of the disc, and the number of passes depends on the speed of the disc. The particle parameters for each run is shown in the table. 4A is a sensitivity run where the path of the particles closest to the disc tip have been shifted by a random distance, within 200µm, away.

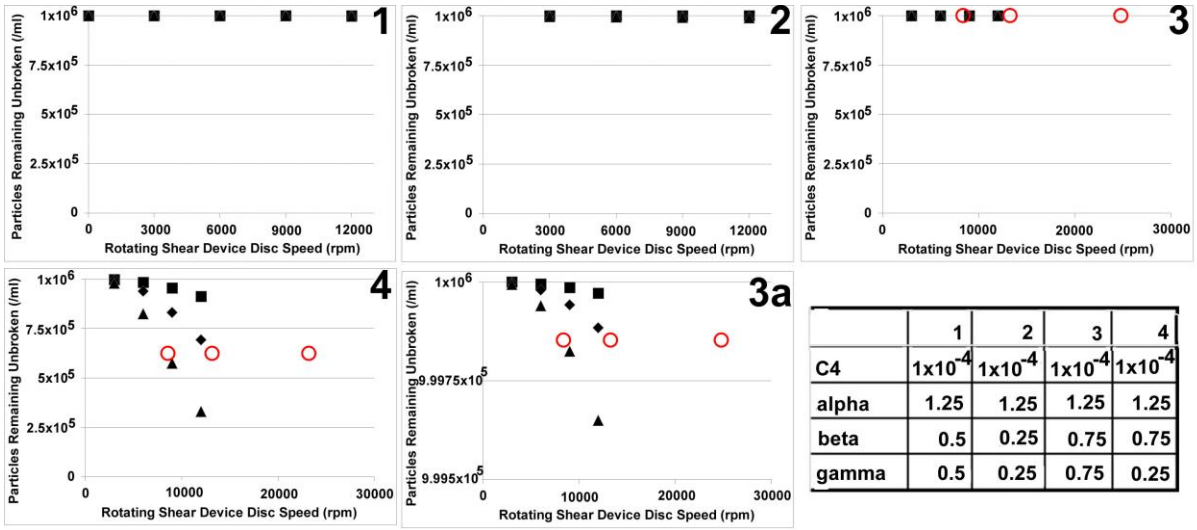

	1	2	3	4
C4	$1x10^{-4}$	$1x10^{-4}$	$1x10^{-4}$	$1x10^{-4}$
alpha	1.25	1.25	1.25	1.25
beta	0.5	0.25	0.75	0.75
gamma	0.5	0.25	0.75	0.25

Figure(C) 3. Predicted particle breakage for a selected set of particle breakage parameters in the rotating disc shear device, for a range of run times: 5seconds (■), 20seconds (◆) and 1 minute (▲). Particle diameters assumed uniform at 100nm. Red circles (◯) are the predictions for the PKII centrifuge.

The impact of PSC-5 geometry sensitivities on outputs, as measured by rotating disc speed required to replicate particle breakage, is shown in Figure(C) 4.

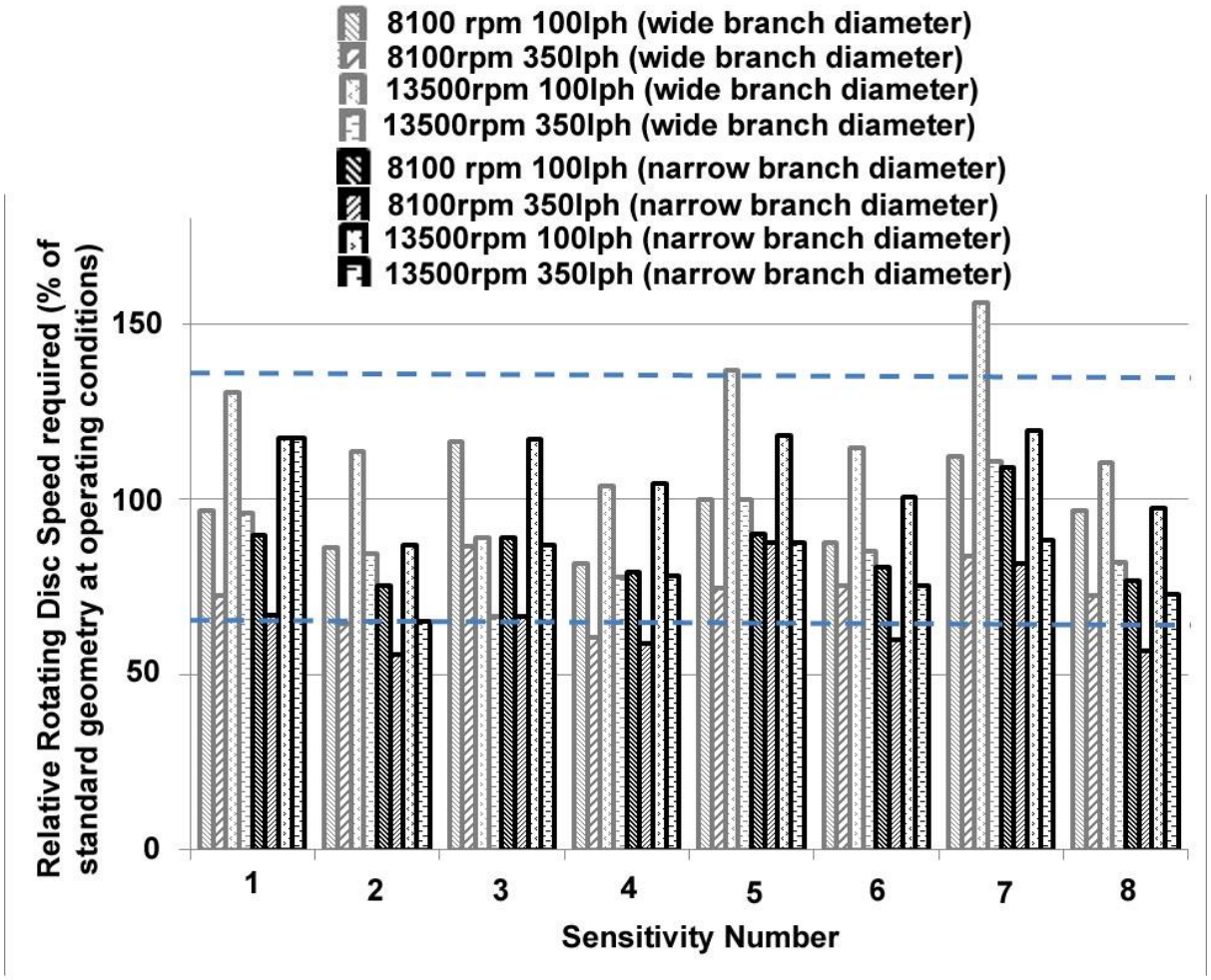

Figure(C) 4. Sensitivity run results for the geometric features of a PSC style centrifuge feed zone, including inner and outer radius and angle and diameter of inlet branches, over a range of speeds and flowrates. The relative equivalent disc speed in the rotating disc shear device is based on particle breakage modelling as illustrated in Figure 3.2-22. The dashed lines indicate the equivalent range for the PSC-5 measured-geometry used in the main PSC-5 simulation. Sensitivity run parameters are detailed in Table 2.2-1.

Appendix D: Chapter 4 Supplementary Data

Initially the count ratio measured on the Casy counter (Figure(D) 2) and the equivalent (number based) Mastersizer 90%ile (Figure(D) 1) parameter were used. This gave a higher than expected prediction of shear; 8.3 to 9.5krpm instead of the expected 6krpm.

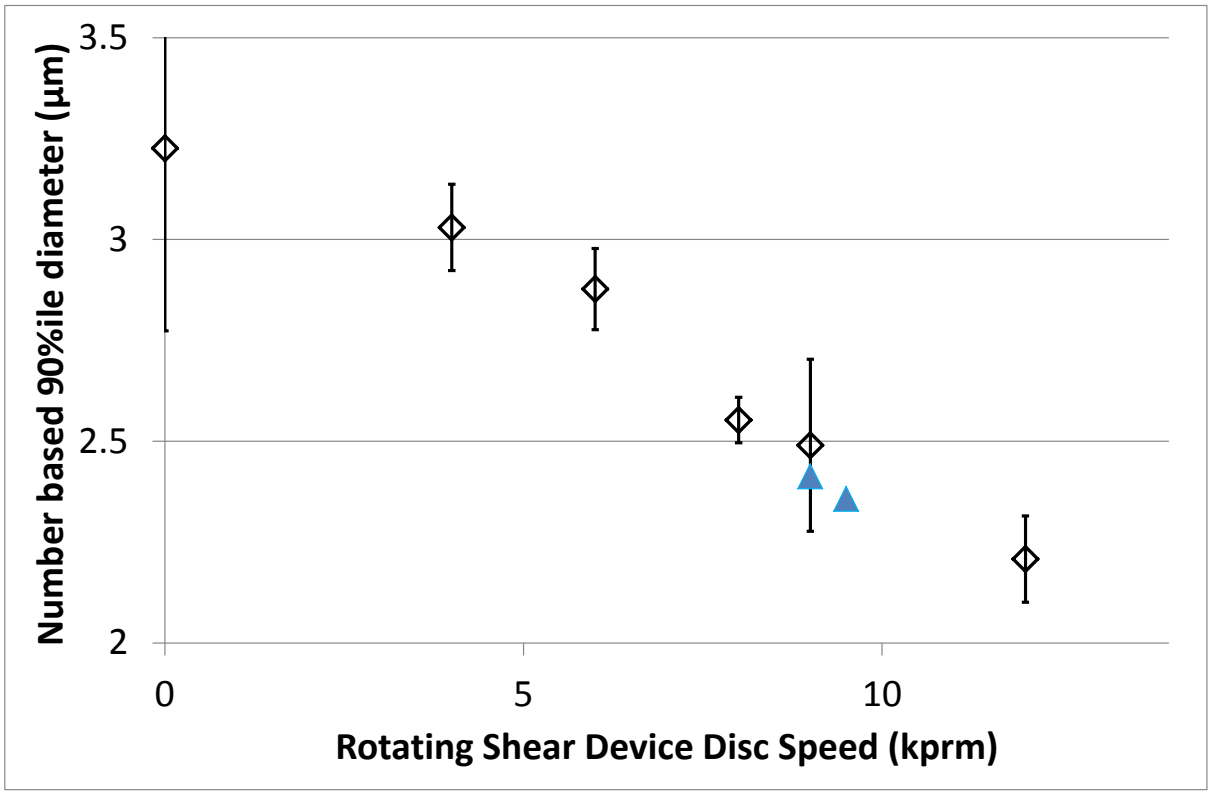

Figure(D) 1. Effect of shear on a 1%v/v Adju-Phos suspension using the USD rotational shear device at varying shear rates, based on Mastersizer 2000 data. Error bars represent 95% confidence intervals using student t-test (n=4). Open diamonds (◇) represent Adju-phos runs on the rotating disc shear device, filled triangles (▲) are Adju-phos runs on the pilot scale disc stack centrifuge (CSA-1) with solids manually removed from the solids collection chamber within the centrifuge bowl.

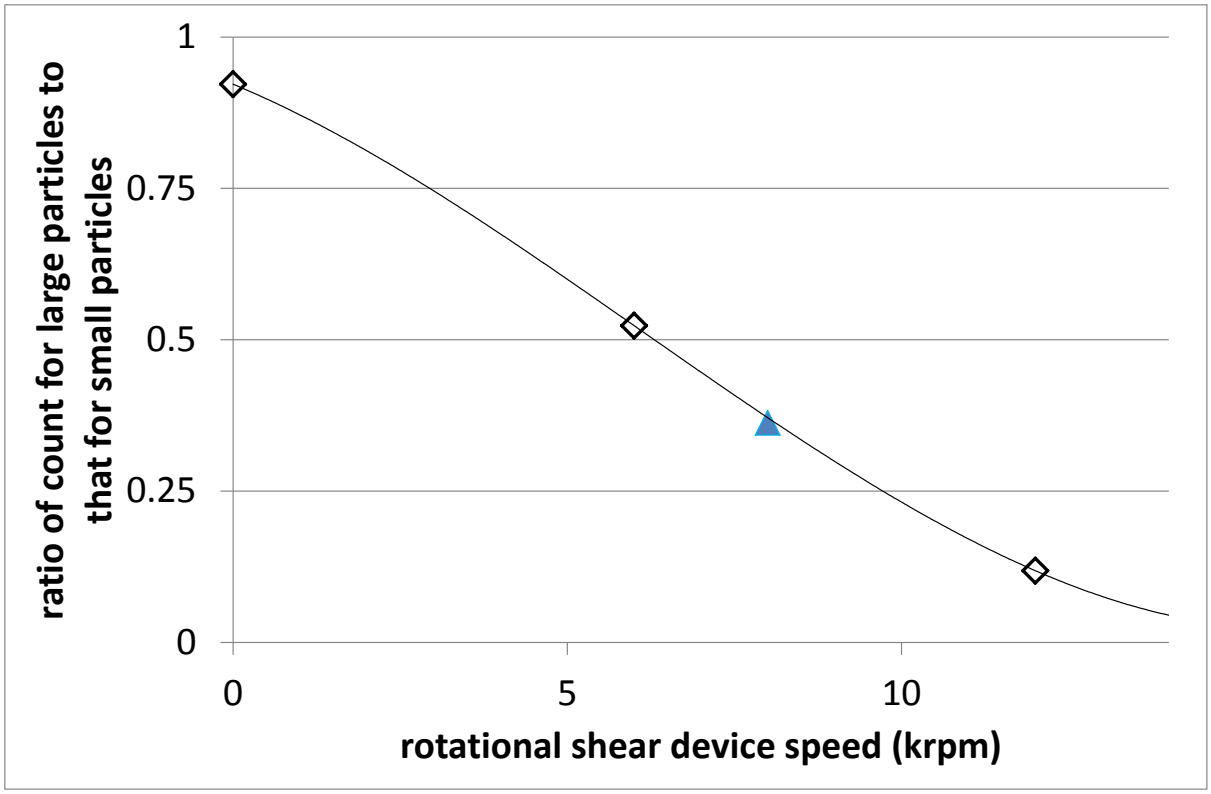

Figure(D) 2. Effect of shear on a 1%v/v Adju-Phos suspension using the USD rotational shear device at varying shear rates, based on Casy Counter data. Error bars represent 95% confidence intervals using student t-test (n=4). Open diamonds (◇) represent Adju-phos runs on the rotating disc shear device, filled triangles (▲) are Adju-phos runs on the pilot scale disc stack centrifuge (CSA-1) with solids manually removed from the solids collection chamber within the centrifuge bowl.

The figures below illustrate, in order, the steps taken to analyse the position of the peak for the raw mastersizer data.

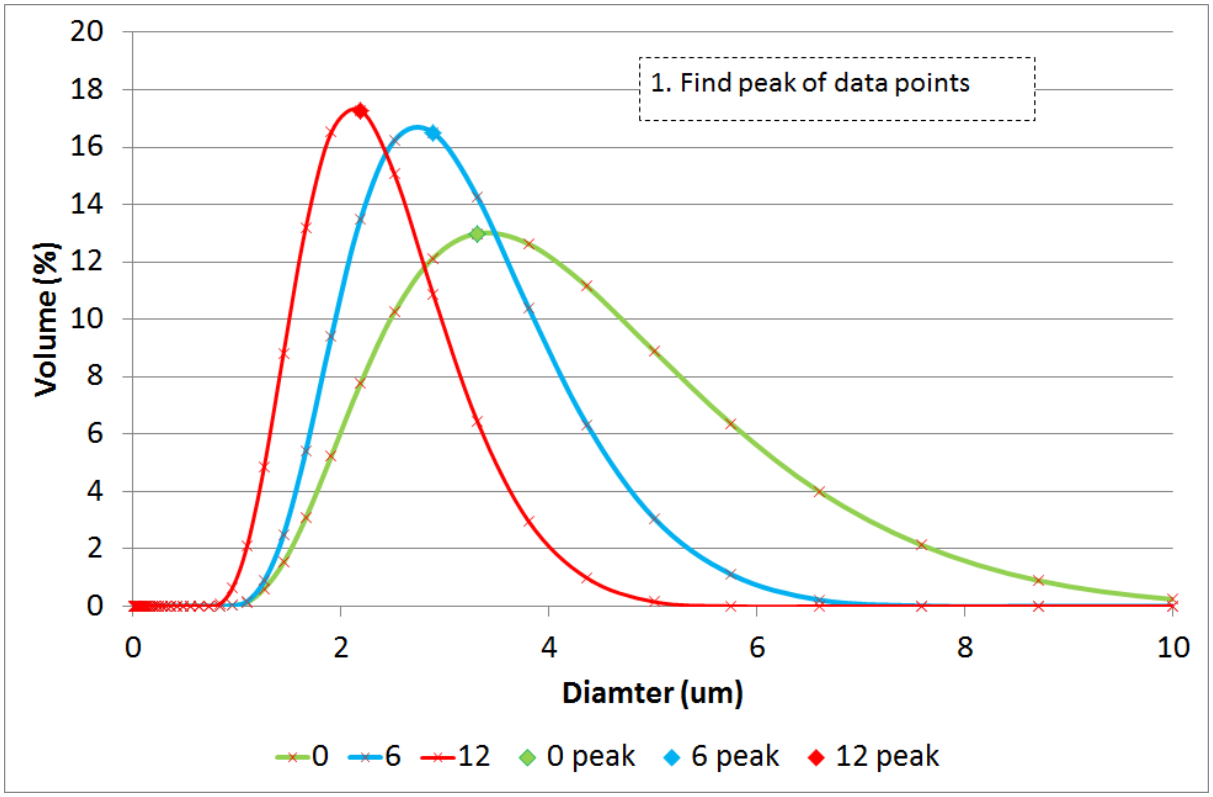

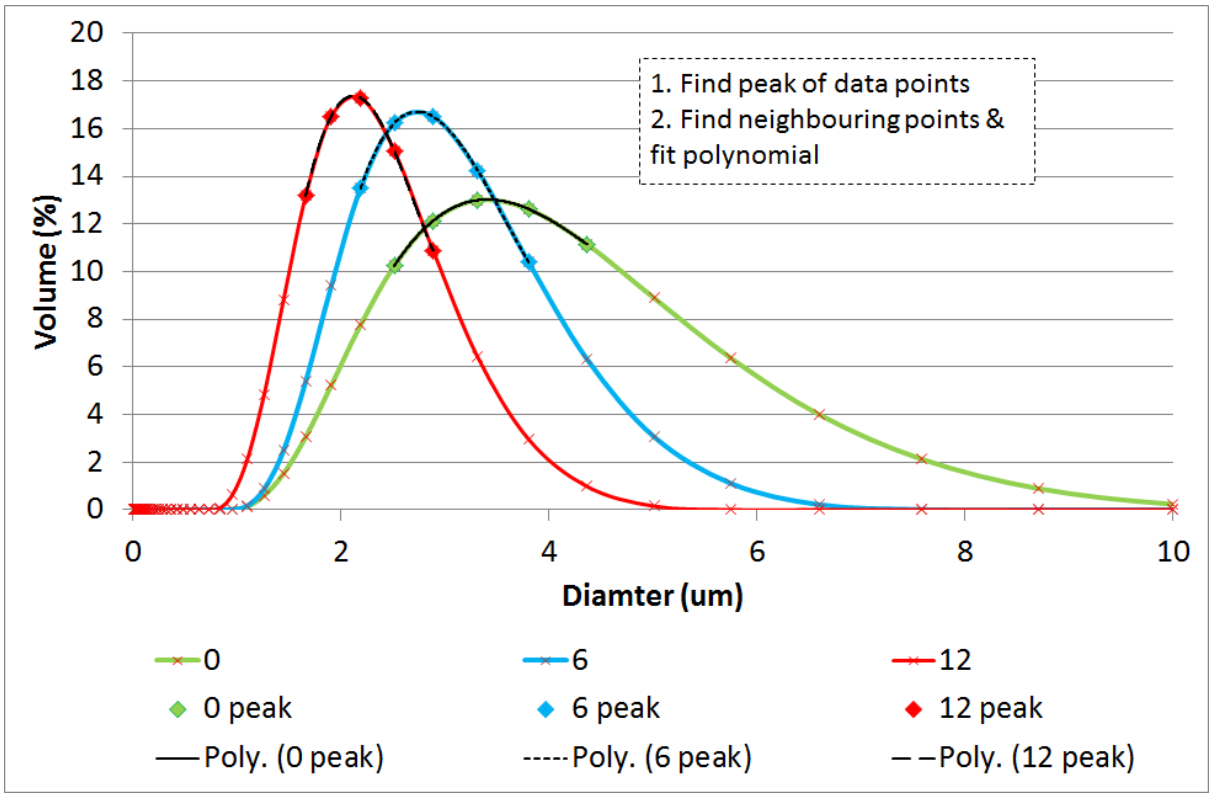

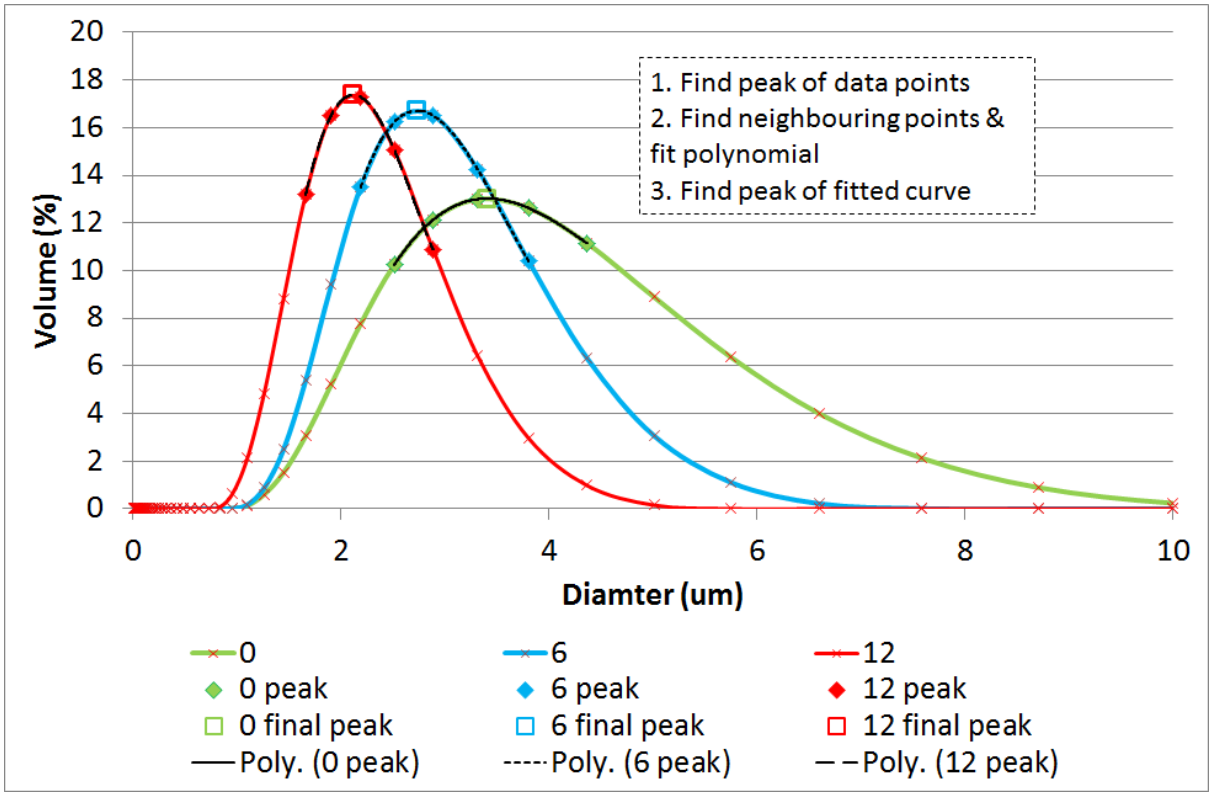
1. Find peak of data points
2. Find neighbouring points & fit polynomial
3. Find peak of fitted curve
Volume (%)
Diamter (um)
0
2
4
6
8
10
12
14
16
18
20
0
6
12
0 peak
6 peak
12 peak
0 final peak
6 final peak
12 final peak
Poly. (0 peak)
Poly. (6 peak)
Poly. (12 peak)

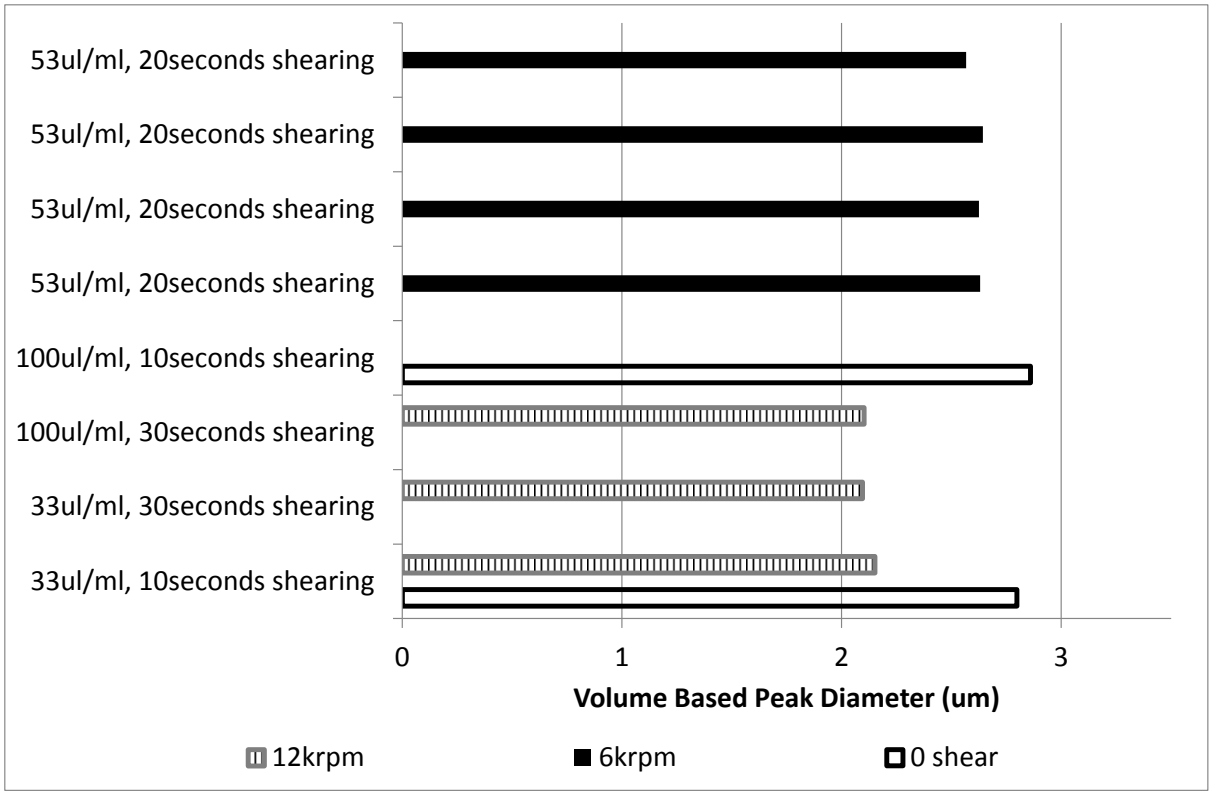

Figure(D) 3. Sensitivity analysis on rotating shear device speed, Adju-Phos concentration and shearing period on the volume based peak diameter, as measured using the Mastersizer 2000MS.

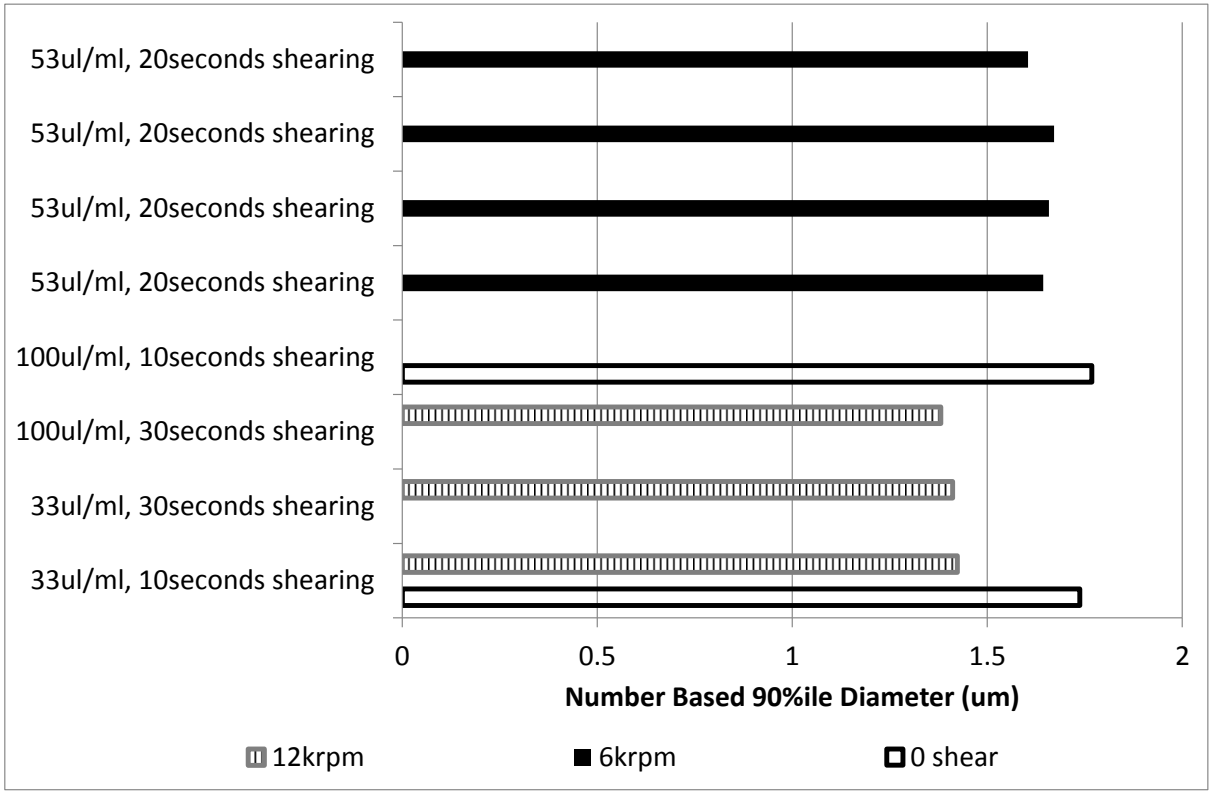

Figure(D) 4. Sensitivity analysis on rotating shear device speed, Adju-Phos concentration and shearing period on the number based 90%ile diameter, as measured using the Mastersizer 2000MS.

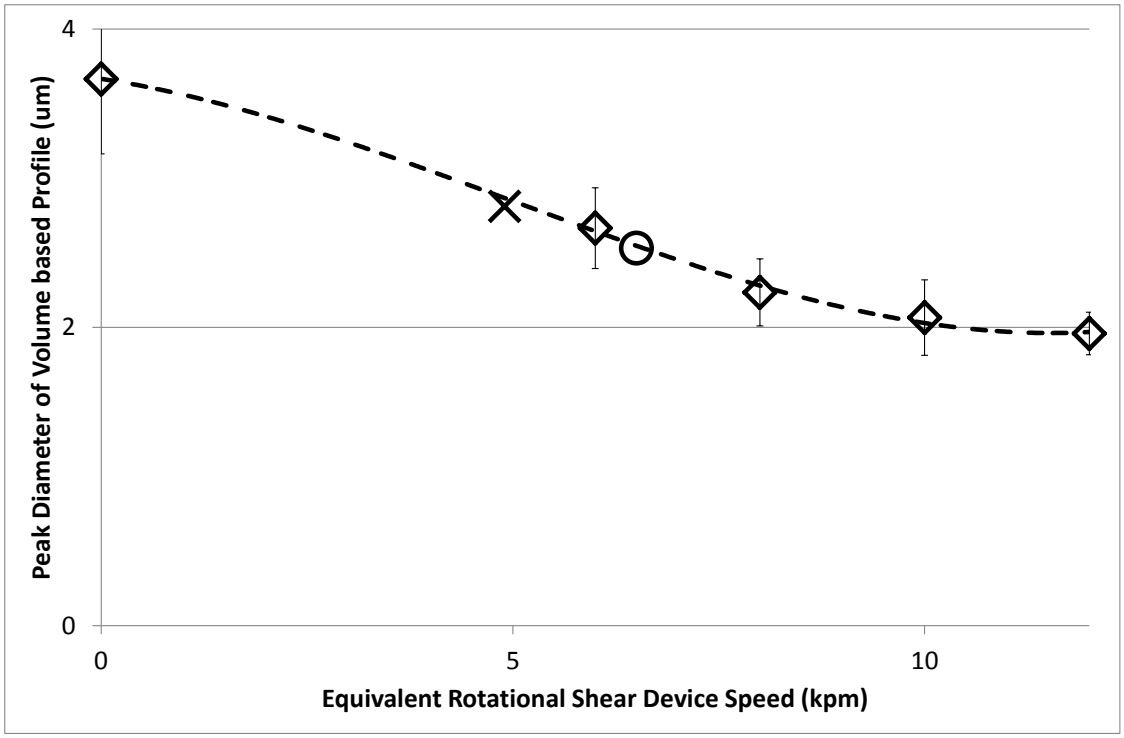

Figure(D) 5. Effect of disruption shear rate on the particle size distribution for 1%v/v Adju-Phos suspension by a USD rotational shear device over a range of shear rates. The peak diameter on a volume basis is generated using a single peak based distribution on Mastersizer 3000 SV. Open diamonds (◇) are the results from Adju-phos sheared in the rotating shear device. Error bars represent 95% confidence intervals using student t-test (n=3). The open circle (○) is a run at top speed and minimum flow, and the cross (X) a run at min speed and max flow, on the PSC-1 centrifuge (which automatically discharges before stopping), with solids removed manually.

Appendix E: Chapter 5 Supplementary Data

1. A constant amount of fluorescein is added to a dilution series of nanobeads, and a 4 parameter logistic fit against the data used to identify the concentration parameter C.

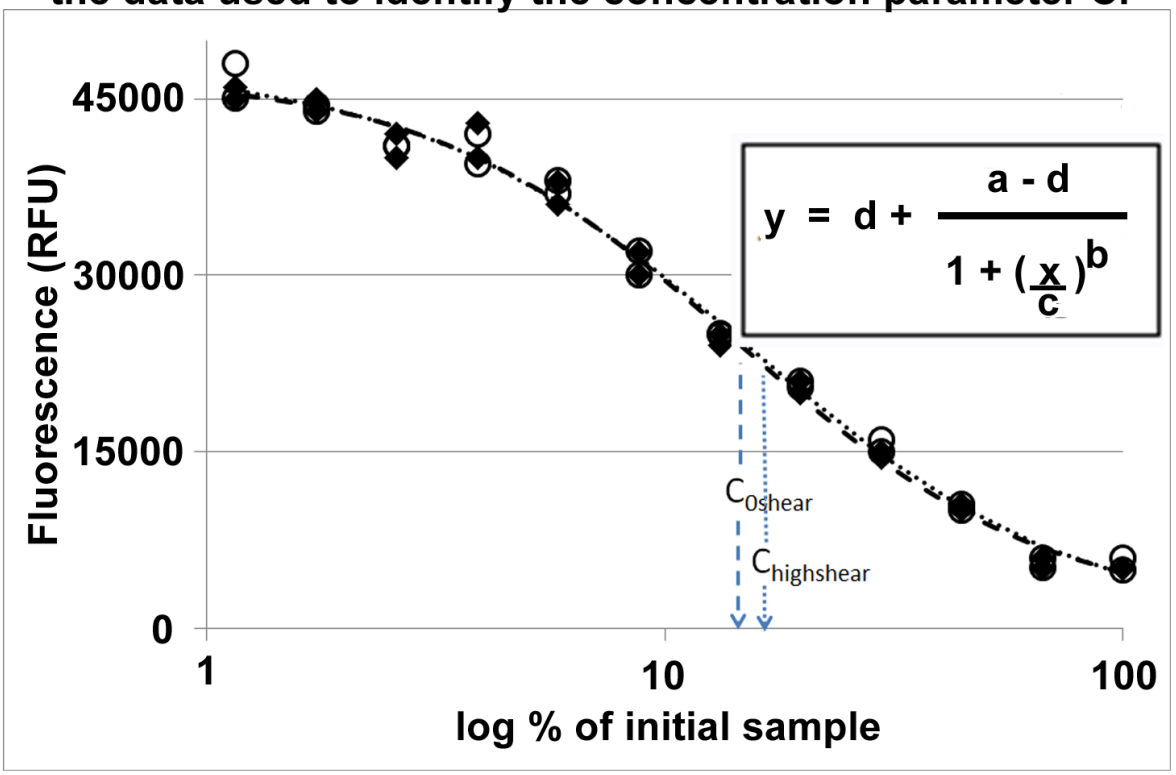

2. Fluorescence assay used to correct count

Count with Fluorescence Concentration correction =
Concentration as measured on nanosight x C / 100

Figure(E) 1. Derivation of the Fluorescence assay corrected concentration whereby the count from the nanosight is calibrated against the expected number of nanobeads based on the streptavidin concentration derived from the fluorescence assay.

Appendix F: Chapter 6 Supplementary Data

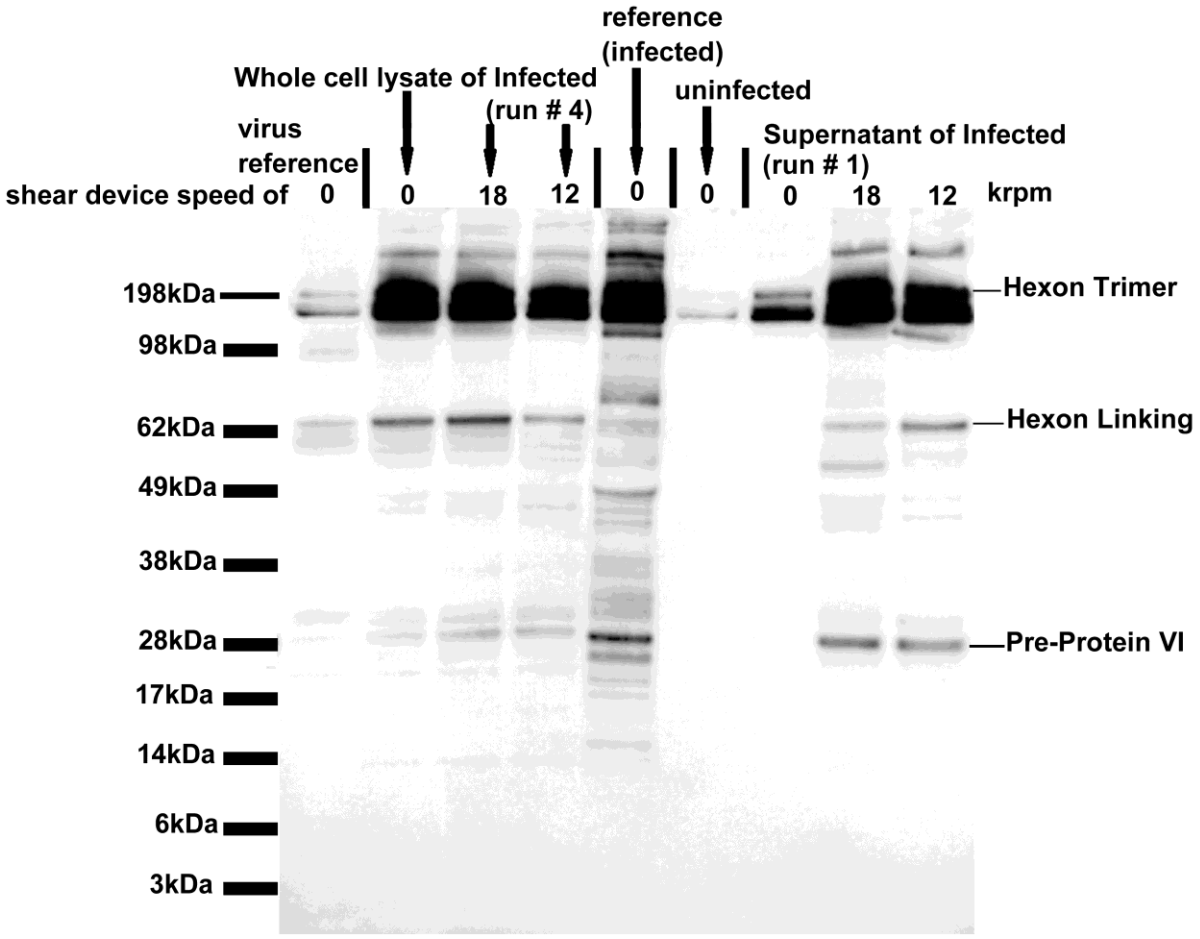

Figure(F) 1. Sample immunoblot, tagged with polyclonal antibodies against adenovirus type 5 coat proteins. Lanes, Ad5 reference, lysate of HEK cells infected with adenovirus and subjected to rotating shear device speeds of 0, 18 and 12krpm, a reference of adenovirus infected HEK cells, lysate of uninfected HEK cells, and supernatant of HEK cells infected with adenovirus and subjected to rotating shear device speeds of 0, 18 and 12krpm. Equal mass of protein was loaded in each lane.

An attempt was made to produce a similar immunoblot against HA influenza proteins (Figure(F) 2) but the quality of the blot was too poor for analysis. There was insufficient time to repeat this assay.

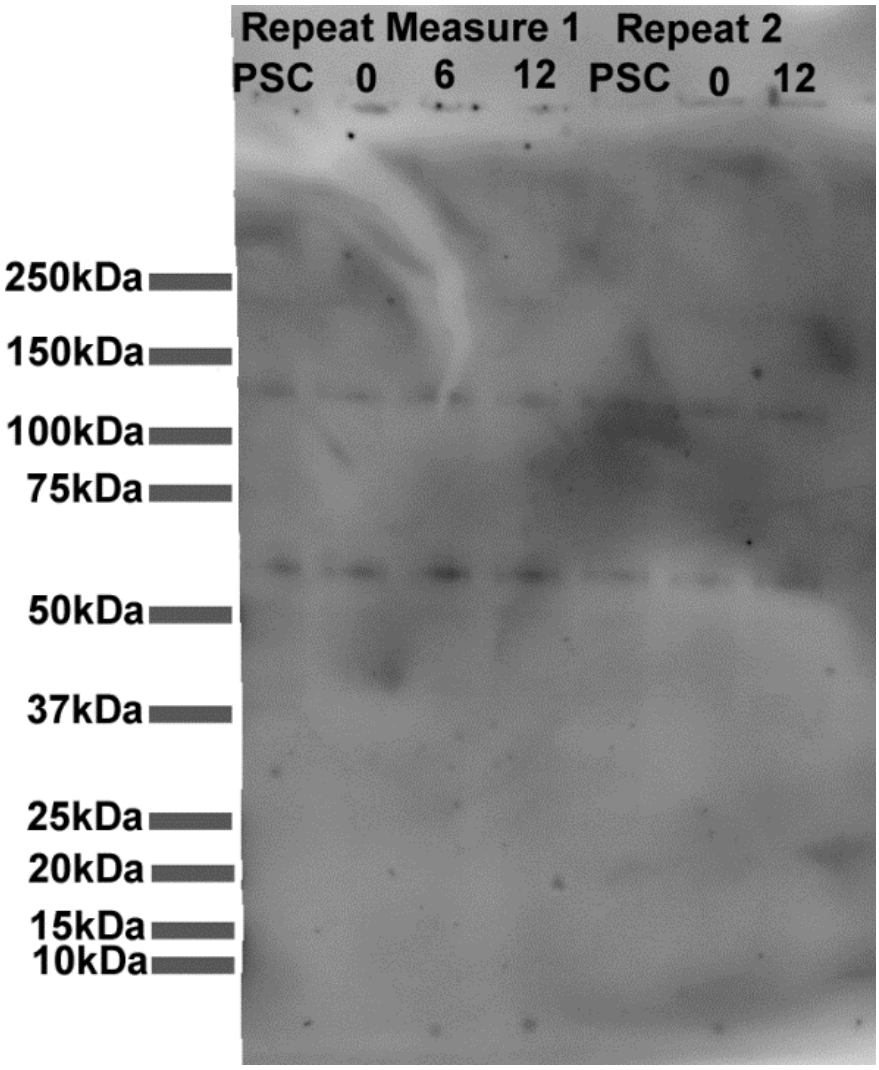

Figure(F) 2. Sample immunoblot, tagged with antibodies against HA proteins. Lanes are, in order, molecular weight markers, EB66 cells infected with influenza and clarified using the PSC-5 centrifuge, subjected to shear in the rotating shear device at speeds of 0, 6 and 12krpm before being clarified at laboratory scale, and repeat measurements of the large scale centrifuge supernatant (PSC-5) and shearing at rotational shear device speeds of 0 and 12krpm and clarification at laboratory scale. N.B. equal volume of sample loaded in each lane. Laboratory scale samples have been clarification at conditions equivalent to those used at large scale.

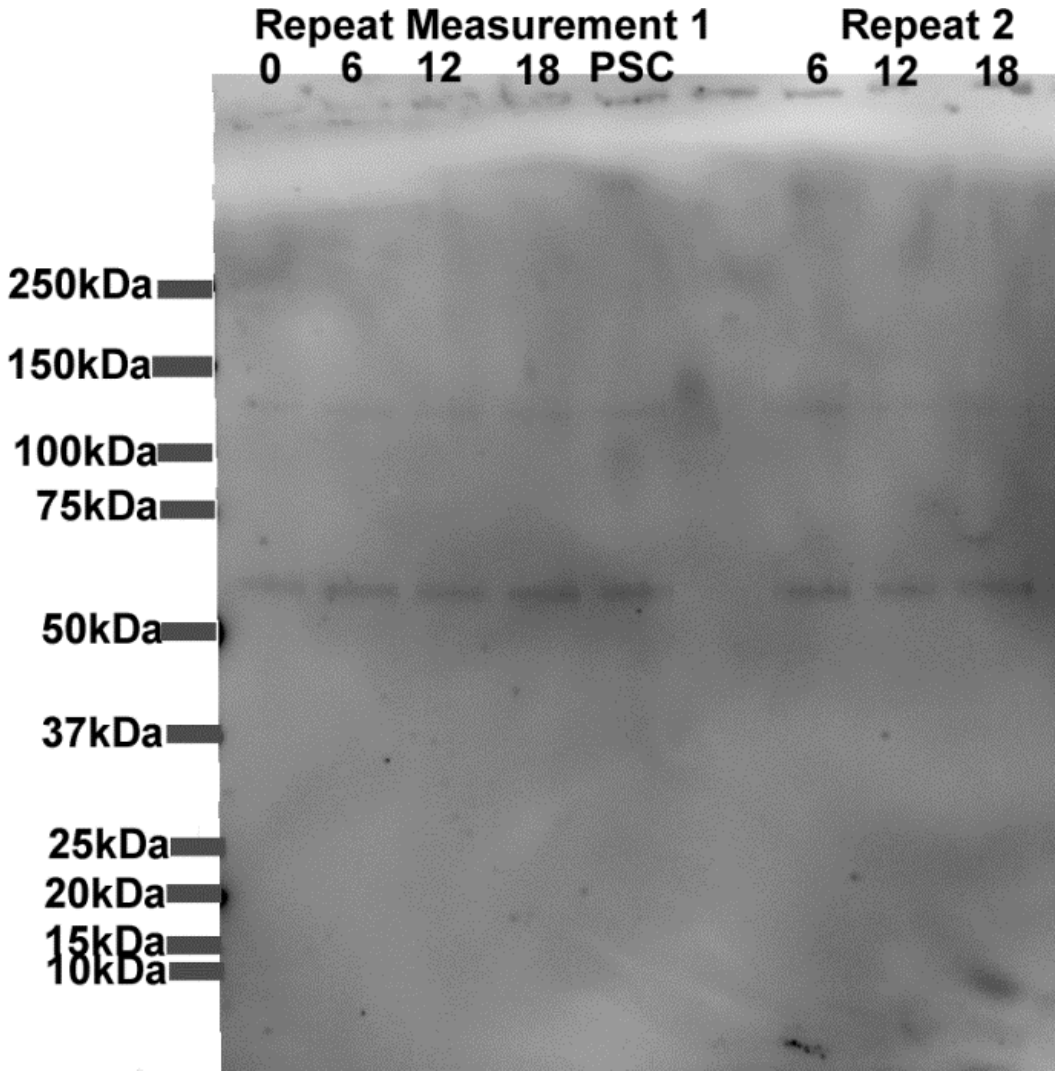

Figure(F) 3. Sample immunoblot, tagged with antibodies against HA proteins. Lanes are, in order, molecular weight markers, EB66 cells infected with influenza and subjected to rotating shear device speeds of 0, 6, 12 and 18krpm, large scale PSC-5 centrifuge processed influenza infected EB66 cells, a blank lane and repeat measurements for EB66 cells infected with influenza and subjected to rotating shear device speeds of 6, 12 and 18krpm. N.B. Equal mass of protein in each lane as measured by peak absorption. The laboratory scale samples have been clarified at conditions equivalent to those used at large scale, and all samples have been fractionated using a sucrose gradient.

Appendix G: Chapter 2 Buffer Recipes

PBS

PBS tablets (Sigma Aldrich) were dispersed in RO milliq water. The concentration was 1 x 1.95-9g tablet in approximately 200ml. A magnetic stirrer was used to ensure the PBS was fully dissolved.

PBS was used to suspend nanobeads, chromatographic beads, adju-phos, al-hydrogel and sucrose.

Tris HCl

10xTris-HCl was made up as follows: 61g of Trizma Hydrochloride (T3253, Sigma, UK) was dissolved in 1000ml of milliq water, and NaOH (71692-1KG, Sigma) added drop-wise to adjust the pH to 8.1.

10mM Tris-HCl was made by adding 10ml of 10xTris-HCl to 490ml of milliq water. 10mM Tris-HCl was used to make up CsCl density gradients, and to suspend the virus sample before adding to the density gradient.

Tris Base

6g Tris base (SC-3715A, santa cruz) and 8.766g NaCl (746398-1kg, sigma-aldrich, UK) was added to 1litre of milliq water, and 1M HCl added drop-wise to adjust pH to 7.6.

NP40 buffer

NP40 buffer was made-up by addition to 50ml of milliq water of the following, in the following order: 3.48g NaCl (746398-1kg, sigma-aldrich), 0.242g Tris (SC-3715A, Santa Cruz Biotechnology Inc), 0.292g EDTA (E6758-10G, Sigma), 1M HCl (258148-2.5L, Sigma) added drop-wise to adjust the pH to 7.3, 2ml NP40 (I3021-100ML, Sigma). The volume was made up to 100ml with milliq water. NP40 was stored refrigerated.

STB Sample buffer

Non-reducing STB (Laemmli) buffer was made-up by addition to 50ml of milliq water of the following, in the following order: 0.605g Tris, HCl added drop-wise to adjust the pH to 6.8, milliq water to make up the volume of 100ml, of which 7ml was taken, and 0.4g SDS (L3771-25g, sigma), 2ml glycerol (G5516-100ML, Sigma) and a trace of bromophenol blue (114391-5g, sigma-aldrich) added. For reducing STB an additional 1ml of 2-mercaptoethanol (M3148-25ml, sigma) was added along with the SDS.

Acids and Base

10ml of 99% sulphuric acid, H_2SO_4 (BDH AnalaR) was diluted in 190ml milliq water to create a 1 molar stock solution.

6ml of 37% HCl was diluted in 193ml milliq water to create a 1 molar stock solution.

42g of sodium bicarbonate, $NaHCO_3$, powder (Fluka Analytical) was dispersed in 500ml milliq water to create a 1 molar stock solution.

Both 1 molar and concentrated acids were used to treat Agarose and the streptavidin coated nanobeads as described in section 2.1.2.1 and $NaHCO_3$ used to neutralise the acid following treatment.

Acid treatment was used to stress test shear mimic candidates, with the aim of demonstrating that the assay techniques chosen/ developed were capable of measuring damage to the shear mimics. It was also used as a simple, single step treatment, in an attempt to weaken chromatographic bead materials, and make them more susceptible to damage by shear.

Silver stain solutions

Fixing solution: 400ml methanol (M/3900/17, Fischer scientific), 100ml acetic acid (126040010, Acros Organics) and 500ml milliq water;

Sensitising solution, prepared by addition, in order of:

- 100ml milliq water
- 10ml sodium thiosulphate (72049-250G, Sigma Aldrich) (5%w/v)
- 17g sodium acetate (S5636-500G, Sigma Aldrich)
- And, once the above was dissolved, 75ml ethanol and milliq water to 250ml

Silver stain solution:

- 25ml milliq water
- 2.5mg silver nitrate (209139-25G, Sigma Aldrich)
- And, once the above was dissolved, milliq water to 250ml

Developing solution:

- 2.5g sodium carbonate (791768-500G, Sigma Aldrich)
- 500ml milliq water
- 200µl Formaldehyde (F8775-25ml, Sigma Aldrich)

Stopping solution:

- 3.65g EDTA-$Na_2 2H_2O$ (E5134-100G, Sigma Aldrich);
- Filled to 250ml with milliq water

Sypro Tangerine solutions

Fixation solution consists of 250ml of 7.5% acetic acid with 50µl sypro tangerine added and mixed vigorously. 7.5% acetic acid.